Selected Papers in the Hydrologic Sciences 1987

December 1987

United States Geological Survey Water-Supply Paper 2330

AVAILABILITY OF BOOKS AND MAPS OF THE U.S. GEOLOGICAL SURVEY

Instructions on ordering publications of the U.S. Geological Survey, along with prices of the last offerings, are given in the current-year issues of the monthly catalog "New Publications of the U.S. Geological Survey." Prices of available U.S. Geological Survey publications released prior to the current year are listed in the most recent annual "Price and Availability List." Publications that are listed in various U.S. Geological Survey catalogs (**see back inside cover**) but not listed in the most recent annual "Price and Availability List" are no longer available.

Prices of reports released to the open files are given in the listing "U.S. Geological Survey Open-File Reports," updated monthly, which is for sale in microfiche from the U.S. Geological Survey, Books and Open-File Reports Section, Federal Center, Box 25425, Denver, CO 80225. Reports released through the NTIS may be obtained by writing to the National Technical Information Service, U.S. Department of Commerce, Springfield, VA 22161; please include NTIS report number with inquiry.

Order U.S. Geological Survey publications **by mail** or **over the counter** from the offices given below.

BY MAIL

Books

Professional Papers, Bulletins, Water-Supply Papers, Techniques of Water-Resources Investigations, Circulars, publications of general interest (such as leaflets, pamphlets, booklets), single copies of Earthquakes & Volcanoes, Preliminary Determination of Epicenters, and some miscellaneous reports, including some of the foregoing series that have gone out of print at the Superintendent of Documents, are obtainable by mail from

U.S. Geological Survey, Books and Open-File Reports
Federal Center, Box 25425
Denver, CO 80225

Subscriptions to periodicals (Earthquakes & Volcanoes and Preliminary Determination of Epicenters) can be obtained ONLY from the

Superintendent of Documents
Government Printing Office
Washington, D.C. 20402

(Check or money order must be payable to Superintendent of Documents.)

Maps

For maps, address mail orders to

U.S. Geological Survey, Map Distribution
Federal Center, Box 25286
Denver, CO 80225

Residents of Alaska may order maps from

Alaska Distribution Section, U.S. Geological Survey,
New Federal Building - Box 12
101 Twelfth Ave., Fairbanks, AK 99701

OVER THE COUNTER

Books

Books of the U.S. Geological Survey are available over the counter at the following Geological Survey Public Inquiries Offices, all of which are authorized agents of the Superintendent of Documents:

- **WASHINGTON, D.C.**--Main Interior Bldg., 2600 corridor, 18th and C Sts., NW.
- **DENVER, Colorado**--Federal Bldg., Rm. 169, 1961 Stout St.
- **LOS ANGELES, California**--Federal Bldg., Rm. 7638, 300 N. Los Angeles St.
- **MENLO PARK, California**--Bldg. 3 (Stop 533), Rm. 3128, 345 Middlefield Rd.
- **RESTON, Virginia**--503 National Center, Rm. 1C402, 12201 Sunrise Valley Dr.
- **SALT LAKE CITY, Utah**--Federal Bldg., Rm. 8105, 125 South State St.
- **SAN FRANCISCO, California**--Customhouse, Rm. 504, 555 Battery St.
- **SPOKANE, Washington**--U.S. Courthouse, Rm. 678, West 920 Riverside Ave..
- **ANCHORAGE, Alaska**--Rm. 101, 4230 University Dr.
- **ANCHORAGE, Alaska**--Federal Bldg, Rm. E-146, 701 C St.

Maps

Maps may be purchased over the counter at the U.S. Geological Survey offices where books are sold (all addresses in above list) and at the following Geological Survey offices:

- **ROLLA, Missouri**--1400 Independence Rd.
- **DENVER, Colorado**--Map Distribution, Bldg. 810, Federal Center
- **FAIRBANKS, Alaska**--New Federal Bldg., 101 Twelfth Ave.

Selected Papers in the Hydrologic Sciences 1987

Edited by Seymour Subitzky

December 1987

U.S. GEOLOGICAL SURVEY WATER-SUPPLY PAPER 2330

DEPARTMENT OF THE INTERIOR
DONALD PAUL HODEL, Secretary

U.S. GEOLOGICAL SURVEY
Dallas L. Peck, Director

UNITED STATES GOVERNMENT PRINTING OFFICE: 1988

For sale by the Books and Open-File Reports Section,
U.S. Geological Survey, Federal Center,
Box 25425, Denver, CO 80225

Selected Papers in the Hydrologic Sciences
ISSN 0892–3450

PREFACE

Selected Papers in the Hydrologic Sciences, a U.S. Geological Survey-managed journal-type publication in the Water-Supply Paper series, is aimed at meeting widespread public and professional needs for results of broad-based integrated hydrologic studies derived from the Federal research program, Federal-State cooperative program, and, to some extent, work done on behalf of other Federal agencies. This is the fifth issue of the series and comprises 12 topical papers that address a broad range of topics including biochemistry, atmospheric hydrology, ground- and surface-water hydrology, and selected geologic and chemical techniques for hydrologic studies.

Selected Papers is intended to serve as a forum that encourages dialog between readers and authors. Participation in such dialog among hydroscientists within and outside the Federal sector would be beneficial. Discussion papers by *all* members of the hydroscience community are desired. A discussion section for readers' comments and authors' replies will be included in each issue. Such discussion papers for this issue will be open until September 1989. Address comments to Editor, *Selected Papers in the Hydrologic Sciences*, U.S. Geological Survey, 444 National Center, Reston, VA 22092.

Seymour Subitzky
Editor

SI and Inch-Pound Unit Equivalents

International System of Units (SI), a modernized metric system of measurement. All values have been rounded to four significant digits. Use of hectare (ha) as an alternative name for square hectometer (hm^2) is restricted to measurement of land or water areas. Use of liter (L) as a special name for cubic decimeter (dm^3) is restricted to the measurement of liquids and gases.

Multiply SI units	By	To obtain inch-pound units
Length		
micrometer (μm)	0.000 039 37	inch (in)
millimeter (mm)	0.039 37	inch (in)
centimeter (cm)	0.393 7	inch (in)
meter (m)	3.281	foot (ft)
	1.094	yard (yd)
kilometer (km)	0.621 4	mile (mi)
Area		
centimeter^2 (cm^2)	0.155 0	inch^2 (in^2)
meter^2 (m^2)	10.76	foot^2 (ft^2)
	1.196	yard^2 (yd^2)
	0.000 247 1	acre
hectometer^2 (hm^2)	2.471	acre
kilometer^2 (km^2)	0.386 1	mile^2 (mi^2)
Volume		
centimeter^3 (cm^3)	0.061 02	inch^3 (in^3)
milliliter (mL)	0.061 02	inch^3 (in^3)
liter (L)	61.02	inch^3 (in^3)
	0.035 31	foot^3 (ft^3)
	33.82	ounce, fluid (oz)
	2.113	pint (pt)
	1.057	quart (qt)
	0.264 2	gallon (gal)
meter^3 (m^3)	35.31	foot^3 (ft^3)
	1.308	yard^3 (yd^3)
	264.2	gallon (gal)
	0.000 810 7	acre-foot (acre-ft)
kilometer^3 (km^3)	0.239 9	mile^3 (mi^3)
Mass		
microgram (μg)	0.000 015 43	grain (gr)
gram (g)	0.035 27	ounce, avoirdupois (oz avdp)
kilogram (kg)	2.220 5	pound, avoirdupois (lb avdp)

Multiply SI units	By	To obtain inch-pound units
Mass per unit volume		
microgram per liter (μg/L)	0.000 058 41	grain per gallon (gr/gal)
milligram per liter (mg/L)	0.058 41	grain per gallon (gr/gal)
Mass or volume per unit time (includes flow)		
gram per minute (g/min)	0.035 27	ounce (avoirdupois) per minute (oz/min)
milliliter per minute (mL/min)	0.033 82	ounce (fluid) per minute (oz/min)
	0.035 31	foot^3 per second (ft^3/s)
liter per second (L/s)	15.85	gallon per minute (gal/min)
meter^3 per second (m^3/s)	35.31	foot^3 per second (ft^3/s)
	15 850	gallon per minute (gal/min)
meter per second (m/s)	3.281	foot per second (ft/s)
meter per day (m/d)	3.281	foot per day (ft/d)
Transmissivity		
meter^2 per day (m^2/d)	10.76	foot^2 per day (ft^2/d)
Force per unit area		
kilopascal (kPa)	0.145 03	pound-force per inch^2 (lbf/in^2)
kilogram per meter^2 (kg/m^2)	0.204 8	pound-force per foot^2 (lbf/ft^2)
kilogram per meter^3 (kg/m^3)	0.624 6	pound-force per foot^3 (lbf/ft^3)
Temperature		
degree Celsius (°C)	Temp °F=1.8 temp °C+32	degree Fahrenheit (°F)
Specific conductance		
microsiemens per centimeter at 25 degrees Celsius (μS/cm at 25 °C)	1.000	micromho per centimeter at 25 degrees Celsius (μmho/cm at 25 °C)
millisiemens per meter at 25 degrees Celsius (mS/m at 25 °C)	1.000	millimho per meter at 25 degrees Celsius (mmho/m at 25 °C)

Any use of trade names and trademarks in this publication is for descriptive purposes only and does not constitute endorsement by the U.S. Geological Survey.

National Geodetic Vertical Datum (NGVD) of 1929: A geodetic datum derived from a general adjustment of the first-order level nets of both the United States and Canada, formerly called *"Mean Sea Level."*

CONTENTS

Use of Aeromagnetic Data to Define Boundaries of a Carbonate-Rock Aquifer in East-Central Nevada

By Russell W. Plume

Abstract

A major problem in the study of ground-water flow systems in carbonate rocks in the eastern Great Basin is that of defining flow-system boundaries. Aeromagnetic data have been used to define such boundaries in a part of the White River flow system of eastern Nevada. In the northern part of this flow system, the upper Precambrian and Paleozoic stratigraphic section consists of about 40,000 feet of clastic and carbonate sedimentary rocks. The carbonate-rock aquifer in this area is contained within two units of carbonate rocks that are separated by a relatively thin unit of clastic rocks.

Two models of subsurface geology based on interpretation of aeromagnetic data indicate that the northern part of the flow system is bounded on the east and west by Cretaceous and Tertiary granitic intrusions. In between, the stratigraphic section is underlain by either Precambrian basement or by younger granitic rocks. Although either model is considered geologically reasonable, the Precambrian basement model is favored because the configuration of the basement surface seems to coincide with inferred fault offsets of the base of the stratigraphic section. This suggests that stratigraphic thickness can be used to estimate possible aquifer thickness in the northern part of the White River flow system. In this area, the maximum thickness of the carbonate-rock aquifer is still uncertain but probably is less than about 26,000 feet; its width is about 25 miles, in contrast to an earlier estimate of 15 miles. With this revised value of flow-system width, the transmissivity of the aquifer is an estimated 20,000 feet squared per day, whereas the earlier estimate was 30,000 feet squared per day.

INTRODUCTION

The eastern Great Basin (eastern Nevada and western Utah) is underlain by thick sections of Paleozoic carbonate rocks (limestone and dolomite) that contain several regional ground-water flow systems. A major difficulty involved with the study of these flow systems is that of defining their base and lateral limits. These properties are difficult to define for at least three reasons: first, deep borehole data for the Precambrian and Paleozoic sections generally are not available; second, the complex geology of the Great Basin makes estimates of aquifer thickness based only on stratigraphic thickness uncertain; and third, water-level data from wells, mines, and regional springs representative of the carbonate-rock aquifer are sparse, they generally represent heads in the shallower part of the aquifer, and they indicate only general directions of ground-water movement. This paper shows how aeromagnetic data were used to define the lateral boundaries and possible base of part of a carbonate-rock aquifer in east-central Nevada (fig. 1). These properties are important because they are directly related to other aquifer properties such as transmissivity and cross-sectional area of flow.

This work was done as part of the Great Basin Regional Aquifer-System Analysis Program. The overall study is one of a series of systematic studies of regional aquifer systems being made by the U.S. Geological Survey throughout the United States.

One of the first carbonate-rock flow systems to be recognized and described in the Great Basin was the White River flow system in eastern Nevada (Eakin, 1966); it consists of 13 valleys, 6 of which are tributary to the Colorado River via ephemeral streams and the other 7 of which are topographically closed (Eakin, 1966, p. 251–253). Eakin showed that the flow system is contained within Paleozoic carbonate rocks that underlie the mountains and valleys of the area. Furthermore, he tentatively considered the lateral limits of the flow system to be ground-water divides that coincide with the outer topographic divides of valleys in the system. Eakin described in broad terms the regional geology of the flow system, the regional movement of water, and a water budget. For the northern part of the flow system (north end of White River Valley), he estimated an effective aquifer width of 15 mi and a transmissivity of 30,000 ft^2/d (1966, p. 266).

The area discussed in this paper is near the north end of the White River flow system (figs. 1 and 2). This area includes the north end of White River Valley, Jakes Valley, and parts of the White Pine and Egan Ranges. The line A–A' in figures 1 and 2 shows the location of a geologic section and magnetic profile, both of which are

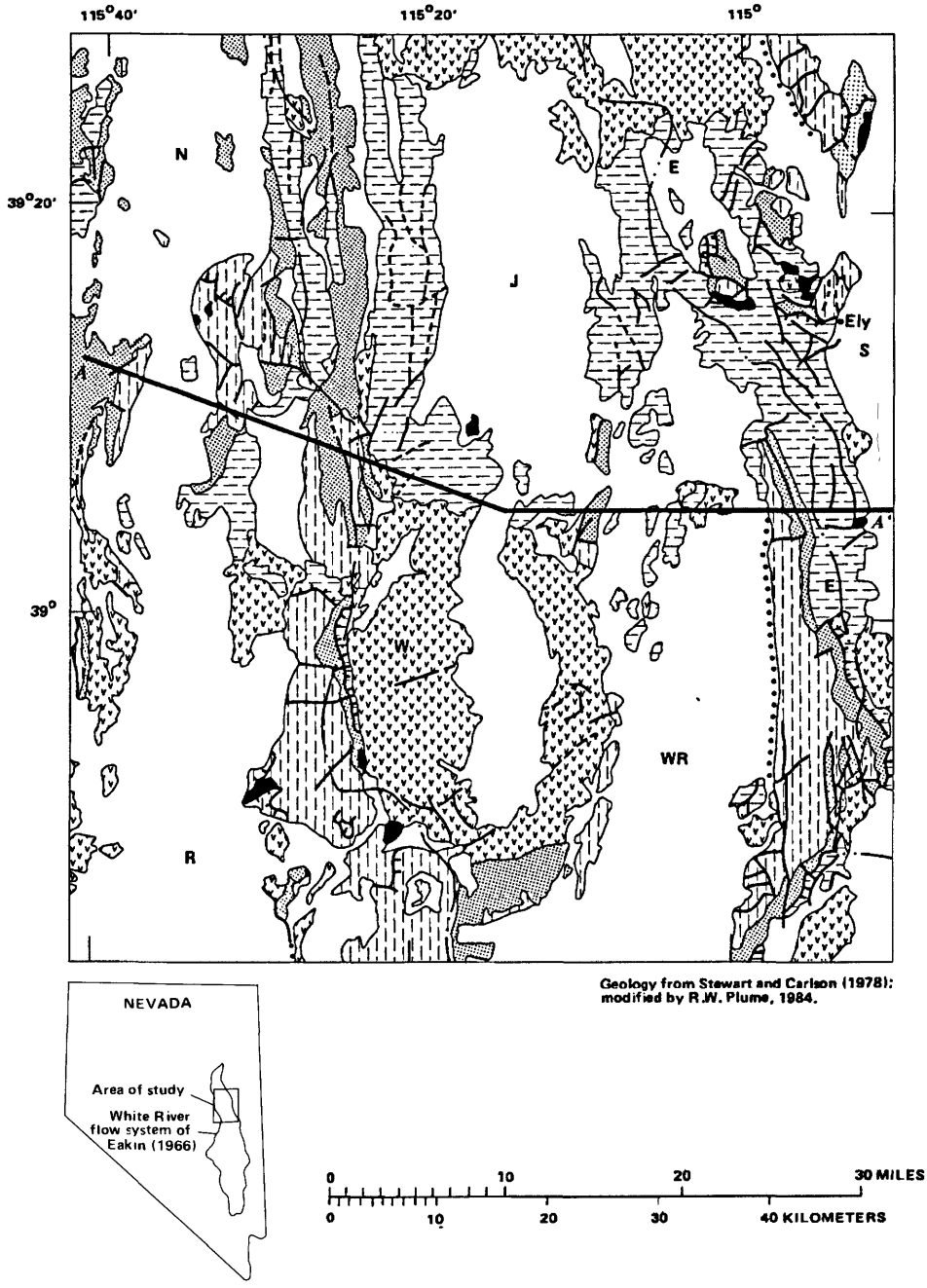

Figure 1. Hydrogeologic map of the study area. Abbreviations: E, Egan Range; J, Jakes Valley; N, Newark Valley; R, Railroad Valley; S, Steptoe Valley; W, White Pine Range; WR, White River Valley.

used to describe the subsurface geology across the flow system and to define aquifer boundaries. The line is normal to the regional southward flow of ground water.

The area of the White River flow system in eastern Nevada is one where north-south-trending mountains and valleys are as much as 100 mi long and 15 mi wide. Altitudes generally range from 2,000 to 6,000 ft above sea level at valley floors and from 5,000 to almost 11,000 ft along the crests of mountain ranges. The area is arid to semi-arid, although the higher mountains receive substantial amounts of winter precipitation, part of which becomes ground-water recharge. Much recharge occurs in the north part of the flow system (part of the study area) because this is the area of highest altitude in the flow system, typically 6,000 ft in valleys and 8,000 to nearly 11,000 ft in mountains.

REGIONAL GEOLOGY

The continental margin of western North America was located in what is now eastern Nevada from late

EXPLANATION

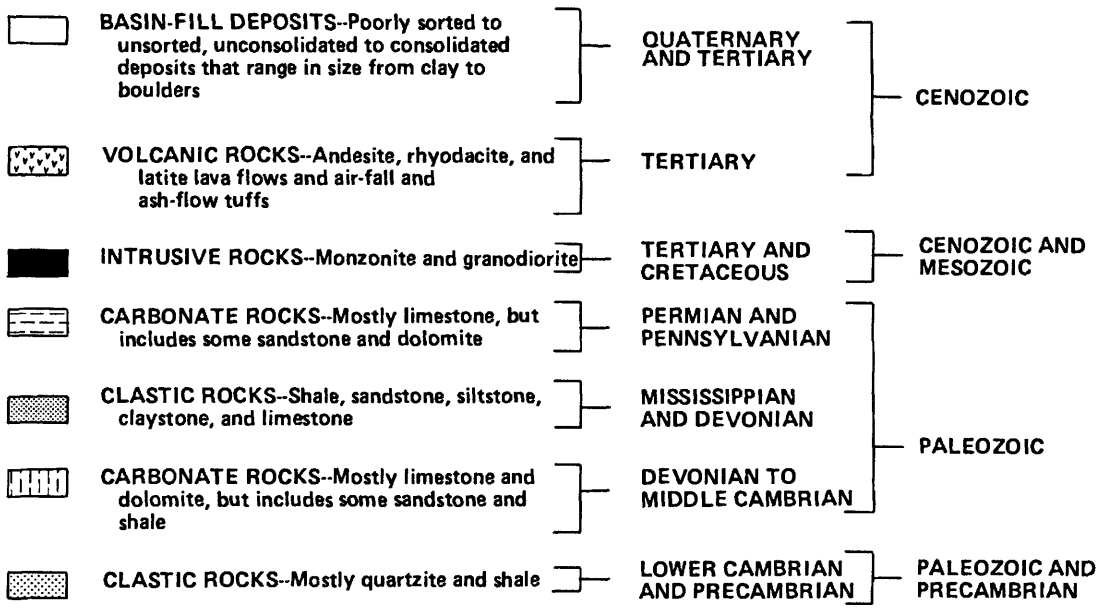

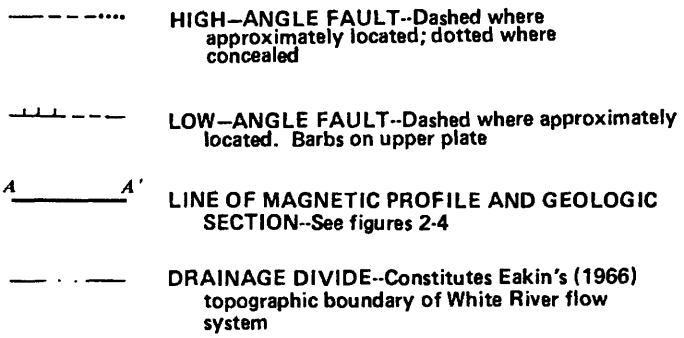

Precambrian time through the Paleozoic and Early Triassic (Hose and Blake, 1976, p. 3; Stewart, 1980, p. 14, 35–36, and 60). During that period, a section of marine clastic and carbonate sedimentary rocks as thick as 40,000 ft accumulated (Humphrey, 1960, p. 9; Drewes, 1967, p. 4–6; Moores and others, 1968, p. 1707; Hose and Blake, 1976, p. 3–16; Stewart, 1980, p. 14–64). For purposes of this study, the section has been divided into four hydrogeologic units (fig. 1): (1) upper Precambrian and Lower Cambrian clastic rocks (about 14,000 ft thick); (2) Middle Cambrian to Devonian carbonate rocks (about 16,000 ft); (3) Upper Devonian and Mississippian clastic rocks (about 3,000 ft); and (4) Pennsylvanian and Permian carbonate rocks (about 6,800 ft). The base of this section is not exposed in east-central Nevada; however, the oldest rocks of the section presumably overlie Precambrian basement (metamorphic and granitic rocks), as they do in southern Nevada and eastern California. Locally, the rocks of the section are intruded by Cretaceous and Tertiary granitic rocks and are overlain by Tertiary volcanic rocks. Basin-fill deposits of Tertiary and Quaternary age overlie large areas of the older rocks, as shown on figure 1.

The major structural features of east-central Nevada are extensional faults of Cenozoic age that include both low- and high-angle normal faults. These faults produced the present-day topography of the region. Low-angle faults generally have moved younger rocks over older ones and have resulted in apparent thinning of the stratigraphic section. These structural features have been recognized in the White Pine Range (Moores and others, 1968, p. 1713–1724), the Egan Range (Hose and Blake, 1976, p. 30), and east of the study area in the Schell Creek and Snake Ranges

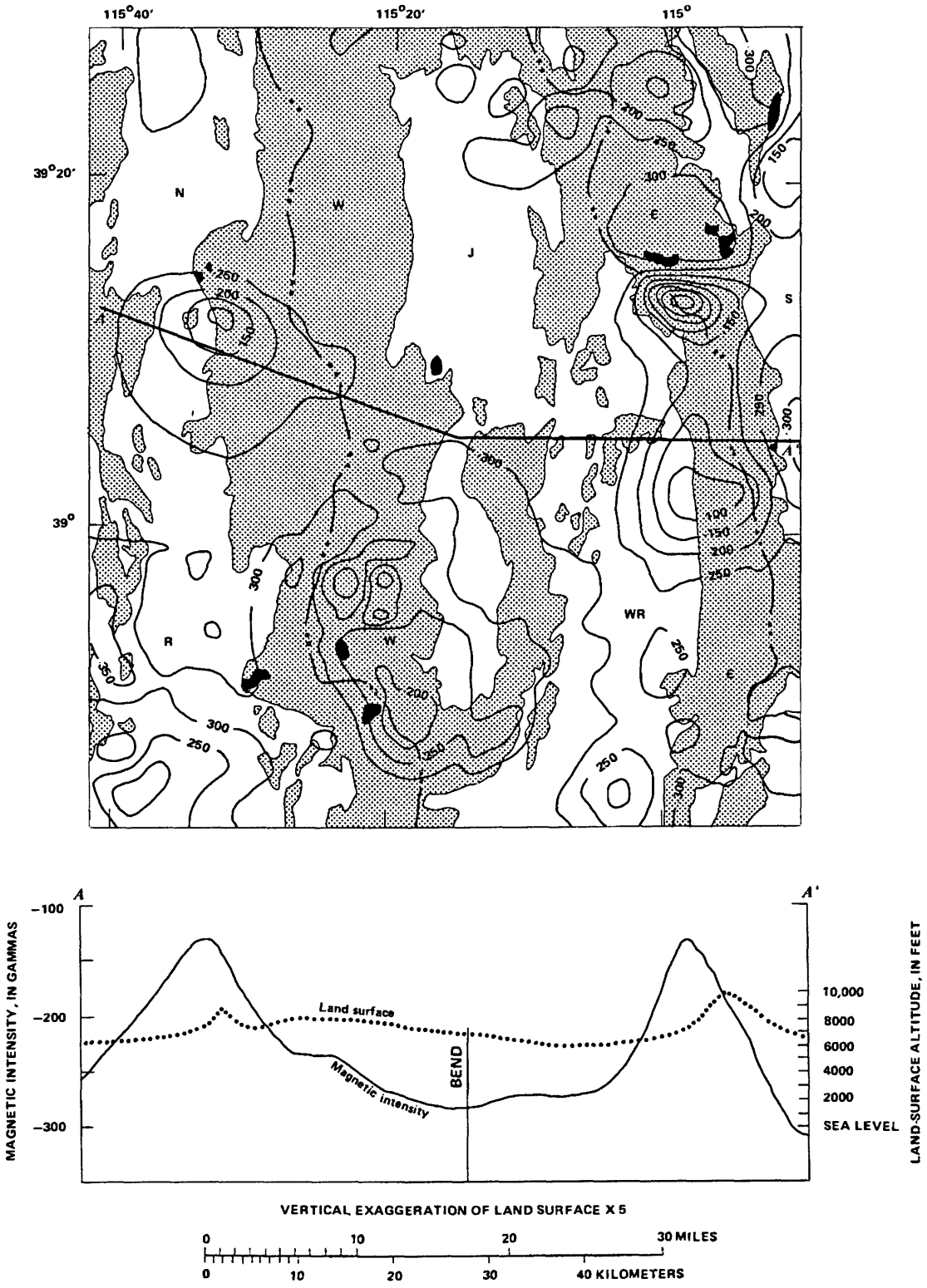

Figure 2. Aeromagnetic map and profile of the study area. Abbreviations: E, Egan Range; J, Jakes Valley; N, Newark Valley; R, Railroad Valley; S, Steptoe Valley; W, White Pine Range; WR, White River Valley.

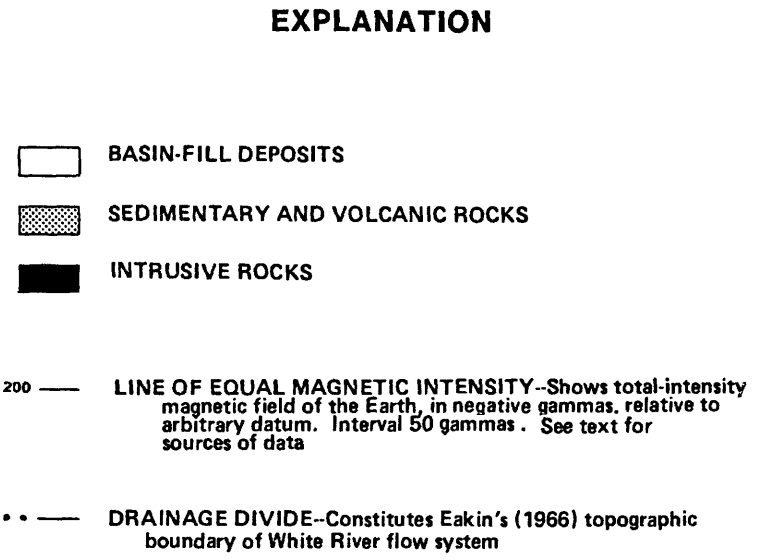

(Drewes, 1967, p. 66–70; Gans and others, 1985). High-angle normal faults cut the upper plates of low-angle faults and in some cases have been shown to flatten and merge at depth with low-angle faults (Allmendinger and others, 1983, p. 535; Gans and others, 1985, p. 193).

The carbonate-rock aquifer of the White River flow system comprises parts of the Pennsylvanian and Permian and the Middle Cambrian to Devonian carbonate rocks, along with the intervening Upper Devonian and Mississippian clastic rocks. The clastic rocks may be a local barrier to ground-water flow. Fault offsets, however, have juxtaposed the upper and lower carbonate-rock units (figs. 1 and 4), and for this reason, the carbonate-rock aquifer, when considered over large areas, can be treated as a single unit even though it consists of parts of three hydrogeologic units. The stratigraphic thickness of this combined carbonate- and clastic-rock unit is about 26,000 ft (see previously listed thicknesses). The base of the aquifer is presumed to be no deeper than the top of upper Precambrian and Lower Cambrian clastic rocks, but it is probably much shallower than that.

MAGNETIC ANOMALIES

Figure 2 shows an aeromagnetic map[1] of the area shown in figure 1 and a magnetic profile along line *A–A'*. The map, which depicts the total-intensity magnetic field of the Earth relative to an arbitrary datum, is based on three aeromagnetic surveys made in 1975 (U.S. Geological Survey, 1976a, b, and c). The surveys were flown at a barometric altitude of 11,500 ft along north-south flight lines spaced at 1-mi intervals.

Three magnetic anomalies on the map may have sources that are hydrologically significant. Two are prominent magnetic highs in the Egan and White Pine Ranges and the third is a broad magnetic low along the west side of White River Valley and the east side of the White Pine Range. This paper demonstrates that source bodies for the two highs are lateral boundaries of the aquifer and that the source for the low can be used to estimate a possible maximum depth to the base of the aquifer. Each anomaly is described below.

The elongate anomaly along the west side of the Egan Range and the east side of White River Valley was described by Brokaw and others (1962) and Carlson and Mabey (1963). They concluded that (1) the source for the high at the north end of the anomaly is a monzonite-porphyry intrusion at the Robinson mining district near Ely, (2) monzonite dikes near the high at the south end of the anomaly suggest a relatively shallow intrusive body, and (3) the two bodies are connected at depth. Carlson and Mabey (1963) estimated that the depth to the top of the source at the south end of the anomaly is about 3,000 ft below the floor of the White River Valley.

The circular high on the west side of the White Pine Range is also associated with nearby intrusive rocks (fig. 2). Two granodiorite stocks have been mapped on the west side of the range (Humphrey, 1960), and the close association of these outcrops with the anomaly strongly suggests that the source is a large igneous intrusion. The depth to the top of the intrusive body on

[1] Changes in the intensity of a magnetic field such as that shown in figure 2 are mainly caused by differences in the magnetic-mineral content of adjacent bodies. For instance, sedimentary rocks such as those of the Paleozoic section usually have low concentrations, at most, of magnetic minerals. In contrast, volcanic and intrusive rocks have relatively high concentrations of magnetic minerals. A magnetic body will produce a relatively strong anomaly when it is at or near land surface, but the intensity of the anomaly becomes weaker as the depth to the body increases.

the south side of the anomaly (the area where line *A–A'* crosses) is estimated to be 9,000 ft, on the basis of the gradient-analysis method of Vacquier and others (1951). The source for the broad low on the west side of White River Valley and east side of the White Pine Range (fig. 2) most likely is either Precambrian basement or Cretaceous and Tertiary granitic rocks. Regardless, the source is deeply buried, possibly beneath the entire accumulation of upper Precambrian and Paleozoic sedimentary rocks.

MODELS OF SUBSURFACE GEOLOGY

The magnetic profile shown in figure 2 was used to develop two theoretical models of the subsurface geology along line *A–A'* (fig. 3). Model bodies are defined in the *x* and *z* directions (horizontal and vertical directions along the profile), and also in the *y* direction (normal to the profile). Each of the models shown in figure 3 is accompanied by two magnetic profiles: the measured data (solid curve) and the profile computed from the model (dotted curve). The close fits of the measured and computed profiles shown in figures 3*A* and *B* were achieved by using reasonable values of magnetic susceptibility for model bodies and then adjusting model geometry. They are not unique solutions, however, because similar fits could be achieved with different susceptibilities and appropriate changes in model geometry.

Some parts of the models are fairly well constrained. For instance, the steep gradients of the anomalies along the observed profile define the horizontal positions of associated source bodies to within several thousand feet. Further, gradient analyses (see previous section) provide estimated depths to these sources. The base of each of the models is loosely constrained by an estimated depth of 60,000 ft to the Curie-point temperature (A.H. Lachenbruch, U.S. Geological Survey, oral commun., 1984), which is the temperature at which rocks become demagnetized. Although this depth is uncertain in eastern Nevada, it provides a tentative lower limit for the models. Model properties that are not constrained are magnetic susceptibilities for all bodies and the geometry of body 2 (fig. 3). Because of these uncertainties, estimated depths based on the models may be in error by 25 percent or more.

The two models shown in figure 3 are presented as possible solutions, both considered to be geologically reasonable. For both models, the dimensions for body 1 in the *y* direction are 4 mi north and 6 mi south of line *A–A'* and those for body 3 are 10 mi north and 7 mi south of the line. Body 2, in contrast, was modeled as a slab of infinite extent in the *y* direction. Bodies 1 and 3 in figures 3*A* and *B* are assumed to be granitic intrusions with magnetic susceptibilities[2] of 0.001. Body 2 was assumed to be either Precambrian basement or Tertiary or Cretaceous granitic rocks. The values of susceptibility used for this body are 0.0001 for figure 3*A* (T.G. Hildenbrand, U.S. Geological Survey, oral commun., 1984) and 0.001 for figure 3*B*.

The values of susceptibility that were used for the models are order-of-magnitude estimates that fall within the ranges of values for granitic and metamorphic rocks (Lindsley and others, 1966, p. 548). In addition, values used for bodies 1 and 3 provided fits within the vertical constraints described above. Figure 3 shows that order-of-magnitude changes in the susceptibility of body 2 do not greatly affect the configuration of either model. However, such changes cannot be made for bodies 1 and 3 without producing unreasonable models.

INTERPRETATION OF THE GEOLOGIC MODELS

The models discussed above and the geology mapped by Hose and Blake (1976) were used to construct a geologic section along line *A–A'* across the north part of the White River flow system (fig. 4). The section shows that the flow system is bounded on the west by a granitic intrusion that underlies the west side of the White Pine Range and on the east by a granitic intrusion that underlies the west side of the Egan Range and the east side of White River Valley. Between the intrusive bodies, a thick section of faulted upper Precambrian and Paleozoic sedimentary rocks overlies either Precambrian basement or a younger granitic intrusion. The long-dashed line in figure 4 is the base of the stratigraphic section, assuming (1) an approximate thickness of 40,000 ft and (2) no structural thinning or thickening caused by low-angle faults, folds, or regional tilting. This second assumption is unverified in the study area but is useful for comparing stratigraphic thickness to estimates of apparent thickness. The line above and the line below the long-dashed line are the modeled configurations for the upper surface of magnetic basement (body 2, fig. 3). The dotted line is the hypothetical surface of Precambrian basement, which is from 35,000 to 45,000 ft below land surface along the section. The deeper dashed-dotted line is a hypothetical granitic intrusion at a depth of about 45,000 ft.

---

[2] Magnetic susceptibility is a dimensionless quantity that differs in magnitude, depending on which system of units is used. The two systems of units conventionally used in geophysics are the meter-kilogram-second (SI) system and the centimeter-gram-second (CGS) system. Values of magnetic susceptibility used in this paper are based on the CGS system. For more details, see Sheriff (1980, p. 134–135 and 143).

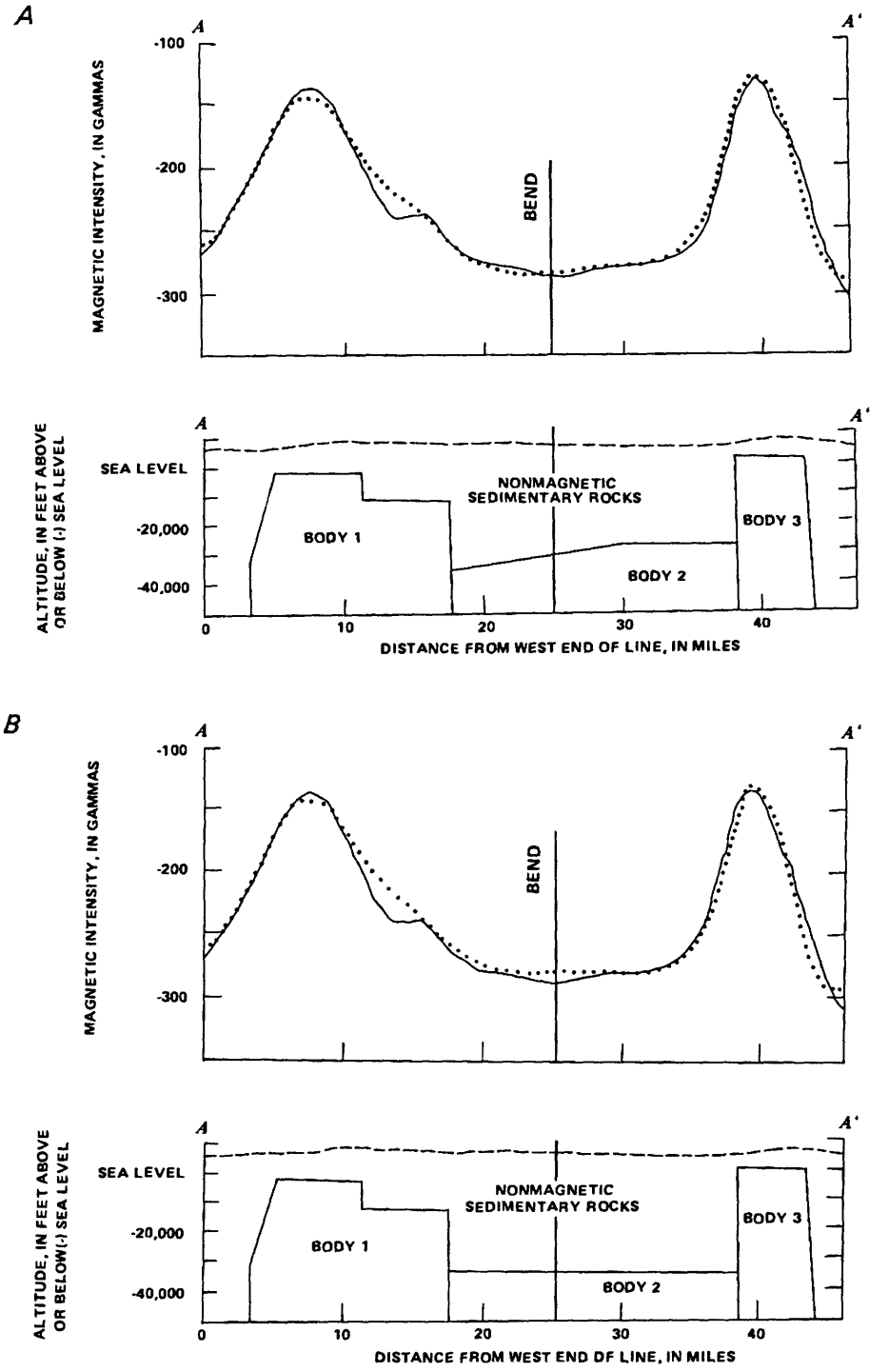

Figure 3. Comparison between measured and computed magnetic profiles for two models of subsurface geology along line *A–A'* (fig. 2). In models, dashed line is land surface; no vertical exaggeration. In magnetic profiles: solid line, measured; dotted line, computed from model. *A*, Magnetic susceptibilities 0.001 for bodies 1 and 3, 0.0001 for body 2. *B*, Magnetic susceptibility 0.001 for all bodies.

The stratigraphic section in figure 4 depicts several structural blocks bounded by high-angle faults. The positions of these faults at depth are considered diagrammatic because no proof exists that they extend to the depths shown. The fault offsets are inferred from the geologic map. Even with these limitations, however, the geologic section suggests a possible relationship between the modeled configuration of the hypothetical Precam-

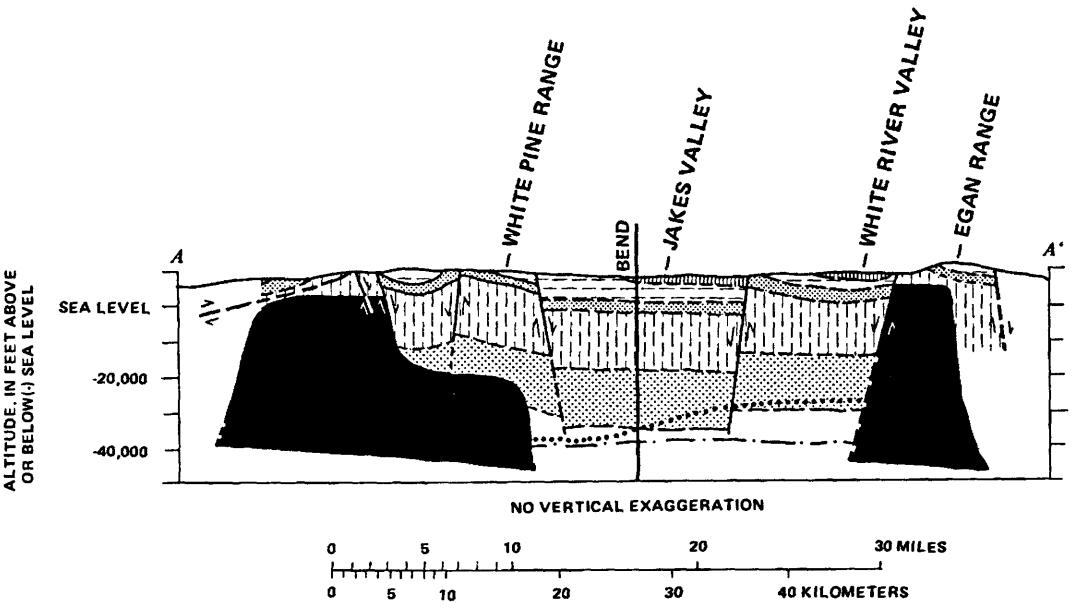

EXPLANATION

BASIN-FILL DEPOSITS--Poorly sorted to unsorted, unconsolidated to consolidated deposits that range in size from clay to boulders	QUATERNARY AND TERTIARY	CENOZOIC	
INTRUSIVE ROCKS--Monzonite and granodiorite	TERTIARY AND CRETACEOUS	CENOZOIC AND MESOZOIC	
CARBONATE ROCKS--Mostly limestone, but includes some sandstone and dolomite	PERMIAN AND PENNSYLVANIAN	PALEOZOIC	
CLASTIC ROCKS--Shale, sandstone, siltstone, claystone, and limestone	MISSISSIPPIAN AND DEVONIAN		
CARBONATE ROCKS--Mostly limestone and dolomite, but includes some sandstone and shale	DEVONIAN TO MIDDLE CAMBRIAN		
CLASTIC ROCKS--Mostly quartzite, sandstone, and shale	LOWER CAMBRIAN AND PRECAMBRIAN	PALEOZOIC AND PRECAMBRIAN	

CONTACT--Approximately located; short-dashed where uncertain; long-dashed at inferred base of Cambrian and Precambrian clastic rocks

TOP OF MAGNETIC BASEMENT--Dotted line is inferred top of Precambrian basement (fig. 3*A*). Dashed-dotted line is inferred top of Tertiary and Cretaceous granitic rocks (fig. 3*B*)

FAULT--Approximately located; dashed where inferred or uncertain. Arrows indicate relative movement

Figure 4. Geologic section along line *A*–*A'* (fig. 1) based on areal geology (Hose and Blake, 1976) and subsurface geologic models (fig. 3).

brian basement and the base (possibly faulted) of the upper Precambrian and Paleozoic section (long-dashed line). The gradual rise in the Precambrian basement surface from west to east, as shown in figure 4, may instead be an abrupt rise owing to fault offset. At these great depths, an abrupt offset of magnetic material, such as Precambrian basement, probably would be reflected as a gradual lateral change in the magnetic field.

The hypothetical Precambrian basement model (dotted line in figure 4) is considered to be the more realistic of the two models in figure 3, although, as stated earlier, either model is geologically reasonable. The Precambrian basement model indicates that the carbonate-rock aquifer in the northern part of the White River flow system may be as thick as 26,000 ft (stratigraphic thickness), and either model indicates that the aquifer is about 25 mi wide. This width contrasts with Eakin's (1966, p. 266) estimate of 15 mi for the flow system at the north end of White River Valley. The actual thickness of the aquifer probably is less than 26,000 ft because lowest parts of the carbonate rocks may not be permeable if fractures are not wide enough to store and transmit water.

HYDROGEOLOGIC IMPLICATIONS

This study has shown that carbonate-rock aquifer boundaries in part of the White River flow system consist of large granitic intrusions rather than ground-water divides that coincide with topographic divides between valleys. Interpretation of aeromagnetic data indicates that the aquifer width is about 25 mi, compared to the width of 15 mi estimated by Eakin (1966, p. 266). This difference in aquifer width would significantly change Eakin's estimate of transmissivity that he made for the flow system at the north end of White River Valley (30,000 ft^2/d). His estimate is based on a form of Darcy's Law:

$$Q = Tiw$$

where Q = underflow through the aquifer, in cubic feet per day;
T = transmissivity, in feet squared per day;
i = gradient of the potentiometric surface, in feet per foot; and
w = aquifer width, in feet.

Using Eakin's values for underflow and gradient and the value of flow-system width determined from this study, the estimate of T would be about 20,000 ft^2/d.

Interpretation of the data also suggests that stratigraphic thickness can be used for estimating possible aquifer thickness in this part of the White River flow system. The techniques used in this study are considered to have potential application for defining similar carbonate-rock aquifer boundaries elsewhere in the Great Basin. The ultimate test of this approach, however, must await the availability of deep borehole data in an area for which such aeromagnetic interpretations are made.

REFERENCES CITED

Allmendinger, R.W., Sharp, J.W., Von Tish, Douglas, Serpa, Laura, Brown, Larry, Kaufman, Sidney, Oliver, Jack, and Smith, R.B., 1983, Cenozoic and Mesozoic structure of the eastern Basin and Range province, Utah, from COCORP seismic-reflection data: Geology, v. 11, no. 9, p. 532–536.

Brokaw, A.L., Gott, G.B., Mabey, D.R., McCarthy, Howard, and Oda, Uteana, 1962, Mineralization associated with a magnetic anomaly in part of the Ely quadrangle, Nevada, *in* Geological Survey Research 1962: U.S. Geological Survey Professional Paper 450–E, p. E1–E10.

Carlson, J.E., and Mabey, D.R., 1963, Gravity and aeromagnetic maps of the Ely area, White Pine County, Nevada: U.S. Geological Survey Geophysical Investigations Map GP–392.

Drewes, Harald, 1967, Geology of the Connors Pass quadrangle, Schell Creek Range, east-central Nevada: U.S. Geological Survey Professional Paper 557, 93 p.

Eakin, T.E., 1966, A regional interbasin ground-water system in the White River area, southeastern Nevada: Water Resources Research, v. 2, no. 2, p. 251–271.

Gans, P.B., Miller, E.L., McCarthy, J., and Ouldcott, M.L., 1985, Tertiary extensional faulting and evolving ductile-brittle transition zones in the northern Snake Range and vicinity—new insights from seismic data: Geology, v. 13, no. 3, p. 189–193.

Hose, R.K., and Blake, M.C., Jr., 1976, Geology, *in* Geology and mineral resources of White Pine County, Nevada: Nevada Bureau of Mines and Geology Bulletin 85, Part I, p. 1–35.

Humphrey, F.L., 1960, Geology of the White Pine Mining District, White Pine County, Nevada: Nevada Bureau of Mines Bulletin 57, 119 p.

Lindsley, D.H., Andreasen, G.E., and Balsley, J.R., 1966, Magnetic properties of rocks and minerals, *in* Clark, S.P., Jr., ed., Handbook of physical constants: Geological Society of America Memoir 97, p. 543–552.

Moores, E.M., Scott, R.B., and Lumsden, W.W., 1968, Tertiary tectonics of the White Pine-Grant Range region, east-central Nevada and some regional implications: Geological Society of America Bulletin, v. 79, no. 12, p. 1703–1726.

Sheriff, R.E., 1980, Encyclopedic dictionary of exploration geophysics: Tulsa, Oklahoma, Society of Exploration Geophysicists, 266 p.

Stewart, J.H., 1980, Geology of Nevada: Nevada Bureau of Mines and Geology Special Publication 4, 136 p.

Stewart, J.H., and Carlson, J.E., compilers, 1978, Geologic map of Nevada: U.S. Geological Survey.

U.S. Geological Survey, 1976a, Aeromagnetic map for part of southwestern Ely 1° by 2° quadrangle, Nevada: U.S. Geological Survey Open-File Report 76–360.

———1976b, Aeromagnetic map for part of central Lund 1° by 2° quadrangle, Nevada: U.S. Geological Survey Open-File Report 76–361.
———1976c, Aeromagnetic map for part of northwestern Lund 1° by 2° quadrangle, Nevada: U.S. Geological Survey Open-File Report 76–362.
Vacquier, V., Steenland, N.C., Henderson, R.G., and Zietz, Isidore, 1951, Interpretation of aeromagnetic maps: Geological Society of America Memoir 47, 151 p.

Collection of Benthic Invertebrates by Drift Net and Dip Net, Little Boulder Creek, Idaho

By Keith V. Slack, Larry J. Tilley, *and* Susan S. Hahn

Abstract

The relative effectiveness of benthic invertebrate collection with drift nets and dip nets was tested in a meadow and in a canyon reach of a mountain stream. Ephemeroptera and Diptera, especially Chironomidae, were most abundant in all collections. The methods provided similar but not identical information on benthic community composition. At both sites the 24-hour drift-net collections contained 2.5 times the number of taxa that were in the dip-net collections. The number of taxa in pooled catches of two nighttime drift-net collections (each of 30-minute duration) or three daytime drift-net collections was the same or larger than the number of taxa collected by dip net. More than 96 percent of the 259 taxa collected during the study occurred in drift-net collections, whereas about 40 percent occurred in dip-net collections. Night drift-net collections contained the largest mean number of taxa per minute of sampling. Dip-net values for mean number of taxa per minute were intermediate between those for a single night and a single day of drift-net collection. We conclude that drift-net collections provided better samples of the benthic invertebrate community with less effort than did dip-net collections.

INTRODUCTION

Benthic invertebrates are the most widely used group of aquatic organisms for characterizing stream water quality (Hellawell, 1978). Besides their use as water-quality indicators, benthic invertebrates serve to characterize surface waters as habitats for aquatic life (Hynes, 1970; Hart and Fuller, 1974). Consequently, benthic invertebrates are commonly collected in reconnaissance, monitoring, and site investigations.

Recent developments in multivariate methods of data analysis and wide availability of computer programs for their use have increased the interpretive power of biological data (Gauch, 1982). However, commensurate improvements in sample acquisition have not occurred. Consequently, sampling continues to be the weak link in ecological studies involving species distribution and abundance.

The distribution of benthic invertebrates in streams is neither uniform nor random, so their quantitative collection is difficult (Elliott, 1977). This is especially true for rocky substrates on which unit area samplers are relatively ineffective. Collection of benthic invertebrates described by Greeson and others (1977) makes use of both active and passive methods. Active collection methods, such as the dip net or the Ponar grab, require the direct participation of the collector in sample acquisition. Passive collection methods, such as artificial substrates or drift nets, result in benthic invertebrate collection without the direct participation of the collector. Passive methods for benthic invertebrate collection require less onsite time, less operator training, and they produce samples with relatively smaller amounts of debris than do most active methods. Also, replicate collections are generally more consistent than are replicate streambed collections of benthic invertebrates (Chutter, 1975; Allan, 1982; Rosenberg and Resh, 1982), and they are less destructive of the natural habitat.

Of the two types of passive methods, drift, the collection of benthic invertebrates suspended in the water column, has some advantages over artificial substrate collection. Drift collections require exposure durations of less than an hour to several hours, whereas artificial substrate collections require exposure durations of days or weeks (Rosenberg and Resh, 1982). Thus, drift collection of benthic invertebrates can be made on a single visit to a site and no equipment remains in place between visits, in contrast to artificial substrate collections. Furthermore, drift-collection data are more clearly associated with related chemical quality and discharge data than are artificial substrate collection data. Reviews in the literature for invertebrate drift are given by Waters (1969, 1972), Bishop and Hynes (1969), Chaston (1972), and Müller (1974).

The downstream transport of benthic invertebrates in the water column has been known since biologists first anchored nets in streams (Needham, 1928). Later studies show that drift of benthic invertebrates occurs in streams from the arctic to the tropics (Müller, 1974; Hynes, 1975) and that drift density is affected by hydrologic, water quality, and biological factors. Large numbers of benthic

invertebrates are swept into the water column during floods (Anderson and Lehmkuhl, 1968), after ice breakup (Maciolek and Needham, 1951), and after spraying with insecticide (Coutant, 1964). Besides catastrophic sources of drift, a small proportion of the benthic invertebrate community is found in the drift under noncatastrophic conditions. Evidence in the literature (McLay, 1970; Elliott, 1971) indicates that individual drifting invertebrates travel only a few meters before they are returned to the streambed by turbulent flow, where their instinctive responses to seek contact with solid objects and to hide (Bishop and Hynes, 1969) cause them to reattach. However, not all drift results from accidental entrainment of the invertebrate in streamflow. Research on behavior of benthic invertebrate species has demonstrated active entry into the water column and return to the streambed by several species in response to biological and environmental stimuli (Walton, 1978, 1980).

Temporal variations in drift abundance and composition range from day-to-night (diel) to year-to-year differences. A prominent feature of noncatastrophic drift is its diel pattern in which the numbers of drifting invertebrates increase at night and decrease during the day. In the few reported instances of prolonged drift sampling, little change in density was found for periods of a week or more, even with a doubling of discharge (Chutter, 1975). Elliott (1967) found drift density to be fairly constant for the same month but not for different months.

The ease of collection, ubiquity, and relation of drift to the benthic community suggested collection of drifting invertebrates as an alternative to streambed sampling for benthic invertebrates (Waters, 1961; Besch, 1966; Larimore, 1974; Slack and others, 1976). These studies show that the species composition of drift samples is similar to that of samples of the benthos in the reach where both are collected, but the relative abundances are different because of differing tendencies of species to drift (Elliott, 1967; Lehmkuhl and Anderson, 1972; Turcotte and Harper, 1982). Because drift and benthos samples were similar in composition at different points in a drainage basin sampled by Elliott and Minshall (1968), they concluded that "in the absence of bottom samples, drift could be used as an index of species composition."

The present study compared an active and a passive method for benthic invertebrate collection in two major habitats of a mountain stream. Both methods collect from many different microhabitats, and the relative effectivenss of each method in collection of benthic invertebrate taxa was determined. The study was carried out over a 2-day period in summer.

We thank W.C. Emmett and M.C. Sanguinneti for generous assistance with drift-net collection and S.F. Muzzio for help with invertebrate identification.

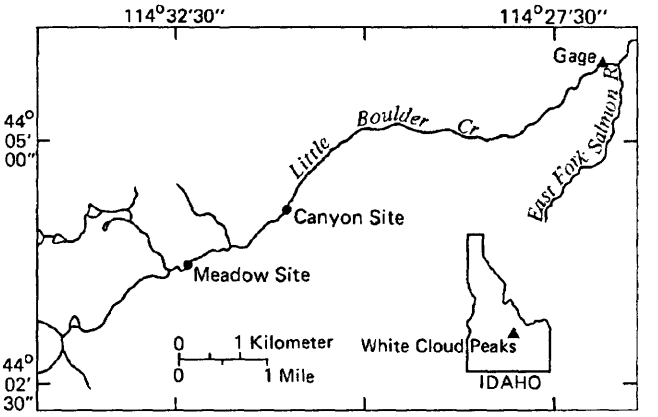

Figure 1. Location of Little Boulder Creek, Idaho, showing the setting of the meadow and canyon study reaches.

DESCRIPTION OF STUDY SITE

Two third-order reaches of Little Boulder Creek were sampled (fig. 1). Little Boulder Creek flows eastward from the White Cloud Peaks into the East Fork Salmon River, Custer County, south-central Idaho. The higher elevation site was at the downstream end of a meadow at an elevation of 2,466 m and an average channel gradient of 12 m/km. The lower elevation site was in a forested canyon, 2.5 stream km downstream from the meadow, at an elevation of 2,362 m and an average channel gradient of 43 m/km. The area is shown on the U.S. Geological Survey 1:24,000-scale topographic map for the Boulder Chain Lakes quadrangle. Emmett (1975) gives additional information on the East Fork Salmon River and its tributaries.

METHODS OF STUDY

Environmental Factors

Stream discharge was measured at the meadow as described by Buchanan and Somers (1969). Because there was no water diversion and only negligible tributary flow between the meadow and the canyon sites, discharge was assumed to be the same at both sites.

The 24-hour study period, July 12–13, 1977, was divided into a 14-hour light and a 10-hour dark period. "Day" was the period from 0700 to 2000 hours mountain daylight time, whereas "night" was the period from 2100 to 0600 hours. Cumulonimbus clouds obscured the sun toward evening of July 12, producing a prolonged twilight.

Biological Collection and Sample Processing

Thirty-minute drift-net samples were collected at each site, beginning on the hour, between 1800 hours

July 12 and 1700 hours, July 13. Nets were made of Nitex nylon, 216 μm mesh opening, mounted on 25×25 cm aluminum frames. The ratio of open area of netting to the area of the drift net mouth was 4:1. A digital flow meter (General Oceanics model 2030) mounted in the mouth of each net measured the volume filtered. One net was installed in the center of flow at each site on vertical rods driven into the bed. The lower edge of the net frame rested on the streambed, and the upper edge was below the water surface. No clogging or back flow from the nets was observed. The meadow net filtered an average of 46.8 ± 2.2 m^3 (mean ± standard deviation) of water per 30-minute collection compared to 29.6 ± 1.2 m^3 for the canyon net. These volumes were 7.0 and 4.4 percent, respectively, of the stream discharge of 0.37 m^3/s (W.W. Emmett, oral commun., July 1977). Drift data, when corrected for volume filtered, are expressed as density, defined as numbers of individuals or taxa per cubic meter.

The dip net was selected as the active collection method for benthic invertebrates because it could be used in the boulder bed of the canyon reach as well as in the gravel bed of the meadow reach. Unit area samplers could not be used effectively in the canyon because of the large size of the streambed rocks. Benthic invertebrates were collected for 45 minutes with a D-shaped dip net (210 μm mesh opening) from the major aquatic habitats at each site (Slack and others, 1976). The sampling effort for each habitat was approximately in proportion to the amount of that habitat at the site. Dip-net samples were collected in the afternoon of July 14 after drift-net collection was completed. The benthic invertebrate samples were preserved in 70 percent ethanol.

In the laboratory, invertebrates were sorted from debris by sugar flotation (Anderson, 1959), and the residue larger than 210 μm was searched with a dissecting microscope to recover invertebrates missed. Aquatic Insecta and Acari, the numerically dominant groups, were identified or discriminated to the lowest practical taxa by use of available references. A few immature insects could be assigned only to family or order, and some Chironomidae larvae were placed in "species groups" when further subdivision was not possible. Uncommon groups were identified to class or order. Terrestrial invertebrates and adult aquatic Insecta other than Coleoptera were not included in the analysis. Although several taxonomic entities, termed "taxa," were used, the treatment was uniform throughout and, we believe, justifies cautious intercollection comparisons.

Diversity of the collections is expressed by using Brillouin's (1962) index, where

$$H=\frac{1}{N}\log\frac{N!}{N_1!\,N_2!\cdots N_s!} \qquad (1)$$

in which H is the diversity index, N is the total number of individuals, N_1, N_2 ... are the number of individuals of species 1, 2 ..., and s is the total number of species. Factorials were computed, not estimated (Kaesler and Herricks, 1976).

The evenness component of diversity is expressed as relative evenness, e (Zand, 1976), which ranges from 0 for the least even sample to 1 for the most even sample. It is the ratio

$$e=\frac{H-H_{min}}{H_{max}-H_{min}} \qquad (2)$$

in which H_{max} and H_{min} are given by

$$H_{max}=\frac{1}{N}\log_2\frac{N!}{\{(m+1)!\}^r\,(m!)^{s-r}} \qquad (3)$$

where m and r are the quotient and remainder, respectively, of N/s; that is, $N = ms + r$ and $r < s$ (Pielou, 1975; Zand, 1976), and

$$H_{min}=\frac{1}{N}\log_2\frac{N!}{(N-s+1)!}\cdot \qquad (4)$$

RESULTS OF STUDY

Composition of the Collections

Immature aquatic Insecta were numerically dominant in all collections, and the greatest numbers of individuals belonged to the orders Ephemeroptera and Diptera, especially the dipteran family Chironomidae (table 1). Chironomids were relatively more abundant in the canyon than in the meadow (probability <0.01, Mann-Whitney test, Zar, 1974). Copepoda were abundant in the meadow daytime drift-net collections, common in nighttime drift-net collections, but rare in dip-net collections at both sites and in the canyon drift-net collections (table 1). Because most onsite work is done during the day, it is of interest to compare the composition of dip-net collections with that of day drift-net collections. In the meadow, the percentage of Insecta in the dip-net collections was larger than in the day drift-net collections (table 1). Simuliidae, Ephemeroptera, Plecoptera, and Coleoptera were relatively more abundant in the meadow dip-net collections than in the day drift-net collections. The percentages of Insecta were the same in canyon dip-net and drift-net collections, although there were differences in abundances of some groups. Plecoptera, Simuliidae (Diptera), and Coleoptera were relatively more abundant in the canyon dip-net collections than in the day drift-net collections. Chironomidae were equally abundant in dip-net and day drift-net collections.

Table 1. Comparison between drift-net and dip-net collections from meadow and canyon reaches, Little Boulder Creek, Idaho

[The 2-, 3-, and 24-hour drift collections are pooled results from successive 30-minute collections; day and night drift periods were selected to avoid dawn and dusk; n.a., not applicable]

	Meadow								Canyon							
	Day drift-net collection times (hours)			Night drift-net collection times (hours)			Total 24-hour drift	Dip net	Day drift-net collection times (hours)			Night drift-net collection times (hours)			Total 24-hour drift	Dip net
	0800	0800,0900	0800-1000	2200	2200,2300	2200-2400			0800	0800,0900	0800-1000	2200	2200,2300	2200-2400		
Relative abundance (percent)																
Insecta (total)	(59.2)	(58.5)	(61.2)	(94.1)	(93.3)	(92.5)	(83.1)	(94.5)	(96.7)	(96.1)	(96.4)	(98.2)	(98.2)	(98.0)	(95.6)	(95.4)
Ephemeroptera	25.1	27.6	27.6	53.5	50.3	50.5	41.2	52.0	21.4	24.1	22.0	54.0	47.4	44.3	29.4	20.3
Diptera (total)	(27.4)	(25.6)	(28.4)	(35.5)	(37.7)	(36.9)	(37.3)	(27.9)	(69.9)	(67.6)	(70.1)	(38.8)	(45.4)	(48.7)	(61.8)	(64.8)
Chironomidae	22.9	21.1	22.9	24.6	25.2	25.0	29.7	17.7	62.5	61.0	63.3	30.2	35.4	37.6	53.0	63.7
Simuliidae	4.3	4.0	5.3	10.8	12.5	11.6	7.2	9.1	(7.5)	6.6	6.8	8.6	10.0	11.0	8.7	.6
Plecoptera	.7	.7	.7	3.7	3.8	3.7	1.9	5.1	2.8	1.9	1.9	2.4	2.3	2.1	1.7	5.6
Trichoptera	2.9	2.8	2.7	.4	.8	.6	1.4	1.9	2.3	2.3	2.0	2.6	2.7	2.6	2.3	3.2
Coleoptera	2.5	1.4	1.2	1.0	.7	.6	1.0	7.4	0	0	.1	0	.1	.1	.2	1.5
Collembola	.7	.7	.6	0	.1	.1	.3	.1	.2	.2	.2	.3	.2	.2	.2	0
Acari	5.8	8.1	7.5	2.1	2.5	2.2	4.7	4.0	2.8	3.6	3.2	1.3	1.4	1.4	3.4	4.2
Crustacea (total)	(35.0)	(33.4)	(30.4)	(3.8)	(4.0)	(5.3)	(12.1)	(0.9)	(0.2)	(0.2)	(0.2)	(0.5)	(0.4)	(0.5)	(0.8)	(0.2)
Ostracoda	1.8	1.2	1.4	.4	.4	.5	.8	.7	.2	.2	.2	.5	.3	.4	.6	.2
Copepoda	33.2	31.6	29.0	3.4	3.6	4.7	11.3	.2	0	0	0	0	.1	.2	.3	0
Other	0	0	0	0	.1	.1	.1	.6	.2	.1	.2	0	0	0	.1	.2
Collection Data																
Number of taxa	47	75	79	57	84	102	193	79	43	59	75	55	81	93	179	73
Taxa per cubic meter	1.0	.8	.6	1.2	.9	.7	.2	n.a.	1.4	1.0	.8	1.9	1.4	1.0	.3	n.a.
Taxa per 100 individuals	10.5	6.5	5.1	5.6	3.6	2.9	1.2	2.8	10.0	5.4	5.0	4.6	3.9	3.0	1.1	4.1
Taxa per minute of sampling effort	1.6	1.2	.9	1.9	1.4	1.1	.27	1.8	1.4	1.0	.8	1.8	1.4	1.0	.25	1.6
Number of individuals	446	1,161	1,534	1,017	2,314	3,480	16,403	2,778	429	1,102	1,464	1,198	2,086	3,073	16,252	1,777
Individuals per cubic meter	9.5	12.4	10.9	21.7	24.7	24.8	14.6	n.a.	14.5	18.6	16.5	40.5	35.2	34.6	22.9	n.a.
Individuals per minute of sampling effort	14.9	19.4	17.0	33.9	38.6	38.7	22.8	62.0	14.3	18.4	16.3	39.9	34.8	34.1	22.6	39.5
Diversity index	3.88	4.07	4.27	4.00	4.48	4.53	4.82	4.60	3.88	3.87	3.87	4.04	4.22	4.20	4.26	4.32
Evenness index	.68	.64	.67	.68	.70	.67	.63	.73	.71	.64	.60	.69	.66	.63	.57	.69

The co-occurrence of the most abundant taxa in the dip-net and drift-net collections at each site was examined by ranking the taxa by their abundances. More than 97 percent of the individuals were in the 10 most abundant taxa in each type of collection. The same 5 taxa were among the 10 most abundant taxa in both collection types at each site. Thirteen taxa in the meadow and 12 taxa in the canyon of the 20 most abundant taxa, accounting for 99 percent of the individuals, occurred in both types of collections at each site. Thus the two methods of benthic invertebrate collection provided similar but not identical information on benthic community composition in the study reaches.

Number of Taxa and Individuals

The composition of single and pooled catches for day and night drift-net collections and the 24-hour mean drift was compared with that of the dip-net collections (table 1). At both sites, the 24-hour drift-net collections caught 2.5 times the number of taxa in the dip-net collections. The number of taxa in the pooled catches of two night drift-net collections (each of 30 minutes duration) or three day drift-net collections was the same or larger than the number of taxa collected by dip net. The diversity of night drift-net collections was larger than that of day drift-net collections and was similar to dip-net values. Night drift-net collections contained significantly larger numbers of taxa and individuals than day collections (probability <0.01). Figure 2 shows that with the onset of darkness the numbers of drift taxa and individuals simultaneously increased above the 24-hour mean values and decreased at dawn below the 24-hour means with only occasional reversals during the day.

Sampling Efficiency

The efficiency of drift- and dip-net sampling for collecting taxa was examined by comparing the number of taxa caught by each method with the number caught by both methods (table 1). Two hundred and fifty-nine taxa were collected at both sites by both methods, 193 in the meadow, and 179 in the canyon. More than 96 percent of the collected taxa occurred in drift-net collections, whereas 40 percent or less occurred in dip-net collections. About half of the total taxa in drift-net collections at both sites were caught in the first three postdusk collections. Comparable day drift-net values required four postdawn collections. However, nearly 65 percent of the 24-hour total number of taxa was obtained at both sites by pooling three daytime and three night drift-net collections.

The number of taxa, or individuals per collection, divided by the sampling duration gives an estimate of

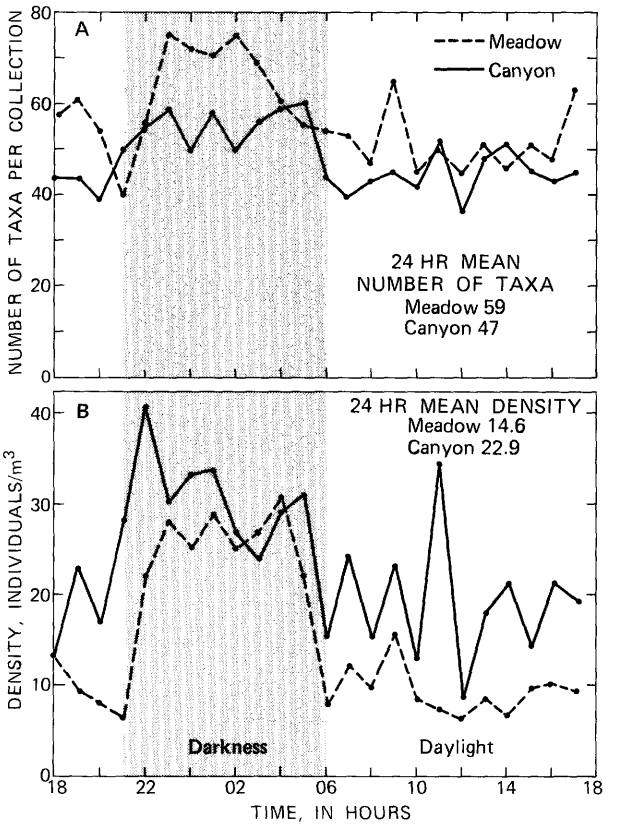

Figure 2. The number of taxa per 30-minute collection *(A)* and the density of individuals per cubic meter *(B)* in drift-net collections of benthic invertebrates, Little Boulder Creek, Idaho, July 12–13, 1977.

effectiveness per minute of sampling. Night drift-net collections contained the largest mean number of taxa per minute of all methods, and it was among the most efficient methods for catching individuals (table 1). The dip-net values for mean number of taxa per sampling effort were intermediate between those for a single day and a single night drift-net collection.

DISCUSSION

Biological methods for water-quality evaluation based on benthic invertebrate community structure require consistent collection of a variety of invertebrate species having different responses to stress. Drift sampling fulfills these requirements (Coutant, 1964; Besch, 1966; Wojtalik and Waters, 1970; Larimore, 1974; Hall and others, 1982). Although many species collected in the drift nets in Little Boulder Creek exhibited day-night differences in abundances, the diel variability did not prevent collection of adequate samples of benthic invertebrates at any time. Pooled collections of any two of the nighttime or three of the daytime 30-minute drift-net

samples contained the same or larger numbers of taxa as did the dip-net collections, which attempted to include all of the aquatic habitats.

The most likely explanation for the larger number of taxa collected by the drift nets compared to the dip nets is the differences in their sample sizes. Large biological collections (large numbers of individuals) include more rare species than do small collections (Hulbert, 1971). Moreover, a wider spectrum of microhabitat sources probably contributed to the drift-net collections than could be recognized and sampled by dip net. Thus the drift nets composited invertebrates from many sources into more comprehensive samples of the benthic fauna than could be obtained with the dip nets. Furthermore, the drift-net collections accumulated without attention while other onsite activities were carried out.

We conclude that the drift-net collections provided better samples of the benthic invertebrate community in each study reach with less effort than did the dip-net collections. However, several sources of variability in composition of the benthic invertebrate collections were evident. These were differences between sites for a given collection method, differences within sites for different collection methods, and differences between day and night drift-net collection. Night appears to be the optimum time for drift collection if study objectives require maximum number of taxa per unit sampling effort. As with other biological methods (Green, 1979), consistency in drift-net collection is essential if the results are to be compared between collection sites or times.

REFERENCES CITED

Allan, J.D., 1982, The effects of reduction in trout density on the inverte brate community of a mountain stream: Ecology, v. 63, p. 1444–1455.

Anderson, N.H., and Lehmkuhl, D.M., 1968, Catastrophic drift of insects in a woodland stream: Ecology, v. 49, p. 198–206.

Anderson, R.O., 1959, A modified flotation technique for sorting bottom fauna samples: Limnology and Oceanography, v. 4, p. 223–225.

Besch, W., 1966, Driftnetzemthode und biologische Fliesswaseruntersuchung: Verhandlungen Internationalen Vereinigung Limnologie, v. 16, p. 669–678.

Bishop, J.E., and Hynes, H.B.N., 1969, Downstream drift of the invertebrate fauna in a stream ecosystem: Archiv für Hydrobiologie, v. 66, p. 56–90.

Brillouin, L., 1962, Science and information theory (2d ed.): New York, Academic Press, 347 p.

Buchanan, T.J., and Somers, W.P., 1969, Discharge measurements at gaging stations: U.S. Geological Survey Techniques of Water-Resources Investigations, Book 3, Chapter A8, 65 p.

Chaston, I., 1972, Non-catastrophic invertebrate drift in lotic system, *in* Clark, R.B., and Wootton, R.J., eds., Essays in Hydrobiology: Exeter, University of Exeter, p. 33–51.

Chutter, F.M., 1975, Variation in the day-time drift of a Natal river: Verhandlungen Internationalen Vereinigung Limnologie, v. 19, p. 1728–1735.

Coutant, C.C., 1964, Insecticide Sevin: Effects of aerial spraying on drift of stream insects: Science, v. 146, p. 420–421.

Elliott, J.M., 1967, Invertebrate drift in a Dartmoor stream: Archiv für Hydrobiologie, v. 63, p. 202–237.

———1971, the distances travelled by drifting invertebrates in a Lake District stream: Oecologia (Berlin), v. 6, p. 350–379.

———1977, Some methods for the statistical analysis of benthic invertebrates: Freshwater Biological Association Scientific Publication 25, 160 p.

Elliott, J.M., and Minshall, G.W., 1968, The invertebrate drift in the River Duddon, English Lake District: Oikos, v. 19, p. 39–52.

Emmett, W.W., 1975, The channels and waters of the Upper Salmon River Area, Idaho: U.S. Geological Survey Professional Paper 870–A, 166 p.

Gauch, H.G., Jr., 1982, Multivariate analysis in community ecology: Cambridge, Cambridge University Press, 298 p.

Green, R.H., 1979, Sampling design and statistical methods for environmental biologists: New York, John Wiley & Sons 257 p.

Greeson, P.E., Ehlke, T.A., Irwin, G.A., Luim, B.W., and Slack, K.V., (eds.), 1977, Methods for collection and analysis of aquatic biological samples: U.S. Geological Survey Techniques of Water-Resources Investigations, Book 5, Chapter A4, 332 p.

Hall, R.J., Pratt, J.M., and Likens, G.E., 1982, Effects of experimental acidification on macroinvertebrate drift diversity in a mountain stream: Water, Air, and Soil Pollution, v. 18, p. 273–287.

Hart, C.W., Jr., and Fuller, S.L.H., 1974, Pollution ecology of freshwater invertebrates: New York, Academic Press, 389 p.

Hellawell, J.M., 1978, Biological surveillance of rivers: Water Research Centre, Stevenage, England, 332 p.

Hulbert, S.H., 1971, The nonconcept of species diversity: A critique and alternative parameters: Ecology, v. 52, p. 577–586.

Hynes, H.B.N., 1970, The ecology of running waters: Toronto, University of Toronto Press, 555 p.

Hynes, J.D., 1975, Downstream drift of invertebrates in a river in southern Ghana: Freshwater Biology, v. 5, p. 515–532.

Kaesler, R.L., and Herricks, E.E., 1976, Analysis of data from biological surveys of streams: Diversity sample size: Water Resources Bulletin, v. 12, p. 125–135.

Larimore, R.W., 1974, Stream drift as an indication of water quality: American Fisheries Society Transactions, v. 103, p. 507–517.

Lehmkuhl, D.M., and Anderson, N.H., 1972, Microdistribution and density as factors affecting the downstream drift of mayflies: Ecology, v. 53, p. 661–667.

Maciolek, J.A., and Needham, P.R., 1951, Ecological effects of winter conditions on trout and trout foods in Convict Creek, California, 1951: American Fisheries Society Transactions, v. 81, p. 202–217.

McLay, Colin, 1970, A theory concerning the distance travelled by animals entering the drift of a stream: Fisheries

Research Board Canada Journal, v. 27, p. 359–370.
Müller, Karl, 1974, Stream drift as a chronobiological phenomenon in running water ecosystems: Annual Review of Ecology and Systematics, v. 5, p. 309–323.
Needham, P.R., 1928, A net for the capture of stream drift organisms: Ecology, v. 9, p. 339–342.
Pielou, E.C., 1975, Ecological diversity: New York, John Wiley & Sons, 165 p.
Rosenberg, D.M., and Resh, V.H., 1982, The use of artificial substrates in the study of freshwater benthic macroinvertebrates, *in* Cairns, John, Jr., ed., Artificial substrates: Ann Arbor, Mich., Ann Arbor Science Publication, p. 175–235.
Slack, K.V., Nauman, J.W., and Tilley, L.J., 1976, Evaluation of three collecting methods for a reconnaissance of stream benthic invertebrates: U.S. Geological Survey Journal of Research, v. 4, p. 491–495.
Turcotte, P., and Harper, P.P., 1982, Drift patterns in a high Andean stream: Hydrobiologia, v. 89, p. 141–151.
Walton, O.E., Jr., 1978, Substrate attachment by drifting aquatic insect larvae: Ecology v. 59, p. 1023–1030.
———1980, Active entry of stream benthic macroinvertebrates into the water column: Hydrobiologia, v. 74, p. 129–139.
Waters, T.F., 1961, Standing crop and drift of stream bottom organisms: Ecology, v. 42, p. 532–537.
———1969, Invertebrate drift-ecology and significance to stream fishes, *in* Northcote, T.G., ed., Symposium on salmon and trout in streams: Vancouver, University of British Columbia, MacMillan Lectures in Fisheries, p. 121–134.
———1972, The drift of stream insects: Annual Review of Entomology, v. 17, p. 253–272.
Wojtalik, T.A., and Waters, T.F., 1970, Some effects of heated water on the drift of two species of stream invertebrates: American Fisheries Society Transactions, v. 99, p. 782–788.
Zand, S.M., 1976, Indexes associated with information theory in water quality: Water Pollution Control Federation Journal, v. 48, p. 2026–2031.
Zar, J.H., 1974, Biostatistical analysis: Englewood Cliffs, New Jersey, Prentice-Hall, 620 p.

Dual-Acidity Titration Curves—Fingerprint, Indicator of Redox State, and Estimator of Iron and Aluminum Content of Acid Mine Drainage and Related Waters

By Arthur N. Ott

Abstract

Titration curves constructed from data obtained from the determination of dual acidities of acid mine drainage samples can be used to estimate a sample's redox state as well as its dissolved ferrous iron, ferric iron, and aluminum content. A nonlinear regression equation with a correlation coefficient of 0.98 was determined for the relation between the titratable acidity to pH 4.0 and the concentration of oxidized iron. A linear regression equation with a correlation coefficient of 0.99 was derived for the relation between the titratable acidity for the hydrogen-peroxide-treated sample from pH 4.0 to 5.0 and the concentration of aluminum. The dual titration curves constitute a characteristic shape, or "fingerprint," for the acid mine drainage sample that should not change—except to contract or elongate, depending on sample dilution—unless a geochemical change occurs to alter the metal proportions.

INTRODUCTION

The acidity of acid mine drainage (AMD) is normally considered only in the context of its total acid concentration. It is, therefore, a value used primarily for comparing the acid strength between AMD samples. Acidity can also be considered as a property of a solution that can be characterized by a titration curve. According to Brown and others (1970) "the construction of a titration curve permits . . . a more reliable understanding of the reactions taking place during the neutralization." In addition, Rainwater and Thatcher (1960) conclude that the concentration of a specific acid compound can be determined by titration with a base to a practical end point. However, this end point differs with the acid compound and makes it impossible to determine the acid concentrations of mixtures of hydrolyzable salts by titration to a single predetermined end point.

The purpose of this report is to describe the use of dual-acidity titration curves and evaluate a technique for identifying and estimating the concentration of dissolved ferrous iron, ferric iron, and aluminum by using different end points in an acidity titration curve produced for AMD and related waters. These waters were collected within the Eastern Coal Province, an area of coal deposits extending from northern Pennsylvania southwestward to central Alabama (fig. 1).

METHODS OF STUDY

Initially, water samples were collected periodically from March 1981 to March 1983 from coal mine shafts and their receiving streams in north-central Pennsylvania (table 1) for a study conducted by Ott (1986).

Acidity titration curves were produced for these samples under temperature-controlled laboratory conditions. Metal concentrations were determined for each acidity titration performed and were correlated to the acid concentration of their respective hydrolyzable salts. Ferrous iron was originally believed to be absent or in low concentration in the AMD sampled, since initial ferrous iron concentrations were found to be 1.5 mg/L or less. This was in line with the general conclusions of previous investigators (L.A. Reed, and J.R. Ward, U.S. Geological Survey, oral commun., 1981). Acidities were therefore not determined on samples oxidized with H_2O_2 (hydrogen peroxide). This omission could be the major reason for the occasional occurrence of poor prediction of iron concentration in samples. The regression equations derived from the correlations of the iron and aluminum concentrations to their respective acidities did, however, allow for reasonable metal estimates to be predicted from field titration data derived from previous studies by Ward (1976) and Reed (1980) for AMD samples collected from the same area in north-central Pennsylvania.

Samples from streams and ground waters affected by AMD were collected in the spring of 1984 from Kentucky, Maryland, Ohio, western Pennsylvania, and West Virginia to test the utility of the technique on water

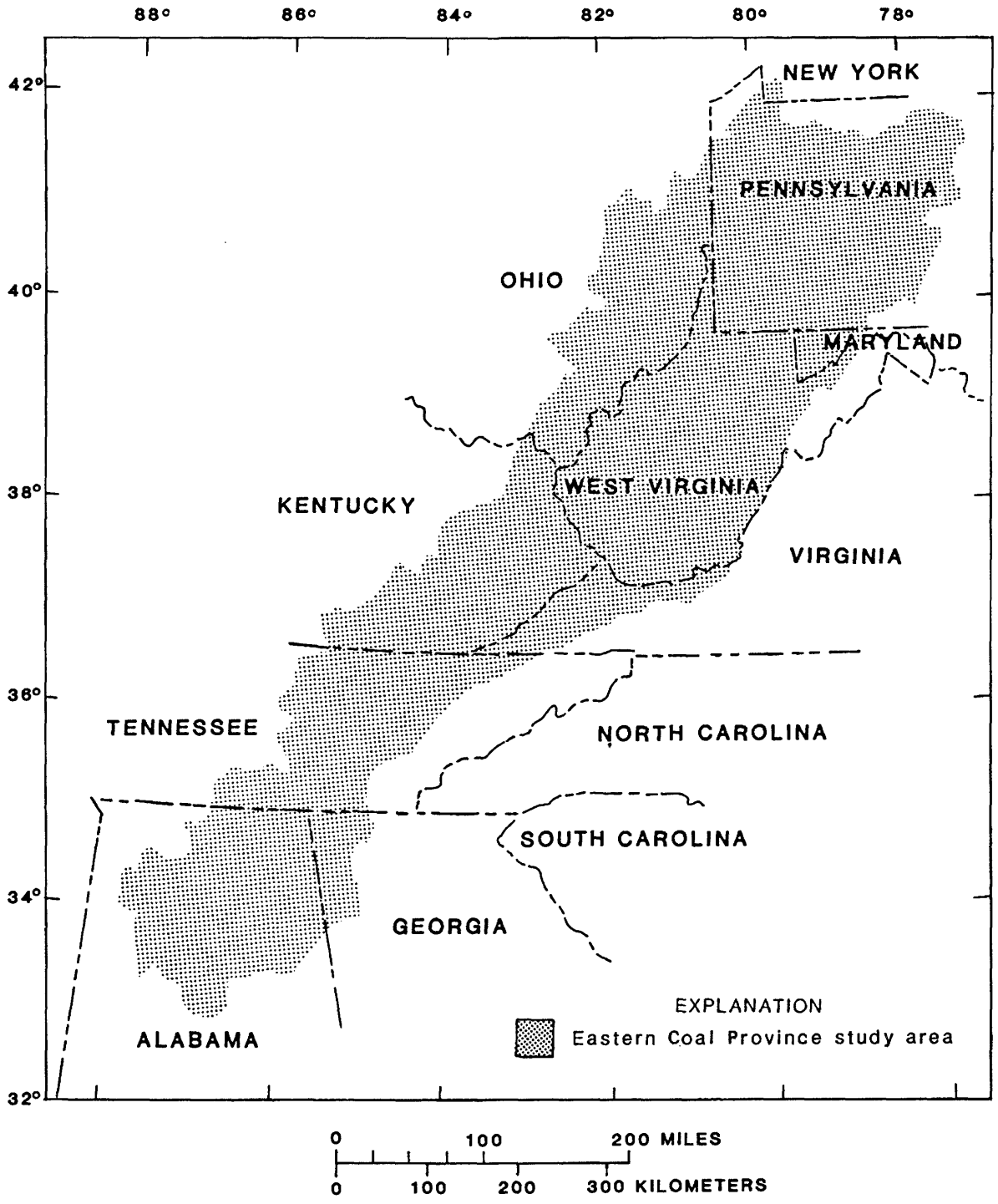

Figure 1. Eastern Coal Province study area.

that contained ferrous iron and originated in areas other than north-central Pennsylvania (table 2). The Pennsylvania samples are ground waters, whereas all other samples are from streams. A combination of high streamflow, which diluted the AMD, and limestone streams whose number increase in a southerly direction caused streams designated to be sampled in Georgia, Tennessee, and Virginia to be above pH 5.0 and therefore not appropriate for use in this study.

LABORATORY PROCEDURES

Samples collected in the field were shipped chilled to the laboratory and then refrigerated until analysis.

Table 1. Sampling site locations for samples collected in north-central Pennsylvania

Site name	Station number	Latitude	Longitude
Mine-discharge sites			
Mitchel No. 2, near Antrim.....	01548413	41°37'43"	77°18'12"
Anna S No. 1, near Antrim.....	01548416	41°37'26"	77°18'07"
Hunter Drift, near Antrim	01548418	41°37'05"	77°18'40"
Stream sites			
Bridge Run, near Antrim.....	01548415	41°37'32"	77°17'43"
Basswood Run, near Antrim.....	01548421	41°36'50"	77°17'38"
Wilson Creek, at Morris	01548423	41°35'51"	77°17'50"
Morris Run, near Blossburg.....	01516256	41°39'47"	77°02'23"
Coal Creek, at Blossburg.....	01516260	41°40'17"	77°03'41"
Bear Creek, at Blossburg.....	01516267	41°41'00"	77°03'53"

Table 2. Sampling site locations for samples collected in Kentucky, Maryland, Ohio, western Pennsylvania, and West Virginia

Site	Station number	Latitude	Longitude
Kentucky			
Flat Creek, near Madisonville ...	03321050	37°15'11"	87°26'50"
Lick Creek, near Rabbit Ridge ..	03384035	37°18'15"	87°24'58"
Maryland			
Abrams Creek, near Mount Storm	01595275	39°18'45"	79°12'43"
Laurel Run, near Wilson.....	01594930	39°14'38"	79°25'41"
Mill Run, near Morrison.....	01598980	39°31'03"	79°25'41"
Three Forks Run, at Vindex	01595550	39°24'53"	79°10'55"
Ohio			
Sandy Run, near Lake Hope	03201600	39°21'45"	82°18'47"
Yost Run, near Nelsonville	03201535	39°25'34"	82°18'37"
Western Pennsylvania			
Control Well no. 1	410950079253411	41°09'50"	79°25'34"
Control Well TH no. 2	410948076253711	41°09'48"	76°25'37"
Main drain	410945079252801	41°09'45"	79°25'28"
Seep 2.....	410939079254701	41°09'39"	79°25'47"
Seep 2A	410939079254702	41°09'39"	79°25'47"
TR2 Well no. 1.....	410951079253211	41°09'51"	79°25'32"
Well T	410945079253211	41°09'45"	79°25'32"
Well U	410947079253213	41°09'47"	79°25'32"
Well 4K	410951079253011	41°09'51"	79°25'30"
Well 7K	410945079252712	41°09'45"	79°25'27"
Well 11K	410948079252911	41°09'48"	79°25'29"
West Virginia			
Canyon Creek, at Canyon	—	39°40'35"	79°53'46"
Conner Run, near Valley Point ..	03070310	39°34'18"	79°40'39"
Dents Run, near Laurel Point ...	—	39°37'59"	80°02'45"
Glade Run, near Valley Point ...	—	39°34'37"	79°39'48"
Sovern Run, near Valley Point...	—	38°37'14"	79°42'17"
West Run, near Morgantown....	—	39°39'09"	79°54'52"

Acidities were performed in the laboratory on whole water samples. Sample aliquots for metal analyses were taken each time an acidity was performed, filtered through a 0.45-μ filter, and acidified with concentrated nitric acid to pH less than 2. Initially, a single acidity titration was performed for each untreated sample. The titration was performed on an untreated sample warmed to 23° to 25°C in a water bath. During the latter part of the study a second titration was performed on a subsample treated with 5 to 10 drops of 30 percent H_2O_2, heated to boiling, and immediately cooled to 23° to 25°C. Sample aliquots of 25 or 50 mL were titrated with standard NaOH (sodium hydroxide) to pH 8.3. Samples were magnetically stirred. A Beckman Altex 71 pH meter with temperature compensation and a Beckman combination glass electrode no. 531013 were used in the titrations.

The instrument was calibrated with pH 4.0 and pH 7.0 buffers at least once daily and occasionally checked with pH 9.18 buffer. Because calibration was with two standards, the instrument automatically computed slope (corrected for temperature) and corrected offset. To obtain consistent results and eliminate operator "judgment," the "Auto Read" function of the pH meter was used. The pH reading in this mode is locked on digital display when the pH readings change by no more than ± 0.004 pH in 10 seconds. Titrant increments were generally on the order of 0.25 mL. Laboratory analyses of iron and aluminum were performed according to procedures described by Skougstad and others (1979).

TITRATION CURVE CHARACTERISTICS

Buffer Zones

Examples of single-acidity titration curves for untreated samples representative of AMD or streams affected by AMD are presented in figure 2. Although the acidity and ionic concentrations for the samples differ, all curves show the same characteristic two-tier buffer zone below pH 6.0. Salotto and others (1967) showed these same characteristic buffer zones when titrating the acidity of 0.02N sulfuric acid solutions containing ferric iron and aluminum salts. Buffering below pH 4.0 occurred with the ferric iron salt solution and between pH 4.0 and 5.0 with the aluminum salt solution. Similar titration curves were obtained by Payne and Yeates (1970) for titrations of ferrous iron in sulfuric acid and ferric iron in sulfuric acid after both solutions had been subjected to oxidation with a 3 percent H_2O_2 solution.

The titration characteristics below pH 5.0 for AMD samples appear to be due to the neutralization of free acid

$$2NaOH + H_2SO_4 \rightarrow Na_2SO_4 + 2H_2O$$

and the subsequent hydrolysis of ferric and aluminum sulfates, which produce additional free acid

$$Fe_2(SO_4)_3 + 6H_2O \rightarrow 2Fe(OH)_3 + 3H_2SO_4$$

$$Al_2(SO_4)_3 + 6H_2O \rightarrow 2Al(OH)_3 + 3H_2SO_4$$

and create the buffering.

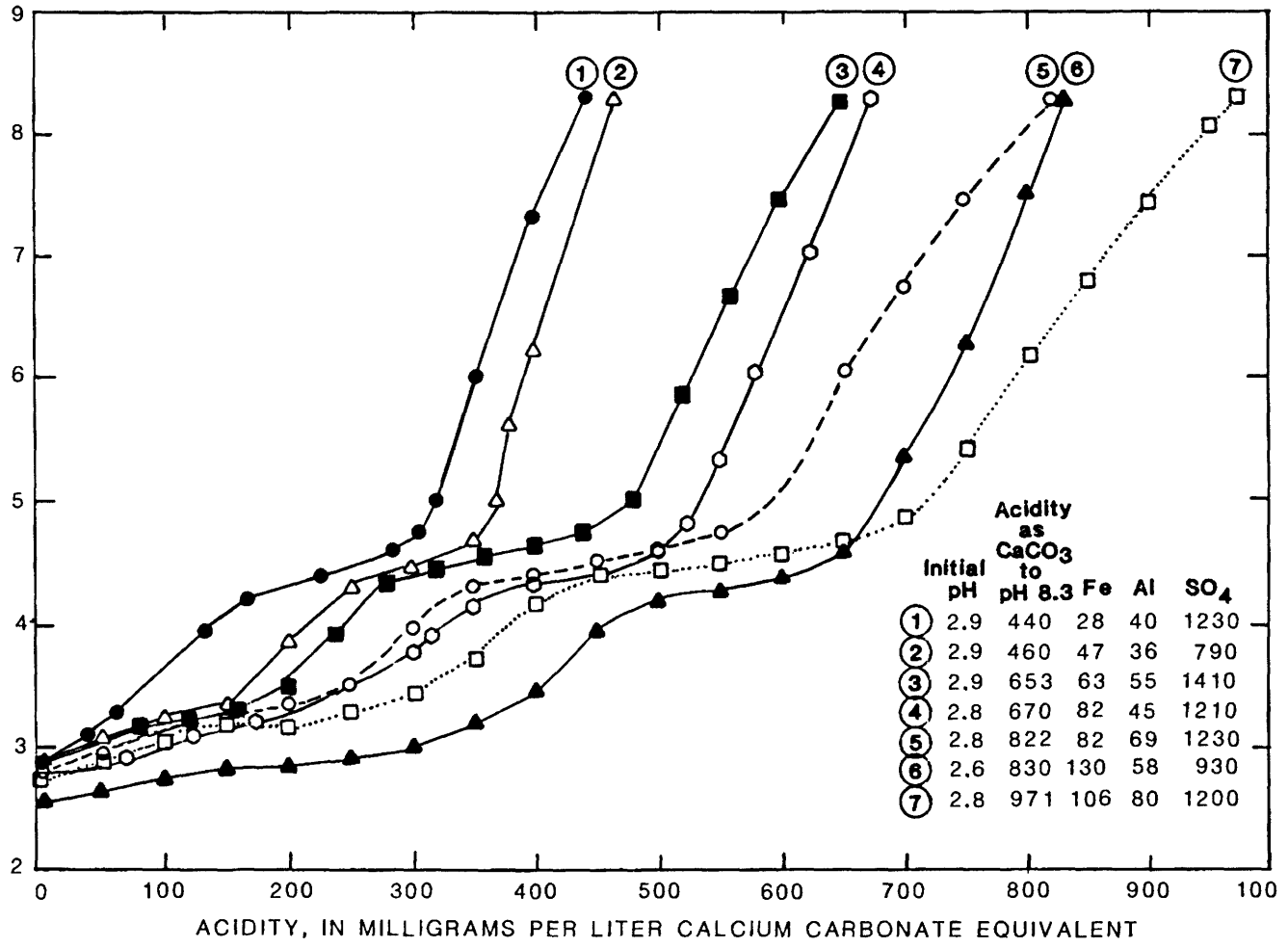

Figure 2. Titration curves for selected acid mine discharges in northeast Pennsylvania.

Relation Between Acidity and Iron and Aluminum Concentration

To see if the acidity derived from metal hydrolysis could be separated as implied by the data of Salotto and others (1967) and Payne and Yeates (1970), subsamples were taken from the sample during the course of an acidity titration to determine the iron and aluminum concentration as the sample titration progressed. An initial titration was performed, curve plotted, and ten points selected along the curve where the metal determinations would be made. Amounts of titrant were added to 10 subsamples equivalent to the titrant volume at the 10 preselected points on the initial titration curve. Samples were stirred until the expected pH was attained and were then filtered and analyzed for iron and aluminum. The titration curve and corresponding reductions of ferric iron and aluminum are shown in figure 3. These data show that midway into the pH 3.0 buffer zone, 55 percent of the iron precipitated and that 97 percent had precipitated at the end of the zone. The aluminum data show that at this latter point, about 25 percent of the dissolved aluminum had coprecipitated with the iron. This is supported by Kolthoff and Sandell (1937), who report that the precipitation of hydrous aluminum oxide begins at pH 3.0.

The precipitation of iron appears essentially complete before the initiation of the second buffer zone at pH 4.0, the area where the majority of the dissolved aluminum precipitates. The precipitation of dissolved aluminum is essentially complete by pH 5.0. Thus, although there appears to be some coprecipitation of aluminum with iron, the first buffer zone represents the neutralization of the initial free acidity and the acidity produced by iron hydrolysis, and the second buffer zone represents the neutralization of acid produced by the hydrolysis of aluminum.

Titration Characteristics of Various Chemical States

The AMD samples represented by the titration curves depicted in figure 2 contained little if any ferrous

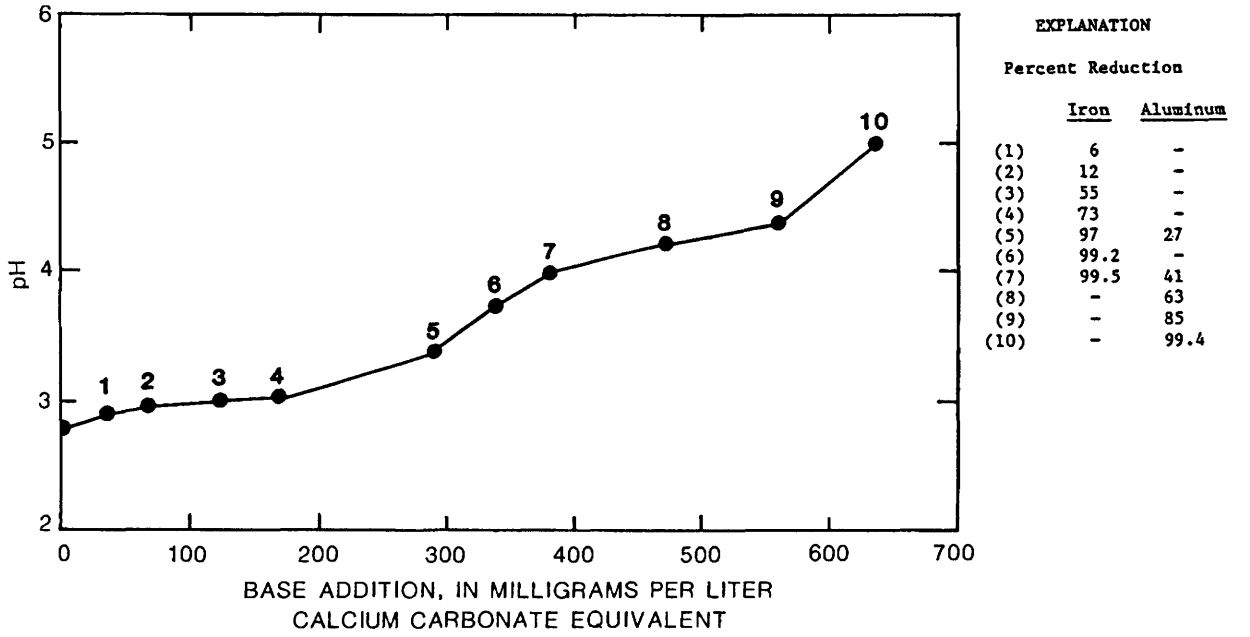

Figure 3. Decrease in ferric iron and aluminum content during neutralization of Mitchel No. 2 discharge at 25°C.

iron. Selvig and Ratliff (1922) found that the methyl orange acidity (to pH 3.7) was a "more nearly correct" free sulfuric acid value if the ferric sulfate in the AMD sample was first reduced. This implies that ferrous iron is not a factor in the hydrolysis reaction at least to pH 3.7. Salotto and others (1967) showed nearly identical titration curves for separate sulfuric acid solutions containing equal milliequivalents of ferric iron and ferrous iron oxidized with H_2O_2 (fig. 4). These curves exhibited a buffer zone to approximately pH 4.0. In contrast, the titration of a non-oxidized sulfuric acid solution containing the same milliequivalents of ferrous iron exhibited the buffer zone from approximately pH 5.5 to 7.5.

Figure 4 indicates that the shape created by the dual titration curves for an AMD sample depends upon the ferrous iron content relative to the ferric iron content. Takai and others (1956) found that in terms of the oxidation-reduction (redox) potential, ferrous iron constitutes more than 50 percent of the ferrous and ferric iron content in waterlogged paddy soils at redox values below +0.2 volts and increases proportionately as the reducing intensity increases. Thus, *the greater the system's reducing intensity*, the greater the proportion of ferrous to ferric iron; conversely, *the greater the system's oxidizing intensity*, the lower the proportion of ferrous to ferric iron.

The titration curves shown in figure 5 illustrate various redox states. These are indicated by the extent of the similarity between the curves of the untreated and H_2O_2-treated samples. The oxidized state is characterized by the two titration curves being nearly superimposed upon each other (Well T); the non-oxidized state is characterized by radically divergent curves that begin with totally different pH values (TR2 Well no. 1); and the intermediate state is characterized by curves that, while divergent, do not radically differ in their initial pH value (Well U).

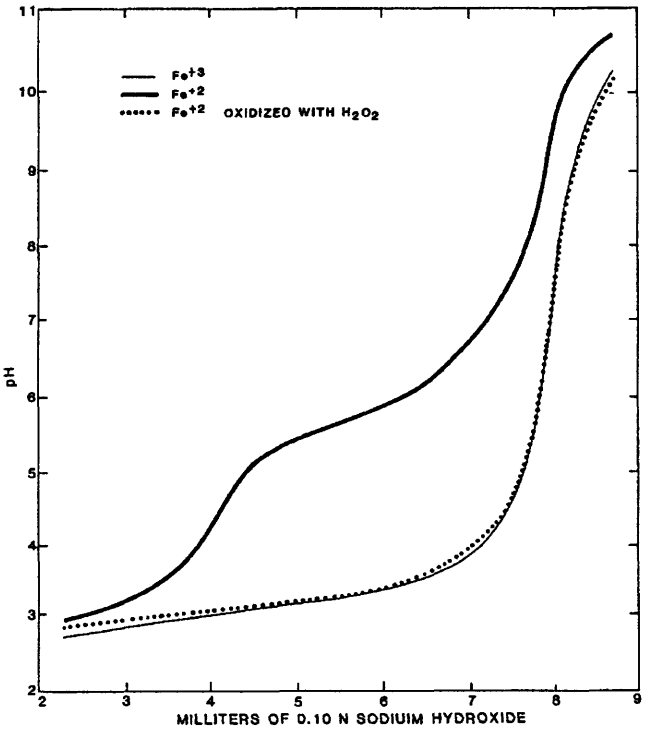

Figure 4. Titration curves for solutions of ferrous iron, ferric iron, and ferrous iron oxidized with H_2O_2.

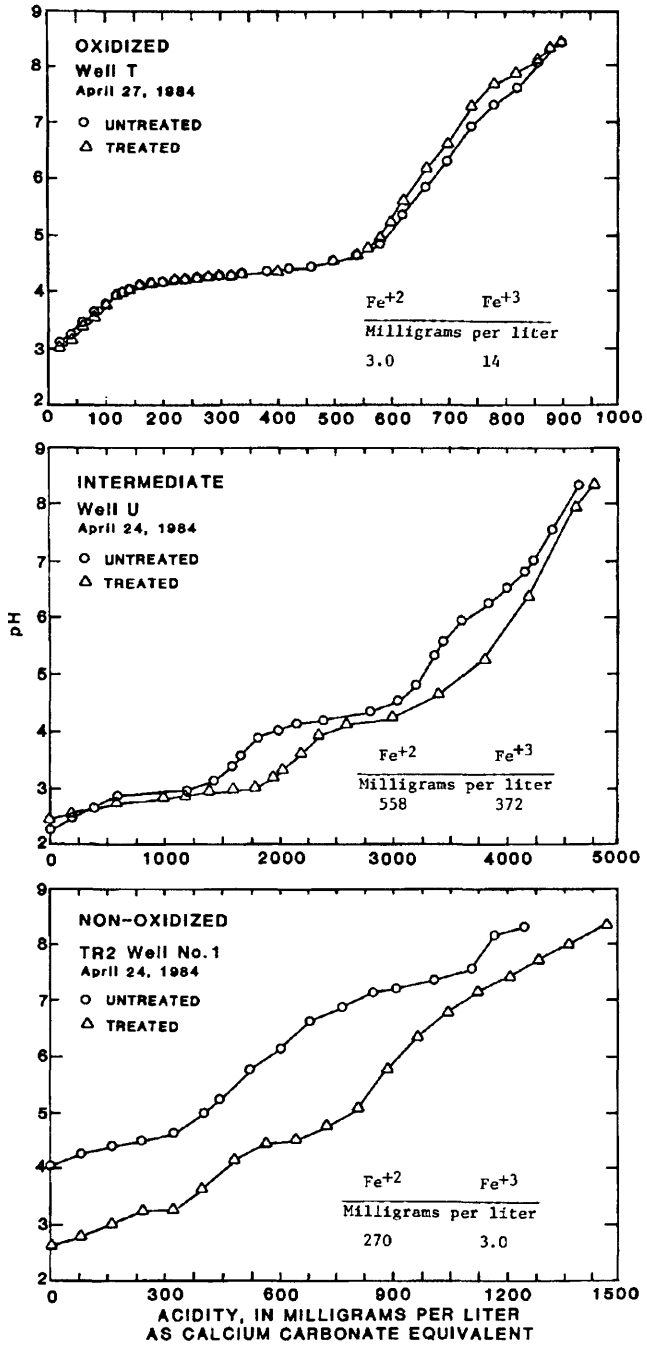

Figure 5. Titration curves characterizing AMD in an oxidized, intermediate, and non-oxidized state.

Site Fingerprint

To further explore the effect the redox state has on the acidity titration curve, samples known to have high concentrations of both ferrous and ferric iron were collected from a reclaimed strip mine located in western Pennsylvania. Duplicate samples were titrated at 25°C as (1) an untreated sample and (2) an oxidized sample, treated with 5 drops 30 percent H_2O_2. The resultant curves for three samples containing different metal concentrations are illustrated in figure 5.

Analysis of the iron species for the three samples showed that the iron in the sample from Well T was 21 percent ferrous iron (3.0 mg Fe^{+2}, 17 mg total dissolved iron); the sample from well U was 60 percent ferrous iron (558 mg Fe^{+2}, 930 mg total dissolved iron); and the sample from TR2 Well no. 1 was 99 percent ferrous iron (270 mg Fe^{+2}, 273 mg total dissolved iron). It appears from the three data sets that the similarity, or conversely, dissimilarity, between the untreated and H_2O_2-treated titration curves is dependent upon the ferrous to ferric iron ratio. The larger the ratio of ferrous iron to ferric iron, the greater the divergence between the untreated and H_2O_2-treated titration curves.

Thus, if the bulk of the iron content is ferrous iron, the dual titration curves characterize the non-oxidized state (TR2 Well no. 1); if the bulk of the iron content is ferric iron, the dual titration curves characterize the oxidized state (Well T). The intermediate state is represented by Well U. To reinforce the "fingerprint" concept, three additional sites were characterized and are presented in figure 6.

The characteristic shape of the dual acidity titration curves does not appear to change significantly for AMD samples taken at the same site over a period of time. This similarity is reflected in figures 7–9 and indicates that if the proportions of the major AMD constituents do not radically change, the general shape of the titration curve will not change. The curves can therefore be looked upon as a "fingerprint" for a mine site that will graphically indicate when a geochemical change occurs to significantly alter the metal proportions.

ESTIMATION OF IRON AND ALUMINUM CONCENTRATION IN ACID MINE DRAINAGE

Description of Technique

Figure 2 indicates a direct relation between metal concentration and the length of the buffer zone for samples in an oxidized state. This implies that the acid concentration may be related to the metal concentration relative to a buffer zone. Various procedures were attempted to relate the buffer acidity (in mg/L $CaCO_3$) to metal concentration. Because of the variability encountered in accurately identifying the inflection points from titration curves representing a variety of AMD samples arbitrary pH end points were used to separate the acidity ascribed to the hydrolysis of ferric iron and acidity due to the hydrolysis of aluminum. The method used in this report involves the relation of the ferric iron concentration to the acidity (as mg/L $CaCO_3$) required to titrate

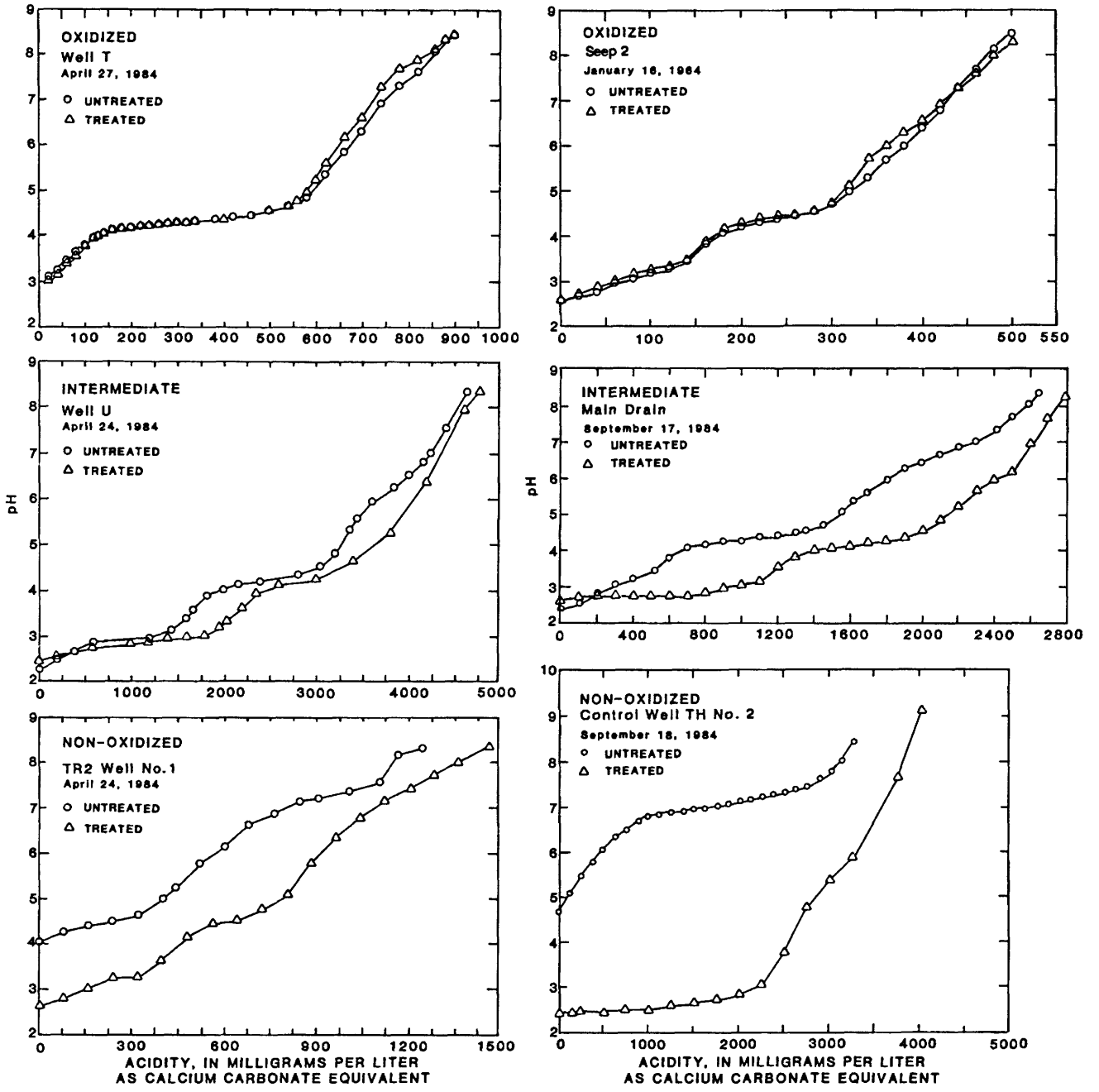

Figure 6. Titration curves for six AMD samples that characterize the oxidized, intermediate, and non-oxidized state.

from the initial pH to pH 4.0 and the aluminum concentration to the acidity value (as mg/L $CaCO_3$) required to titrate from pH 4.0 to 5.0. A statistical analysis of the iron relation to acidity using data from table 3 for samples believed to be in an oxidized state and using a nonlinear least-squares fitting procedure results in a plot (fig. 10) having the general relationship:

$$y=0.0128x^{1.5055} + 0.90 \quad (1)$$
$$r^2=0.98$$

where y = ferric iron concentration, in milligrams per liter,

x = acidity, in milligrams per liter as $CaCO_3$ equivalent, and

r^2 = correlation coefficient.

A linear least squares fitting procedure was used to produce a plot (fig. 11) with the general relationship for the aluminum relation to acidity:

$$y=0.2139x + 1.150 \quad (2)$$
$$r^2=0.97$$

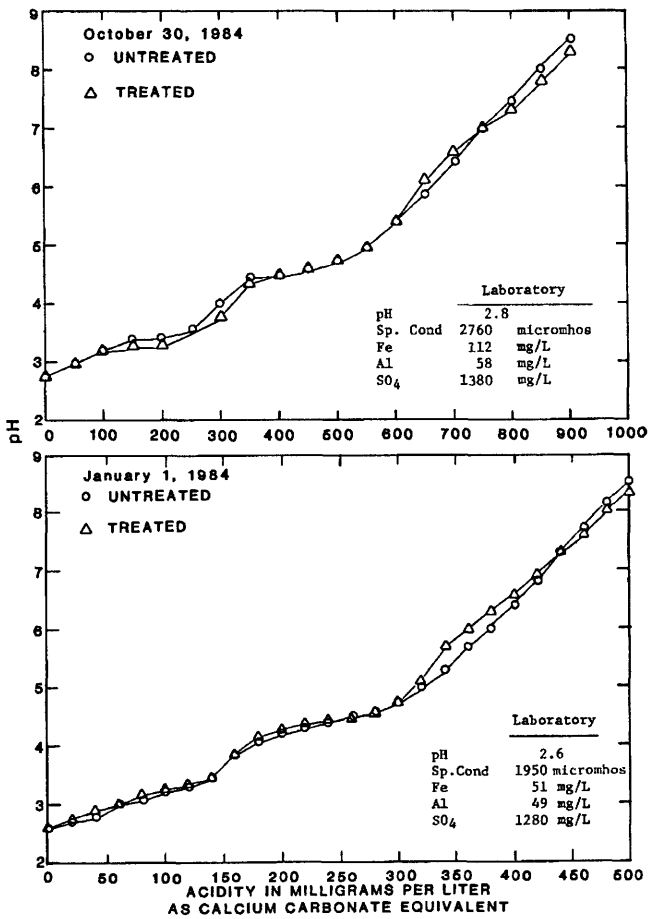

Figure 7. Similarity in titration curve characteristics for AMD from Seep no. 2, Clarion County, Pennsylvania, for samples collected in January 1984 and October 1984.

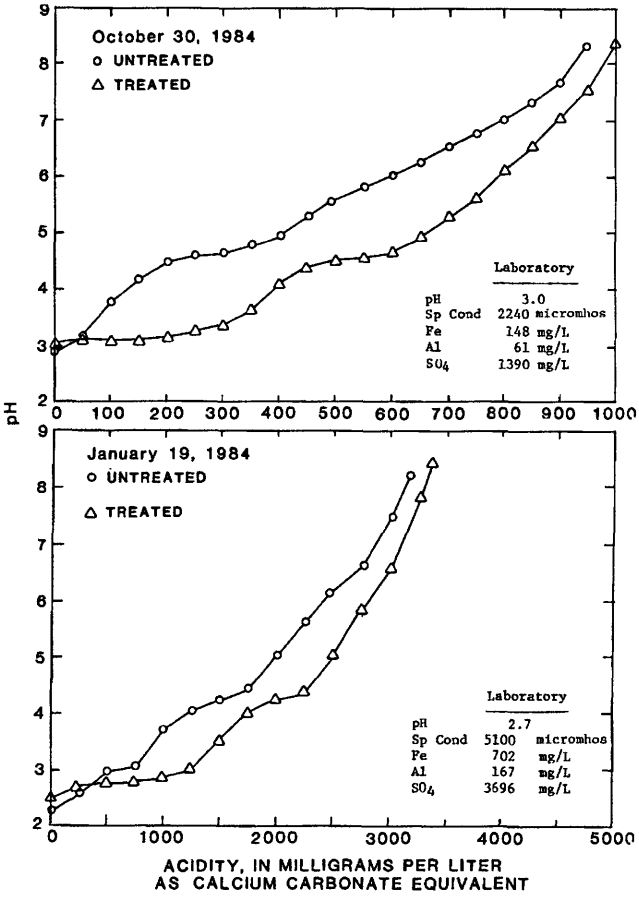

Figure 8. Similarity in titration curve characteristics for AMD from Well 4K, Clarion County, Pennsylvania, for samples collected in January 1984 and October 1984.

where y = aluminum concentration, in milligrams per liter, and

x = acidity, in milligrams per liter as $CaCO_3$ equivalent.

These equations were tested on field titration data and corresponding iron and aluminum values that were determined in the laboratory. These data were collected from 1975 to 1980 for AMD-related water samples from north-central Pennsylvania. Of 122 iron estimates ranging in concentration from 4 to 280 mg/L, 75 percent were less than ±25 percent of the laboratory-determined value, while less than 1 percent were greater than ±50 percent of the laboratory values. For 96 aluminum estimates ranging from 1 to 120 mg/L, 84 percent were less than ±25 percent, whereas 3 percent were greater than ±50 percent of the laboratory values. New regression equations were calculated by using only data collected for the latter part of the study. These data, found in table 4, were from samples that were both untreated and treated with H_2O_2 and heated. Paired t tests were run to compare the estimated iron values with the laboratory-determined values and to make a comparison between the estimated values derived from the two equations. Significant differences at the 95 percent confidence level were not noted between either group of estimated values and the laboratory values. However, the mean difference and the standard error of the mean were much lower for the data obtained using the regression equation associated with the H_2O_2-treated samples. The paired t test was then used to compare the estimated values from both equations. This time a significant difference at the 95 percent confidence level was noted. Therefore, the equation derived from the peroxide treatment is to be used for estimating iron values.

It is believed that the difference between the equations exists primarily because titrations were performed on both untreated and oxidized samples collected during the latter part of the study, while only single titrations were performed on untreated samples collected during the first part of the study.

The modified equation for iron is:

$$y = 0.0386\, x^{1.3256} + 0.90 \qquad (3)$$
$$r^2 = 0.98$$

Table 3. Chemical analyses of acid mine drainage and related waters from north-central Pennsylvania

[Concentrations are in milligrams per liter, unless otherwise indicated; no entry in column means no data available]

Date of collection	pH	Specific conductance (Microsiemens at 25°C)	Acidity ($CaCO_3$ equivalent)	Calcium (Ca)	Magnesium (Mg)	Sodium (Na)	Potassium (K)	Iron (Fe)	Aluminum (Al)	Manganese (Mn)	Zinc (Zn)	Copper (Cu) (µg/L)	Silica (SiO_2)	Phosphorus (P)	Chloride (Cl)	Sulfate (SO_4)
Mitchel 2 Mine Discharge (01548413)																
1981																
March 18.....	2.7	2,450	890					91	64	38				0.01		1,900
April 20.....	2.7	2,310	790	79				83	120	34	5,400		42			1,300
October 15....	2.7	3,160	1,290					160	25	69						2,300
1982																
January 28.....	2.6	3,140	1,390	150	150	1.7	0.9	26	50	62	9,800		30		13	2,200
March 31.....	2.6	2,580	855	102	102	1.3	.9	75	65	36	5,970	420	20	.01	1.0	1,530
April 14.....	2.8	2,490	822	102	91	1.4	1.1	82	69	43	6,050	400	19	.01	2.0	1,230
May 18.....	2.8	2,820	971	144	137	1.7	.8	106	70	43	6,600	450	47	.04	1.0	1,200
June 7.....	2.8	2,200	629	91	75	1.4	1.4	66	55	32	4,180	410	35	.03	2.0	1,410
June 24.....	2.8	2,420	660	118	106	1.7	.9	57	53	33	4,920	370	41	.02	2.0	870
July 16.....	2.8	2,580	796	142	120	1.8	2.2	74	56	34	5,240	370	17	.03	1.0	1,200
August 13.....	2.7	3,000	840	128	112	0.8	1.1	92	63	34	5,150	330	50	.03	3.0	1,050
Anna S Mine Discharge (01548416)																
1981																
March 18.....	2.8	1,800	400					40	28	10				.01		750
April 20.....	2.8	1,600	410	59				34	35	13	2,600		36			630
June 9.....	3.2	1,500						24	20	8.5						540
October 15....	2.7	1,620	487					43	21	15						720
1982																
January 28.....	2.7	1,620	497	66	42	2.7	1.4	39	33	15	2,600		33		1.9	690
Hunter Drift Mine Discharge (01548418)																
1981																
March 18.....	2.7	2,090	800					110	60	22						1,600
April 20.....	2.7	1,865	617	41				84	72	14	2,900		35			800
June 9.....	2.9	2,400						130	59	22						1,200
Bridge Run (01548415)																
1981																
March 18.....	3.1	705	140					4.9	5.8	3.4						220
April 20.....	3.3	650	80	30				3.9	4.5	3.1	210		18			200
June 9.....	3.3	780						4.3	6.0	3.7						230
Wilson Creek at Morris (01548423)																
1981																
March 18.....	3.5	500	140					3.5	8	3.5					.01	180
April 20.....	3.7	317	43	16				2.3	3.9	2.1	300		8.5			100
June 9.....	3.7	430						1.6	5.0	3.4						160
Shoff Mine Discharge (01541414)																
1983																
March 11.....	2.6		2,242					690		8.2						

where y = iron concentration, in milligrams per liter, and

x = acidity, in milligrams per liter as $CaCO_3$ equivalent.

The modified equation for aluminum is

$$y = 0.2161x + 2.0932 \quad (4)$$

$$r^2 = 0.99$$

where y = aluminum concentration, in milligrams per liter, and

x = acidity, in milligrams per liter as $CaCO_3$ equivalent.

The acidity titrated to pH 4.0 for the untreated samples is considered to relate to the free mineral acidity and to the acidity formed from the hydrolysis of ferric sulfate, since it was previously mentioned that ferrous iron does not hydrolyze below at least pH 3.7. The acidity titrated to pH 4.0 for the oxidized sample is also the product of free mineral acidity and the acidity formed from the hydrolysis of ferric sulfate as well as that formed from the oxidation and hydrolysis of ferrous sulfate. As previously shown in figure 4, the curves for the solutions containing equal milliequivalents (meq) of oxidized fer-

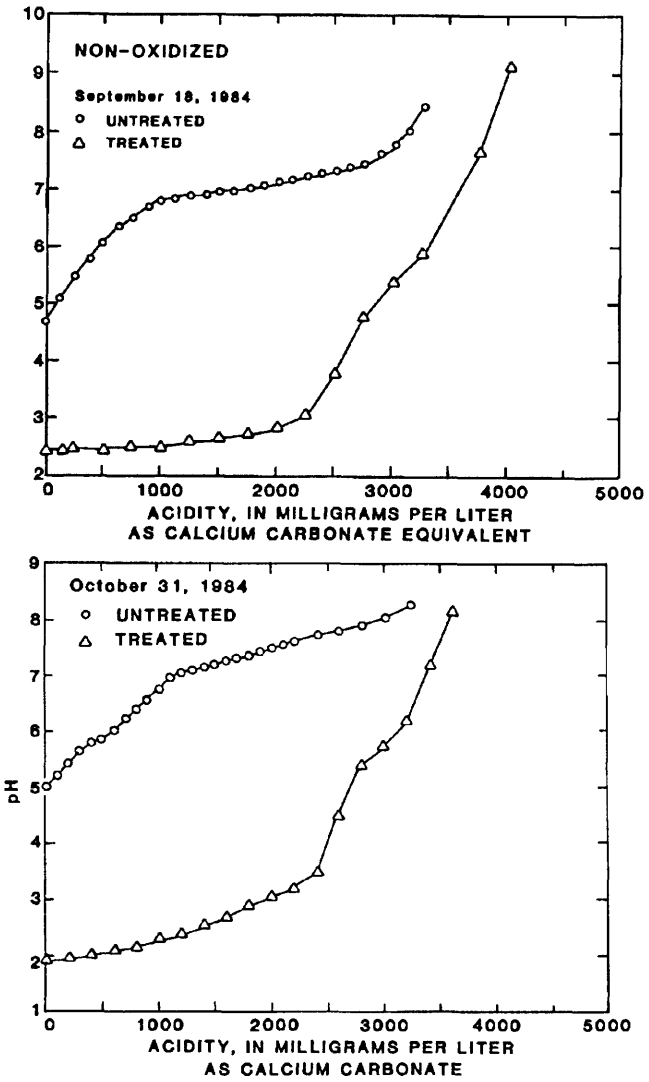

Figure 9. Similarity in titration curve characteristics for AMD from Control Well TH no. 2, Clarion County, Pennsylvania, for samples collected in September 1984 and October 1984.

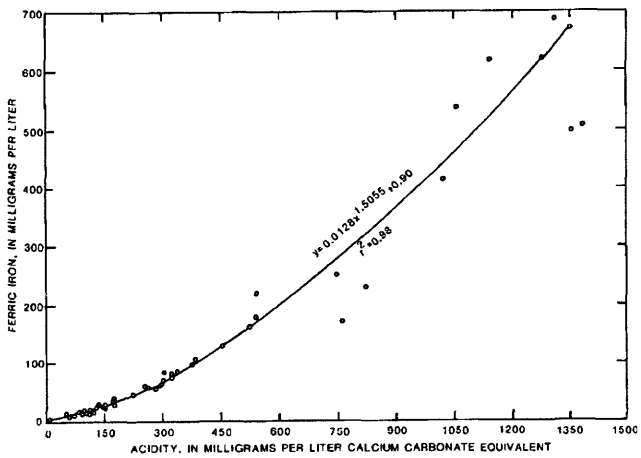

Figure 10. Relation between ferric iron concentration and amount of calcium carbonate equivalent required to raise the initial sample pH to 4.0 at 25°C.

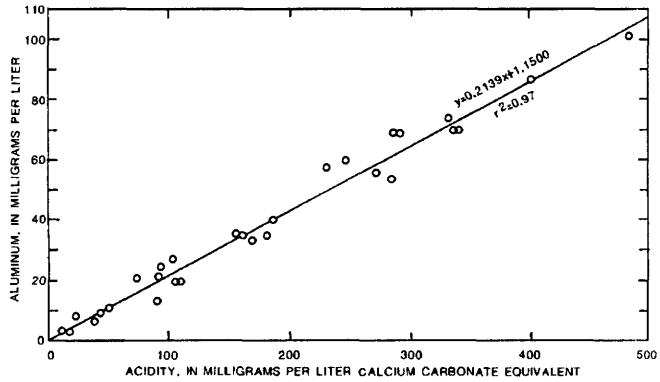

Figure 11. Relation between aluminum concentration and the amount of calcium carbonate equivalent required to raise sample pH from 4.0 to 5.0 at 25°C.

rous iron and ferric iron are, for all practical purposes, identical. This identity means that the acidity equivalent to 1 mg ferric iron is equivalent to

$$\frac{27.9 \text{ mg/meq } Fe^{+2}}{18.6 \text{ mg/meq } Fe^{+3}} = 1.5 \text{ mg ferrous iron.}$$

In estimating the iron content from the titratable acidity of an AMD sample, two titrations should be made—one titration on an untreated (raw) sample and one on a subsample treated with H_2O_2. The iron in the untreated sample may be composed of ferric and ferrous iron. Their estimations are determined separately. This is accomplished by quantifying the ferric iron in the untreated sample and subtracting it from the oxidized iron value determined for the treated sample. The ferric and ferrous iron values are then added together to arrive at a total dissolved iron value.

It should be pointed out that the relation achieved between the iron concentration and acidity to pH 4.0 breaks down at high concentrations of iron and acidity. However, satisfactory estimates for samples having acidities to pH 4.0 greater than 1,300 mg/L $CaCO_3$ can be obtained by halving the acidity value and doubling its corresponding iron concentration to equate with the original acidity value.

Application of Technique

The procedure for the estimation technique follows:

(1) Untreated sample curve

(a) $y = 0.0386\,x^{1.3256} + 0.90$ = mg/L *ferric iron*

where x = acidity to pH 4.0 as mg/L $CaCO_3$

(2) Treated sample curve
(a) $y = 0.0386x^{1.3256} + 0.90$ = mg/L *oxidized iron*
where x = acidity to pH 4.0 as mg/L $CaCO_3$
(b) oxidized iron (2a) − ferric iron (1a) × 1.5 = mg/L *ferrous iron*
(c) *ferric iron* (1a) + ferrous iron (2b) = *total dissolved iron*

Example:

Figure 5, Well T—Sample in an oxidized state
(1) Untreated sample curve
(a) $y = 0.0381x^{1.3256} + 0.90$ = mg/L ferric iron
$0.0381 \times 130^{1.3256} + 0.90 = 25$ mg/L ferric iron
(2) Treated sample curve
(a) $y = 0.0381x^{1.3256} + 0.90$ = mg/L oxidized iron
$0.0381 \times 129^{1.3256} + 0.90 = 25$ mg/L oxidized iron
(b) oxidized iron − ferric iron × 1.5 = ferrous iron
25 mg/L−25 mg/L × 1.5 = 0 mg/L ferrous iron
(c) ferric iron + ferrous iron = total dissolved iron
25 mg/L + 0 mg/L = 25 mg/L
laboratory value = 14 mg/L total dissolved iron

Figure 5, Well U—Sample in an intermediate state
(1) Untreated sample curve
(a) $y = 0.0381x^{1.3256} + 0.90$ = mg/L ferric iron

$$0.0381 \times \frac{1924^{1.3256}}{2} + 0.90 \times 2 = 697 \text{ mg/L ferric iron}$$

(2) Treated sample curve
(a) $y = 0.0381x^{1.3256} + 0.90$ = mg/L oxidized iron

$$0.0381 \times \frac{2422^{1.3256}}{2} + 0.90 \times 2 = 945 \text{ mg/L oxidized iron}$$

(b) oxidized iron—ferric iron × 1.5 = ferrous iron
945 mg/L − 697 mg/L × 1.5 = 372 mg/L ferrous iron
(c) ferric iron + ferrous iron = total dissolved iron
697 mg/L + 372 mg/L = 1,069 mg/L total dissolved iron
laboratory value = 930 mg/L total dissolved iron

Figure 5, TR2 Well no. 1—Sample in a non-oxidized state
(1) Untreated sample curve
(a) $y = 0.0381x^{1.3256} + 0.90$ = mg/L ferric iron
$0.0381 \times 0^{1.3256} + 0.90 = 0$ mg/L ferric iron
(2) Treated sample curve
(a) $y = 0.0381x^{1.3256} + 0.90$ = mg/L oxidized iron
$0.0381 \times 450^{1.3256} + 0.90 = 128$ mg/L oxidized iron
(b) oxidized iron − ferric iron × 1.5 = ferrous iron
128 mg/L − 0 mg/L × 1.5 = 192 mg/L ferrous iron
(c) ferric iron + ferrous iron = total dissolved iron
0 mg/L + 192 mg/L = 192 mg/L total dissolved iron
laboratory value = 270 mg/L total dissolved iron

Comparison between the estimated ferrous and total dissolved iron concentrations and laboratory-determined concentrations are made for samples collected in April 1984 in western Pennsylvania (table 5). These data are tabulated below.

The data show a consistently low estimate of ferrous iron relative to the laboratory-determined ferrous iron values. It also appears that at least more than 11 mg/L ferrous iron need be present before being detected by the estimation technique. The consistently low estimate could be inherent to the method of the acidity titration. Stirring of the sample is required to ensure adequate dispersal of the titrant and metal precipitate. The stirring oxygenates and may oxidize some ferrous iron.

There is little difference between the present regression equation for aluminum and the initial equation derived from the north-central Pennsylvania samples. With the recommendation that two titrations be performed per sample, two acidity values from pH 4.0 to 5.0 are available. A statistical analysis using the paired t test for comparing the estimated aluminum concentration to the laboratory-determined value for the untreated samples and for the oxidized samples indicated that neither the oxidized nor untreated estimated values were significantly different from the laboratory values. However, the standard deviation and the standard error of the mean were lower for the oxidized versus the laboratory values than for the untreated versus the laboratory values. Separate regression equations were calculated for the oxidized acidities from pH 4.0 to 5.0 and laboratory aluminum values and for the untreated acidities from pH 4.0 to 5.0 and the laboratory aluminum values. There was less of a difference between the equations representing the oxidized samples and the original data than between the equation representing the untreated and original data. An example is presented that shows that complete oxidation is required to best estimate the aluminum content. Separate titrations were performed on subsamples from Well C-2 that contained over 1,000 mg/L ferrous iron. The titrations were performed on an untreated sample, H_2O_2-treated sample, and H_2O_2-treated and heated sample. The three curves are illus-

Table 4. Titration curve, laboratory-analyzed, and estimated metal data for samples from Kentucky, Maryland, Ohio, western Pennsylvania, and West Virginia collected for the period from December 1983 to June 1984

[—, no data]

Location	pH	Specific conductance (microsiemens at 25°C)	Acidity (milligrams per liter as $CaCO_3$)			Iron (milligrams per liter)			Aluminum (milligrams per liter)		
							Laboratory[1]			Laboratory[1]	
			pH 4	pH 5	pH 8.3	Estimate	1	2	Estimate	1	2
Kentucky											
Flat Creek											
Untreated	3.3	1,870	35	87	200	—	—	—	—	—	—
Treated	3.3	—	35	89	193	3.6	2.6	—	21	17	—
Lick Creek											
Untreated	3.9	817	2	20	42	—	—	—	—	—	—
Treated	3.9	—	3	17	50	1.0	0.3	—	6	4	—
Maryland											
Abrams Creek											
Untreated	4.2	610	0	34	60	—	—	—	—	—	—
Treated	3.4	—	15	22	60	3.4	0.5	—	7	9	—
Laurel Run											
Untreated	3.4	485	40	31	102	—	—	—	—	—	—
Treated	3.1	—	46	31	100	5.4	8.5	—	9	7	—
Mill Run											
Untreated	3.8	719	4	27	49	—	—	—	—	—	—
Treated	3.4	—	16	15	50	1.7	0.3	—	5	6	—
Three Forks Run											
Untreated	3.3	580	29	27	78	—	—	—	—	—	—
Treated	3.3	—	36	21	81	3.7	4.7	—	7	5	—
Ohio											
Sandy Run											
Untreated	3.5	465	13	22	53	—	—	—	—	—	—
Treated	3.4	—	17	17	55	2.8	0.5	—	6	5	—
Yost Run											
Untreated	3.4	1,150	20	75	160	—	—	—	—	—	—
Treated	3.3	—	27	68	160	4.5	0.7	—	17	14	—
West Virginia											
Canyon Creek											
Untreated	2.8	2,640	245	350	785	—	—	—	—	—	—
Treated	2.7	—	240	342	745	50	38	—	76	82	—
Conner Run											
Untreated	3.0	1,800	150	240	550	—	—	—	—	—	—
Treated	2.8	—	150	230	535	25	26	—	52	52	—
Dents Run											
Untreated	2.6	5,110	670	920	2,220	—	—	—	—	—	—
Treated	2.3	—	717	873	2,220	268	142	74	191	180	151
Glade Creek											
Untreated	2.9	4,180	190	498	990	—	—	—	—	—	—
Treated	2.8	—	190	495	955	35	25	47	—	—	—
Sovern Run											
Untreated	3.6	675	12	110	184	—	—	—	—	—	—
Treated	3.3	—	32	90	168	4.1	4.5	—	22	24	—
West Run											
Untreated	2.8	2,280	292	196	630	—	—	—	—	—	—
Treated	2.6	—	300	190	630	75	71	—	43	44	—
Western Pennsylvania											
Dec. 1983											
Main Drain											
Untreated	2.35	6,600	1,300	975	3,450	—	—	—	—	—	—
Treated	2.45	—	1,825	900	3,515	768	700	605	197	200	155
Seep 2											
Untreated	3.18	580	105	60	245	—	—	—	—	—	—
Treated	3.18	—	110	60	245	22	35	10	15	11	4
Well U											
Untreated	2.85	1,600	150	215	585	—	—	—	—	—	—
Treated	2.85	—	200	185	565	51	15	14	42	55	42
Well 4K											
Untreated	2.77	3,000	330	515	1,350	—	—	—	—	—	—
Treated	2.89	—	550	458	1,450	208	210	219	101	100	79

Table 4. Titration curve, laboratory-analyzed, and estimated metal data for samples from Kentucky, Maryland, Ohio, western Pennsylvania, and West Virginia collected for the period from December 1983 to June 1984—Continued

Location	pH	Specific conductance (microsiemens at 25°C)	Acidity (milligrams per liter as $CaCO_3$) pH 4	pH 5	pH 8.3	Iron (milligrams per liter) Estimate	Laboratory[1] 1	2	Aluminum (milligrams per liter) Estimate	Laboratory[1] 1	2
Western Pennsylvania—Continued											
Well 7K											
Untreated	3.28	5,500	210	380	2,220	—	—	—	—	—	—
Treated	2.60	—	1,360	480	2,520	638	870	383	106	96	69
Well 11K											
Untreated	2.56	5,000	735	955	2,590	—	—	—	—	—	—
Treated	2.62	—	1,020	910	2,680	444	420	385	199	190	161
Feb. 1984											
Main Drain											
Untreated	2.5	5,000	640	620	2,220	—	—	—	—	—	—
Treated	1.90	—	1,140	540	2,260	553	—	606	118	—	144
Well 4K											
Untreated	2.9	2,600	152	273	1,090	—	—	—	—	—	—
Treated	2.1	—	535	255	1,160	226	—	324	57	—	57
Well 7K											
Untreated	2.4	4,000	650	630	2,480	—	—	—	—	—	—
Treated	1.9	—	1,020	700	2,400	462	—	561	153	—	179
Mar. 1984											
Main Drain											
Untreated	2.2	4,000	885	715	2,740	—	—	—	—	—	—
Treated	2.0	—	1,380	650	2,800	518	—	505	142	—	129
Apr. 1984											
Control no.1											
Untreated	2.5	6,000	504	802	2,740	—	—	—	—	—	—
Treated	2.7	—	1,540	745	3,000	705	720	630	163	160	107
Main Drain											
Untreated	2.4	5,200	889	826	2,620	—	—	—	—	—	—
Treated	2.4	—	1,354	793	2,800	500	550	498	173	190	119
Seep 2											
Untreated	3.0	1,950	202	189	573	—	—	—	—	—	—
Treated	2.9	—	201	189	589	45	60	54	42	39	24
Seep 2A											
Untreated	3.6	1,750	27	97	345	—	—	—	—	—	—
Treated	2.9	—	151	75	367	45	80	76	17	15	41
TR2 Well no. 1											
Untreated	4.0	6,000	0	200	1,237	—	—	—	—	—	—
Treated	2.7	—	457	322	1,455	196	290	273	72	200	91
Well T											
Untreated	3.0	2,000	130	460	880	—	—	—	—	—	—
Treated	3.0	—	129	454	880	25	14	13	100	120	83
Well 4K											
Untreated	2.9	2,700	216	389	1,090	—	—	—	—	—	—
Treated	2.2	—	506	303	1,075	207	190	197	67	70	60
Well 11K											
Untreated	2.6	4,500	529	755	2,050	—	—	—	—	—	—
Treated	2.7	—	850	690	2,180	365	340	330	151	130	168
Well U											
Untreated	2.3	6,500	1,924	1,335	4,650	—	—	—	—	—	—
Treated	2.4	—	2,422	1,311	4,730	1,069	930	781	285	280	195

[1]Laboratory 1 and 2 represent split samples analyzed by two different laboratories.

trated in figure 12. It should be noted that the oxidized unheated sample is incompletely oxidized as evidenced by its lower acidity content to pH 4.0, as opposed to the acidity contained by the oxidized and heated sample. The acidity from 4 to 5 for the oxidized sample correlates with 73 mg/L aluminum, while the acidity from the oxidized and heated sample correlates with 36 mg/L aluminum. The laboratory-determined aluminum value is 27 mg/L. Thus it appears that ferrous iron can be an interference between pH 4.0 and 5.0 and must be completely oxidized before aluminum can be properly estimated.

Therefore the acidity from pH 4.0 to 5.0 for the oxidized (treated) and heated samples should be used for the estimation of aluminum.

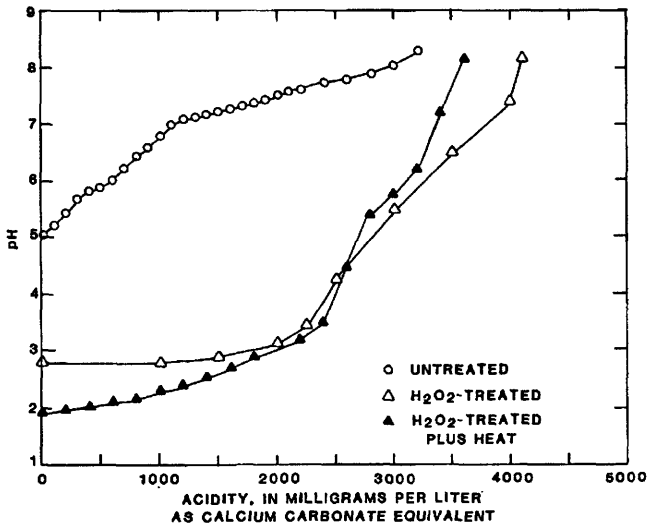

Figure 12. Titration curves for subsamples from Well C-2 that are untreated, treated with H_2O_2, and treated with H_2O_2 and heated.

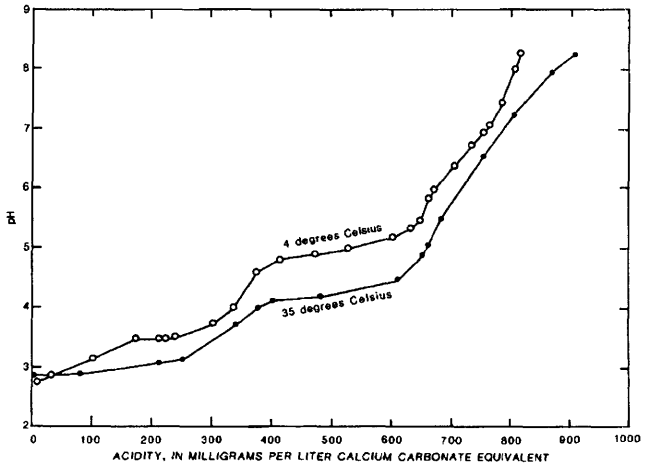

Figure 13. Effect of temperature on titration curve characteristics.

Estimation of aluminum for the samples in figure 5 follows:

Well T—Sample in an oxidized state

(1) Treated sample curve

(a) acidity from pH 4.0 to 5.0 = X (regression equation) = mg/L aluminum

455 mg/L $CaCO_3$ = X (0.2161x + 2.0932) = 100 mg/L aluminum

laboratory value = 120 mg/L aluminum

Well U—Sample is in an intermediate state

(1) Treated sample curve

(a) acidity from pH 4.0 to 5.0 = X (regression equation) = mg/L aluminum

1,275 mg/L $CaCO_3$ = X (0.2161x + 2.0932) = 278 mg/L aluminum

laboratory value = 280 mg/L aluminum

TR2 Well no. 1—Sample in a non-oxidized state

(1) Treated sample curve

(a) acidity from pH 4.0 to 5.0 = X (regression equation) = mg/L aluminum

336 mg/L $CaCO_3$ = X (0.2161x + 2.0932) = 75 mg/L aluminum

laboratory value = 91 mg/L aluminum

A decrease of 1.0 to 1.5 pH units was observed by Salotto and others (1967) for the inflection points of iron, aluminum, and manganese titration curves derived at 90°C as opposed to the inflection points obtained for titration curves at 25°C. Therefore, temperature appears to be an important factor when use is made of the metal estimation technique.

Curves for duplicate AMD samples titrated at 4°C and 35°C are depicted in figure 13. The samples at ambient room temperature contained 96 and 69 mg/L of iron and aluminum, respectively. The estimated iron and aluminum concentrations at 4°C are 86 and 43 mg/L, respectively, and at 35°C are 101 and 63 mg/L, respectively. This indicates that, particularly in the case of aluminum, poor estimates are obtained from titrations determined at low temperature.

Fortunately, field titrations are probably seldom performed at these temperatures because of the care required to adjust the electrolyte concentration of the pH electrode filling solution. The electrolyte used to fill the electrode at room temperature will "salt out" at low temperatures because of supersaturation and will be undersaturated at the elevated temperatures. Either case will produce erroneous pH readings unless the electrolyte concentration is adjusted.

Table 5. Comparison between estimated and laboratory-determined concentrations of ferrous and total disssolved iron

[Values are in milligrams per liter]

Site	Ferrous iron		Total dissolved iron	
	Estimate	Laboratory	Estimate	Laboratory
Well T	0	3.5	25	14
Well 4K	150	210	199	197
Seep 2	0	11	45	54
Seep 2A	41	90	45	76
Control Well no. 1	557	630	705	720
TR2 Well no. 1	200	270	196	273
Control Well TH no. 2	599	798	617	566
Well 11K	207	325	365	340
Well U	372	558	1,069	930
Main drain	186	364	500	498

SUMMARY AND CONCLUSIONS

The acidity determination provides a value that denotes the quantitative capacity of the water sample to neutralize a strong base to pH 8.3. However, much additional information can be obtained when dual acidities are determined and their respective titration curves constructed. This is accomplished by titrating (1) an untreated sample at room temperature and (2) a sample treated with H_2O_2, heated to boiling, and cooled to room temperature. Titration curves for each are then constructed from the recorded data of titrant increments and their corresponding pH values. After the two curves are plotted, an indication can be obtained of the sample's redox state and its dissolved ferrous iron, ferric iron, and aluminum content.

Redox states are indicated by the extent of similarity between the titration curves of the untreated and H_2O_2-treated samples. The oxidized state is characterized by the dual titration curves being nearly superimposed upon each other; the non-oxidized state characterized by radically divergent titration curves and totally different initial pH values; and the intermediate state characterized by curves that, while divergent, do not radically differ in their initial pH value.

A nonlinear regression equation with a correlation coefficient of 0.98 was determined for the relation between the titratable acidity (as mg/L $CaCO_3$) to pH 4.0 and the concentration of oxidized iron as determined by laboratory analysis. This correlation was achieved despite the fact that the titratable acidity is due not only to the hydrolysis of ferric iron but also to the free mineral acidity and to the hydrolysis of some aluminum that co-precipitates with the iron.

The estimation of ferrous, ferric, and total dissolved iron is achieved by using the titration curves of the oxidized and untreated samples. The oxidized iron is estimated from the oxidized sample and represents the combined concentration of the oxidized ferrous and original ferric iron. The ferric iron concentration is estimated from the untreated, raw sample and represents the ferric iron concentration in the original sample. The concentration value of the ferric iron is subtracted from the oxidized iron value and multiplied by 1.5 to obtain the estimated ferrous iron concentration. The total dissolved iron concentration is then obtained by adding the ferrous iron value with that of ferric iron.

A linear regression equation with a correlation coefficient of 0.99 was derived for the relation between the titratable acidity (as mg/L $CaCO_3$) for the oxidized sample from pH 4.0 to 5.0 and the concentration of aluminum. The relationship suggests that although some aluminum hydrolysis occurs below pH 4.0, the total dissolved aluminum is directly proportional to the dissolved aluminum in solution between pH 4.0 and 5.0.

The dual titration curves constitute a characteristic shape, or fingerprint, for the AMD sample collected at a site. This configuration should not change for the sampling site except to contract or elongate, depending on sample dilution, unless a geochemical change occurs to alter the metal proportions.

The dual acidity titration curves provide a useful tool in reconnaissance studies of AMD sites in that they indicate the redox state of a sample and allow an estimate of the samples's ferrous, ferric, and total dissolved iron and aluminum content.

REFERENCES CITED

Brown, Eugene, Skougstad, M.W., and Fishman, M.J., 1970, Methods for collection and analysis of water samples for dissolved minerals and gases: U.S. Geological Survey Techniques of Water-Resources Investigations, Book 5, Chapter A1, 160 p.

Kolthoff, I.M., and Sandell, E.B., 1937, Textbook of quantitative inorganic analysis: New York, The Macmillan Company, 749 p.

Ott, A.N., 1986, Estimating iron and aluminum content of acid mine drainage from a north-central Pennsylvania coal field by use of acidity titration curves: U.S. Geological Survey Water-Resources Investigations Report 84–4335, 25 p.

Payne, D.A., and Yeates, T.E., 1970, The effect of magnesium on acidity determinations of mine drainage: Proceedings—Third Symposium on Coal Mine Drainage Research: Pittsburgh, Pennsylvania, Coal Industry Advisory Committee to the Ohio River Valley Water Sanitation Commission, p. 200–226.

Rainwater, F.H., and Thatcher, L.L., 1960, Methods for collection and analysis of water samples: U.S. Geological Survey Water-Supply Paper 1454, 301 p.

Reed, L.A., 1980, Effects of strip mining the abandoned deep Anna S Mine on the hydrology of Babb Creek, Tioga County, Pennsylvania: U.S. Geological Survey Water Resources Investigations Report 80–53, 41 p.

Salotto, B.V., Barth, E.F., Ettinger, M.B., and Tolliver, W.E., 1967, Determination of mine waste acidity, *in* Internal report of FWPCA, presented at 154th National Meeting of American Chemical Society, Chicago, Illinois, September 1967: U.S. Department of the Interior, Federal Water Pollution Control Administration, Cincinnati, Ohio, January 1967, 26 p.

Selvig, W.A., and Ratliff, W.C., 1922, The nature of acid water from coal mines and the determination of acidity: Journal of Industrial and Engineering Chemistry, v. 14, no. 2, p. 125–127.

Skougstad, M.W., and others, 1979, Methods of determination of inorganic substances in water and fluvial sediments: U.S. Geological Survey Techniques of Water-Resources Investigations, Book 5, Chapter A1, 626 p.

Takai, Y., Koyama, T., and Kamura, T., 1956, Microbial metabolism in reduction process of paddy soils (part 1): Soil and Plant Food, v. 2, p. 63–66.

Ward, J.R., 1976, Preliminary results of preimpoundment water quality studies in the Tioga River basin, Pennsylvania and New York: U.S. Geological Survey Water-Resources Investigations Report 76–66, 79 p.

Pesticides in Rainfall Samples Collected at Fresno, California, December 1981 through March 1983

By Michael V. Shulters, Richard N. Oltmann, *and* Rolland R. Grabbe

Abstract

Rainfall samples from 21 storms were collected at two sites in Fresno, California, from December 1981 through March 1983. These samples were analyzed for 7 organophosphorus insecticides, 13 organochlorine insecticides, and 4 chlorophenoxy-acid herbicides. Eight of these compounds exceeded detection levels. The three detected organophosphorus insecticides had the highest concentrations: median concentrations of parathion, diazinon, and malathion were 0.16, 0.11, and 0.02 micrograms per liter, respectively. The four detected organochlorine insecticides occurred less frequently: median concentrations of chlordane, lindane, methoxychlor, and endosulfan were <0.10, 0.01, <0.01, and <0.01 micrograms per liter, respectively. The only chlorophenoxy-acid herbicide detected was 2,4–D, which had a median concentration of <0.01 micrograms per liter. The mean rainfall of all sampled storms was 11.0 millimeters.

INTRODUCTION

As part of a study to characterize the quality of urban runoff for four different land-use sites in Fresno, California, rainfall samples were collected at two sites approximately 11 km apart over two rainy seasons from December 1981 through March 1983.

In addition to analysis of these rainfall samples for such conventional quality constituents as metals, nutrients, and major ions, analysis was also done for 26 selected pesticides known to have been used in the Fresno area. The pesticides consisted of organophosphorus and organochlorine insecticides and chlorophenoxy-acid herbicides. The analytical results showed that concentrations for eight of these compounds exceeded analytical detection levels for at least 1 of the 21 sampled storms. Of greatest concern was that several concentrations were above the "freshwater aquatic life" criteria established by the U.S. Environmental Protection Agency (EPA) (1976). The urban-characterization study was part of the EPA's National Urban Runoff Program and was a cooperative effort between the U.S. Geological Survey and the Fresno Metropolitan Flood Control District.

The city of Fresno is located about 260 km southeast of San Francisco, California, within the highly agricultural San Joaquin Valley (fig. 1). The valley is bounded by the Coast Ranges on the west and the Sierra Nevada on the east. Fresno is subject to winter storms that move from the Pacific Ocean over the Coast Ranges and into the valley. The average annual rainfall for the study area is about 250 mm, nearly all of which falls from October to April. During the first year of this study, the rainfall total was near this average; during the second year the total was about 2.3 times the average. The mean rainfall of the 21 sampled storms was 11.0 mm. The topography of the study area is virtually flat; the average gradient is approximately 1.5 m/km.

DATA COLLECTION

Rainfall samples for pesticide analyses were collected with sheet-metal collectors, which measured about 610 by 750 mm (fig. 2). The collectors were located on instrument-shelter rooftops about 3 m above ground level. Each collector was placed in position at the beginning of a storm and removed at the end. During a storm, rainfall landing on the metal collector drained into a glass jar for storage until the end of the storm. Each composite sample represents a single storm. A tipping-bucket rain gauge and a digital recorder were used to document the quantity of rainfall during each storm. After collection, the samples were transferred to 1-L glass bottles, sealed with foil-lined caps, and chilled to 4°C for shipment to the U.S. Geological Survey laboratory in Arvada, Colorado. The glass bottles were baked at 350°C prior to use.

ANALYTICAL METHODS

Organochlorine and organophosphorus compounds were extracted with hexane. The hexane extract was dried and concentrated to 1.0 mL, and a small portion of the extract was analyzed for organophosphorus compounds by gas chromatography on two dis-

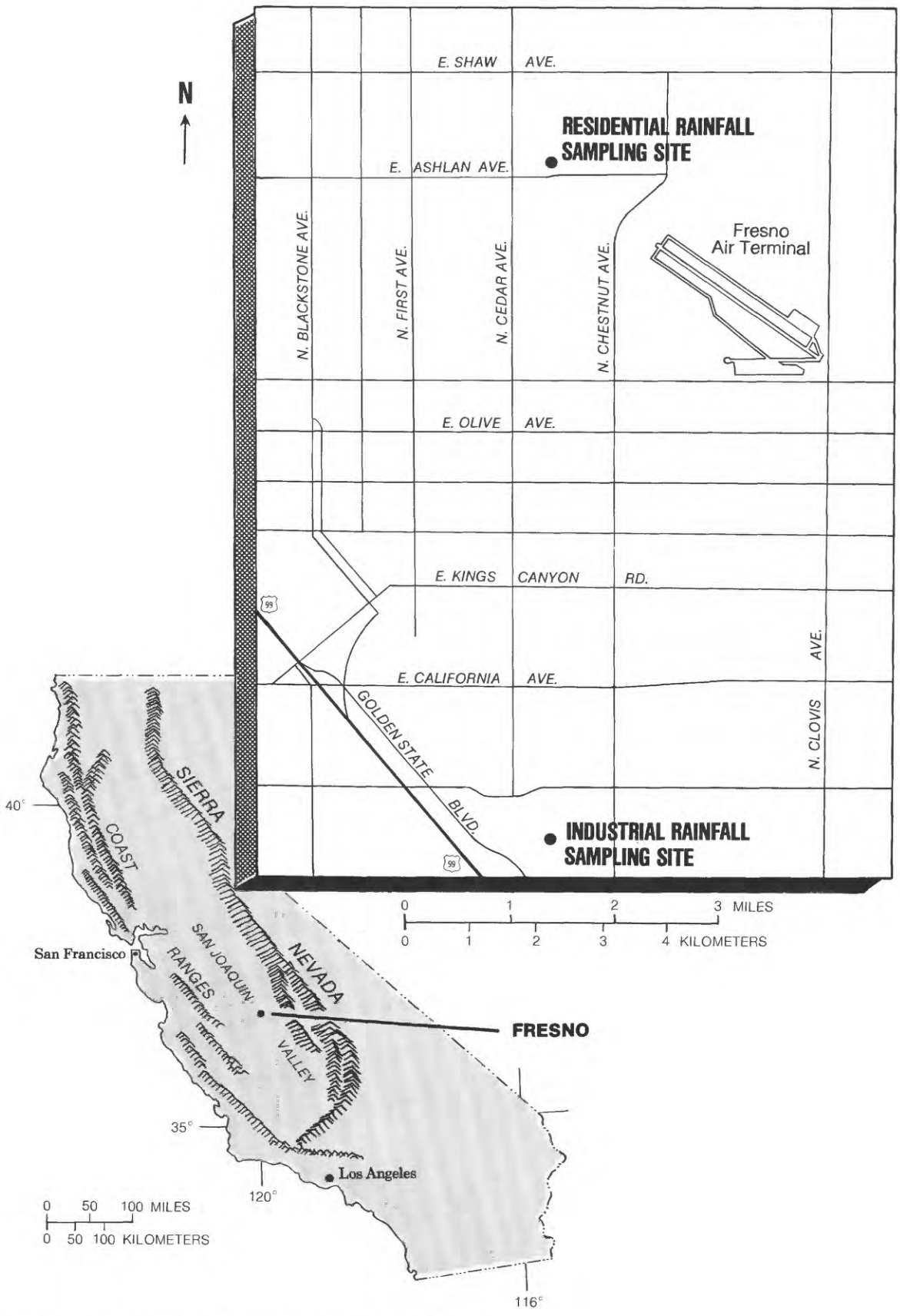

Figure 1. Location of rainfall sampling sites, Fresno, California.

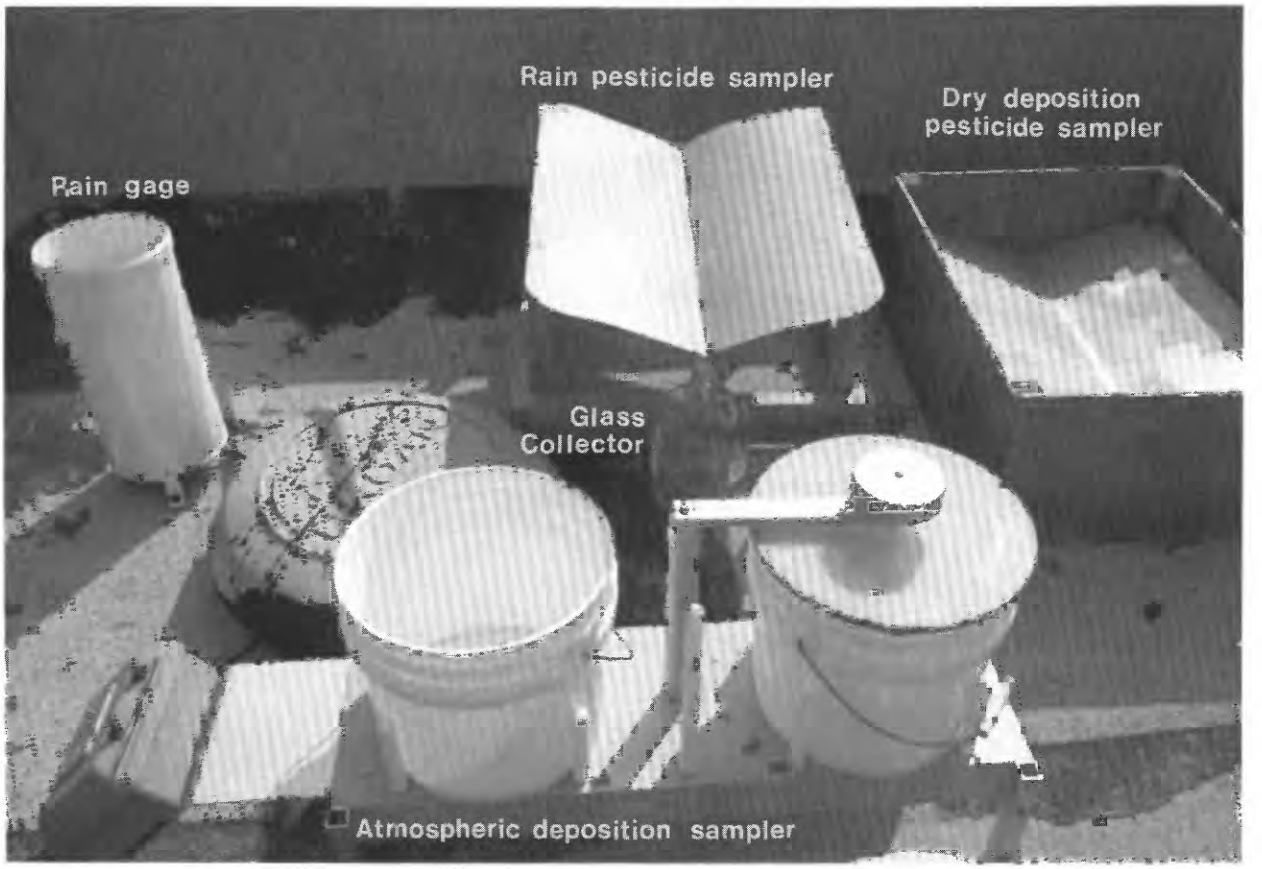

Figure 2. Equipment used to collect rainfall samples for pesticide analysis.

similar columns by use of flame photometric detectors operating in the phosphorus mode. The remaining portion of the extract was then chromatographed with hexane on deactivated alumina columns to remove compounds that would interfere with the organochlorine analyses. The extract was concentrated to 1.0 mL and analyzed by gas chromatography on two dissimilar columns by use of electron-capture detectors.

Pesticide analyses were performed in accordance with the standard method given in Wershaw and others (1987). The samples submitted for chlorophenoxy-acid herbicide analyses were acidified with sulfuric acid and extracted with unpreserved diethyl ether. The extract was heated with aqueous potassium hydroxide to saponify the esters and evaporate the ether. To reduce interference with the chlorophenoxy-acid analysis, the basic and neutral organic compounds were removed by extracting the basic solutions with diethyl ether. The remaining aqueous solution was acidified, and the chlorophenoxy-acid herbicides were extracted with ether. Benzene was added to the extract, and the extract was concentrated to about 1 mL. Boron trifluoride-methanol reagent was added to the benzene solution to produce methyl esters of the chlorophenoxy acids. The benzene solutions were chromatographed on florisil columns to remove compounds that would interfere with the analyses. The chlorophenoxy-acid methyl esters were then determined by gas chromatography on two dissimilar columns by use of electron-capture detectors.

DISCUSSION

The eight pesticides identified in rainfall during the 2-year study and their statistical summary are shown in table 1. The 18 pesticides that sample analysis did not detect during the study follow. The organophosphorus insecticides not detected were ethion, methyl parathion, trithion, and methyl trithion; the organochlorine insecticides not detected were aldrin, DDD, DDE, DDT, dieldrin, endrin, heptachlor, heptachlor epoxide, mirex, perthane, and toxaphene; the chlorophenoxy-acid herbicides not detected were 2,4–DP, 2,4,5–T, and silvex.

The organophosphorus compounds parathion, diazinon, and malathion were the most prevalent pesticides during the study period. The occurrences of parathion and diazinon correlated ($R = 0.71$). These two insecticides are used in the San Joaquin Valley primarily as

Table 1. Statistical summary of pesticides identified in rainfall samples from Fresno, California, December 1981 through March 1983

[Values are in micrograms per liter; mean and standard deviation were determined for diazinon because all values were greater than or equal to the detection limit]

Pesticide	Number of samples	Number of samples showing concentration at or above detection level	Mean	Median	Standard deviation	Minimum value	Maximum value
Organophosphorus							
Parathion	41	37	—	0.16	—	<0.01	1.00
Diazinon	41	41	0.15	.11	0.17	.01	.93
Malathion	41	37	—	.02	—	<.01	.11
Organochlorine							
Chlordane	40	8	—	<.10	—	<.10	.40
Lindane	40	29	—	.01	—	<.01	.04
Methoxychlor	40	6	—	<.01	—	<.01	.12
Endosulfan	40	12	—	<.01	—	<.01	.08
Chlorophenoxy							
2,4–D	35	9	—	<.01	—	<.01	.08

dormant sprays on fruit trees. The most common application method of these insecticides is a high-volume, truck-mounted sprayer, which tends to suspend large quantities of spray in the air and thus facilitate movement by wind currents. This form of application probably accounts for the presence of parathion and diazinon in rainfall.

Low concentrations of diazinon were detected in the early season storms in September, October, and November 1982 (fig. 3), but parathion did not become generally evident until the January 18, 1983, storm. Both compounds were detected throughout the remainder of the rainy season. The observed concentrations seem to depend on the total rainfall for each storm and the length of time since the last storm. Concentrations were generally higher during the first rainy season, but loadings were generally higher during the second rainy season, owing to the higher rainfall totals. An example of these concentrations and loading variations can be seen for parathion in figure 4.

Malathion concentrations were lower than parathion and diazinon during the study, and occurrence of this pesticide was more variable than for either parathion or diazinon (fig. 5). Malathion use has decreased in recent years; it is used mainly for mosquito control rather than for agricultural purposes. The organochlorine insecticides and the chlorophenoxy-acid herbicide 2,4–D were not detected as often or in as large concentrations as parathion or diazinon. Insecticides in the organochlorine group and 2,4–D are applied primarily by aircraft in the San Joaquin Valley. Organochlorine insecticides have been reported in rainfall in previous studies, including those by Bevenue and others (1972), Eisenreich and others (1981), and Strachan and Huneault (1979). Most of the occurrences in this study were during the first rainy

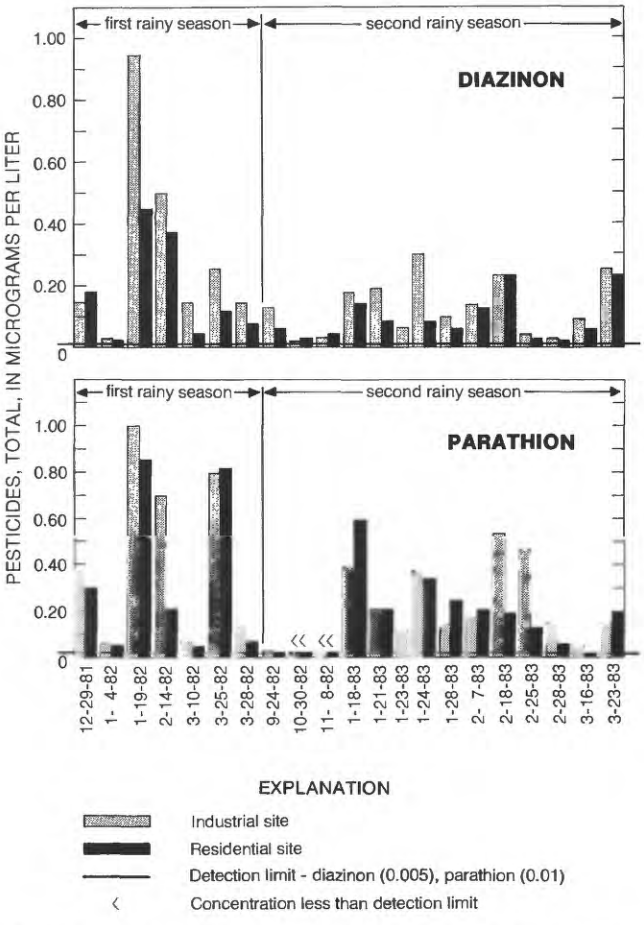

Figure 3. Concentrations of diazinon and parathion in storm-composite samples collected at two sites in Fresno, California.

Figure 5. Concentrations of selected pesticides in storm-▶ composite samples collected at two sites in Fresno, California.

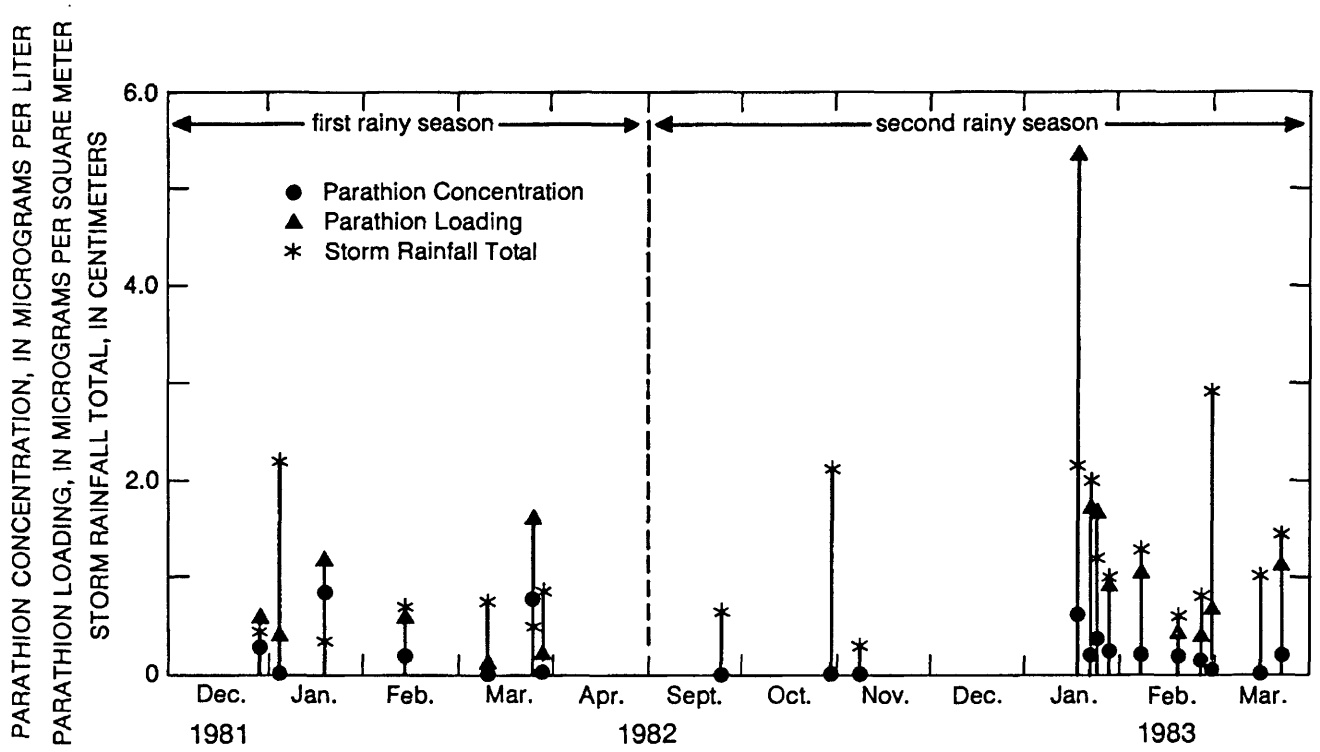

Figure 4. Parathion concentrations, parathion loading, and storm rainfall totals at the residential site.

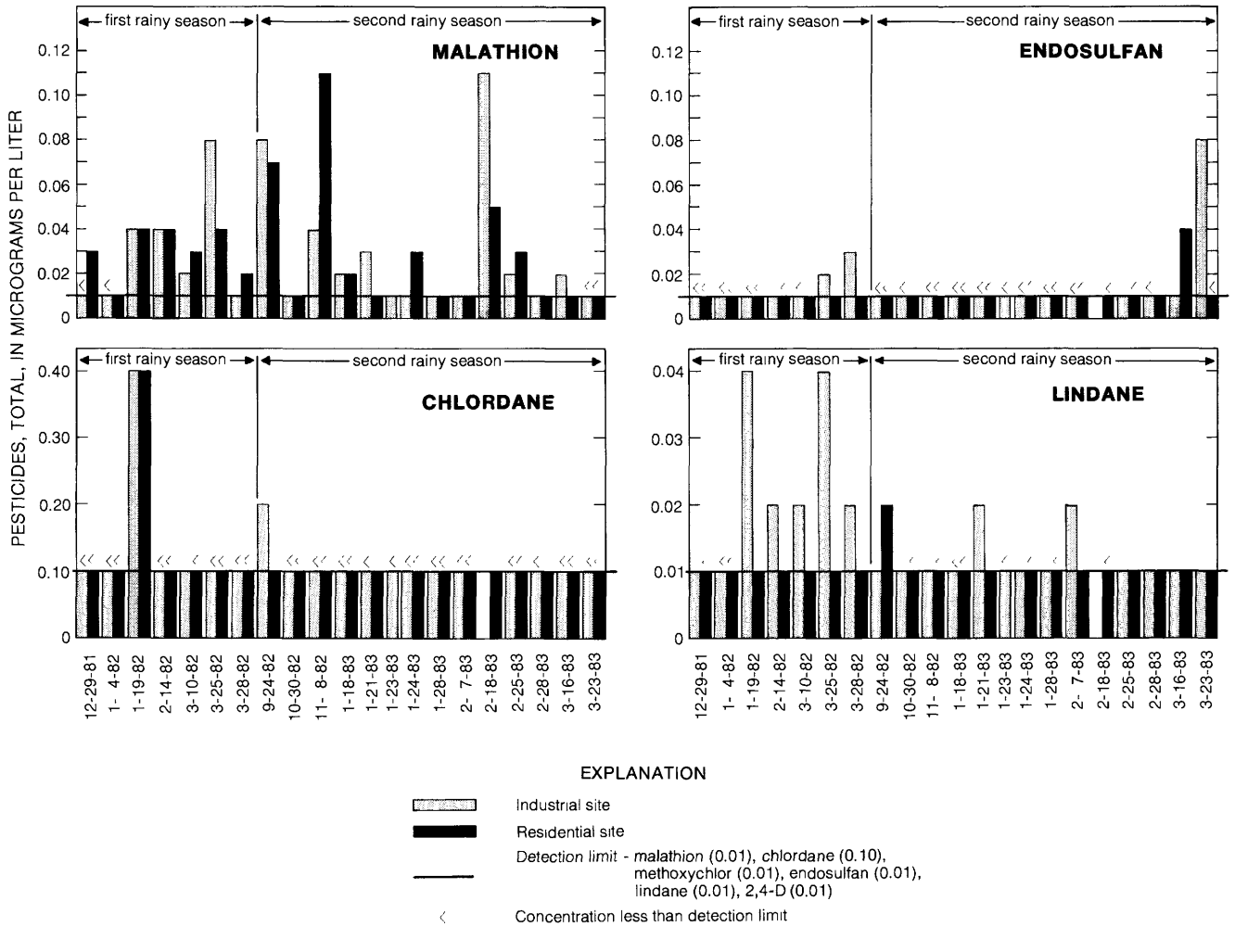

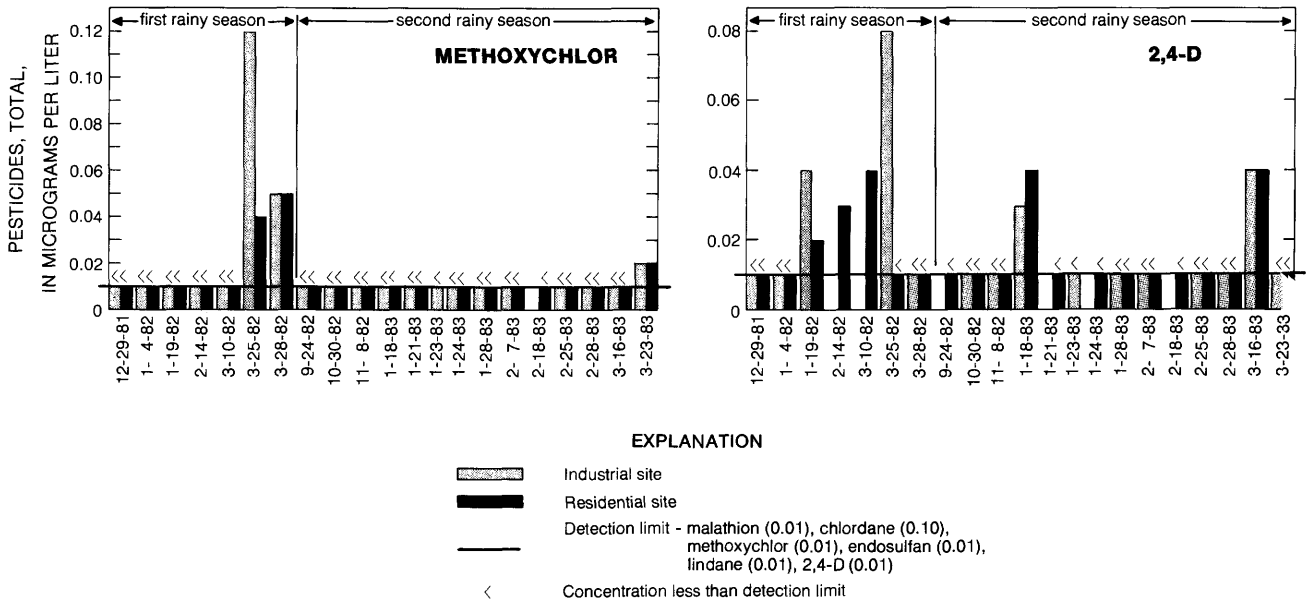

Figure 5.—Continued

season, which had considerably less rainfall than the second rainy season. Chlordane was found mostly at or below detection level (0.10 μg/L), except during one storm in the first rainy season, when the pesticide exceeded detection level at both sites, and then once more at the industrial site only (fig. 5). Methoxychlor and endosulfan exceeded detection level only during March of both years (1982 and 1983) (fig. 5). Lindane exceeded detection level only once at the residential site, but for unknown reasons it exceeded detection level seven times at the industrial site, five of them during the first year of the study (fig. 5). The chlorophenoxy-acid herbicide 2,4–D exceeded detection level only during January through March (fig. 5) of both rainy seasons (1982 and 1983).

The detection of most of these pesticides in the Fresno area rainfall generally coincided with periods in which pesticides are known to be applied to the trees and fields in the surrounding agricultural areas. This coincidence suggests that the rainfall quality is related to localized activities. Data are not available, however, to show to what extent these pesticides are transported from their application points.

REFERENCES CITED

Bevenue, A., Ogata, J.N., and Hylin, J.W., 1972, Organochlorine pesticides in rainwater, Oahu, Hawaii, 1971–72: Bulletin of Environmental Contamination and Toxicology, v. 8, no. 4, p. 238–241.

Brown and Caldwell, 1984, Fresno nationwide urban runoff program project, final report: Fresno, California, Fresno Metropolitan Flood Control District.

Eisenreich, W.J., Looney, B.B., and Thornton, J.D., 1981, Airborne organic contaminants in the Great Lakes ecosystem: Environmental Science and Technology, v. 15, no. 1, p. 30–38.

Strachan, W.M.J., and Huneault, H., 1979, Polychlorinated biphenyls and organochlorine pesticides in Great Lakes rainfall: Journal of Great Lakes Research, v. 5, no. 1, p. 61–68.

U.S. Environmental Protection Agency, 1976, Quality criteria for water: U.S. Environmental Protection Agency, 256 p.

Wershaw, R.L., Fishman, M.F., Grabbe, R.R., and Lowe, L.E., 1987, Methods for the determination of organic substances in water and fluvial sediments: U.S. Geological Survey Techniques of Water-Resources Investigations, Book 5, Chapter A3, 80 p.

The Flux of Particulate Organic Carbon in Estuaries: Phytoplankton Productivity and Oxygen Consumption

By David H. Peterson, Laurence E. Schemel, Richard E. Smith, Dana D. Harmon, *and* Stephen W. Hager

Abstract

Phytoplankton are by definition the principal source of organic matter in phytoplankton-based estuaries. Conceptually, such estuaries with higher phytoplankton productivity (higher carbon flux) have the capacity to maintain higher organic-matter mineralization rates and thus higher oxygen consumption rates than estuaries with lower productivity. To test this concept in a preliminary way we compare two possible phytoplankton-based estuaries: Chesapeake Bay (and its tributary Potomac estuary) and northern San Francisco Bay. Reported estimates of annual mean phytoplankton productivity are higher for Chesapeake Bay than for northern San Francisco Bay and, indeed, the rates of water-column oxygen consumption are also consistently higher in Chesapeake Bay than in San Francisco Bay. Furthermore, the literature values of water-column oxygen consumption rates from other estuaries are within the approximate range observed for San Francisco and Chesapeake Bays, or, are even higher. Apparently our estimate of the "average" rate of water-column oxygen consumption in northern San Francisco Bay, 6 micromoles O_2 per liter per day, represents a low estuarine value, but this rate is still higher than similar rates reported for the photic ocean.

INTRODUCTION

Variability in the biogeochemistry of many aquatic systems is controlled predominately by rates of supply, dilution, and removal of organic matter. Since phytoplankton are often the principle source of such organic matter, aquatic systems are often classified solely on the basis of their phytoplankton productivity. In very large systems such as the oceans, however, observed local biogeochemical rates are not always representative of the system as a whole or even major portions of the system. For example, observations of dissolved silica fluxes estimated from benthic chamber experiments off the northwest coast of Africa (Rowe and others, 1977) appear to overestimate the average benthic flux beneath shelf waters when extrapolated to this entire region (Carothers and Grant, 1983).

Estuaries are also difficult to fully characterize by a few discrete observations such as phytoplankton productivity and benthic exchange because estuaries are located at the crossroads between terrestrial and marine environments. As a result, estuarine distributions are highly variable, and few generalizations about estuarine systems have ever been attempted. For these reasons a review from the early 1970's stated ". . . what we know of the broadest biotic functions of estuaries is still largely guess work" (Woodwell and others, 1973).

One generality that does seem to be broadly applicable in understanding the biogeochemistry of estuaries is that estuaries with higher concentrations of suspended sediment and consequently higher diffuse-light extinction coefficients have lower phytoplankton productivity than estuaries with lower suspended sediment concentrations (table 1; see also Wofsy, 1983; Day, 1981; Pennock and others, 1983; and Peterson and Festa, 1984). And, to the extent that phytoplankton are the major source of organic matter, we propose that phytoplankton productivity in estuaries is a controlling mechanism for many biogeochemical processes. We test this premise in a preliminary way by comparing rates of oxygen consumption in the water column of northern San Francisco Bay, an estuary with below-average annual phytoplankton productivity, to rates in Chesapeake Bay, an estuary with above-average productivity. The link, if any, between phytoplankton-based systems and oxygen consumption is a relatively recent subject of research because oxygen consumption rates in most systems are poorly defined (Packard and others, 1983). Thus, in an attempt to put the oxygen consumption rates for northern San Francisco Bay and Chesapeake Bay into perspective, we have reviewed published oxygen consumption rates from the ocean and other estuaries.

Table 1. Estuarine phytoplankton productivity and optical depth

[Optical depth is the inverse of the diffuse-light extinction coefficient; see text and references for details regarding this and other estuarine parameters]

Estuary	Phytoplankton productivity ($g\ C\ m^{-2}y^{-1}$)	Optical depth (m)	References
Neuse River	520	0.77	Fisher and others, 1982a.
Chesapeake Bay	480	.91	Boynton and others, 1982; Champ and others, 1980.
Narragansett	310	.98	Furnas and others, 1976; Oviatt and others, 1981.
Delaware Estuary	290	.67	Pennock and others, 1983.
South River	290	.40	Fisher and others, 1982b.
Northern San Francisco Bay	110	.50	Cole, 1982; Peterson, 1979.
Wassaw Estuary	90	.56	Turner and others, 1979.
Ems	55	.48	Cadee and Hegman, 1974.
Dollart	13	.11	Cadee and Hegman, 1974.

Reviews by W. Broenkow, R.S. Carney, R. Harvey, D. Johnson, and A.Y. Ota, discussions with T. Callender, T.J. Conomos, Douglas Hammond, J.F. Festa, F.H. Nichols, and J.K. Thompson, and technical assistance of S. Chapralis, J.S. DiLeo-Stevens, and the San Francisco Bay and Potomac Estuarine research teams are appreciated.

A CONCEPTUAL MODEL

In this report, the concept of estuaries is simplified by assuming light intensity as the principal forcing function for the in-situ production of organic matter. Several estuaries follow a broad relation between mean annual productivity and optical depth (table 1). Optical depth is the reciprocal of the diffuse-light extinction coefficient.

Our model assumes that estuaries having higher rates of productivity (more available light) support higher rates of mineralization. This simple model provides a frame of reference for evaluating some of the many positive (and negative) feedback mechanisms that considerably complicate estuaries and facilitates broad comparisons between diverse estuaries. In general, then, high rates of mineralization are considered a consequence rather than the cause of high productivity. Additional assumptions include neglect of water circulation and mixing effects and nutrient sources, but to some extent water circulation and mixing must control light intensity and, therefore, is considered.

METHODS OF STUDY

Phytoplankton productivity was studied in northern San Francisco Bay during 1976 and 1977 (daylight and 24-hour rates, Peterson and others, 1984, unpub. data) and 1980 (24-hour rates, B.E. Cole, 1982) and by others in Chesapeake Bay during 1977 and 1978 (Kemp and Boynton, 1981) and in its tributary Potomac estuary during 1977 and 1978 (short term, daylight and 24-hour rates, Cole and Harmon, 1981). Dark-bottle oxygen consumption was studied in northern San Francisco Bay during 1976 and 1977 (12- and 24-hour rates, Peterson and others, 1984, unpub. data), and in Chesapeake Bay during 1977 and 1978 (Kemp and Boynton, 1981), and in its tributary Potomac estuary during 1977 and 1978 (12- and 24-hour rates, Cole and Harmon, 1981). Sample locations and methods are detailed in these reports.

For purposes of comparison the following conversion factors were used throughout this paper: optical depth equals Secchi depth times 1.5 (Holmes, 1970), 1 mole O_2 produced equals 1 mole C fixed, and 1 mole C mineralized equals 1 mole O_2 consumed. Oxygen consumption rates from the various sources were not normalized for temperature effects.

RESULTS AND DISCUSSION

Although observations of dark-bottle oxygen consumption are a gross and relatively low-precision measurement, the results are reproducible. For example, in agreement with Williams (1982), we saw no significant differences in dark-bottle rates during the Potomac estuarine study between daylight and 24-hour incubation experiments (for a range in values of 14 to 130 μmole O_2 $L^{-1}d^{-1}$ (μmole = 10^{-6} molecular weight) (the daylight rate = 0.02 + 1.01 times the 24-hour rate and with a mean deviation $\pm$4.4 μmole O_2 $L^{-1}d^{-1}$; the correlation coefficient, R^2, = 0.94; the number of samples, n, = 22). Also, many oxygen consumption rates observed in San Francisco Bay are probably near our limit of analytical detection and, therefore, these rates are clearly lower than those observed in the outer Potomac estuary by use of the same techniques (fig. 1). Further validation of this estuarine difference in rates is provided by Kemp and Boynton (1981). Their measurements in Chesapeake Bay by different techniques but at the same time of the year as our Potomac estuary rates showed similar or even higher values (fig. 1).

On the basis of presently available data, Chesapeake Bay has one of the highest phytoplankton productivities and presumably highest oxygen consumption rates, whereas northern San Francisco Bay is an estuary with lower productivity and oxygen consumption rates (tables 1 and 2). We explore this difference in the following way. First the offshore decrease in concentration of organic matter in the ocean and some of the consequences with regard to oxygen consumption are briefly reviewed. Then we characterize some of the

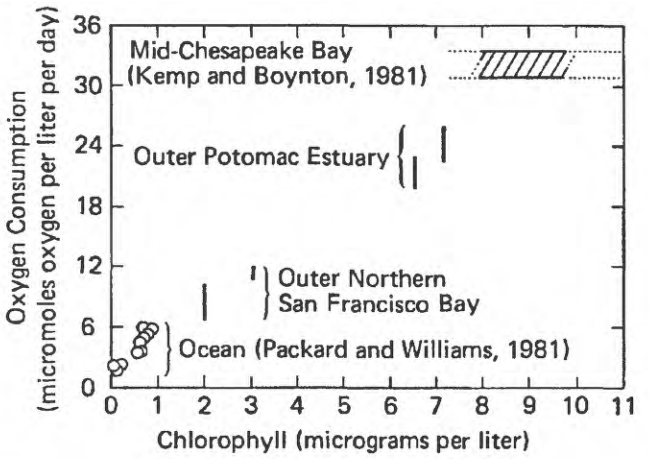

Figure 1. Oxygen consumption rates and chlorophyll concentrations for outer San Francisco Bay estuary, Chesapeake Bay (including outer Potomac estuary), and the ocean.

Table 2. Water-column oxygen consumption rates in estuaries and the ocean

Location	Temperature (°C)	Chlorophyll concentration ($\mu g L^{-1}$)	Water column oxygen consumption ($\mu mole\ O_2\ L^{-1} d^{-1}$)	References
Chesapeake Bay . .	18	6	16	Kemp and Boynton, 1981; Flemer, 1970.
Northern San Francisco Bay . . .	18.9	6.2	6.4	Peterson and others, unpub. data 1984.
Shelf water	16.7	.83	5.5	Packard and Williams, 1981.
Shelf water	16.4	.66	3.9	Packard and Williams, 1981.
Slope water	20.9	.24	2.1	Packard and Williams, 1981.
Slope water	21.2	.18	1.9	Packard and Williams, 1981.

possible biological differences between Chesapeake Bay and northern San Francisco Bay that could be related to observed differences in oxygen consumption rates. Lastly, we provide an additional basis for comparison by summarizing published observations of oxygen consumption in other estuaries.

The Ocean

Estuaries are open to the ocean and intuitively there must be a continuum of processes from the outer estuary into the ocean. Most of the oxygen consumption in the photic zone of the ocean is attributable to phytoplankton and bacterial respiration (Williams, 1981, 1982). Consequently, when phytoplankton and bacterial abundance decrease in waters beyond the continental

Table 3. Macroscopic benthic biomass in estuaries and the ocean

[Calculated as ash-free dry weight based on conversion factors of Lie (1969) for wet weight; see text for details concerning calculation]

Location	Water depth (m)	Benthic biomass ($g\ m^{-2}$)	References
Chesapeake Bay	3–6	1–35	Kemp and Boynton, 1981.
Northern San Francisco Bay.	1–11	.07–9	Thompson and Nichols, 1984.
Continental shelf/slope.	<2,000	2–14	Cary, 1972.
Deep sea (Gulf of Mexico). . . .	<2,000	>.02	Rowe, 1971; Rowe and Menzel, 1971.

Table 4. Benthic oxygen consumption in estuaries and the ocean

Location	Benthic oxygen consumption ($\mu mole\ m^{-2} d^{-1}$)	References
Chesapeake Bay	34[1]	Kemp and Boynton, 1981.
San Francisco Bay	25	D. D. Hammond, oral commun., 1984.[2]
California Shelf	3–11	Smith and others, 1983; Hartwig, 1974.[3]
North Pacific deep sea	.3	Smith and others, 1983.

[1]Annual mean.
[2]Based primarily on studies in south San Francisco Bay.
[3]Cited in Fisher and others, 1982a.

shelf (J.J. Cole, 1982; Fenchel, 1982; Ducklow, 1983, Linley and others, 1983), oxygen consumption rates also decrease (table 2).

Decreasing benthic activity beyond the continental shelf is attributed largely to increasing water depth (Rowe, 1983; Theil, 1983; Carney and others, 1983). Thus, the relative abundance of marine benthic animals in the deep sea is thought to reflect the incoming organic carbon flux to that region. For instance, animal biomass decreases dramatically from the continental shelf to the deep sea (table 3) apparently in response to a similar decrease in flux of particulate organic carbon (Suess, 1980). Similarly, decreases in benthic biomass with increasing depth in the sea is apparently greatest in regions of low phytoplankton productivity (Rowe, 1971). However, the abundance of macrobenthic organisms is only one of several indicators of the incoming organic carbon flux (Lyle, 1983); another is the rate of benthic oxygen consumption (Nixon, 1981; Smith and others, 1983; table 4).

In summary, relative to most estuarine systems the photic waters of the open ocean must represent low abundances of phytoplankton and bacteria and, therefore, are near or lower than the lowest rates of oxygen

consumption observed in estuarine waters. Similarly, benthic biomass and oxygen consumption in the deep ocean is, obviously, considerably less than for estuarine and coastal shelf systems.

San Francisco Bay and Chesapeake Bay

Annual mean phytoplankton productivity for Chesapeake Bay (fig. 2) is clearly higher than for San Francisco Bay (Flemer, 1970; Biggs and Flemer, 1972; Kemp and Boynton, 1981; Officer and others, 1984; B.E. Cole, 1982). Estuarine oxygen consumption rates , however, are less well documented but must be higher than oceanic rates. To illustrate this, it is instructive to estimate a possible contribution of phytoplankton respiration to oxygen consumption by using allomeric equations (Peters, 1983; Seim and Seather, 1983; Fenchel and Finley, 1983) for respiration in agreement with Williams (1982). In coastal and outer estuarine waters of San Francisco Bay (an area of deep photic depth and high productivity relative to the inner estuary), the phytoplankton population is assumed to be 2.6×10^6 cells L^{-1} (annual mean value near Golden Gate, Wong and Cloern, 1982). Using an allomeric phytoplankton respiration equation (Banse, 1976) and assuming 86 pg C $cell^{-1}$ and 2.8 μg chlorophyll L^{-1} (Wong and Cloern, 1982), we arrive at an oxygen consumption of 1.7 μmoles O_2 $L^{-1}d^{-1}$ (μg chlorophyll)$^{-1}$, or 4.8 μmoles O_2 $L^{-1}d^{-1}$. This estimate of phytoplankton respiration in the outer estuarine waters of the bay suggests the observed rates are reasonable.

Perhaps even less is known about estuarine benthic communities than is known about estuarine oxygen consumption rates. Whether or not estuarine benthic biomass is a valid indicator of organic carbon flux has not yet been established. Nevertheless, for completeness, some information on benthic biomass in San Francisco Bay and Chesapeake Bay is included.

Macrobenthic animal biomass in northern San Francisco Bay tends to be lower than in Chesapeake Bay (table 3). Winter-fall average biomass in the outer estuary, which is least influenced by fresh water inflow, was 50 g/m^2 wet weight (Thompson and Nichols, 1984). This is less than 4 g/m^2 ash-free dry weight. (To make this conversion, a phylum-weighted conversion factor of 0.07 g ash-free dry weight per gram of wet weight was used (Lie, 1968). Almost 90 percent of the wet biomass was mollusca, with the remainder annelida and arthropoda (Thompson and Nichols, 1984).)

Although macrobenthic organisms account for only a fraction of benthic oxygen consumption (Smith, 1973), benthic oxygen consumption in San Francisco Bay is lower than in Chesapeake Bay (table 4). Annual-mean benthic oxygen consumption in San Francisco Bay is estimated to be 24 mmoles O_2 $m^{-2}d^{-1}$ (Douglas Hammond, oral commun., 1984). This estimate is based largely on observations from south San Francisco Bay. Interestingly, benthic biomass is highest at locations in south San Francisco Bay where phytoplankton productivity is highest (B.E. Cole, 1982) and where phytoplankton standing stock is possibly controlled by benthic filter feeding (Cloern, 1982).

In general, differences in oxygen consumption rates (water column and benthic) between northern San Francisco Bay and Chesapeake Bay are consistent with their differences in phytoplankton productivity. The oxygen consumption rates seem to be realistic, but to further verify this, we review the oxygen consumption rates from other estuarine studies on a case by case basis.

Narragansett Bay, Rhode Island

An estimate of phytoplankton productivity in Narragansett Bay is 310 g C $m^{-2}y^{-1}$ (based on 24-hour carbon-14 incubation experiments, Furnas and others, 1976). Of course temporal, spatial, and experimental design variability are all complications in estimating both annual productivity (Oviatt and others, 1981) and oxygen consumption, but oxygen consumption is further complicated because most wet chemical methods cannot measure small rates. Oxygen consumption rates less than 30 μmole O_2 $L^{-1}d^{-1}$ in Narragansett Bay were considered to be unreliable (38 of 46 observations were less than 30 μmole $L^{-1}d^{-1}$, Oviatt and others, 1981). Thus, an alterna-

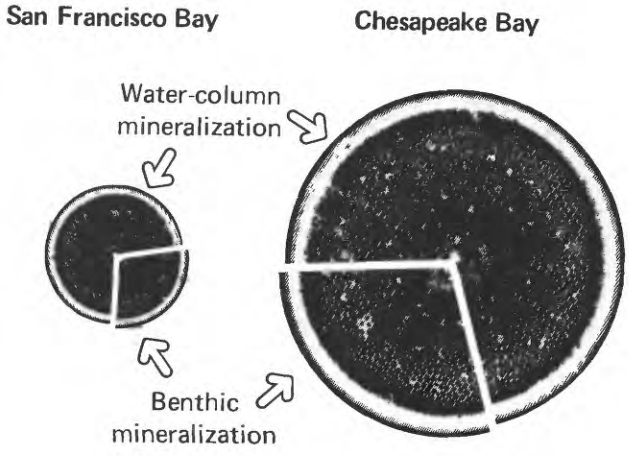

Figure 2. Simplified pie diagrams of relative magnitudes of phytoplankton productivity and mineralization in San Francisco Bay and Chesapeake Bay (illustrated with the diatom *Thalassiosira wongii*). The relative proportions of water-column to benthic mineralization are idealized and are virtually unknown. See text for some discussion of data and assumptions. Range of chlorophyll for Chesapeake Bay is roughly estimated from determinations of suspended particulate organic carbon (Kemp and Boynton, 1981) and chlorophyll distributions for this mid-estuarine region (Flemer, 1970).

tive to direct estimate of oxygen consumption was made. It was assumed that the ratio of daylight water-column oxygen productivity to night respiration was the same in Narragansett Bay as their observed ratio in experimental microcosm tanks. Note that annual-mean respiration in the microcosm tanks including the walls and water but not bottom sediment was 15 μmole O_2 $L^{-1}d^{-1}$ (Oviatt and others, 1981). Assuming, then, that night oxygen consumption equals daylight oxygen productivity divided by 1.7 (Oviatt and others, 1981) and assuming a 12-hour night, oxygen consumption in the bay is 94 mmole $m^{-2}d^{-1}$. Therefore, for a mean water depth of 9 m (Kremer and Nixon, 1978) annual mean oxygen consumption is 10 μmole O_2 $L^{-1}d^{-1}$. Annual mean benthic oxygen consumption is 32 mmole O_2 $m^{-2}d^{-1}$ (Nixon and others, 1976).

Newport River Estuary, Rhode Island

Results for this estuary are included because they provide an estuarine example in which phytoplankton biomass is relatively low. As a caution, however, a simple profile of this system could be misleading because in contrast to the previously described systems the average water depth, 1.2 m, is less than the photic depth (Williams and Murdoch, 1966; Williams, 1966) and benthic filter feeding is considered to be an important control on phytoplankton standing stock (Officer and others, 1982).

Annual mean phytoplankton standing stock is 2 $\times$ 10^6 cells L^{-1} and (or) 4 μg chlorophyll L^{-1} (Williams and Murdoch, 1966; Williams, 1966). Annual (net) productivity, 48 g C $m^{-2}y^{-1}$, must be less than the potential productivity because the mean depth of the estuary is less than the photic depth. Using their observation that water-column respiration is 48 percent gross photosynthesis per unit area, oxygen consumption is 13 μmole O_2 $L^{-1}d^{-1}$ (19 in summer and 7 μmole O_2 $L^{-1}d^{-1}$ in winter).

In this estuary annual mean oxygen consumption is two times higher than the value observed for San Francisco Bay, whereas productivity is two times lower than for San Francisco Bay. However, Newport estuary is very shallow and although productivity on an area basis is two times lower than for San Francisco Bay, on a volume basis productivity is about two times higher than for San Francisco Bay (and oxygen consumption on a volume basis is also correspondingly higher than for San Francisco Bay).

Dollart Estuary, The Netherlands

This is an organic-waste-dominated estuary tributary to the Ems estuary (Van Es and Ruardij, 1982). Annual mean phytoplankton standing stock is 9 μg chlorophyll L^{-1}, and productivity is only 13 g C $m^{-2}y^{-1}$, but waste input is 400 g C $m^{-2}y^{-1}$ and benthic oxygen consumption is high, between 50 and 60 mmole O_2 $m^{-2}d^{-1}$.

Waste waters of the Dollart are partially mixed and diluted with waters from the major Ems estuary (Van Es and Ruardij, 1982). In the Ems, the lowest oxygen consumption rates are only 6 μmole $L^{-1}d^{-1}$ (except in the outer estuary during phytoplankton blooms, when oxygen consumption rates are 10 to 15 μmole $L^{-1}d^{-1}$). An annual average value of oxygen consumption in the Dollart is about 16 μmole $L^{-1}d^{-1}$. During summer, when average water temperatures are higher (20°C), oxygen consumption rates in the Dollart vary from 7 μmole O_2 $L^{-1}d^{-1}$ near the mouth to 30 μmole O_2 $L^{-1}d^{-1}$ near the waste-dominated inner reaches. Thus, the carbon fluxes (phytoplankton plus waste-derived) and oxygen consumption rates are higher than for San Francisco Bay and similar to values estimated for Chesapeake Bay.

Wassaw Estuary, Mississippi

This system is similar to the Dollart in that nonphytoplankton sources of organic matter apparently support higher rates of oxygen consumption than might be expected from phytoplankton productivity alone. Annual mean oxygen consumption is 14 μmole O_2 $L^{-1}d^{-1}$ and varies between about 15 to 60 μmole O_2 $L^{-1}d^{-1}$ in summer (Turner, 1978). Although annual mean phytoplankton productivity, 90 g C $m^{-2}y^{-1}$, is not sufficient to support these observed rates of dissolved-oxygen consumption (Turner and others, 1979), the shortfall of organic matter is met by dissolved organic carbon exudates from nearshore macroscopic algae (about 190 g C $m^{-2}y^{-1}$, Turner, 1978).

Southhampton Estuary, England

Background rates of oxygen consumption in the upper estuary were between 5 and 10 μmole O_2 $L^{-1}d^{-1}$ (Lima and Williams, 1978). Rates increased to about 23 μmole O_2 $L^{-1}d^{-1}$ when chlorophyll peaked to about 24 μg chlorophyll L^{-1}, but these rates may have been up to 2 times higher because phytoplankton activity varied between 50 and 100 percent after sample processing (Lima and Williams, 1978).

IMPLICATIONS

Oxygen consumption rates in San Francisco Bay are consistently lower than in Chesapeake Bay (table 2 and references cited therein) and seem to be in the range expected on the basis of results from the ocean, other estuaries, and differences in organic carbon flux such as phytoplankton productivity per unit area. However, esti-

mating annual rates of water-column oxygen consumption in estuaries is confounded by two limitations: in many instances the observed rates are near analytical precision and the temporal and spatial sampling frequency is minimal. Thus, these differences between estuaries are considered qualitatively valid only.

There is a link between phytoplankton productivity and benthic oxygen consumption in many shallow-water coastal marine environments including estuaries, even though only 25 to 50 percent of the supply of organic matter is mineralized on the bottom (Nixon, 1981). Potentially, then, almost 50 to 75 percent of the organic matter is available for mineralization in the water column, burial in the bottom sediment, or export to the sea. As an example calculation for the water column, using a mean-tide water depth of 4 m for northern San Francisco Bay and our estimated mean oxygen consumption rate of 6 μmole O_2 $L^{-1}d^{-1}$, annual water-column consumption of organic carbon in northern San Francisco Bay is 100 g C $m^{-2}y^{-1}$. This rough estimate suggests that the observed rates of oxygen consumption are reasonable and close to what might be expected if phytoplankton are the principal source of organic matter that is mineralized in the northern bay (table 1).

Sediment-associated organic matter borne by rivers is also an important source, but some of this organic matter is undoubtedly refractile and, as such, accumulates in bottom sediment. It is also unknown what fraction of annual phytoplankton productivity supports benthic oxygen consumption. Nevertheless, it seems impressive that annual mean benthic oxygen consumption rates in Chesapeake Bay (table 4) are equivalent to 150 g C $m^{-2}y^{-1}$, because this makes benthic organic-matter mineralization rates in Chesapeake Bay similar to, or even possibly higher, than annual mean phytoplankton productivity in northern San Francisco Bay (table 1).

Spatial variability in oxygen consumption rates are poorly defined but are probably very important to estuarine budgets. For example, oxygen consumption rates in near-surface waters can be higher than at depth because oxygen consumption in near-surface photic waters includes respiratory growth and maintenance processes, whereas oxygen consumption in aphotic waters at depth may be attributed solely to maintenance processes (Rivkin and others, 1982). As an example calculation, using a mean water depth of 7 m (Jaworski, 1981) and an annual mean oxygen consumption rate of 16 μmole O_2 $L^{-1}d^{-1}$ makes annual water-column consumption of organic carbon in Chesapeake Bay 490 g C $m^{-2}y^{-1}$. This calculation used average rates of oxygen consumption from water depths of 3 to 6 m (Kemp and Boynton, 1981). As such the oxygen consumption rates may be weighted to higher near-surface values than an average value for Chesapeake Bay as a whole, because more than 30 percent of the area of Chesapeake Bay is at a water depth greater than 9 m (Pritchard, 1952). The average depth of Narragansett Bay is 9 m, and Oviatt and others (1981) observed that oxygen consumption rates from samples at depth were frequently less than near-surface samples (see also Turner and Allen, 1982). On the average, obviously, amounts of light and photosynthesis are lower at depth. Similarly, estuary respiration (per unit volume) in the Newport River was a smaller percentage, 19 percent, of gross maximum photosyntheses (per unit volume at the 50 percent light intensity) in the two instances of extremely high turbidity (optical depths of 0.13 and 0.19 m) in comparison to the estuarine average of 29 percent (Williams, 1966).

Oxygen consumption rates tend to increase with increasing chlorophyll concentrations (noted in discussion above and Fisher and others, 1982b). Because annual mean chlorophyll concentrations in San Francisco Bay and Chesapeake Bay are apparently similar (table 2), specific photosynthetic activity in Chesapeake Bay is most likely, higher on the average than San Francisco Bay. This is probably a physical and physiological consequence of the lower average suspended sediment concentration in surface waters of Chesapeake Bay than in San Francisco Bay (Flemer, 1970; Biggs and Flemer, 1972; Conomos and others, 1979; Wofsy, 1983; Cole and Cloern, 1984; Peterson and Festa, 1984).

Although observations of dissolved-oxygen consumption rates are a very gross parameter, such rates seem to provide a general frame of reference for unanswered questions regarding Chesapeake and San Francisco Bays. High phytoplankton biomass and productivity support high bacterial biomass and productivity (J.J. Cole, 1982; Linley and others, 1983; Ducklow, 1983; Azam and others, 1983) but it remains to be seen if the average bacterial biomass, productivity, and associated microbial activities are indeed higher in Chesapeake Bay than in northern San Francisco Bay.

Estuaries having very high annual rates of phytoplankton productivity (table 1) tend to have low ambient concentrations of dissolved inorganic nutrients, in comparison to estuaries having low productivity (Chesapeake Bay versus San Francisco Bay). Narragansett Bay, in fact, is considered slightly oligotrophic (Kremer and Nixon, 1978). In the broad range of estuaries considered, we assumed that organic-matter recycling rates largely depend on phytoplankton productivity. But in the estuaries of relatively high phytoplankton productivity, phytoplankton productivity also depends on organic-matter recycling rates (positive feedback). This is one explanation why long-term increases in nutrient sources are considered to be an important control altering the biogeochemistry of Chesapeake Bay (Officer and others, 1984), but perhaps less so for northern San Francisco Bay.

In summary, it is understandable that there is a reluctance to make generalizations about the biogeochemistry of estuaries because they are very complex systems and to a large degree each system is unique. Preliminary interpretations indicate that estuarine oxygen consumption rates make sense when the magnitude of organic source is known or approximately known and when considered on annual or, possibly, seasonal time scales.

REFERENCES CITED

Azam, F., Fenchel, Thomas, Field, J.G., Gray J.S., Meyer-Reiland, L.A., Thingstad, F., 1983, The ecological role of water-column microbes in the sea: Marine Ecology—Progress Series, v. 10, p. 257–263.

Banse, Karl, 1976, Rates of growth, respiration and photosynthesis of unicellular algae as related to cell size—a review: Journal of Phycology, v. 12, p. 135–140.

Biggs, R.B., and Flemer, D.A., 1972, The flux of particulate carbon in an estuary: Marine Biology, v. 12, p. 11–17.

Boynton, W.R., Kemp, W.M., and Keefe, C.W., 1982, A comparative analysis of nutrients and other factors influencing estuarine phytoplankton production, *in* Kennedy, V.S., ed., Estuarine comparisons: Academic Press, New York, p. 69–90.

Cadee, G.C., and Hegman, John, 1974, Primary production of phytoplankton in the Dutch Wadden Sea: Netherlands Journal of Sea Research, v. 8, p. 240–259.

Carney, R.S., Haedrich, R.L., and Rowe, G.T., 1983, Zonation of fauna in the deep sea, *in* Rowe, G.T., ed., The sea, v. 8, Deep-sea biology: John Wiley and Sons, p. 371–398.

Carothers, P.E., and Grant, W.E., 1983, Systems analysis and simulation of the N.W. African marine upwelling region: Ecological Modelling, v. 19, p. 73–103.

Cary, A.G., 1972, Ecological observations on the benthic invertebrates from the central Oregon continental shelf, *in* Pruter, A.T., and Alverson, D.L., eds., The Columbia River estuary and adjacent ocean waters: Bioenvironmental studies: University of Washington Press, p. 422–433.

Champ, M.A., Gould, G.A., and Bozzo, W.E., 1980, Characterization of light extinction and attenuation in Chesapeake Bay, August 1977, *in* Kennedy, V.S., ed., Estuarine perspectives: Academic Press, New York, p. 263–277.

Cloern, J.E., 1982, Does the benthos control phytoplankton biomass in south San Francisco Bay?: Marine Ecology—Progress Series, v. 9, p. 191–202.

Cole, B.E., 1982, Size-fractionation of phytoplankton production in northern San Francisco Bay: 1980: EOS, Transactions American Geophysical Union, v. 63, p. 947.

Cole, B.E., and Coern, J.E., 1984, Significance of biomass and light availability to phytoplankton productivity in San Francisco Bay: Marine Ecology—Progress Series, v. 17, p. 15–25.

Cole, B.E., and Harmon, D.D., 1981, Phytoplankton productivity, respiration, and nutrient uptake and regeneration in the Potomac River, August 1977-August 1978: U.S. Geological Survey Open-File Report 81–700, 51 p.

Cole, J.J., 1982, Interactions between bacteria and algae in aquatic ecosystems: Annual Review of Ecological Systems, v. 13, p. 291–314.

Conomos, T.J., Smith, R.E., Peterson, D.H., Hager, S.W., and Schemel, L.E., 1979, Processes affecting seasonal distributions of water properties in the San Francisco Bay estuarine system, *in* Conomos, T.J., ed., San Francisco Bay: The urbanized estuary: Pacific Division, AAAS, San Francisco, p. 15–142.

Day, J.H., 1981, Summaries of current knowledge of 43 estuaries in Southern Africa, *in* Day, J.H., ed., Estuarine ecology: A.A. Balkema, Rotterdam, p. 241–330.

Ducklow, H.W., 1983, Production and fate of bacteria in the oceans: Bioscience, v. 33, p. 494–501.

Fenchel, Thomas, 1982, Ecology of heterotrophic microflagellates: IV, Quantitative occurrence and importance as bacterial consumers: Marine Ecology—Programs Series, v. 9, p. 35–42.

Fenchel, Thomas, and Finley, B.J., 1983, Respiration rates in heterotrophic, free-living protozoa: Microbiology and Ecology, v. 9, p. 99–122.

Fisher, T.R., Carlson, P.R., and Barber, R.T., 1982a, Sediment nutrient regeneration in three North Carolina estuaries: Estuarine, Coastal and Shelf Science, v. 14, p. 101–116.

———1982b, Carbon and nitrogen primary productivity in three North Carolina estuaries: Estuarine, Coastal and Shelf Science, v. 15, p. 621–644.

Flemer, D.A., 1970, Primary production in the Chesapeake Bay: Chesapeake Science, v. 11, p. 117–129.

Furnas, M.J., Hitchcock, G.L., and Smayda, T.J., 1976, Nutrient-phytoplankton relationships in Narragansett Bay during the 1971 summer bloom, *in* Wiley, M., ed., Estuarine processes: New York, Academic Press, p. 118–133.

Hartwig, E.O., 1974, Physical, chemical and biological aspects of nutrient exchange between the marine benthos and the overlying water: Sea Grant Publication, No. 40.

Holmes, R.W., 1970, The secchi disk in turbid coastal waters: Limnology and Oceanography, v. 15, p. 688–694

Jaworski, N.A., 1981, Sources of nutrients and the scale of eutrophication problems in estuaries, *in* Neilson, B.J., and Cronin, L.E., eds., Estuaries and nutrients: The Humana Press, Clifton, New Jersey, p. 83–110.

Kemp, W.M., and Boynton, W.R., 1981, External and internal factors regulating metabolic rates of an estuarine benthic community: Oecologia, v. 51, p. 19–27.

Kremer, J.N., and Nixon, S.W., 1978, A coastal marine ecosystem: Simulation and analysis: Ecological studies, v. 24, Springer-Verlag, Heidelberg, 217 p.

Lie, Ulf, 1969, A quantitative study of benthic infauna in Puget Sound, Washington, USA, in 1963–64: Fiskeridirektoratet skrifter serie Havŭndersøkelser, v. 14, p. 229–556.

Lima, H. de S., and Williams, P.J., 1978, Oxygen consumption by the planktonic population of an estuary—Southhampton water: Estuarine and Coastal Marine Science, v. 6, p. 515–521.

Linley, E.A., Newell, R.C., and Lucas, M.I., 1983, Quantitative relationships between phytoplankton, bacteria and heterotrophic microflagellates in shelf waters: Marine Ecology—Progress Series, v. 12, p. 77-89.

Lyle, T.M., 1983, The brown-green color transition in marine sediments; a marker of the Fe (III)–Fe (II) redox boundary: Limnology and Oceanography, v. 28, p. 1026–1033.

Nixon, S.W., 1981, Remineralization and nutrient cycling in coastal marine ecosystems, *in* Neilson, B.J., and Cronin, L.E., eds., Estuaries and nutrients: The Humana Press, Clifton, New Jersey, p. 111–138.

Nixon, S.W., Oviatt, C.A., and Hale, S.S., 1976, Nitrogen regeneration and the metabolism of coastal marine bottom communities, *in* Anderson, J.M., and Macfayden, T.A., eds., The role of terrestrial and aquatic organisms in decomposition processes: Blackwell Scientific Publications, Oxford, p. 269–283.

Officer, C.B., Smayda, T.J., and Mann, T.R., 1982, Benthic filter feeding: A natural eutrophication control: Marine Ecology—Progress Series, v. 9, p. 204–210.

Officer, C.B., Biggs, R.B., Taft, J.L., Cronin, L.E., Tyler, M.A., Boynton, W.R., 1984, Chesapeake Bay Anoxia: Origin, development, and significance: Science, v. 223, p. 22–27.

Oviatt, C.C., Buckley, B.N., and Nixon, Scott, 1981, Annual phytoplankton metabolism in Narragansett Bay calculated from survey field measurements and microcosm observation: Estuaries, v. 4, p. 167–175.

Packard, T.T., and Williams, P.J., 1981, Rates of respiratory oxygen consumption and electron transport in surface seawater from the northwest Atlantic: Oceanologica Acta, v. 4, p. 351–358.

Packard, T.T., Garfield, P.C., and Codispoti, L.A., 1983, Oxygen consumption and denitrification below the Peruvian upwelling, *in* Suess, E., and Thiede, J., eds., Coastal upwelling, Part A: Plenum Publishing Corporation, p. 147–173.

Pennock, J.R., Sharp, J.H., and Canamier, W.J., 1983, Phytoplankton, *in* Sharp, J.H., ed., The Delaware Estuary: Research as background for estuarine management and development: University of Delaware College of Marine Studies, Lewes, Delaware, p. 133–168.

Peters, R.H., 1983, The Ecological implications of body size: Cambridge University Press, 229 p.

Peterson, D.H., 1979, Sources and sinks of biologically reactive oxygen, carbon, nitrogen and silica in Northern San Francisco Bay, *in* Conomos, T.J., ed., San Francisco Bay: The urbanized estuary: Pacific Division, AAAS, p. 176–193.

Peterson, D.H., and Festa, J.F., 1984, Numerical simulation of phytoplankton productivity in partially mixed estuaries: Estuarine Coastal and Shelf Science, v. 19, no. 5, p. 563–589.

Pritchard, D.W., 1952, Salinity distribution and circulation in the Chesapeake Bay estuarine system: Journal of Marine Research, v. 11, p. 106–123.

Rivkin, R.B., Voytek, M.A., and Seliger, H.H., 1982, Phytoplankton division rates in light-limited environments: Two adaptations: Science, v. 215, p. 1123–1125.

Rowe, G.T., 1971, Benthic biomass and surface productivity, *in* Costlow, J.D., Jr., ed., Fertility of the sea, v. 2: Gordon and Breach Science Publishers, p. 441–454.

———1983, Biomass and production of the deep-sea macrobenthos, *in* Rowe, G.T., ed., The sea, v. 8, Deep-sea biology: John Wiley and Sons, p. 97–122.

Rowe, G.T., and Menzel, D.W., 1971, Quantitative benthic samples from the deep Gulf of Mexico with some comments on the measurement of deep sea biomass: Bulletin of Marine Science, v. 21, p. 556–566.

Rowe, G.T., Clifford, C.H., and Smith, K.L., Jr., 1977, Nutrient regeneration in sediments off Cap Blane, Spanish Sahara: Deep Sea Research, v. 24, p. 57–64.

Seim, E.M., and Seather, B., 1983, On rethinking allometry which regression model to use?: Journal of Theoretical Biology, v. 194, p. 161–168.

Smith, K.L., 1973, Respiration of a sublittoral community: Ecology, v. 54, p. 1065–1075.

Smith, K.L., Lauer, M.P., and Brown, N.O., 1983, Sediment community oxygen consumption and nutrient exchange in the central and eastern North Pacific: Limnology and Oceanography, v. 28, p. 882–898.

Suess, Edwin, 1980, Particulate organic carbon flux in the oceans—surface productivity and oxygen utilization: Nature, v. 288, p. 260–263.

Theil, T.H., 1983, Meiobenthic and nanobenthic of the deep sea, *in* Rowe, G.T., ed., The sea, v. 8, Deep-sea biology: John Wiley and Sons, p. 167–230.

Thompson, J.K., and Nichols, F.H., 1984, Benthic macrofaunal biomass of San Francisco Bay, California: January/February and August 1973: U.S. Geological Survey Open-File Report 81–1331, 39 p.

Turner, R.E., 1978, Community plankton respiration in a salt marsh estuary and the importance of macrophytic leachates: Limnology and Oceanography, v. 23, p. 442–451.

Turner, R.E., and Allen, R.L., 1982, Plankton respiration rates in the bottom waters of the Mississippi River Delta bight: Contributions in Marine Science, v. 5, p. 173–179.

Turner, R.E., Woo, S.W., and Jitts, H.R., 1979, Phytoplankton production in a turbid, temperate salt marsh estuary: Estuarine and Coastal Marine Science, v. 9, p. 603–613.

Van Es, F.B., and Ruardij, V.P., 1982, The use of a model to assess factors affecting the oxygen balance in the water of the Dollart: Netherlands Journal of Sea Research, v. 15, p. 313–330.

Williams, P.J., 1981, Microbial contribution to overall marine plankton metabolism: Direct measurements of respiration: Oceanologica Acta, v. 4, p. 359–364.

———1982, Microbial contribution to overall plankton community respiration-studies in CEE's, *in* Grice, G.D., and Reeve, M.R., eds., Marine mesocosms: Biological and chemical research in experimental ecosystems: Springer-Verlag, p. 305–321.

Williams, R.B., 1966, Annual phytoplankton production in a system of shallow temperate estuaries, *in* Barnes, H.R., ed., Some contemporary studies in marine science: George Allen and Unwin, Ltd., London, p. 689–716.

Williams, R.B., and Murdoch, M.B., 1966, Phytoplankton production and chlorophyll concentration in the Beaufort Channel, North Carolina: Limnology and Oceanography, v. 11, p. 73–82.

Wofsy, S.C., 1983, A simple model to predict extinction coefficients and phytoplankton biomass in eutrophic waters: Limnology and Oceanography, v. 28, p. 1144–1155.

Wong, R.L., and Cloern, J.E., 1982, Plankton studies in San Francisco Bay, IV, Phytoplankton abundance and species

composition, January 1980–February 1981: U.S. Geological Survey Open-File Report 82–443, 152 p.
Woodwell, G.M., Rich, P.H., and Hall, C.A.S., 1973, Carbon in estuaries, *in* Woodwell, G.M., and Pecan, E.V., eds., Carbon and the biosphere: United States Atomic Energy Commission, p. 221–240.

Steady-State Solutions for Concentration of a Solute with First-Order Decay in a River

By Nobuhiro Yotsukura

Abstract

Many dissolved substances transported in a river are not conservative and often lose their mass at a rate described by a first-order reaction. For these types of substances or solutes, the transport process in an open-channel flow is linear and the principle of superposition of solutions is valid.

This paper describes the mathematical aspects of obtaining the steady-state solutions for solute concentration in steady, nonuniform, riverine flow by application of the superposition principle. The resulting solutions should be applicable to a one-, two-, or three-dimensional (space) problem and be particularly useful for the determination of first-order decay coefficients from field data.

INTRODUCTION

Many dissolved substances or solutes transported in rivers are not conservative and often lose their mass at a rate described by a first-order reaction. One basic description of the concentration of a nonconservative solute, C, is to relate it to that of a conservative solute, C_c, by

$$C(x,y,z,t)=\frac{M}{M_c}C_c(x,y,z,t)\exp(-Kt)\,. \qquad (1)$$

Equation 1 is based on the initial condition that a mixture of mass, M, of the nonconservative solute and mass, M_c, of the conservative solute is released instantaneously to the river at $t=0$. The variables x,y,z, and t are measures of longitudinal channel distance, cross-channel distance, vertical distance above a datum, and time, respectively. The subscript, c, indicates a "conservative" solute concentration or "conservative" mass. Equation 1 combines the concept of first-order decay,

$$\frac{dC}{dt}=KC,$$

with that of the hydraulic transport by advection and diffusion, which are assumed identical for for both solutes. The decay coefficient, K, is assumed to be effective from the instant of solute release and to be constant with respect to time, t. Equation 1 is, thus, valid for unsteady flow, and provides the most practical description of first-order decay for the three-dimensional transport problem in rivers (Holley and Yotsukura, 1984).

When the river flow is steady, it is desirable to have the steady-state version of equation 1, because the experimental determination of transport parameters tends to be accomplished more easily and the results are more reliable statistically under steady-state conditions than under transient-state conditions. In addition, the steady-state solution is more compatible with procedures used to measure naturally occurring solute plumes. These plumes often exhibit steady-state, transport/decay patterns. It is the purpose of this report to obtain the steady-state solutions from equation 1, which will be particularly useful for the determination of K from field data.

The mathematical technique used throughout this report is the principle of superposition for a linear system. It will be applied, first, to the one-dimensional problem in uniform, open-channel flow to reconfirm the well-known steady-state solution. This not only provides a clue to the expected form of solution for nonuniform flow but also provides physical insight into the relationship between diffusion and decay. The steady-state solutions for nonuniform flow will then be derived by application of the same principle. These solutions will be compared term-by-term with the one-dimensional, uniform-flow solution to demonstrate the exactness of mathematical derivations.

STEADY-STATE SOLUTIONS FOR UNIFORM FLOWS

Consider the one-dimensional transport equation for a nonconservative solute in steady, uniform flow,

$$\frac{\delta C}{\delta t}+U\frac{\delta C}{\delta x}=D_x\frac{\delta^2 C}{\delta x^2}-KC\,, \qquad (2)$$

in which both U, the longitudinal velocity, and D_x, the longitudinal dispersion coefficient, are assumed constant. For an instantaneous release of mass, M, at $x=0$, the transient-state solution is

$$C=\frac{M}{A\sqrt{4\pi D_x t}}\exp(-Kt)\exp\left\{-\frac{(x-Ut)^2}{4D_x t}\right\}, \quad (3)$$

where A is the constant cross-sectional area. Note that equation 3 with $K=0$ provides the expression for C_c/M_c of the conservative solute so that equation 3 is a one-dimensional form of equation 1.

Because equation 2 is a linear, homogeneous, partial differential equation, the principle of superposition of solutions is valid (Churchill, 1941). A continuous, uniform release of mass per time, m, is equivalent to an infinite number of sequential instantaneous releases with $m d\tau=M$, where τ designates the time of solute release having the same origin as τ. The superposition of equation 3 for all releases between $\tau=0$ and $\tau=t$ is (Yotsukura and Kilpatrick, 1973)

$$C(x,t)=\frac{m}{A\sqrt{4\pi D_x}}\int_0^t \frac{1}{\sqrt{t-\tau}} \exp\left\{-K(t-\tau)-\frac{[x-U(t-\tau)]^2}{4D_x(t-\tau)}\right\} dt . \quad (4)$$

By introducing a new variable of integration, $p=\sqrt{t-\tau}$, increasing t to infinity, and utilizing the well-known integration formula

$$\int_0^\infty \exp\left(-p^2-\frac{\lambda^2}{p^2}\right)dp=\frac{\sqrt{\pi}}{2}\exp(-2\lambda), \quad (5)$$

equation 4 yields the steady-state solution

$$C(x)=\frac{m}{AU\sqrt{1+\alpha}}\exp\left\{\frac{xU}{2D_x}(1-\sqrt{1+\alpha})\right\}, \quad (6)$$

where the nondimensional parameter, α, is defined by

$$\alpha=\frac{4D_x K}{U^2}. \quad (7)$$

Equation 6 is identical to the form obtained by O'Connor and Lawler (1965), who solved the second-order ordinary differential equation obtained by eliminating the $\delta C/\delta t$ term from equation 2.

In order to further simplify equation 6, one needs to assume that α is much smaller than unity. The term $\sqrt{1+\alpha}$ in the denominator of equation 6 will thus be approximated by unity, while the $\sqrt{1+\alpha}$ term in the exponential function of equation 6 can be approximated by $1+\alpha/2$. Equation 6 is then simplified to

$$C(x)=\frac{m}{AU}\exp\left(-\frac{kx}{U}\right). \quad (8)$$

Equation 8 is simpler to use than equation 6 for the determination of K from experimental data. Also, equation 8 is the solution of equation 2 without the $\delta C/\delta t$ and $D_x\delta^2 C/\delta x^2$ terms. For this reason, equation 8 is called the "plug-flow" solution. Fischer and others (1979) have discussed the physical conditions for which application of equation 8 in natural rivers is appropriate and concluded that α must be less than 0.06 for equation 8 to be a satisfactory solution for nonconservative solutes.

The two- and three-dimensional solutions could be obtained by employing the same technique as above, assuming rectangular channel flow, constant velocity, and diffusion coefficients. Reference is made to Glover (1964), who applied the superposition principle to a two-dimensional equation. This solution suggests that one major condition for the two- and three-dimensional plug flow solutions is that the nondimensional parameter, α, be much smaller than unity, as is required for the one-dimensional solution, also. The deficiency of this approach, however, is that the velocity is assumed constant in a cross section. As is well known from the hydraulics of transport (Fisher and others, 1979), the major contributor to the longitudinal dispersion coefficient is the variation of longitudinal velocity within a cross section. Thus, any set of two- or three-dimensional transport equations with constant velocity, U, is unable to describe correctly the process of longitudinal dispersion in which the coefficient is never constant and continues to increase with time toward an asymptotic one-dimensional value. Because of this problem, the two- and three-dimensional steady-state solutions with constant parameters, though elegant in mathematics, do not provide any more useful information than the one-dimensional solution and, thus, will not be presented here.

STEADY-STATE SOLUTIONS FOR NONUNIFORM FLOWS

In this approach, one again assumes that the solute transport is described by a set of linear homogeneous equations including boundary conditions, whatever these equations may be. Moreover, strong justification for use of the principle of superposition comes from empirical observations that "the one thing that seems to be agreed, whatever theory one may have about diffusion, is that diffusing distributions are superposable" (Taylor, 1959).

This approach, similar to the method of unit hydrograph for linear runoff process, considers that the form of equation 1 remains the same at a fixed point in a steady nonuniform flow, as long as the time, t, is measured relative to the time of release.

Consider equation 1 as a superposition response function. Then by introducing the normalized response function, $f(x,y,z,t)$, as

$$f(x,y,z,t)=\frac{C_c(x,y,z,t)}{\int_0^\infty C_c(x,y,z,t)dt}, \quad (9)$$

where $f(x,y,z,t)$ has the dimension of time^{-1}, one notes that the area under the curve, f versus t, is unity. The denominator of equation 9 is an expression of the total solute mass that passed through the point (x,y,z) and is, thus, variable in a cross section.

This variability is accounted for by introducing the mass distribution factor, $\phi(x,y,z)$, as

$$\phi(x,y,z)=\frac{Q\int_0^\infty C_c(x,y,z,t)dt}{M_c}, \quad (10)$$

where Q is the steady river discharge. Because of the requirement for conservation of mass,

$$M_c=\int_0^A u(x,y,z)\int_0^\infty C_c(x,y,z,t)dtda, \quad (11)$$

where $u(x,y,z)$ is the longitudinal velocity and da designates an infinitesimal cross-sectional area and the integration with respect to da covers the entire cross-sectional area, A.

Note that $\phi(x,y,z)$ is defined as a nondimensional parameter independent of t and in view of equations 10 and 11,

$$\int_0^A \phi(x,y,z)\,u(x,y,z)da=Q. \quad (12)$$

When the integral, $\int_0^\infty C_c(x,y,z,t)dt$, of equation 10 is constant in a cross section, equations 10 and 11 show that $\phi(x,y,z)$ becomes unity.

Substituting equations 9 and 10 into equation 1, one is able to reduce the latter to

$$C(x,y,z,t)=\frac{M}{Q}\phi(x,y,z)\,f(x,y,z,t)\,\exp(-Kt). \quad (13)$$

A continuous uniform release of mass per time, m, of a nonconservative solute is again considered as equivalent to an infinite number of sequential releases with $md\tau=M$, so that the superposition of equation 13 is

$$C(x,y,z,t)=\frac{m}{Q}\phi(c,y,z)\int_0^t f(x,y,z,t-\tau)\exp\{-K(t-\tau)d\tau\}. \quad (14)$$

Introducing a new variable of integration $p=t-\tau$, and increasing t to infinity, one obtains the steady-state solution by superposition that is expressed as

$$C(x,y,z)=\frac{m}{Q}\phi(x,y,z,)\int_0^\infty f(x,y,z,p)\,\exp(-Kp)dp. \quad (15)$$

In order to reduce equation 15 to a more tractable form, first revert to the more familiar notation, t, from p without losing generality of the discussion. Following the definition of equation 9, one obtains

$$\int_0^\infty f(x,y,z,t)dt=1. \quad (16)$$

The mean travel time, $\bar{t}(x,y,z)$, is the first-order moment of f, or

$$\bar{t}(x,y,z,t)=\int_0^\infty f(x,y,z,t)dt. \quad (17)$$

The results of uniform flow analysis, in particular, equation 8, strongly suggest that the integral of equation 15 will be related to $\exp\{-K\bar{t}(x,y,z)\}$, where $\bar{t}$ is analogous to x/U of equation 8. This was confirmed, also, by numerical integration of the one-dimensional response functions measured in Cowaselon Creek (Yotsukura and others, 1983). Following this clue, assuming K to be constant, utilizing equation 16 and 17, and expanding the exponential functions into series form, one obtains

$$\int_0^\infty f(x,y,z,t)\,\exp(-Kt)dt-\exp\left\{k\bar{t}(x,y,z)\right\}$$

$$=\sum_{n=2}^{\infty}\frac{(-1)^nK^n}{n!}\left[\int_0^\infty {}^n f(x,y,z,t)dt-(\bar{t}(x,y,z))^n\right], \quad (18)$$

where n is an integer index.

The right-hand side of equation 18 can be shown by some tedious mathematical manipulations to be

$$\sum_{n=2}^{\infty}\frac{(-1)^nK^n}{n!}\left[\int_0^\infty t^n f(x,y,z,t)dt-(\bar{t}(x,y,z,))^n\right]$$

$$=\exp\left\{-K\bar{t}(x,y,z)\right\}\sum_{n=2}^{\infty}\frac{(-1)^nK^n}{n!}$$

$$\int_0^\infty (t-\bar{t}(x,y,z))^n f(x,y,z,t)dt \quad (19)$$

so that the integral term of equation 15 reduces to

$$\int_0^\infty f(x,y,z,t)\exp(-Kt)dt$$

$$=\exp\left\{-K\bar{t}(x,y,z)\right\}1+\sum_{n=2}^{\infty}\frac{(-1)^nK^n}{n!}$$

$$\int_0^\infty (t-\bar{t}(x,y,z))^n f(x,y,z,t)dt\,. \qquad (20)$$

Designating the bracketed term of equation 20 as the correction term, $E(x,y,z)$, one can obtain the final form of the steady-state solution, which may be written from equation 15 as

$$C(x,y,z)=\frac{m}{Q}\phi(x,y,z)E(x,y,z)\exp\left\{-K\bar{t}(x,y,z)\right\} \qquad (21)$$

where

$$E(x,y,z)=1+\sum_{n=2}^{\infty}\frac{(-1)^nK^n}{n!}$$

$$\int_0^\infty (t-\bar{t}(x,y,z))^n f(x,y,z,t)dt\,. \qquad (22)$$

Because the above superposition involves only time-dependent variables, equations 21 and 22 are independent of spatial dimensions and thus valid for one-, two-, or three-dimensional problems, except that $\phi=1$ for a one-dimensional problem as noted before. For a typical form of $f(x,y,z,t)$ in natural rivers and for a moderate value of K, the summation term of equation 22 tends to be much smaller than unity, so that equation 21 may be approximated by

$$C(x,y,z)=\frac{m}{Q}\phi(x,y,z)\exp\left\{-K\bar{t}(x,y,z)\right\}. \qquad (23)$$

Equation 23 is comparable to equation 8 for uniform flow and may be designated as the plug flow solution for nonuniform flows. The requirement that the summation term of equation 22 must be much smaller than unity corresponds to the condition that α of equation 7 be much smaller than unity for the use of equation 8. Equations 21, 22, and 23, therefore, generalize the description of steady-state solute concentration, which appears so far to have been provided only by the one-dimensional, uniform-flow solution (Fischer and others, 1979).

EXAMPLE CALCULATIONS

Because the development from equation 15 to equations 21 and 22 involves rather tedious manipulations that are cumbersome to present in detail, it is worthwhile to illustrate the equivalence of these two sets of equations by means of examples.

For the first example, assume a rectangular normalized response function such that $f(t)$ is constant, 1/L for $t_A \le t \le t_D$, where $t_D - t_A = L$, and $f(t)$ is zero for all other t values. The spatial dimension of the response function is immaterial, thus the following equations will neglect it. Assuming $m\phi/Q=1$ for simplicity, equation 15 is written and integrated directly as

$$C=\int_{t_A}^{t_D}\frac{1}{L}\exp(-Kt)dt$$

$$=\frac{1}{KL}\left\{\exp\left(\frac{KL}{2}\right)-\exp\left(\frac{-KL}{2}\right)\right\}\exp(-K\bar{t}), \qquad (24)$$

where

$$\bar{t}=\frac{t_D+t_A}{2}\,. \qquad (25)$$

Equations 21 and 22 may be combined as

$$C=\left[1+\sum_{n=2}^{\infty}\frac{(-1)^nK^n}{n!}\int_{t_A}^{t_D}(t-\bar{t})^n\frac{1}{L}dt\right]\exp(-K\bar{t}), \qquad (26)$$

in which the integration can be carried out directly. Equation 26 thus becomes

$$C=\left[1+\frac{K^2L^2}{(2)(12)}+\frac{K^4L^4}{(24)(80)}+\frac{K^6L^6}{(720)(448)}+\ldots\right]\exp(-K\bar{t})\,. \qquad (27)$$

By expanding $\exp(KL/2)$ and $\exp(-KL/2)$ and arranging the terms in series form with increasing power of KL, the first four terms of equation 24, which represents equation 15, can be shown to be identical to those evident in equation 27, which represents equations 21 and 22. This example demonstrates that equation 21 is valid for the response function, which has a finite duration between t_A and t_D, but is discontinuous at t_A and t_D.

For the second example, consider the one-dimensional problem in a uniform flow discussed previously. The normalized response function, $f(x,t)$, can be obtained from equation 3 by letting $K=0$ for the conservative solute and noting that

$$\int_0^\infty C_c(x,t)dt=M_c/AU.$$

Following the definition of equation 9, then

$$f(x,t)=\frac{U}{\sqrt{4\pi D_x t}}\exp\left\{\frac{(x-Ut^2)}{4D_x t}\right\}. \quad (28)$$

The steady-state solution expressed by equation 15 was obtained previously as equation 6. Assuming $m/AU=1$ for simplicity, equation 6 is rewritten as

$$C(x)=\frac{1}{\sqrt{1+\alpha}}\exp\left\{\beta(1-\sqrt{1+\alpha})\right\} \quad (29)$$

where the nondimensional parameter, α, was defined by equation 7, and β is defined by

$$\beta=\frac{xU}{2D_x}. \quad (30)$$

By expanding the $\sqrt{1+\alpha}$ term in the exponential function of equation 29 by means of the binomial formula and noting that $\alpha\beta/2=Kx/U$, equation 29 is expanded partially as

$$C(x)=(1+\alpha)^{-1/2}\exp\left[\frac{\beta\alpha^2}{8}-\frac{\beta\alpha^3}{16}+\frac{5\beta\alpha^4}{128}-\ldots\right]\exp\left[\frac{Kx}{U}\right]. \quad (31)$$

The preliminary step needed to express equation 21 and 22 in a form comparable with equation 31 is to calculate various moments from equation 28. The first four moments are given as the following:

$$\bar{t}(x)=\int_0^\infty t\,f(x,t)dt=\frac{x}{U}\frac{(\beta+1)}{\beta}, \quad (32)$$

$$\int_0^\infty (t-\bar{t}(x))^2 f(x,t)dt=\frac{x^2}{U^2}\frac{(\beta+2)}{\beta^2}, \quad (33)$$

$$\int_0^\infty (t-\bar{t}(x))^3 f(x,t)dt=\frac{x^3}{U^3}\frac{(3\beta+\beta)}{\beta^3}, \text{ and} \quad (34)$$

$$\int_0^\infty (t-\bar{t}(x))^4 f(x,t)dt=\frac{x^4}{U^4}\frac{(3\beta^2+27\beta+60)}{\beta^4}. \quad (35)$$

The specific form of equations 32 through 35, in which the term $(\frac{x}{U})^n$ is retained for the purpose of combining it with the term Kn of equation 22, permits one to express $(\frac{Kx}{U})^n=(\frac{\alpha\beta}{2})^n$. Substituting equations 32 through 35 into equations 21 and 22 with some manipulations, one obtains

$$C(x)=\exp\left[-\frac{\alpha}{2}\right]\left[1+\frac{(\beta+2)\alpha^2}{8}-\right.$$

$$\left.\frac{(3\beta+8)\alpha^3}{48}+\frac{(3\beta+27\beta+60)\alpha^4}{384}-\ldots\right]\exp\left[-\frac{Kx}{U}\right]. \quad (36)$$

Expanding equations and 31 and 36 further, except the term $\exp(-\frac{Kx}{U})$, calculating the product terms, and arranging the resulting series in the increasing order of power of α, one can show that equation 31, which represents equation 15, and equation 36, which represents equations 21 and 22, are identical term by term up to the order of α^4. This calculation confirms that the term $\sqrt{1+\alpha}$ in the demoninator of equation 6 is necessary to provide the exact superposition solution. Also, note that $\bar{t}(x)$ given by equation 32 is not the same as x/U, and the third moment given by equation 34 is not zero. This is because equation 28 has a slightly skewed distribution with respect to $\bar{t}(x)$, as it is considered to be the function of t at a fixed distance x.

The above example calculations, though limited to several initial terms of the infinite series, appear sufficient in demonstrating that equation 21 and 22 are the exact steady-state solution obtained by the principle of superposition.

SUMMARY

It has been shown that, if the mass of a nonconservative solute decays according to a first-order reaction rate, the steady-state solution for solute concentration in nonuniform, open-channel flow can be obtained by applying the principle of superposition to an unspecified response function. Equations 21 and 22 provide a solution that is applicable to any one-, two-, or three-dimensional problem. Equation 23 is a plug flow approximation of the steady-state solution and provides the simplest form for the calculation of decay coefficients from experimental data. For this approximation, however, the summation term of equation 22 must be much less than unity. For a typical response function of several hours duration in rivers and for a moderate value of K on the order of 4 day^{-1} or less, the summation term may not exceed 0.04, normally. However, the assessment of physical situations suitable for use of these solutions is beyond the scope of this report and will be based on future experimental observations.

REFERENCES CITED

Churchill, R.V., 1944, Fourier series boundary value problems: New York, McGraw-Hill Book Co., 206 p.

Fischer, H.B., List, E.J., Koh, R.C.Y., Imberger, Jorg, and Brooks, N.H., 1979, Mixing in inland and coastal waters: New York, Academic Press, 483 p.

Glover, R.E., 1964, Dispersion of dissolved or suspended materials in flowing streams: U.S. Geological Survey Professional Paper 433–B, 32 p.

Holley, R.R., and Yotsukura, Nobuhiro, 1984, Field techniques for reaeration measurements in rivers, *in* Brutsaert, W., and Jirka, G.H., eds., Gas transfer at water surface: D.

Reidel Publishing Co., Dordrecht, Netherlands, p. 381–401.

O'Connor, D.J., and Lawler, J.P., 1965, Mathematical analysis of estuarine pollution: 55th National Meeting, American Institute of Chemical Engineers, Reprint No. 31a, Houston, Texas.

Taylor, G.I., 1959, The present position in the theory to turbulent diffusion: Advances in Geophysics, v. 6, Academic Press, New York, p. 101–112.

Yotsukura, Nobuhiro, and Kilpatrick, F.A., 1973, Tracer simulation of soluble waste concentration: American Society of Civil Engineers, Journal of Environmental Engineering Division, v. 99, no. EE4, p. 499–515.

Yotsukura, Nobuhiro, Steadfast, D.A., Draper, R.E., and Brutsaert, W.H., 1983, An assessment of steady-state propane-gas tracer method for reaeration coefficients—Cowaselon Creek, New York: U.S. Geological Survey Water-Resources Investigations Report 83–4183, 88 p.

Fire-Related Debris Flows in the Beaver Creek Drainage, Lewis and Clark County, Montana

By Charles Parrett

Abstract

A moderate August 1984 rainstorm produced substantial debris flows from tributaries of Beaver Creek, a small Missouri River tributary located near Helena, Montana. The debris flows occurred only in the parts of the drainage that had been burned by an extensive forest fire just prior to the rainstorm. Peak debris discharges were determined at 31 sites by using a variation of the slope-area, superelevation, and critical-flow methods and were determined to be close to or larger than maximum known water floods in Montana.

Unit peak discharges ranged from 0.4 to 34,000 cubic feet per second per square mile, with the largest value and most spectacular debris flow occurring in Bear Gulch Creek. The Bear Gulch Creek debris flow apparently was triggered by mass erosion of burned topsoil near the drainage divide. The flow increased by bulking until it reached an estimated peak of 29,900 cubic feet per second at a measurement site 0.7 mile upstream from the mouth. The discharge rapidly attenuated to 3,100 cubic feet per second about 0.4 mile downstream. The large peak and rapid attenuation are presumed to result from debris damming and subsequent release near the upstream measurement site.

The peak debris discharge at the upstream measurement site on Bear Gulch Creek was determined by the superelevation method. The computed discharge was then used in the slope-area equation to solve for Manning's *n* value, and it was found that the *n* value had to be doubled to account for the additional energy loss caused by the debris load. The doubling of *n* values was presumed to be applicable to all other discharge-measurement sites where the slope-area method was used.

The solids-to-water ratio of the Bear Gulch Creek debris flow was estimated by mixing water with a dried sample of deposited debris. The reconstituted debris slurry was 87 percent solids by weight and 72 percent solids by volume. Thus, the peak water discharge at the measurement sites can be estimated as 28 percent of the peak debris discharge. Making this adjustment to the data still results in two peak discharges occurring above the envelope curve for maximum floods in Montana.

INTRODUCTION

In August 1984, several large forest and range fires in Montana became the focus of national attention as they burned thousands of acres and threatened numerous rural residences. One of the largest fires—the North Hills fire—burned in the mountains north of Helena. The North Hills fire consumed more than 20,000 acres of timber and rangeland, including several thousand acres within the Beaver Creek drainage, a small tributary stream of the Missouri River. Rainfall on August 30 and 31 largely eliminated the fire but resulted in unprecedented debris flows from most small tributaries to Beaver Creek. Although the rainfall volumes were not enough to cause any significant runoff from unburned areas, soils in the burned area were easily eroded so that substantial volumes of runoff composed of a sediment-water mixture were generated. The resultant debris flows temporarily dammed Beaver Creek at one or two locations and formed debris fans at the mouths of several tributaries. Such an ironic hydrologic phenomenon is probably not uncommon in the Rocky Mountain region, but little or no documentation exists in the literature. Established techniques for determining peak discharge of clear-water floods were applied to the debris flows with some adjustments made to friction coefficients to account for the non-Newtonian characteristics of the debris fluid.

The purpose of this paper is to describe and document the rather unique fire-caused flooding and debris flows that occurred in the Beaver Creek drainage. Indirect measurements of peak discharge were made at 31 sites in the basin. In addition, precipitation and streamflow data and aerial photography obtained from the U.S. Forest Service, Helena National Forest, were used to estimate storm magnitude, stream discharge from Beaver Creek, and the percentage of the drainage burned.

ACKNOWLEDGMENTS

William C. Putnam, hydrologist, and Dean A. Suricek, soil scientist, from the U.S. Forest Service, Helena National Forest, provided the author with precipitation and streamflow records, photographs, refer-

ence material, and assistance with delineation of the burned area. In addition, both individuals provided valuable descriptive information and insight gleaned from their experience and many trips through the burned area. Their assistance and willingness to help the author are greatly appreciated.

THE BEAVER CREEK AREA

Beaver Creek is a small perennial stream (drainage area of 73.3 mi^2) that flows into the Missouri River on its right bank about 20 air miles northeast of Helena. The Beaver Creek drainage lies entirely within the forested Big Belt Mountains. The forest is made up mostly of pine and fir interspersed with open meadow areas. The mountains are fairly rugged, with elevations ranging from about 3,800 ft at the mouth of Beaver Creek to almost 8,000 ft at the basin divide. Most of the landscape is characterized as steep, with slopes ranging from 25 to 60 percent. The Beaver Creek basin is underlain chiefly by limestone, shale, and sandstone. Outcrops and talus mostly are limestone and are especially predominant within the study area (fig. 1) near measurement site 13, where Beaver Creek flows through a narrow gorge. Soils mostly are calcareous gravelly loams and generally are easily erodible. Although average precipitation in the basin is about 20 to 25 in. annually, the vegetative cover generally is more characteristic of a drier climate, probably because of the abundant permeable limestone bedrock. None of the Beaver Creek tributaries are perennial; the bigger tributaries such as Hunters Gulch and Big Log Gulch probably flow intermittently. All other tributaries are ephemeral and flow only in response to large storms.

THE FIRE AND SUBSEQUENT RAINSTORM

The North Hills fire began on August 27, 1984, about 6 mi west of Beaver Creek. Prevailing westerly winds spread the fire rapidly eastward in spite of concentrated fire-fighting efforts. Although the Missouri River ordinarily would have been an effective firebreak and prevented any further eastern movement, the winds and high intensity of the fire enabled it to jump the river near the mouth of Beaver Creek on August 29.

By August 30, the fire had moved east beyond Bear Gulch Creek (see fig. 1). The fire burned mostly along the north side of Beaver Creek, although the area along both banks was burned. The fire varied in intensity along the Beaver Creek drainage, depending upon the available fuel and the wind conditions.

Rainfall that began in the late afternoon of August 30 and continued throughout most of August 31 finally halted and largely extinguished the fire. The rain was sporadic and relatively light until the morning of August 31. From about 1000 to 1200 hours the rain increased in intensity and reportedly culminated in a downpour of rain mixed with hail near the community of Nelson. The nearest recording precipitation gage is a Forest Service gage about 6 mi northeast of Nelson, near the Beaver Creek tributary of Pike Creek. The Pike Creek gage showed a precipitation total of 1.64 in. for the 2-day storm, with 1.25 in. occurring on August 31. Incremental volumes of rain at the Pike Creek gage were measured in 6-hour increments, so the maximum hourly rate of rainfall could not be determined. The maximum 6-hour rain volume was 0.63 in. Both the maximum 6-hour and the maximum 24-hour rain volumes for the Pike Creek location are less than the estimated volumes for storms with a 2-year recurrence interval (Miller and others, 1973). Although eyewitness reports indicate that the storm was more intense near Nelson than at Pike Creek, it is doubtful that the total precipitation anywhere within the Beaver Creek drainage could have been more than about 2 to 3 in. A storm of 24-hour duration with a total precipitation volume of 3 in. has a recurrence interval of about 10 years in the Beaver Creek area.

FLOODING AND DEBRIS FLOWS

During the late afternoon of August 31, virtually all tributary gulches draining the burned areas of Beaver Creek (fig. 1) began flowing. In all instances, the flows were made up of a mixture of ash, soil, rock, and water. Debris fans were formed near the mouths of several gulches where they terminated on the relatively flat flood plain along Beaver Creek. Fine gray ash was deposited on several of the fans among the otherwise green, vegetated landscape. Although the duration of flow probably was very short (less than 1 hour) in all drainages, the channel scour and estimated peak debris discharges generally were dramatically large. As might be expected from the relatively small volumes of precipitation that were recorded at the Pike Creek gage, the tributary gulches draining the unburned parts of the Beaver Creek drainage showed no evidence of flow.

In addition to burning the vegetative cover that normally would intercept some rainfall, the fire may have burned the forest soils enough to make them water-repellent (hydrophobic). Hydrophobic soil conditions following fires have been reported for forested watersheds, particularly in southern California chaparral where the water-repellent layer is sometimes driven downward a few inches from the surface by intense heat (Krammes and Debano, 1965). A study of controlled burning and its effect on water-repellency in a fir and spruce forest in northwestern Montana found a marked increase in water-repellency in the top 4 in. of soil

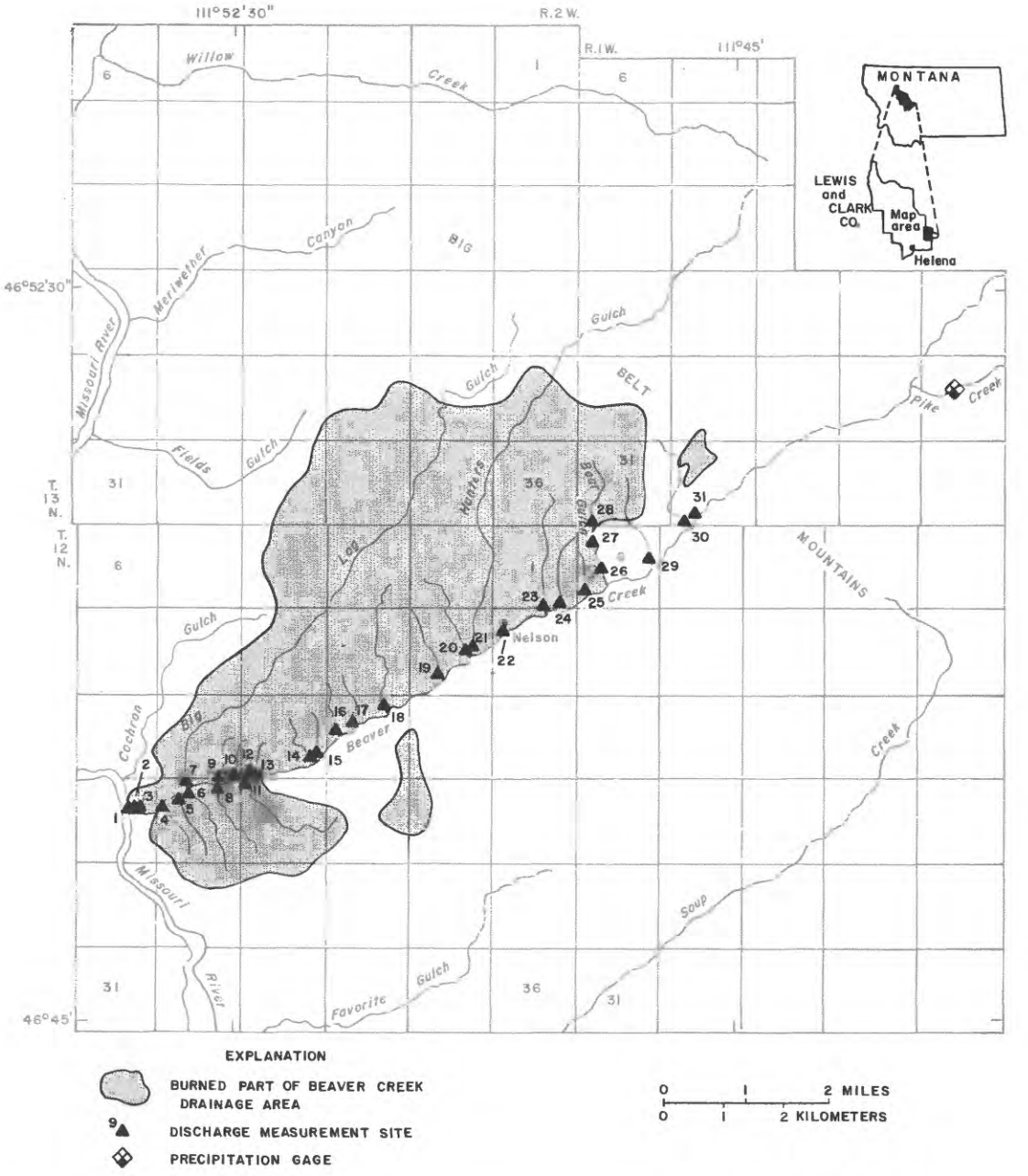

Figure 1. Location of burned area and measurement sites, Beaver Creek drainage, Montana.

(DeByle, 1973). The somewhat drier pine and fir forest in the Beaver Creek drainage probably reacted similarly. In any case, almost all the precipitation ran off the burned slopes, and the lack of vegetation made the normally erodible soils even more erodible.

In most headwater areas, massive quantities of soil were removed through erosion. Sheet erosion of the ash layer and soil surface began within a few feet of the ridgetops and progressed downslope into rill and gully erosion (fig. 2). As the soil-water slurries from the rills and gullies moved into the channel system, debris flows evidently formed. Slope failures, which are commonly the cause of debris flows in steep mountainous areas (Campbell, 1975, and Pierson, 1980) were noticeably absent in the Beaver Creek drainage.

On some of the steeper hill slopes where only a thin layer of soil covered bedrock, however, mass failure of the thin soil layer may have been the initiating mechanism for the debris flow. In these few instances, virtually all topsoil was removed and no rill erosion is evident (fig. 3). Because the impermeable bedrock lies just a few inches below the soil surface, the soil layer could have become saturated and slipped en masse (T.C. Pierson, U.S. Geological Survey, written commun., 1986).

Figure 2. Area of rill erosion on hill slope in Bear Gulch Creek drainage. Photograph by U.S. Forest Service shows complete lack of organic material on the soil surface. Pen near center of photograph shows relative scale.

Following the flood, personnel from the U.S. Geological Survey visited the area and collected data for determining peak discharge at 27 tributary gulches and at 4 locations on Beaver Creek (fig. 1). Indirect measurements were made at three locations along Bear Gulch Creek, where the largest and most spectacular debris flow occurred. Because most of the gulches are too small to be named, they are numbered consecutively upstream on each bank of Beaver Creek. Each site is further identified by the letter L for left-bank tributary or the letter R for right-bank tributary. Thus, the first gulch upstream from the mouth of Beaver Creek that enters the creek on the right bank is identified as Gulch 1R. The types of indirect measurements and the results of the discharge determinations are given in table 1.

As indicated in table 1, the largest peak debris discharges occurred in Bear Gulch Creek where one discharge was estimated to be almost 30,000 ft^3/s. The largest unit peak debris discharge (discharge per square mile of contributing drainage area) also occurred in Bear Gulch Creek. Because the debris flows in Bear Gulch Creek were so much larger and more spectacular than in any of the other gulches, the Bear Gulch Creek debris flow is discussed separately in a subsequent section of this paper. Unit peak debris discharges greater than 3,000 $(ft^3/s)/mi^2$ also occurred in eight other gulches.

Determination of Discharge

Peak discharge at all measurement sites in the Beaver Creek basin was estimated using either a basic energy-balance equation (superelevation method or critical-flow method) or the Manning form of the nonuniform flow equation (slope-area method). Even though each method was developed for clear-water flow

Figure 3. Area of possible soil mass failure in the Bear Gulch Creek drainage. The light-gray areas are bedrock. The photograph, by the U.S. Forest Service, shows conditions in the upstream reaches of Bear Gulch.

under steady-flow conditions, apparently reasonable estimates of debris-flow discharge have been obtained in Oregon and Washington from the superelevation method (Gallino and Pierson, 1985). Therefore, this approach was used where a suitable location could be found. The superelevation method was used at site 3 on Gulch 2R, and sites 27 and 28 on Bear Gulch Creek. The calculated peak debris discharges at all locations are considered to be poor at best because of the uncertainty about the applicability of clear-water flow equations to non-Newtonian debris flows.

At sites 3 and 27, a level was used to survey profiles of high-water marks along both banks and to survey a channel-thalweg profile for a distance of about 50 ft upstream and downstream from a surveyed channel cross section. The radius of curvature of the channel at each site was determined by swinging an arc through the plotted thalweg points on a plan view of the measurement site. The peak discharge then was calculated from the following simplified equation for flow around a bend (modified from Chow, 1959):

$$Q = (g\,\Delta h\, r/b)^{0.5} A, \qquad (1)$$

Table 1. Results of indirect discharge measurements

[--, no data]

Site number	Stream	Drainage area (mi^2)	Computed peak debris discharge (ft^3/s)	Method of computation	Average Manning's *n*	Average velocity (ft^3/s)	Average Froude number	Unit peak discharge [$(ft^3/s)/mi^2$]
1.....	Beaver Creek at mouth	73.3	[1]2,870	Slope-area	0.045	9.3	0.66	39
2.....	Gulch 1R	.02	106	Slope-area	.070	8.8	1.37	5,300
3.....	Gulch 2R	.03	571	Super-elevation	--	14.2	2.81	19,000
4.....	Gulch 1L	.14	414	Slope–area	.070	10.8	1.33	2,960
5.....	Gulch 2L	.07	110	Slope-area	.070	6.6	1.12	1,570
6.....	Gulch 3L	.56	979	Slope-area	.090	7.4	.94	1,750
7.....	Big Log Gulch	9.68	896	Slope-area	.075	6.0	.87	93
8.....	Gulch 4L	.29	694	Slope-area	.060	8.5	1.15	2,390
9.....	Gulch 3R	.10	381	Slope-area	.080	6.6	1.00	3,810
10.....	Gulch 4R	.07	142	Slope-area	.100	7.5	1.22	2,030
11.....	Gulch 5L	.76	982	Slope-area	.070	10.5	1.33	1,290
12.....	Gulch 5R	.07	267	Critical-flow	--	7.8	1.00	3,810
13.....	Beaver Creek at U.S. Forest Service gaging station	61.0	[1]522	Slope-area	.048	7.4	.74	8.6
14.....	Gulch 6R	.14	56	Slope-area	.067	8.4	1.64	400
15.....	Gulch 7R	.40	57	Slope-area	.063	6.8	1.19	143
16.....	Gulch 8R	.11	215	Critical-flow	--	6.7	1.00	1,950
17.....	Gulch 9R	.07	93	Slope-area	.060	8.6	1.45	1,330
18.....	Gulch 10R	.81	1,250	Slope-area	.067	11.6	1.21	1,540
19.....	Gulch 11R	.41	1,570	Slope-area	.070	12.6	1.24	3,830
20.....	Gulch 12R	.20	709	Slope-area	.063	12.8	1.63	3,550
21.....	Hunters Gulch	8.84	872	Slope-area	.067	.66	.78	99
22.....	Beaver Creek at Nelson	40.5	281	Slope-area	.037	6.0	.77	6.9
23.....	Gulch 13R	.47	600	Critical-flow	--	10.2	1.00	1,280
24.....	Gulch 14R	.12	163	Slope-area	.073	6.8	1.04	1,360
25.....	Gulch 15R	.13	404	Slope-area	.070	12.0	1.68	3,110
26.....	Bear Gulch Creek 1	1.13	3,100	Slope-area	.120	9.3	.91	2,740
27.....	Bear Gulch Creek 2	.92	15,800	Superelevation	--	23.2	1.71	17,200
28.....	Bear Gulch Creek 3	.88	29,900	Superelevation	--	32.0	2.76	34,000
29.....	Gulch 16R	.15	871	Slope-area	.093	13.3	1.44	5,810
30.....	Gulch 17R	.88	202	Slope-area	.080	6.0	.93	230
31.....	Beaver Creek above Bear Gulch Creek	33.6	[1]13.7	Measurement extension	.040	1.2	--	.4

[1]Peak discharge presumed to be water flow and not debris flow.

where Q = peak discharge, in cubic feet per second;
g = acceleration of gravity, in feet per second squared;
Δh = superelevation of the flow (average difference, in feet, between high-water marks on opposite banks);
r = radius of curvature of the channel bend, in feet;
b = width of the channel cross section, in feet; and
A = cross-sectional area of flow, in square feet.

At site 28, high-water profiles were surveyed along both banks for a distance of about 250 ft. Two channel cross sections were surveyed, spaced about 120 ft apart. The channel thalweg was not surveyed because the high-water profiles adequately defined the channel curvature. Cross-sectional area, channel width, discharge, and velocity (discharge divided by cross-sectional area) were computed for each surveyed cross section and the results were averaged to obtain a single value for the measurement site.

The results of the surveys and discharge computations for the two sites on Bear Gulch Creek are given in table 2. Flow velocities at both sites were very rapid, all greater than 20 ft/s. Froude numbers, which are an index to the state of flow in a channel, were substantially larger than 1.0, indicating rapid flow. Although such large velocities and Froude numbers rarely, if ever, occur with clear-water flow in natural channels (Jarrett, 1984), they are not unusual with debris flows (Gallino and Pierson, 1985). Evidence that flow velocities were extremely rapid was found at several locations within the Bear Gulch Creek channel where trees as much as 14 in. in diameter were sheared off almost flush to the ground (fig. 4).

Table 2. Results of superelevation computations for sites on Bear Gulch Creek

Site number	Cross section no. (in down-stream order)	Average depth at peak (ft)	Channel width at peak (ft)	Superelevation, Δh, at peak (ft)	Radius of curvature (ft)	Cross-sectional area (ft^2)	Channel gradient (ft/ft)	Mean velocity (ft/s)	Peak discharge (ft^3/s)	Froude number
27.....	1	9.8	69.8	7.0	167	681.5	0.095	23.2	15,800	1.71
28.....	1	11.7	82.0	17.0	136	961.6	.119	30.1	28,900	2.39
28.....	2	11.4	80.5	21.0	136	914.0	.119	33.8	30,900	3.12

Figure 4. Tree trunk sheared by the force of the debris flow.

The critical-flow method was used to estimate peak discharge at three sites where large vertical drops in the channel bed were present. At these sites, a channel cross section and high-water marks were surveyed approximately 10 to 15 ft upstream from each drop where the critical-flow section was presumed to occur. The discharge was calculated from the following critical-flow equation (Henderson, 1966, p. 51):

$$Q=A(gA/b)^{0.5} \quad (2)$$

where all terms are as defined in equation 1 for flow around a bend.

The assumption of a critical-flow section (Froude number = 1.0) occurring just upstream from a vertical drop generally is valid for clear-water flow but may be erroneous for debris flows where Froude numbers commonly exceed 1.0. Thus, peak-discharge estimates using the critical-flow method probably are conservatively small when applied to debris flows. For sites in steep channels where the superelevation method cannot be applied or where the several cross sections required for the slope-area technique cannot be obtained, the critical-flow method provides a procedure for obtaining a lower-bound estimate of peak debris discharge.

Using the slope-area method to compute peak discharge requires a subjective estimate of the flow resistance provided by the channel bed and banks. Although much experience has been obtained in making acceptably accurate estimates of the resistance factor (Manning's n value) for clear-water flows, the method has not been widely used for debris flows.

To find how Manning's n might differ for a debris flow, the slope-area method was applied to the surveyed data obtained at site 28. Though far from an ideal slope-area site as defined by Dalrymple and Benson (1967), site 28 is a contracting reach without substantial channel scour. The Manning's n was selected by the author and an experienced hydrologic technician without any allowance for debris; therefore, clear-water flow was assumed just for the n-value selection. On this basis, the average n value through the reach was 0.040. In addition to the two surveyed channel sections, an interpolated channel section midway between the two surveyed sections was used to generate a three-section slope-area computation. The computed discharge using the 0.040 n value was almost 60,000 ft^3/s, or about twice the discharge computed from the superelevation method. Using a Manning's n of 0.080 resulted in a computed discharge from the slope-area method of 29,600 ft^3/s, a value almost identical to that obtained from the superelevation computation. On that basis, it was concluded that for this particular debris flow in Bear Gulch Creek, a doubling of the conventionally determined n values would yield acceptable results by the slope-area method.

For lack of similar comparisons on the other tributary gulches, it was assumed that the same doubling of the n values would be required to produce reasonable slope-area results. Such a broad generalization may result in large error at some sites where the debris composition was substantially different from that of Bear Gulch Creek.

Discharges from Mainstem and Large Tributaries

In contrast to the small tributary discharges, the smallest unit peak discharges occurred in the Beaver Creek mainstem and in the two largest tributaries, Big Log Gulch and Hunters Gulch. At the Beaver Creek site

at the upstream boundary of the fire (site 31), the peak discharge was only 13.7 ft^3/s (unit peak discharge = 0.4 $(ft^3/s)/mi^2$), or about 8 ft^3/s greater than the estimated base flow before the storm began. Storm runoff from the unburned areas of the drainage upstream from site 31 was, thus, very minor.

Although the peak discharge of Beaver Creek increased to 281 ft^3/s (unit peak discharge = 6.9 $(ft^3/s)/mi^2$) at Nelson (site 22), the flow contributions from Bear Gulch Creek and Gulches 16R and 17R (sites 29 and 30) normally would be expected to produce a much larger increase in flow in the mainstem. Because the tributary discharges were debris flows, much of the flowing material settled out on the Beaver Creek flood plain before reaching the Beaver Creek channel. Resulting flows in the Beaver Creek channel were thus more fluid and much smaller in magnitude than those from the tributaries. Although flows in the Beaver Creek channel were still very heavily silt laden, the flow is presumed to have been more nearly like clear-water flow than flow from any of its tributaries, and the conventional fluid-flow equations were considered to be applicable without any adjustments for friction effects or for contained solids. Similarly, the unit discharges from Big Log Gulch (site 7) and from Hunters Gulch (site 21) are substantially smaller than those from the smaller tributary gulches. Although many of the small tributary gulches to Big Log Gulch and Hunters Gulch undoubtedly had large debris flows, most of the debris settled out before reaching the main channels or settled out within the main channels before reaching the measurement sites at the mouths of the two large gulches. As would be expected, the debris fans deposited at the mouths of these two gulches were composed exclusively of fine material (ash, silt, and sand). The discharges determined at the mouths of Big Log Gulch and Hunters Gulch are still presumed to have been debris flows rather than clear-water flows because of the large quantities of fine material deposited. The composition of the debris probably is substantially different from that on the smaller gulches, however.

At site 13 on the Beaver Creek mainstem, a continuous-flow record from the streamflow-gaging station operated by the U.S. Forest Service is available in addition to the peak discharge determination. The discharge of Beaver Creek from 1600 hours on August 31 through 1600 hours on September 1 is shown by hydrograph (fig. 5). The sharply rising curve illustrates the sudden increase in discharge normally associated with thunderstorm-caused floods. Unlike most floods, however, the hydrograph in figure 5 exhibits three separate peaks that are presumed to be the result of temporary damming of the mainstem by debris from tributaries. Debris from Gulch 10R (site 18) formed one blockage upstream from the gage site and may account for the two initial spikes of the hydrograph. If so, the sudden

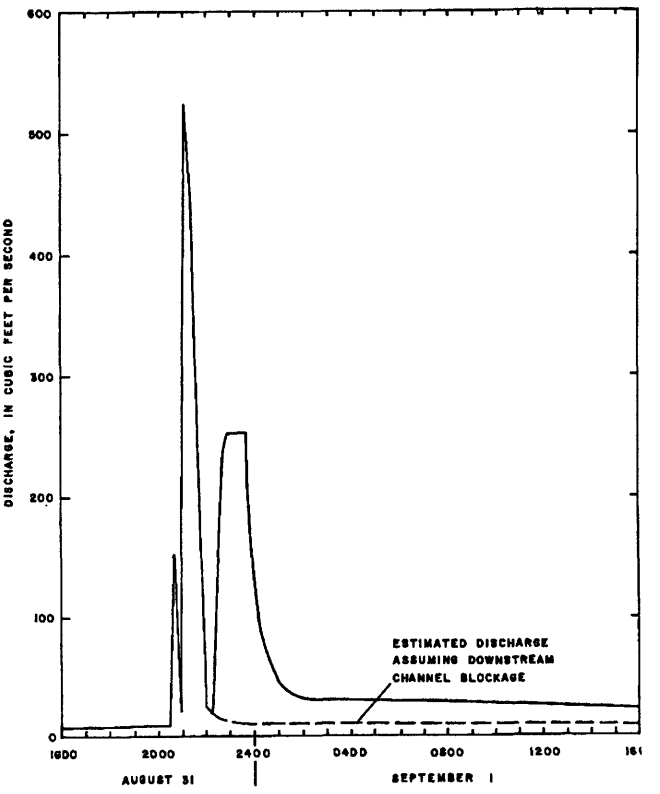

Figure 5. Discharge hydrograph for Beaver Creek at U.S. Forest Service streamflow-gaging station (site 13).

decrease in flow at 2100 hours was due to the sudden damming of the mainstem channel. When the temporary dam was breached only a few minutes later, the surge of flow caused the second hydrograph peak at 2115 hours. The third, unusually flattened hydrograph peak may not be a discharge peak but rather an increase in stage at the site resulting from a temporary dam forming just downstream from the gaging station. Debris from Gulch 5R (site 12) may have dammed Beaver Creek, but the evidence was not so conclusive as it was for the damming upstream. If a downstream blockage did occur, then the estimated actual discharge hydrograph from 2115 hours would be represented by the dashed line in figure 5. In this instance, the third hydrograph peak represents an increase only in stage at the gage pool as water is backed up behind the downstream dam. The stage evidently increased until water began flowing over the top of the dam, then held steady until the dam breached at about 2345 hours on August 31.

Discharges from Small Tributaries

The unit peak debris discharges from the tributary gulches (excluding Big Log Gulch and Hunters Gulch) range from 143 $(ft^3/s)/mi^2$ at site 15 on Gulch 7R to 34,000 $(ft^3/s)/mi^2$ at site 28 on Bear Gulch Creek. Even

excluding Bear Gulch Creek, where the extremely large unit debris discharges may be partly due to debris damming and subsequent release, the magnitude of the discharges from the small tributary gulches generally is very large, and the variation in unit discharge from site to site also is large. The magnitudes of the peak discharges from the Beaver Creek tributaries with maximum known flood discharges from comparably sized drainages in Montana are graphically compared in figure 6. Many of the peak discharges from the 1984 debris flows plot close to or even above the envelope curve for largest known water floods in Montana. Indeed, the 1984 peak debris discharges for two sites on Bear Gulch Creek (sites 27 and 28) plot well above the envelope curve for maximum known water floods in the United States.

Because the peak discharges from the Beaver Creek tributaries were debris flows rather than clear-water flows, subtracting the estimated solids component of the flows would result in equivalent water discharges that would be more directly comparable to the maximum flood envelope curves. Unfortunately, the solids concentration of the debris flows can only be estimated. On the basis of the composition of a debris slurry reconstituted from a debris sample taken near the mouth of Bear Gulch Creek (described in a later section of this report), the estimated solids component of the debris flow from Bear Gulch Creek was 72 percent by volume. Assuming that the flows from the other Beaver Creek tributaries had about the same solids concentrations (except for Big Log Gulch and Hunters Gulch), the author estimates peak water discharges from the tributaries would be 28

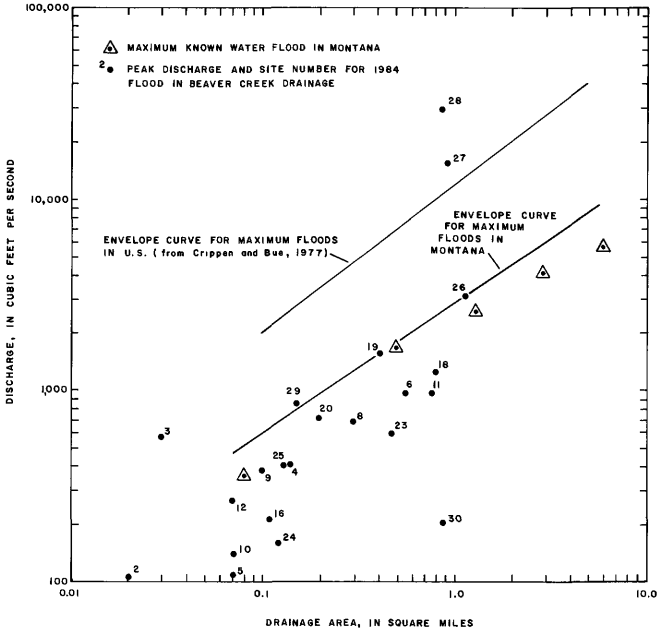

Figure 6. Comparison of selected 1984 debris flows with maximum known water floods in Montana and the United States.

Table 3. Percentages of tributary drainage areas burned

Site number	Stream	Unit peak discharge [(ft³/s)/mi²]	Percentage of drainage area burned	Percentage of drainage area burned severely
2.....	Gulch 1R	5,300	100	0
3.....	Gulch 2R	19,000	100	21
4.....	Gulch 1L	2,960	50	50
5.....	Gulch 2L	1,570	70	70
6.....	Gulch 3L	1,750	68	68
8.....	Gulvh 4L	2,390	90	90
9.....	Gulch 3R	3,810	100	0
10.....	Gulch 4R	2,030	100	7
11.....	Gulch 5L	1,290	84	84
12.....	Gulch 5R	3,810	100	14
14.....	Gulch 6R	400	100	20
15.....	Gulch 7R	143	100	2
16.....	Gulch 8R	1,950	100	18
17.....	Gulch 9R	1,330	100	4
18.....	Gulch 10R	1,540	100	9
19.....	Gulch 11R	3,830	100	0
20.....	Gulch 12R	3,550	100	20
23.....	Gulch 13R	1,280	100	35
24.....	Gulch 14R	1,360	100	0
25.....	Gulch 15R	3,110	100	0
26.....	Bear Gulch Creek 1	2,740	89	26
27.....	Bear Gulch Creek 2	17,200	95	32
28.....	Bear Gulch Creek 3	34,000	97	33
29.....	Gulch 16R	5,810	73	7
30.....	Gulch 17R	230	24	7

percent of the values shown in table 1 and figure 6. Making this adjustment to the plotted points in figure 6 results in all the 1984 peak discharges (except for sites 27 and 28 on Bear Gulch Creek) falling below the envelope curve for maximum floods in Montana. The 1984 peak discharges for sites 27 and 28 on Bear Gulch Creek would fall below the envelope curve for maximum floods in the United States.

The large variability in unit discharges from site to site within the study area originally was believed to be largely caused by the variability of the intensity of the fire and its effect on the soil. Thus, the largest unit discharges were expected to occur from drainages where the soil was burned most severely. In testing this hypothesis, aerial color photographs were used to delineate areas that had been burned moderately and areas that had been burned severely. Dean A. Suricek, a soil scientist with the U.S. Forest Service who had walked most of the burn area, assisted in the delineation of the burn area. An area was considered to have been burned moderately if the burn destroyed soil surface litter and humus on less than 40 percent of the area, and the classification was considered severe if the burn destroyed soil surface litter and humus on more than 40 percent of the delineated area. Delineations of the burn area were transferred to a map showing tributary drainage so that the percentages of each drainage area that burned moderately and severely could be determined. The results of those determinations for the tributary gulches are given in table 3, and the

Figure 7. Debris from Bear Gulch Creek. View is from the middle of the channel looking toward right bank.

correlation between percentage of burned area or percentage of area burned severely and unit discharge is not very strong. A simple multiple regression analysis relating percentage of burned area and percentage of area burned severely to unit discharge had a coefficient of determination (R^2) of 0.1, indicating only a very weak linear relationship.

Thus, although floods resulted only from drainages that experienced some degree of burning, the variability in the magnitude of flooding from site to site within the burned area evidently was caused by a complex combination of many factors, including variability of storm intensity, soil type, vegetative cover, and land slope in addition to the variability in the intensity of burning. Also, debris damming within the channel most likely contributed to the large discharges from Bear Gulch Creek, and such damming may have occurred to a lesser extent in the other tributary gulches. Finally, the calculated debris discharges are subject to considerable error because the conventional clear-water equations that were used may not be applicable to non-Newtonian debris flows.

Discharges from Bear Gulch Creek

The debris flow from Bear Gulch Creek was particularly impressive because of the size and quantity of debris transported through the drainage. Large trees (fig. 7) and rocks as big as 3 ft in diameter were a substantial part of the flow. The debris flow apparently originated near the drainage divide where severe sheet, rill, and gully erosion removed much of the soil mantle. The soils were severely burned and evidently became water repellent along the divide as a result. The virtual lack of infiltration capacity coupled with burned, fragile soils and steep hillslopes provided ideal conditions for erosion of

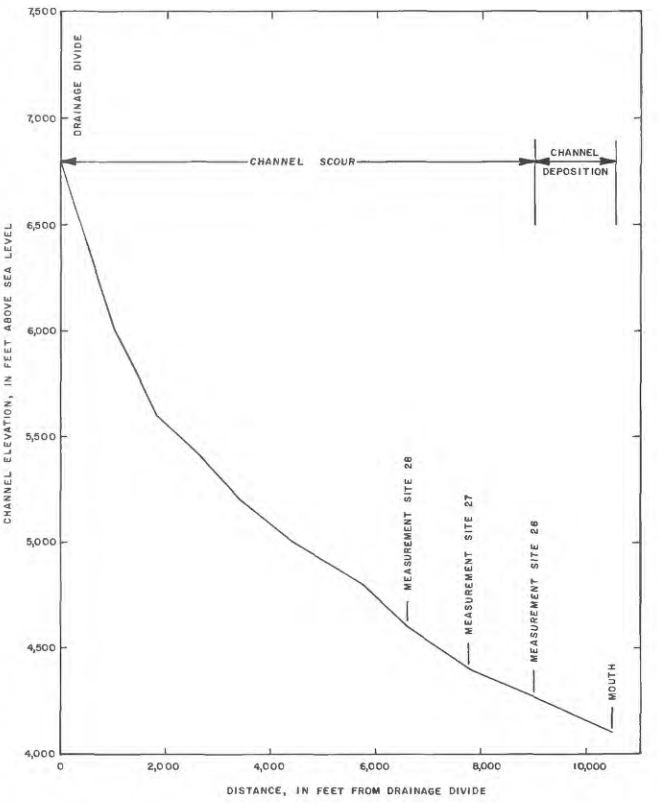

Figure 8. Profile of Bear Gulch Creek channel.

massive quantities of soil downslope and into the Bear Gulch Creek channel. Mass movement of soil also may have occurred on some steeper hill slopes where the soil mantle was severely burned and was only a few inches thick.

The initial flow of soil-water mixture down the channel quickly grew in size as material from the channel bed was incorporated into the flow (bulking). The debris flow probably reached its peak magnitude at site 28, which is just downstream from a major Bear Gulch Creek tributary and about 0.7 mi upstream from the mouth. The largest computed discharge is believed to be largely caused by temporary damming of the flow behind a bouldery, log-rich front. The damming and subsequent release of these debris dams tend to occur in particularly narrow and sinuous channel reaches. Measurement site 28 is especially narrow and sinuous and is, thus, a likely location for damming to occur. From site 28 downstream to site 27, a distance of about 0.2 mi, the peak discharge decreased from 29,900 to 15,800 ft^3/s. Likewise, from site 27 downstream 0.2 mi to site 26 the flow further decreased to 3,100 ft^3/s.

Near site 26, deposition began and generally increased downstream to the mouth as channel slope decreased. A profile view of the Bear Gulch Creek channel (fig. 8) illustrates the change in channel slope from the drainage divide to the mouth and the resultant areas of channel erosion and deposition. Estimates of the

cross-sectional area of channel erosion were made at various locations along the channel reach from near the drainage divide to site 26. The areal estimates were multiplied by their respective channel reach lengths to determine the estimated volume of material eroded from the Bear Gulch Creek channel. The total volume of solid material eroded from just the channel was thus estimated to be 20,000 yd^3. A team of soil scientists from Montana State University investigating topsoil erosion from selected sites estimated that 2.4 in. of soil were eroded from a site near the drainage divide of Bear Gulch Creek (Clifford Montagne, written commun., 1985). If the 2.4 in. of erosion occurred from the part of the Bear Gulch Creek drainage that had burned severely, about 60,000 yd^3 of soil were removed from the drainage outside the channel limits. The total volume of solids transported in the debris flow is thus estimated to be 80,000 yd^3.

A sample of debris from a levee formed at the inside of a channel bend located between sites 26 and 27 was used for particle-size analysis and to estimate the solids-water ratio of the debris flow. The results of the particle-size analysis together with the range of data reported in other debris flow studies are shown in figure 9. The cumulative distribution of particle size for the Bear Gulch Creek debris flow is reasonably comparable to those reported in other mountainous areas.

In the estimation of the solids-water ratio of the flow, water was slowly added to a weighed, dry portion of the debris sample and thoroughly mixed until the heterogeneous mixture became fluid like freshly mixed concrete. The water-solids ratio of this reconstituted debris mixture was presumed to be the same as that of the actual debris flow. Although this procedure may seem to be subjective, results are reportedly fairly precise (Gallino and Pierson, 1985). For the sample from Bear Gulch Creek, the percentage of solids by weight was found to be 87 and the percentage by volume was 72. Thus, the peak water discharge from Bear Gulch Creek can be estimated by multiplying the computed discharges reported in table 1 by 28 percent. Again for lack of sediment sample data from the other tributary gulches, the same percentage reduction is considered to be applicable to the other small tributary measurement sites. As with the Manning's n adjustment, the largest expected errors from such an areal generalization are for those tributaries where the debris composition was significantly different from that of Bear Gulch Creek.

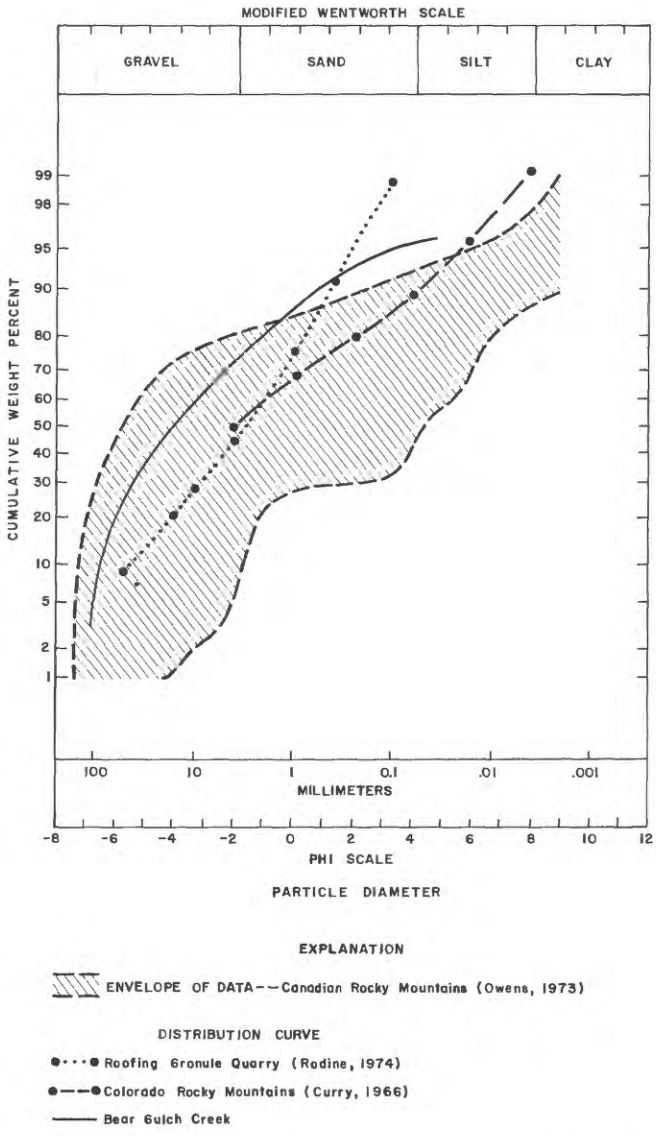

Figure 9. Cumulative distribution of particle size for the Bear Gulch Creek debris flow compared to distribution curves and envelope of data from other studies.

SUMMARY

An August rainstorm of moderate intensity and duration resulted in debris flows from tributaries draining burned parts of the Beaver Creek watershed. Although no significant runoff occurred from unburned tributaries, the peak debris discharges from the burned areas were close to or above an envelope curve for maximum known water floods in Montana. Peak discharges were determined at 31 sites by using superelevation, critical-flow, and conventional slope-area methods. On the basis of results at one site where both the superelevation method and the slope-area method were used, Manning's n values were doubled to account for the additional energy loss of the highly viscous debris flows.

Peak discharges in the Beaver Creek mainstem were more fluid than in the tributaries, and the unit peak discharges were significantly smaller as the debris from tributaries settled out before reaching the Beaver Creek channel. In at least one instance, however, debris from a tributary spilled into Beaver Creek and formed a temporary dam across the channel. Unit peak discharges from

the two largest tributaries of Beaver Creek within the burned area also were considerably smaller than from the other tributary gulches because only parts of the larger drainage areas produced debris flows and presumably also because debris loads were deposited before reaching the channels of these larger streams.

Unit peak debris discharges in the smaller tributary gulches ranged from 143 to 34,000 $(ft^3/s)/mi^2$. A multiple-regression analysis relating unit peak debris discharge to percentage of drainage area burned and percentage of drainage area burned severely (more than 40 percent of the area with surface litter and humus destroyed) showed only a weak linear relationship ($R^2=0.1$). The large variability in unit peak debris discharge thus is presumed to be the result of a complex combination of contributing causes such as variability in storm intensity, soil type, vegetative cover, land slope, degree of burning, possible debris damming, and inaccurate determinations of peak debris discharge.

The largest unit peak debris discharge and most spectacular debris flow occurred in Bear Gulch Creek. The debris flow evidently was triggered by mass erosion of the intensely burned soil surface along the drainage divide. Once the flow began down the Bear Gulch Creek channel, it increased by bulking and probably peaked at measurement site 28, 0.7 mi upstream from the mouth, where a peak discharge of 29,900 ft^3/s was computed. The flow rapidly decreased from this point to the next measurement point 0.2 mi downstream, where a peak discharge of 15,800 ft^3/s was computed, and to the last measurement point 0.2 mi farther downstream, where the computed peak discharge was 3,100 ft^3/s. The rapid decrease in flow is believed to be the result of debris damming that occurred in the narrow, sinuous channel near measurement site 28. The total volume of material moved through the Bear Gulch Creek channel was estimated to be 80,000 yd^3, of which 20,000 yd^3 was eroded from just the channel.

The composition of the debris flow in Bear Gulch Creek was estimated by adding water to a sample of debris until a concrete-like slurry resulted. The percentage of solids by volume of the reconstituted debris flow was 72. Thus, estimates of peak water discharge at the measurement sites can be approximated by multiplying the computed peak debris discharges by 28 percent. When this adjustment is made, peak discharges at two sites on Bear Gulch Creek still plot above the envelope curve for maximum known floods in Montana but below the envelope curve for maximum known floods in the United States.

REFERENCES CITED

Campbell, R.H., 1975, Soil slips, debris flows, and rainstorms in the Santa Monica Mountains and vicinity, southern California: U.S. Geological Survey Professional Paper 851, 51 p.

Chow, V.T., 1959, Open-channel hydraulics: New York, McGraw-Hill, 680 p.

Crippen, J.R., and Bue, C.D., 1977, Maximum floodflows in the conterminous United States: U.S. Geological Survey Water-Supply Paper 1887, 52 p.

Curry, R.R., 1966, Observations of alpine mudflows in the Tenmile Range, central Colorado: Geological Society of America Bulletin 77, p. 771–776.

Dalrymple, Tate, and Benson, M.A., 1967, Measurement of peak discharge by the slope-area method: U.S. Geological Survey Techniques of Water-Resources Investigations, Book 3, Chapter A2, 12 p.

DeByle, N.V., 1973, Broadcast burning of logging residues and the water repellency of soils: Northwest Science, v. 47, no. 2, p. 77–87.

Gallino, G.L., and Pierson, T.C., 1985, The 1980 Polallie Creek debris flow and subsequent dam-break flood, East Fork Hood River basin, Oregon: U.S. Geological Survey Water-Supply Paper 2273, 22 p.

Henderson, F.M., 1966, Open channel flow: New York, The Macmillan Company, 522 p.

Jarrett, R.D., 1984, Hydraulics of high-gradient streams: Journal of Hydraulic Engineering, v. 110, no. 11, p. 1519–1539.

Krammes, J.S., and Debano, L.F., 1965, Soil wettability—A neglected factor in watershed management: Water Resources Research, v. 1, no. 2, p. 283–286.

Miller, J.F., Frederick, R.H., and Tracey, R.J., 1973, Precipitation-frequency atlas of the western United States, Volume 1—Montana: U.S. Department of Commerce, National Weather Service, NOAA Atlas 2, 41 p.

Owens, I.F., 1973, Alpine mudflows in the Nigel Pass area, Canadian Rocky Mountains: University of Toronto, unpublished Ph.D. thesis, 218 p.

Pierson, T.C., 1980, Erosion and deposition by debris flows at Mt. Thomas, North Canterbury, New Zealand: Earth Surface Processes, v. 5, p. 227–247.

Rodine, J.D., 1974, Analysis of the mobilization of debris flows: Final report to the U.S. Army Research Office, Durham, N.C., Report No. ARO 9973.1–EN, 226 p.

Methods and Importance of Suspended-Organic-Carbon Determination in Hydrologic Studies

By Ronald L. Malcolm *and* Patrick W. McKinley

Abstract

Detailed procedures are presented for the determination of suspended organic carbon in water by two different methods: the silver-membrane-filter method and the difference method (total organic carbon minus dissolved organic carbon). Both methods are applicable to a wide range of suspended-sediment concentrations in streams. The silver-membrane-filter method is recommended at low suspended-sediment concentrations, less than 50 milligrams per liter, when the sample contains appreciable quantities of organisms and biodegradable organic substances, and when the most precise data are desired. The difference method is recommended when on-site filtration in the field is precluded by time or field sampling conditions or when the complete filtering assembly is not available for field use. Minor disadvantages of the silver-membrane-filter method include the necessity of trained technicians for field sampling, the cost of silver-membrane filters for duplicate or triplicate sampling, the time required for on-site filtration, and the maintenance required to keep equipment clean in the field. The major disadvantage of the difference method is that if the sample is not adequately chilled during storage or shipment, organic carbon can be redistributed between dissolved and suspended phases or even lost from the sample by decomposition.

Both methods are free of interferences and agree closely to simple and environmental organic-carbon standards. Precision of the silver-membrane-filter method is slightly superior to that of the difference method.

INTRODUCTION

The amount of organic matter in streams, lakes, and wastewaters is important to the hydrologist evaluating water quality. The quantity of carbon transported to the oceans by rivers in both dissolved and particulate forms is a critical factor in evaluating carbon dioxide (CO_2) sources and fluxes into the atmosphere. Traditional parameters, such as biochemical oxygen demand (BOD) and chemical oxygen demand (COD), have served as useful indices of organic-wastewater quality, but both have been misused frequently and often results are misinterpreted. BOD and COD data are nonquantitative for organic substances; both indices have several limitations (Jones, 1969; Grady, 1971; Malcolm and Leenheer, 1973). Total organic carbon (TOC) data have become more popular with hydrologists but are difficult to interpret and usually are limited by analytical sources of error and precision (Malcolm and Leenheer, 1973). The on-site separation of TOC into dissolved organic carbon (DOC) and suspended organic carbon (SOC), the quantitative nature of DOC and SOC data, the many interpretations of DOC and SOC data, and the ease of DOC and SOC analytical determinations have led to general use of these parameters. DOC is defined as that part of the organic carbon in water that passes through a 0.45-μm silver-membrane filter. SOC is defined as that part of the organic carbon in water that remains on the 0.45-μm silver-membrane filter. Previous papers (Malcolm and McKinley, 1972; Malcolm and Leenheer, 1973; Leenheer and others, 1974) have emphasized DOC methods and the usefulness of DOC data. The purpose of this paper is to present two methods for SOC determination and to discuss the usefulness of SOC data in hydrologic studies.

METHODS OF STUDY

Method A—Silver-Membrane-Filter Method

Field Sampling

Collect duplicate representative water samples, each containing 0.2 to 0.8 mg of organic carbon. Place a silver-membrane filter of 47-mm diameter and 0.45-μm pore size on the stainless-steel filter support. The silver-membrane filter needs to be handled very carefully with metal forceps to prevent contamination or breakage. Hand tighten the stainless-steel bottom-end cap to the filter barrel. Fill the stainless-steel filter barrel (fig. 1) with water. Replace the stainless-steel top-end cap, pressurize with carbon-free nitrogen to as much as 100 lb/in^2, and continue filtration until all water has passed through

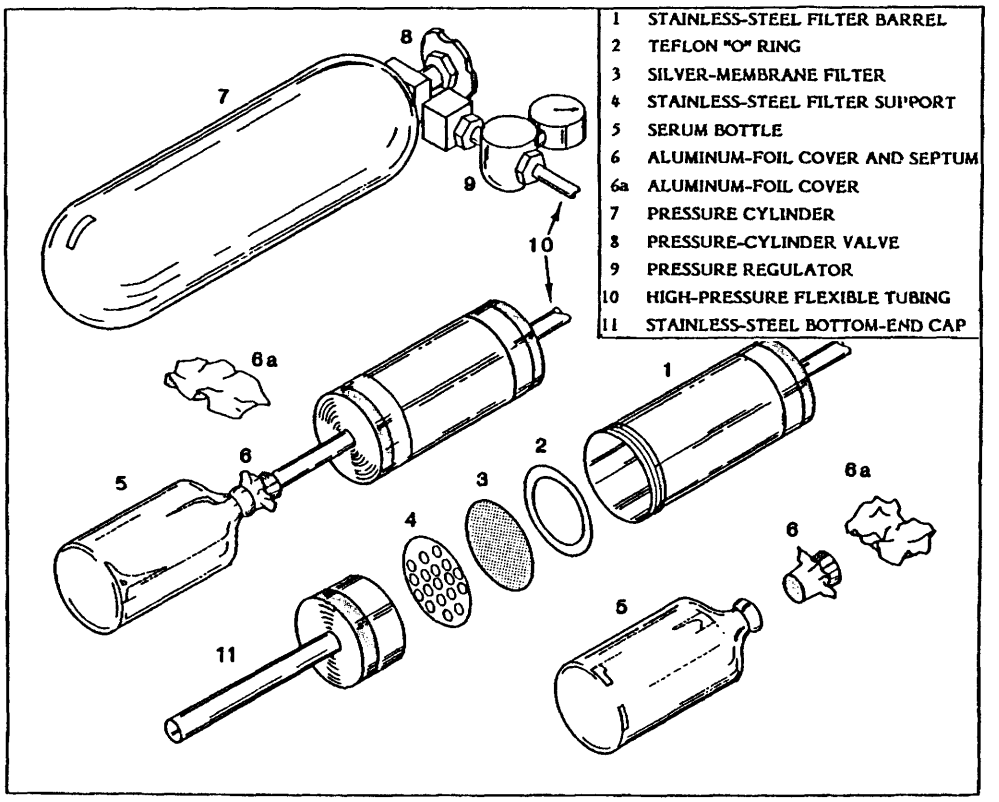

Figure 1. Equipment for field sampling of suspended organic carbon and dissolved organic carbon.

the filter. Refill the filter barrel with the water sample until sediment containing 0.2 to 0.8 mg of organic carbon accumulates on the silver-membrane filter, noting the volume of water filtered (see "Discussion of Methods"). Remove the silver-membrane filter containing sediment from the filter assembly with metal forceps; roll the filter into a small coil with the sediment side inward; and place it in an airtight, clean container (such as a 2.5 cm × 5 cm vial) for shipping to the laboratory. Repeat the procedure for the sample duplicate or triplicate.

Laboratory Procedure

Place the silver-membrane filter containing sediment into a 10-mL glass ampoule, previously baked at 500°C to free it of organic contamination. Add 10 mL of doubly distilled water and 1 mL of concentrated phosphoric acid to the ampoule. Heat the ampoule overnight on a steam bath. Cool the ampoule to room temperature; purge with oxygen gas flow through a glass capillary purge tube for 6 min; dry the neck of the ampoule in a small flame; and add 0.2 g of potassium persulfate. Seal the neck of the ampoule with a torch or a special sealing apparatus similar to the Oceanography International Carbon Analyzer Sealing Unit. Place several ampoules into a pressure vessel containing water, seal the vessel, and heat overnight at 175°C. Organic carbon is converted to CO_2 by this digestion. Break each ampoule in a closed system and determine the amount of CO_2 released by the infrared analyzer while sweeping the ampoule with CO_2-free air. Organic carbon in the ampoule is computed from a working standard curve of integrator counts versus milligrams of organic carbon. SOC, in milligrams per liter in the sample, is calculated from the volume of the original water sample represented within the 10-mL ampoule. This laboratory procedure is essentially the same as written by Wershaw and others (1983).

Method B—Difference Method (Total Organic Carbon Minus Dissolved Organic Carbon)

Field Sampling

Collect a representative 0.5- to 1-L water sample. The sample may be collected in a glass shipping container or transferred to a glass shipping container after collection. Pack the sample in ice for transport to the laboratory.

Laboratory Procedure

For TOC determination, blend the sample in a blender for 2 min and pour into a 2-L glass cyclinder. While the sample is vigorously being mixed with nitrogen

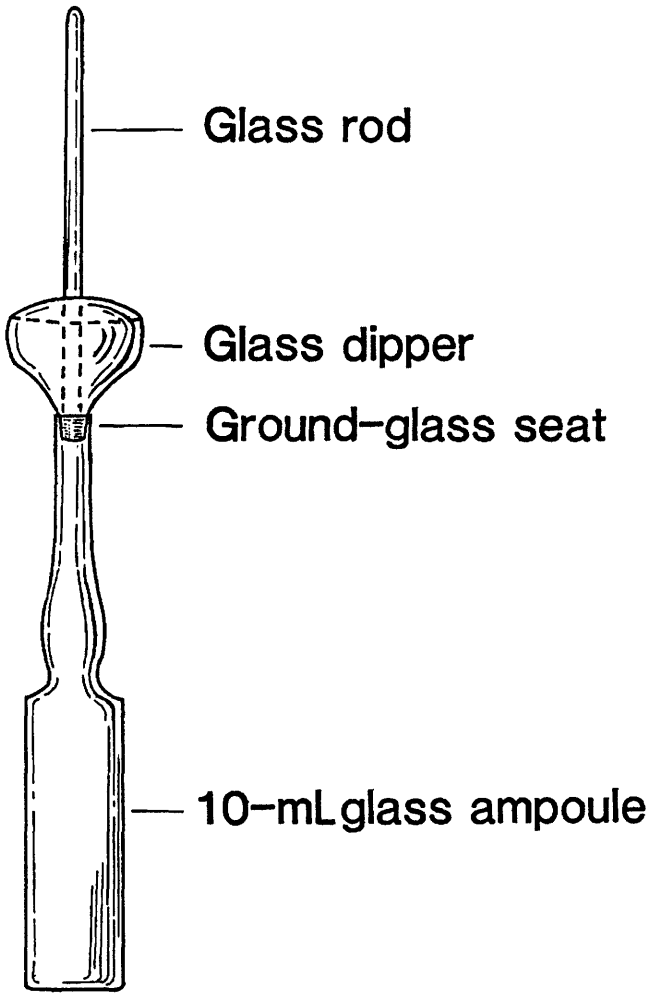

Figure 2. Device for laboratory subsampling of total organic carbon.

gas, remove a subsample from the suspension with a 10-mL glass dipper (fig. 2). Place the glass dipper over the mouth of a 10-mL glass ampoule; dislodge the glass-rod stopper by gentle twisting; and flow the sample quantitatively into the ampoule. Add 1 mL of concentrated phosphoric acid into the ampoule; heat overnight on a steam bath; and proceed as in Method A.

For SOC determination, place five aliquot samples with the glass dipper into a stainless-steel filter assembly with a 0.45-μm silver-membrane filter, as used for field filtration in Method A.

For DOC determination, place five aliquot samples with the glass dipper into a stainless-steel filter assembly with a 0.45-μm silver-membrane filter, as used for field filtration in Method A. Filter the sample and collect the effluent water for DOC analysis. Pipette 10 mL of filtered water into an ampoule containing 0.2 g of potassium persulfate and 0.5 mL of concentrated phosphoric acid. Purge the ampoule with CO_2-free oxygen for 6 min; then seal the ampoule. Proceed with DOC analysis as for SOC in Method A. DOC analysis may also be performed on a modified Beckman 915 Carbon Analyzer (Malcolm and others, 1973), on a Technicon DOC module, or on an Oceanography International wet oxidation carbon analyzer (Wershaw and others, 1983).

DISCUSSION OF METHODS

During field collection of surface water for SOC determination by the silver-membrane-filter method, the volume of sample to be filtered (to accumulate 0.2 to 0.8 mg SOC on the filter) can be determined by estimating the suspended-sediment concentration and its expected relationship to SOC (table 1). The expected relationship between suspended-sediment concentration and SOC has been derived from more than 1,000 published (Malcolm and Durum, 1976) and unpublished values (from the authors' field experience) for numerous streams and lakes throughout the United States. Experience has shown that sample collectors who have had minimal training can easily estimate suspended-sediment concentrations within the concentration ranges listed in table 1.

Table 1. Expected relationship between estimated suspended-sediment and suspended-organic-carbon concentrations

Estimated suspended-sediment concentration (mg/L)	Expected suspended-organic-carbon concentration of sediment (percent dry weight)	Volume of sample to be filtered (mL)
25 or less	5–10	400–600
25–50	4–7	300–500
50–100	3–5	200–300
100–1,000	1–4	100–150
1,000 or greater	0.5–1.5	40–60

Extremely low or high suspended-sediment concentrations may cause sampling problems. Samples containing suspended-sediment concentrations in excess of 1,000 mg/L commonly contain so much sand that they are difficult to accurately subsample in the field or in the laboratory. These samples may be treated as bottom sediments and analyzed accordingly for organic carbon by the Leco method and Van Slyke method (Malcolm and others, 1973). Surface-water samples containing less than 25 mg/L of suspended sediment commonly contain silt- and clay-size particles of living organisms, organic detritus, and inorganic minerals coated with organic matter. Even though suspended-sediment concentration is low, a proportionally smaller volume of sample is needed for filtration, because the small sediment particles contain a higher content of organic matter than coarse silt and sand particles. In surface waters that have low

suspended-sediment concentration, SOC would be equivalent to the seston in biological terminology.

Low concentrations of SOC are common in ground water. Unlike surface water, the organic matter in ground water is more likely to occur as coarse silt-size particles or as a coating on silt- and sand-size particles. In some unfiltered ground-water samples, SOC can cause a significant error in DOC, if it is assumed that the water contains no sediment. In contrast, large volumes of water may need to be filtered to accumulate sufficient SOC on the silver-membrane filter for SOC analysis. Wells contaminated with organic materials commonly have a large population of organisms in the water. Some of these samples may appear relatively free of suspended sediment, but the organisms will rapidly clog the silver-membrane filter soon after filtration begins.

The error associated with SOC determination by both methods is quite variable and usually large (table 2); the error associated with SOC determination is due largely to sampling and subsampling as verified by the data in tables 3 and 4. As shown in table 3, the analytical error in SOC measurement is quite small. Precision error is 1.5 percent or less, using a phthalate solution as an organic-carbon standard, in the operating range of 10 to 40 mg/L, and almost all of this error is a result of pipetting. Accuracy of the determination is 1.4 percent of the true value, using phthalate, sucrose, and quinildic-acid standards, in the operating range of 10 to 40 mg/L. Precision of the SOC methods decreased threefold (table 4) when three dried SOC samples were ground to less than 100 mesh (0.15 mm) and used as organic-carbon standards. This precision error was due largely to organic-carbon heterogeneity in the ground samples and to the difficulty of weighing small representative samples. Accuracy of the determinations was within 3 percent of the true organic-carbon value, as determined by Leco analysis in three independent laboratories. Sample standard No. 2 contained 4.7 percent inorganic carbon; whereas, sample standards Nos. 1 and 3 contained no inorganic carbon. All three sample standards were routinely treated for carbonate removal by heating overnight on a steam bath; no losses of organic carbon were found.

Error in the SOC determination because of sampling and subsampling is expected; obtaining a representative sample of suspended sediment from a stream is not a simple task. Even with the best equal-transient-rate (ETR) sampling techniques, where composite depth-integrated samples are collected from several stream cross sections, duplicate ETR samples commonly may vary between 5 to 20 percent in suspended-sediment concentration. The magnitude of this error generally is correlated with sediment concentration.

SOC analysis of a number of selected stream samples is given in table 1. These samples represent streams under various flow conditions from several geographical regions of the country. Precision of the silver-membrane-filter method is approximately twice as good as the difference method (7 percent versus 12 percent).

Table 2. Comparison of data for suspended organic carbon determined by the silver-membrane-filter and the difference methods

[Avg, average]

Total organic carbon (mg/L)	Dissolved organic carbon (mg/L)	Suspended organic carbon, silver-membrane-filter method (mg/L)	Suspended organic carbon, difference method (mg/L)
Clear Creek near Denver, Colo., 1/30/73			
3.5	2.6	1.1	0.9
3.4	2.2	1.0	1.2
3.5	2.3	.9	1.2
Avg 3.5	2.4	1.0	1.1
Clear Creek near Denver, Colo., 12/21/72			
12.9	8.2	3.6	4.7
12.2	7.9	3.7	4.3
10.9	7.6	3.3	3.3
11.5	7.9	4.2	3.6
Avg 11.9	7.9	3.7	4.0
Clear Creek near Denver, Colo., 12/26/72			
22.5	19.2	4.3	3.3
22.5	19.5	4.7	3.0
22.8	17.6	4.0	5.2
22.8	19.4	3.6	3.4
Avg 22.6	18.9	4.1	3.7
South Platte River near Denver, Colo., 12/26/72			
27.0	17.1	9.4	8.9
23.5	16.0	12.2	7.5
27.0	15.3	10.0	11.7
24.5	15.8	9.4	8.7
Avg 25.5	16.0	10.2	9.2
Houston Ship Channel near Houston, Tex., 3/1/73			
12.5	10.9	2.8	1.6
13.0	10.8	3.6	2.2
13.6	11.2	3.6	2.4
13.4	10.8	3.4	2.6
Avg 13.1	10.9	3.4	2.2
Brazos River near Houston, Tex., 3/15/74			
14.8	5.4	4.5	9.4
14.2	5.6	8.1	8.6
13.9	5.2	4.6	8.7
Avg 14.3	5.4	5.7	8.9
Sopchoppy River near Tallahassee, Fla., 1/17/73			
33	33	.5	0
34	33	.4	1.0
32	32	.5	0
31	32	.5	-1.0
Avg 32	32	.5	0.

COMPARISON OF METHODS

On-site silver-membrane filtration for SOC has several advantages: (1) immediate separation of dissolved and particulate phase; (2) efficient coordination with DOC sampling; (3) less sample handling and shipment; and (4) accumulation of more data for each sample. On-site silver-membrane filtration is a prerequisite for DOC sampling. Suspended-sediment accumulations on the silver-membrane filter during DOC sampling can be used directly for SOC analysis, without

Table 3. Background and precision values for the two suspended-organic-carbon methods with aqueous phthalate used as an organic-carbon standard

[--, no data]

Solution concentration (mg/L)	Integrator counts	Average	Error (percent)	Standard deviation
Reagent blanks.	32, 40, 38, 45, 39, 61, 33, 47, 55, 57	45	--	--
4	1,050, 995, 1,004, 973, 1,025, 954, 1,016, 922, 944, 1,044	993	3.5	43
10	2,008, 2,028, 1,982, 2,109, 2,023, 2,046, 2,097, 2,018, 2,053, 2,063	2,043	1.5	40
20	3,122, 3,233, 3,183, 3,291, 3,250, 3,241, 3,289, 3,278, 3,237, 3,255	3,238	1.2	52
40	5,450, 5,367, 5,540, 5,470	5,441	1.0	71

Table 4. Precision values for the suspended-organic-carbon method using ground (100 mesh =0.15 mm) particulate sediment as organic-carbon standard

Sample standard no.	Milligrams of standard in 10 mL vial	Percent suspended organic carbon	Average percentage suspended organic carbon	Error (percent)	Standard deviations
1	10.0	3.85	3.86	4.1	0.20
	11.0	4.23			
	17.5	3.60			
	22.4	3.84			
	21.2	3.73			
	21.5	3.76			
	20.6	3.59			
	30.0	3.93			
	32.2	4.01			
	30.0	4.06			
2	21.8	2.66	3.60	4.3	0.15
	12.1	2.81			
	15.3	2.61			
	21.6	2.45			
	15.0	2.47			
3	24.2	1.85	1.85	3.6	0.10
	12.3	1.81			
	11.1	1.98			
	8.0	1.75			

removal of the sediment from the silver-membrane filter. The immediate separation of DOC and SOC prevents exchange from one phase to the other as a result of assimilation, sorption or desorption, precipitation, solubilization, decomposition, or changes in general chemistry, such as dissolved oxygen, pH, or temperature. Because DOC commonly is much lower in concentration and more susceptible to rapid changes than SOC, DOC values may change markedly from in-situ stream values during transport of whole-water samples to the laboratory. On-site freezing or addition of inorganic preservatives to whole-water samples does not prevent the exchange of organic compounds between phases, because dissolved organic species commonly co-precipitate with inorganic constituents and because various analytical problems are associated with mercury (Hg_2Cl_2) and other preservatives. In addition to exchange between organic phases, organic carbon can be converted to inorganic carbon (CO_2) by decomposition. On-site separation of SOC by silver-membrane filtration and immediate chilling or drying of the sample prevents undesirable sample changes.

The ease of sample filtration and the color and consistency of the suspended sediment on the filter add to the interpretive value of the sample. Frequently, certain hydrologic phenomenon, such as colloidal inanimate organic debris, algal or microbial growth, and finely divided inorganic colloidal matter may not be observed in the whole-water sample but can be readily observed during filtration and observation of the filter.

Some of the possible limitations of silver-membrane filtration for SOC are (1) the training of fastidious technicians for sample collection and the time required for on-site personnel to filter samples; (2) the undesirable on-site conditions for filtration, such as wind, blowing dust, and cold; and (3) the desirability of collecting suspended sediment on two separate silver-membrane filters. Duplicate samples generally are needed because of the definite possibility of sample loss by ampoule breakage in the laboratory. When only one sample is collected, the SOC data would be lost if the ampoule were broken. The potential problems of undesirable field conditions are lessening, because more van-type vehicles are being used for on-site sample handling.

Advantages of the difference method of SOC analysis are related to the time savings and convenience that result from not having to perform on-site filtration, not transporting additional equipment, and not needing additional training of personnel. Almost all analysis is conducted within the laboratory. The major disadvantage of the difference method of SOC analysis is the potential redistribution of carbon in the whole-water sample during shipment and storage. This problem can be minimized by chilling the sample on ice during shipment and by prompt sample analysis on receipt in the laboratory. As mentioned previously, neither freezing nor inorganic preservatives seem to solve the problem.

In the laboratory, analytical aspects of both methods are very similar and relatively free of interference, if adequate quality-control precautions are exercised. A potential interference is the inclusion of suspended inorganic carbon (SIC) with SOC. This may occur if the SIC is not completely dissolved from the ampoule containing the sample during acid treatment. After acidification, DOC analysis requires only a 6-min gas purge to remove dissolved inorganic carbon (DIC), but well-crystallized carbonates that may be present in suspended sediment require acidification and overnight heating on a steam

bath for complete dissolution. It is imperative that persulfate oxidant not be added to the sample for SOC analysis until the steam-bath treatment is complete and the sample is ready to be sealed. Within 1 hr at room temperature, significant oxidation losses of organic carbon to CO_2 may be detected from the unsealed ampoule.

Organic carbon in reagents that contribute to the background blank value usually is quite low. Some of the organic-carbon contamination in the standard blank is due to doubly distilled water. Organic-carbon content of doubly distilled water can vary considerably, depending on the original organic content of the water and the means of purification. The most pure waters are produced routinely in our laboratory by doubly distilling deionized water that had passed three mixed-bed, cation-anion exchangers. The water produced contains 0.25 mg/L or less of organic carbon. When this water is stored in clean plastic jugs, the organic-carbon content is decreased to 0.15 mg/L or less. Obviously, the rate of organic-carbon sorption on the walls of the plastic container is greater than the release of plasticizers or other organic constituents from the container into the water. Because of this sorptive effect, which decreases the organic-carbon content of the sample, only glass bottles are used for sample collection and shipment. Glass sampling containers and glass ampoules used in both methods are heated to 500°C for 24 hr to free them of organic contamination.

Another possible source of organic contamination is the silver-membrane filter. As received from the factory, silver-membrane filters contain low levels of organic carbon (< 1.0 mg/g). Organic carbonaceous material in or on the filter is not soluble in water and remains with the filter after extensive washings (1,000 mL of reagent water). This 1 mg/L of organic-carbon blank is the largest source of analytical error in the SOC measurement by the silver-membrane-filter method. This source of error results in an approximate 3 to 5 percent error in the SOC measurement. This small quantity of organic carbon on the silver-membrane filter results in no significant source of error in both SOC and DOC determinations. Reagent blanks, which include silver-membrane filters, need be determined periodically for contamination.

Only silver-membrane filters are acceptable for either of the SOC methods. Plastic-membrane filters, commonly used to filter water for analysis of inorganic constituents, are undesirable because they commonly contain high concentrations of water-soluble organic substances and because they sorb water-soluble hydrophobic organic compounds. These problems do not exist with silver-membrane filters.

Another source of organic contamination associated with silver-membrane filters can result from handling the filter while placing it into the filter assembly; use forceps to prevent this contamination. Such contamination can lead to error in both SOC and DOC determinations.

Some of the hydrologic interpretive uses of SOC data include inferences about the possibility of metallo-organic association, exchange characteristics, organic sorptive capacities, food sources, nitrogen reserves, and water-purification properties of the suspended-sediment load. Organic matter is known to have 5 to 100 times the cation-exchange capacity of clay minerals, with many of the exchange functional groups capable of forming complexes and chelates with certain metal ions. The capacity of suspended sediment for this type of reactivity per unit weight of sediment should positively correlate with organic-carbon content.

Many heterotrophic organisms depend on organic detritus as a source of food. The organisms grow directly on the particulate sediment in direct contact with the food source, and the exchangeable and complexed ions are a nutrient source. Decomposition of the organic detritus and the microbial exudates generate low-molecular-weight organic substances that serve as food and nutritional sources for other organisms. With an SOC value, the amount of nitrogen, an important nutrient affecting trophic conditions in streams or lakes, can be approximated. In previous studies (Malcolm and Durum, 1976), it has been documented that stream sediments are accumulators of organic nitrogen, with carbon to nitrogen ratios of six selected rivers of the United States at 9:1 or smaller.

Hydrophobic organic substances entering the aqueous system tend to be removed from leave solution or suspension by sorption on organic surfaces by hydrogen bonding and weak van der Waals forces. Therefore, it is not surprising to find many pesticides, polychlorinated biphenyls, and other organic substances intimately associated with the organic phase in stream sediments. Hydrophilic functional groups on organic matter can also attract hydrophilic organic substances and metal ions. SOC has a scavenging ability or serves as a sink for many undesirable constituents found in water.

Considerable effort is being expended to quantify the sources of possible increased CO_2 fluxes into the atmosphere. The relative quantity of SOC transported in freshwater streams, the quantity of SOC deposited into the oceans by streams, as compared to in-situ production within estuaries and oceans, and the relative decomposition rate of SOC in various environments are important considerations in solving this important problem. Methods for determination of SOC presented in this paper may assist in appropriate data collection for this activity.

ETR sampling with adequate and well-maintained sampling equipment is essential to obtaining a representative SOC sample (Guy and Norman, 1970; Meade and others, 1979a,b; and Stevens and others, 1980). The

authors of this paper believe that sampling is the weakest link in obtaining correct and meaningful SOC data. Other sampling errors that may be large or larger than those associated with sampling equipment or river sampling techniques are due to sampling bias associated with the collection of small volumes of sample and (or) subsampling of larger volumes of sample. Subsampling was documented as a large part of the method error for the difference method in this paper. Analytical errors of both methods described in this paper are small once the sample is in the ampoule. The instrumentation and method for accurate and precise carbon measurement and the low detection limits for carbon often encourage the scientist to collect samples that may be too small and nonrepresentative. Both of the methods presented in this paper may have this type of bias, resulting in consistently low SOC values. Future experiments are planned that will compare SOC values by the methods presented in this paper with methods using large volumes of filtered water to accumulate larger representative quantities of suspended sediment.

SUMMARY AND CONCLUSIONS

Detailed procedures are presented for the determination of SOC in water by two different methods: the silver-membrane-filter method and the difference method. Both methods are applicable to a wide range of suspended-stream-sediment concentrations. The silver-membrane-filter method is recommended when suspended-sediment concentrations are less than 50 mg/L, when the sample contains appreciable quantities of organisms and biodegradable organic substances, and when the most precise data are desired. The difference method is recommended when filtration is precluded by time or field sampling conditions or when the complete filtering assembly is not available for on-site use. Minor disadvantages of the silver-membrane-filter method include the necessity of having trained technicians for field sampling, the cost of silver-membrane filters for duplicate or triplicate sampling, the time required for on-site filtration, and the maintenance of clean equipment in the field. The major disadvantage of the difference method is that, if the sample is not adequately chilled during storage or shipment, organic carbon can be redistributed between dissolved and suspended phases or even lost from the sample by decomposition.

Both methods are free of interferences and agree closely to simple and environmental organic-carbon standards. Precision of the silver-membrane-filter method is slightly superior to that of the difference method.

SELECTED REFERENCES

Grady, C.P.L., 1971, The BOD test and its meaning, hazardous chemical handling and disposal, *in* Howe, R.H.L., ed., 2d Symposium Proceedings: Lafayette, Ind., 1971, p. 128–142.

Guy, H.P., and Norman, V.W., 1970, Field methods for measurement of fluvial sediment: U.S. Geological Survey Techniques of Water-Resources Investigations, Book 3, Chapter C2, 59 p.

Hughes, J.L., Eccles, L.A., and Malcolm, R.L., 1974, Dissolved organic carbon (DOC), an index of organic contamination in ground water near Barstow, California: Ground Water, v. 12, p. 283–289.

Jones, R.H., 1969, Total organic carbon analysis and its relationship to biochemical and chemical oxygen demand, *in* Chapman, R.L., ed., Environmental pollution instrumentation: Pittsburg, Instruments Society of America, p. 116–125.

Leenheer, J.A., Malcolm, R.L., McKinley, P.W., and Eccles, L.A., 1974, Occurrence of dissolved organic carbon in selected ground-water samples in the United States: U.S. Geological Survey Journal of Research, v. 2, no. 3, p. 361–369.

Malcolm, R.L., and Durum, W.H., 1976, Organic carbon and nitrogen concentrations and annual organic carbon load of six selected rivers of the United States: U.S. Geological Survey Water-Supply Paper 1917–F, 21 p.

Malcolm, R.L., and Leenheer, J.A., 1973, The usefulness of organic carbon parameters in water quality investigations: Institute of Environmental Science, Anaheim, Calif., 1973, Proceedings of Annual Meeting, p. 336–340.

Malcolm, R.L., Leenheer, J.A., McKinley, P.W., and Eccles, L.A., 1973, Supplement II—Disolved organic carbon, *in* Goerlitz, D.F., and Brown, Eugene, eds., Methods for analysis of organic substances in water: U.S. Geological Survey Techniques of Water-Resources Investigations, Book 5, Chapter A3, 34 p.

Malcolm, R.L., and McKinley, P.W., 1972, Supplement I—Collection and preservation of water samples for carbon analysis, *in* Goerlitz, D.F., and Brown, Eugene, eds., Methods for analysis of organic substances in water: U.S. Geological Survey Techniques of Water-Resources Investigations, Book 5, Chapter A3, 6 p.

Meade, R.H., Nordin, C.F., Jr., and Curtis, W.F., 1979a, Sediment in Rio Amazonas and some of its principal tributaries during the high-water seasons of 1976 and 1977: Associagao Brasileira de Hidrologia e Recursos Hidricos, Simposio Brasileiro de Hidrologia, III Hidrologia da Amazonia, Anais, v. 2, p. 472–485.

Meade, R.H., Nordin, C.F., Jr., Curtis, W.F., Mahoney, H.A., and Delaney, B.M., 1979b, Suspended-sediment and the velocity data, Amazon River and its tributaries, June-July 1976 and May-June 1977: U.S. Geological Survey Open-File Report 79–515, 42 p.

Stevens, H.H., Jr., Lutz, G.A., and Hubbell, D.W., 1980, Collapsible-bag suspended-sediment sampler: American Society of Civil Engineers, Hydraulics Division Journal, v. 106, no. H.Y. 4, 1980, Proceedings, p. 611–616.

Wershaw, R.L., Fishman, M.J., Grabbe, R.R., and Lowe, L.E., 1983, Methods for the determination of organic substances in water and fluvial sediments: U.S. Geological Survey Open-File Report 82–1004, USGS TWRI Book 5, Laboratory Analysis, Chapter A3, p. 22–30.

Unit Hydraulic Geometry—An Indicator of Channel Changes

By Rhea P. Williams

Abstract

Water-discharge and sediment-transport data collected at selected gaged sites and surveyed reaches of streams in the Western United States were used with hydraulic variables of the energy equation to evaluate channel changes at stream sections. The coefficients and exponents of hydraulic-geometry relations were based on unit discharge rather than on total discharge. Unit hydraulic geometry has greater application to defining channel changes than conventional analysis. The unit-hydraulic-geometry relations were used to infer sectional competence of coarse-sediment discharge and expected channel changes and to define quasi-equilibrium of near-bankfull streams.

Results of this study suggest that long-term projections of coarse-sediment transport initially involve an evaluation of past hydraulic changes in the stream reach. Although the primary analysis used streamflow measurements, slope-area techniques can be used to analyze ungaged reaches. The methods described are applicable to a broad range of stream conditions and provide techniques for evaluating natural changes and man's influence on stream reaches.

INTRODUCTION

Knowledge of changes in channel hydraulics is necessary to understand the mechanisms associated with coarse-sediment transport; however, the relations between coarse-sediment transport and changes in channel hydraulics are not fully known, and channel changes cannot be reliably predicted. Statistical and advanced mathematics are often necessary to define complex relations, but for the nonmathematician involved in stream dynamics, cause and effect become increasingly difficult to follow. There is a need to return to and explore the basic laws of flow dynamics that govern coarse-sediment transport.

The objective of this paper is to present a method to evaluate channel changes by using steady- and unsteady-flow criteria and modified hydraulic-geometry relations. The hydraulic-geometry relations can then be used to understand and infer probable channel changes at gaged sites and along surveyed stream reaches.

BACKGROUND

Laws of thermodynamics apply to hydraulic and sediment-transport processes of most, if not all, stream systems. The first law of thermodynamics involves the external processes of conservation of mass and energy of streamflow. Energy cannot be created or destroyed within channel boundaries, meaning that the mass flux of the water-sediment mixture entering a stream reach must be continuous or the same as that leaving the reach. The second law of thermodynamics involves internal processes of energy decay, entropy, or energy dissipation (usually as heat) caused by the internal stress of the fluid to overcome resistance to flow. The internal loss owing to friction is directly related to the velocity gradient, $\frac{\Delta V}{\Delta D}$, or shear stress, of the flow.

Although these laws of thermodynamics appear to be dichotomous, they are often expressed by the Bernoulli energy equation, "the most universally applicable of all the equations of hydraulics, relating as it does the changes in mechanical energy to the internal processes in the system causing friction loss" (Morris and Wiggert, 1972, p. 27).

The Bernoulli equation for varied steady and unsteady flow is expressed graphically in figure 1 and can be used to identify quasi-equilibrium (no scour and fill apparent during time period under consideration) and nonequilibrium (changing channel bottom during time period under consideration) in channels.

Changes in stream boundaries during steady flow or quasi-equilibrium, such as aggradation and degradation, have, with time, adjusted the stream's hydraulics to where head loss owing to friction (h_f) may be meaningfully expressed as a function of the Manning n or Chezy C roughness coefficients.

For unsteady flow or nonequilibrium, an additional term (h_a) is included to define head loss owing to acceleration or deceleration, in feet, of the changing flow. Unit discharge (q), in cubic feet per second per foot, changes with time (dt) and along channel distance (dx). Short-term channel changes, such as scour and fill, are assumed to result from momentary or local energy gains

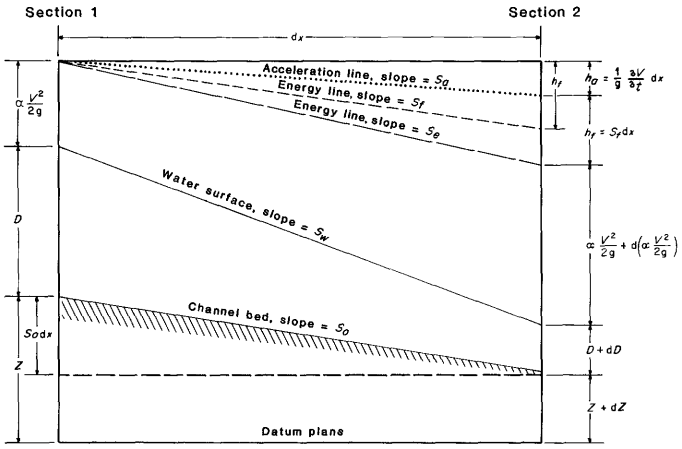

Figure 1. Simplified graphical representation of energy in unsteady flow. (Modified from Chow, 1959.)

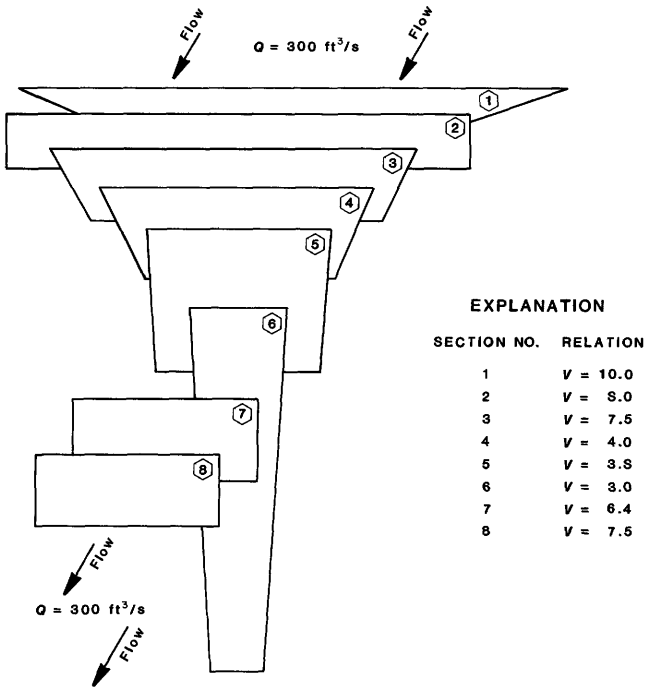

Figure 2. Cross sections of a hypothetical stream reach.

or losses in total energy heads caused by obstructions, debris, and vegetation. Conversely, short-term fluctuations in velocity and depth (see fig. 1) also may result from energy losses in flow because of changing resistance or roughness caused by changing bed forms. Thus, a mechanism of continual feedback exists for the variables in figure 1 influencing short-term changes in the water-sediment discharge. The relations of these variables are numerous and complex, but the resultant effect on alluvial boundaries is integrated to those variables believed common to the Bernoulli energy equation and hydraulic geometry.

If h_a and h_f can be adequately defined at channel sections, then changes in h_a and h_f with time should be relatable to energy-consuming events such as periodic scour and fill. Should $h_a=0$, a steady-state condition or unchanging channel bottom is assumed. However, if a streambed cannot adjust (rock outcrop) and $h_a \neq 0$, channel adjustments affecting bed (armoring) and banks (meandering) may be occurring elsewhere than at the section(s) under consideration.

Factors comprising the energy-head losses (h_a, h_f) of unsteady flow are analyzed by examination of energy distribution between sections and at sections with time. Rates of change include $\frac{\Delta V}{\Delta t}$, $\frac{\Delta D}{\Delta t}$, $\frac{\Delta V}{\Delta x}$, $\frac{\Delta D}{\Delta x}$ and $\frac{\Delta V}{\Delta D}$ as related to Δq. For example, suppose that in figure 1 the incoming sediment rate decreases upstream at section 1 because material normally transported is diverted or trapped. Local adjustments occur at section 1, whereas at section 2, the existing hydraulic gradient, in feet per foot (S_e), must be reduced because the energy expenditure exceeds the work needed. Possible interrelated adjustments at section 2 might include (1) an increase in boundary roughness (n), (2) an increase in the velocity head coefficient distribution factor (α), (3) a decrease in average velocity (V), (4) an increase in average water depth of a cross section, in feet, (D), or (5) a decrease in bed elevation (Z), where Z is the elevation of a point as it refers to a horizontal datum, in feet.

Should the incoming sediment rate at section 1 increase, h_a at section 2 should increase because greater energy expenditure is required to transport the load. Possible interrelated adjustments at section 2 might include (1) a decrease in boundary roughness (n) by decreasing grain roughness and changing bed forms, (2) a decrease in the velocity distribution factor (α), (3) an increase in average velocity (V), (4) a decrease in average depth (D), or (5) an increase in average bed elevation (Z).

Hydraulic Geometry of a Hypothetical Reach

An example of quasi-equilibrium and nonequilibrium between channel sections is illustrated using unit-hydraulic-geometry analysis. The hypothetical stream reach chosen describes possible combinations between water-sediment mixture in the reach and probable changes in hydraulics to transport the mean sediment load (fig. 2). Arbitrary values of V, D, and W (average width of section, in feet) for flows of 50, 175, and 300 ft³/s (table 1) were chosen to represent typical ranges of a small western stream.

Leopold and Maddock (1953) described hydraulic-geometry relations of a variety of natural channels by providing empirical power relations of W, D, and V to water discharge (Q).

Table 1. Data for a hypothetical eight-section reach

Observation number	Section number	Discharge (ft^3/s)	Width (ft)	Velocity (ft^3/s)	Unit sediment load [(ton/d)/ft]	Unit discharge [(ft^3/s)/ft]	Depth (ft)	Froude number	Instantaneous sediment load (ton/d)
1	1	300	30.0	10.00	181.0	10.00	1.00	1.76	5,430
2	1	175	25.0	7.50	100.0	7.00	.93	1.37	2,500
3	1	50	20.0	5.00	40.0	2.50	.50	1.25	800
4	2	300	25.0	8.00	140.0	12.00	1.50	1.15	3,500
5	2	175	25.0	5.75	70.0	7.00	1.22	.92	1,750
6	2	50	25.0	2.67	6.0	2.00	.74	.55	150
7	3	300	20.0	7.50	130.0	15.00	2.00	.94	2,600
8	3	175	19.0	5.63	60.0	9.21	1.63	.78	1,140
9	3	50	18.0	2.78	10.0	2.77	.99	.49	180
10	4	300	15.0	4.00	30.0	20.00	5.00	.32	450
11	4	175	13.5	3.33	12.0	12.96	3.89	.30	162
12	4	50	12.0	2.08	1.0	4.16	2.00	.26	12
13	5	300	10.0	3.75	20.0	30.00	8.00	.23	200
14	5	175	9.5	3.05	10.0	18.42	6.03	.22	95
15	5	50	9.0	1.85	1.0	5.55	3.00	.19	9
16	6	300	5.0	3.00	6.0	60.00	20.00	.12	30
17	6	175	4.5	2.67	3.5	38.88	14.56	.12	16
18	6	50	4.0	2.00	.8	12.50	6.25	.14	3
19	7	300	10.0	6.43	120.0	30.00	4.66	.53	1,200
20	7	175	10.0	5.18	65.0	17.50	3.37	.50	650
21	7	50	10.0	3.20	14.0	5.00	1.56	.45	140
22.....	8	300	10.0	7.54	150.0	30.00	3.97	.67	1,500
23	8	175	10.0	5.46	75.0	17.50	3.20	.54	750
24	8	50	10.0	2.57	4.0	5.00	1.94	.33	40

To obtain a cross-sectional comparison of hydraulic variables using q, Q was divided by W, and V and D were regressed with q. Regressions are given in figures 3 and 4 where $V = K'q^{M'}$ and $D = C'q^{F'}$, $F' + M' = 1.0$, $C' \times K' = 1.0$, and $M' = \frac{\Delta \log_{10} V}{\Delta \log_{10} q}$ and $F' = \frac{\Delta \log_{10} D}{\Delta \log_{10} q}$, where C' and K' are regression coefficients in relation to discharge, and where F' and M' are regression exponents in relation to discharge.

Width is treated not as a constant but as an independent variable with some finite change in time. The effects of W on hydraulic geometry are integrated into the exponents M' and F'. Reduction in the number of dependent variables allows relations of V and D to q to conform with theory and notation represented in figure 1.

The modified hydraulic-geometry relations for sections 1 to 8 in figures 3 and 4 can be compared to each other by plotting the coefficients against the exponents. For example, the velocity relations for Q = 175 and 300 ft^3/s are shown in figure 5. A line representing the bankfull q (the average Q of 175 ft^3/s divided by W, table 1) is drawn through each point of the established relations. The line through the point represents multiple combinations of K' and M' where any choice of K' and M' along the established line gives identical numerical values of V for the given q. The line is assumed to represent a near-constant hydraulic regime for the selected flow. Hydraulic regime is herein defined by use of Froude

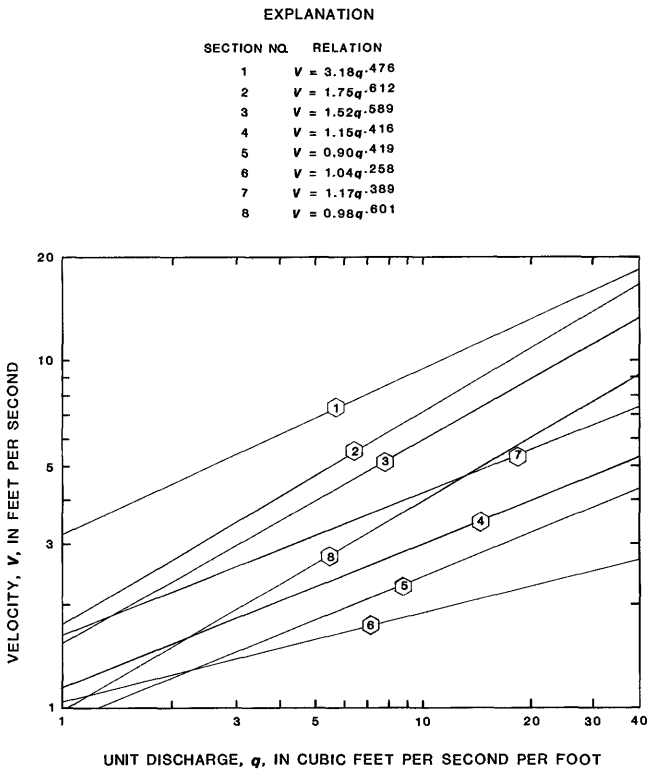

Figure 3. Relation of velocity and unit discharge for a hypothetical stream reach.

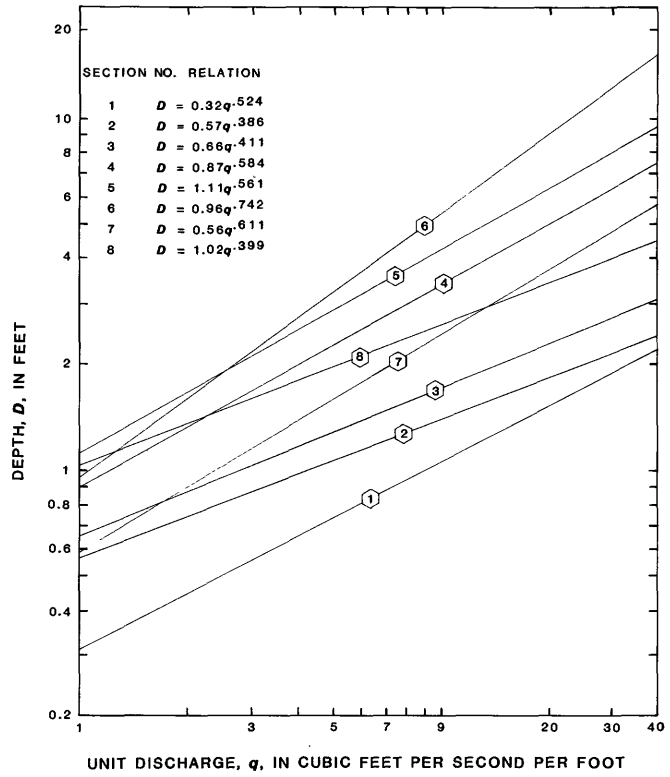

Figure 4. Relation of depth to unit discharge for a hypothetical stream reach.

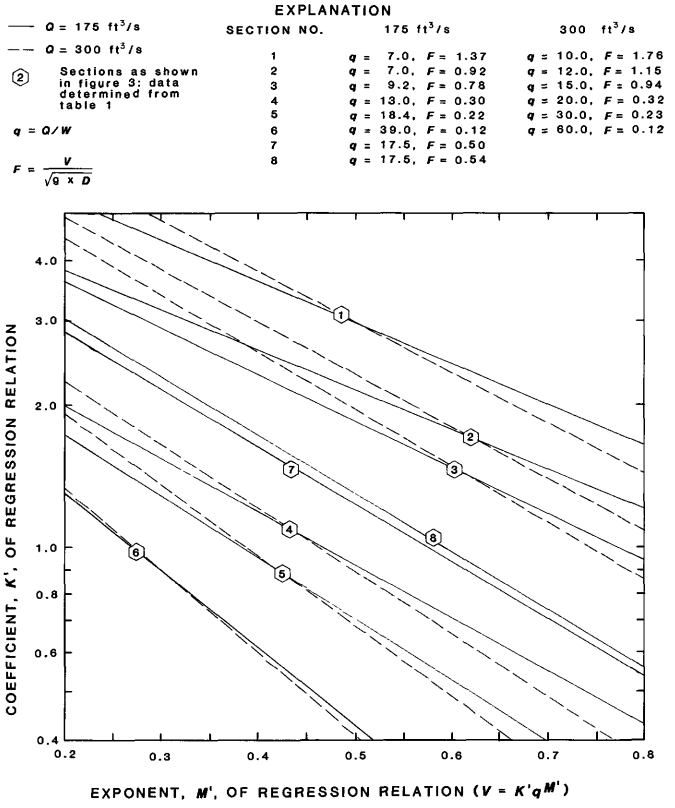

Figure 5. Relation of velocity coefficients and exponents for an eight-section hypothetical stream reach.

numbers (F), where $F = V/\sqrt{gD}$. Dashed lines represent a higher value of q if a Q of 300 ft ^{3}/s had been selected.

These examples purposely represent a case of extreme variation in channel shape. Such extreme shapes probably would not occur in nature except for pronounced pool and riffle sequences, as rates of change in V and D between sections generally are gradual and reflect the shape of the channel, slope of water surface, roughness of the wetted perimeter, and sediment discharge and sizes. In natural channels with gradually developed pool and riffle sequences assumed to be in equilibrium, F for each q considered would be expected to vary slightly between adjacent sections as slight changes in n and S_e occur. The F can be assumed equal to (see footnote on $\sqrt{g}$, Chow, 1959, p. 98) or proportional to $\frac{1.49}{n} R^{1/6} S_e^{1/2}$; if $F = CS_e^{1/2}$, then roughness is $C = \frac{1.49}{n} R^{1/6}$ (Chow, 1959, p. 100), where R is the hydraulic radius, in feet, and C is the roughness coefficient in Chezy equation, in units of $\sqrt{\text{ft/s}}$ and dimensions of $\sqrt{g}$.

Relation of Hydraulic Geometry to Hypothetical Sediment Loads

Natural channel sections usually reflect continuity of the transported sediment load. That is, adjacent cross sections should be hydraulically competent to transport coarse-sediment loads moving downstream (coarse sediment is defined as greater than 0.062 mm in average diameter). Leopold and Maddock (1953) found that coarse suspended-sediment loads were an index of total loads and a function of D, W, V, temperature, particle size, turbulence, and other variables. They further showed that the rate of increase of coarse-suspended-sediment transport varies with Q as a direct function of the following ratio: rate of increase of V with Q divided by rate of increase of D with Q.

Colby (1964), Culbertson and others (1967), and Nordin (1977) presented graphic aids to describe changes in V, D, and q to various sand sizes and water temperatures. Their graphs were used to estimate depth of scour required to maintain equilibrium or continuity of sediment load past two sections. Their experiments were made with readily available sand of uniform size where energy adjustments could be freely distributed by scour, fill, and bed-form adjustments. Any changes in the

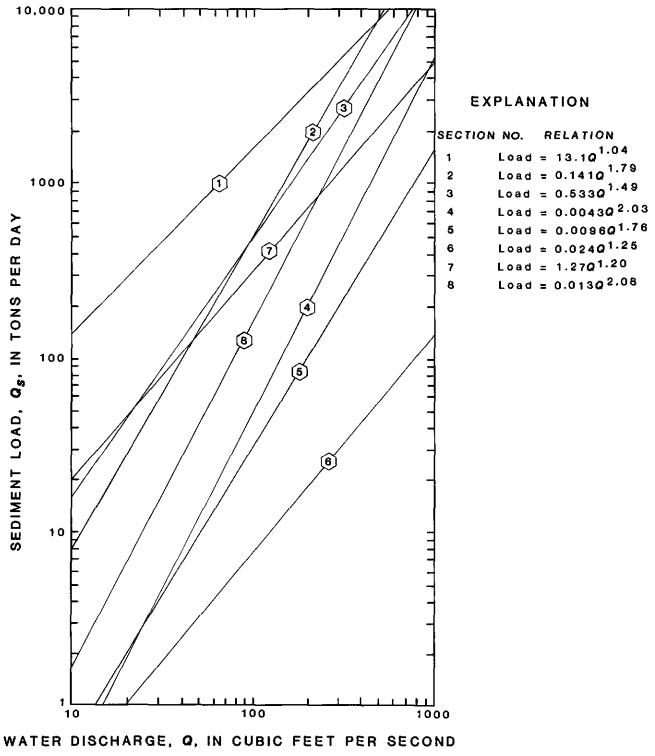

Figure 6. Relation of discharge to sediment load of a hypothetical stream reach.

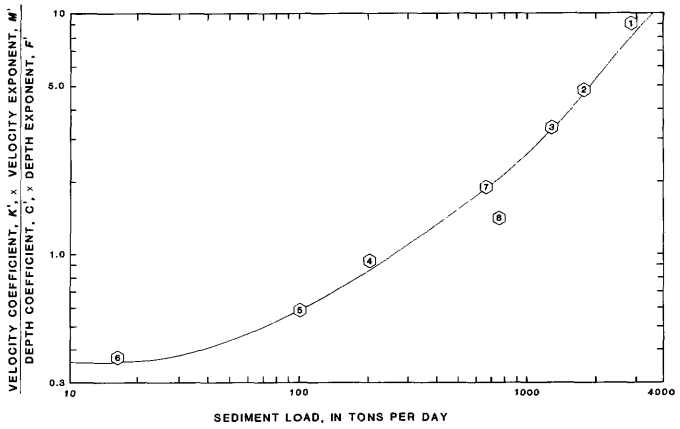

Figure 7. Plot of velocity-depth ratio (three-sample average) to sediment loads for a hypothetical stream reach.

unmeasured variables and n usually were assumed to be constant or integrated into the measured variables. These assumptions become more restrictive with gravel-bottom streams as adjustments may not be freely achieved through similar (usually short) time periods. However, overall hydraulic concepts should apply to coarse-sediment load streams.

Interpolation of Nordin's (1977) graph was used to provide representative values of sediment loads for each discharge and combination of D, V, and W given in table 1. Particle size and temperature selected were 0.8 mm at 15.6°C. The computed sediment discharges, in tons per day and tons per day per foot, (Q_s) were regressed with water discharge (Q) to establish water-sediment relations, or $Q_s = pQ^J$ for each section (fig. 6).

Leopold and Maddock (1953, p. 25) examined the ratio of M/F to p and J for several exponential values of the W and Q relation. Increase in the ratio of M/F implies that the J exponent in relation to discharge should increase and that coarse suspended-sediment load should increase with Q. Analysis of figure 7 tends to confirm this observation; however, because W is now integrated in the V and D relations, both exponents and coefficients of V and D relations are used in figure 7. Sediment loads in figure 7 represent the three-sample average of the three discharges for each of the eight sections. A Q of 175 ft^3/s and an average sediment load of 970 ton/d are assumed to be representative of average transport conditions in and through the eight-section stream reach.

If equilibrium for sediment supply, transport, and Q is to prevail, each section must adjust by scour or fill to transport this average sediment load because the duration or magnitude of water discharge is not likely to vary within a short stream reach. According to Leopold and Maddock (1953, p. 21), equilibrium in stream channels is a function not only of magnitude and duration of Q, but perhaps more importantly, of the average sediment load inflow.

Application to Natural Streams

Modified hydraulic-geometry techniques have been applied to streams in several Western States where sediment data have been collected and the author had access to the data. Included are the Snake River in Idaho and Washington; the Clearwater (Jones and Seitz, 1980; Emmett, 1976), North Fork Teton (Williams, 1979), and Big Lost Rivers (Williams and Krupin, 1984) in Idaho; and the Owens River in California (Williams, 1975).

Hydraulic geometry was evaluated by location of the measurement site (upstream or downstream of gaging station), time (season, year) of measurement, and Q at time of measurement. Relations of V and D to q were compared for each river site from measurement notes (see example, figs. 8 and 9). Yearly regressions and correlation coefficients (r^2) of V and D for the Big Lost River are listed in table 2. Comparison of V relations (regressions) was made by plotting the value of the V exponent (M') against the V coefficient (K') (fig. 10). Plots of exponents (F') and coefficients (C') from regression relations of D to q gave similar but reversed patterns because $F' = 1.0 - M'$ and $C' = 1.0/K'$ (fig. 11). A numerical

Table 2. Hydraulic geometry of Big Lost River at Howell Ranch, Idaho, 1904–82

[r^2, correlation coefficient for depth regression and velocity regression]

Year	F'	Depth r^2	Number of samples	M'	Velocity r^2	C'	K'	Velocity (ft/s)	Depth (ft)	Unit discharge [(ft³/s)/ft]	Froude number
1904	0.292	0.984	4	0.759	0.988	1.354	0.682	6.63	3.25	21.5	0.65
05	.364	.998	6	.627	.996	1.215	.842	5.51	3.61	19.9	.51
09	.141	.981	3	.848	.999	2.310	.447	5.67	3.52	20.0	.53
10	.377	.977	4	.624	.990	1.180	.844	5.47	3.66	20.0	.50
11	.428	.988	7	.574	.993	1.051	.947	5.30	3.78	20.0	.48
1912	.353	.989	4	.647	.997	1.175	.850	5.90	3.39	20.0	.57
21	.443	.981	9	.557	.998	.970	1.030	5.47	3.66	20.0	.50
22	.370	.984	9	.630	.995	1.148	.872	5.75	3.48	20.0	.54
23	.312	.891	10	.687	.976	1.177	.851	6.66	3.00	20.0	.68
24	.422	.897	11	.589	.888	.936	1.026	5.99	3.31	19.8	.58
1925	.531	.933	8	.467	.915	.694	1.442	5.83	3.41	19.9	.56
26	.579	.900	8	.420	.828	.693	1.443	5.07	3.93	20.0	.45
27	.505	.971	8	.495	.970	.723	1.385	6.10	3.28	20.0	.59
28	.441	.997	7	.559	.998	.839	1.191	6.36	3.15	20.0	.63
29	.404	.991	7	.596	.996	.888	1.123	6.69	2.98	20.0	.68
1930	.418	.978	10	.581	.989	.854	1.172	6.69	2.99	20.0	.68
31	.534	.996	9	.466	.995	.694	1.441	5.83	3.43	20.0	.55
32	.517	.991	11	.482	.990	.697	1.436	6.09	3.28	20.0	.59
33	.494	.988	12	.506	.989	.703	1.424	6.48	3.08	20.0	.65
34	.552	.990	9	.453	.980	.645	1.533	5.95	3.38	20.1	.57
1935	.472	.924	14	.528	.938	.766	1.307	6.35	3.15	20.0	.63
36	.504	.903	10	.498	.902	.729	1.370	6.08	3.30	20.1	.59
37	.412	.898	7	.588	.946	.834	1.199	6.98	2.86	20.0	.73
38	.433	.958	10	.567	.975	.852	1.172	6.42	3.12	20.0	.64
39	.354	.747	8	.647	.908	.669	1.040	7.21	1.94	14.0	.91
1940	.435	.951	9	.565	.970	.814	1.229	6.67	2.99	20.0	.68
41	.381	.969	8	.619	.988	.873	1.145	7.32	2.73	20.0	.78
42	.238	.786	9	.763	.974	1.232	.810	7.97	2.51	20.0	.89
43	.387	.919	7	.613	.966	.929	1.077	6.75	2.96	20.0	.69
44	.295	.894	4	.707	.980	1.099	.908	7.54	2.66	20.0	.82
1945	.450	.855	6	.549	.897	.816	1.228	6.37	3.14	20.0	.63
46	.451	.996	6	.549	.997	.738	1.352	7.01	2.85	20.0	.73
47	.423	.858	6	.577	.918	.817	1.225	6.89	2.90	20.0	.71
48	.385	.962	6	.616	.985	.914	1.093	6.91	2.90	20.0	.72
49	.445	.998	8	.555	.999	.751	1.330	7.02	2.85	20.0	.73
1950	.429	.968	6	.570	.982	.776	1.289	7.11	2.81	20.0	.75
51	.428	.969	7	.571	.983	.795	1.259	6.97	2.87	20.0	.73
52	.480	.996	6	.519	.996	.724	1.382	6.55	3.05	20.0	.66
53	.461	.958	8	.561	.972	.750	1.265	6.79	2.98	20.3	.69
54	.428	.982	8	.572	.990	.821	1.218	6.75	2.96	20.0	.69
1955	.433	.960	7	.566	.977	.830	1.206	6.58	3.04	20.0	.67
56	.449	.996	9	.551	.997	.977	1.259	6.56	3.75	24.6	.60
57	.482	.998	7	.518	.998	.747	1.338	6.32	3.16	20.0	.63
58	.428	.988	7	.572	.993	.850	1.175	6.52	3.07	20.0	.66
59	.430	.974	6	.572	.985	.877	1.137	6.30	3.18	20.0	.62
1960	.466	.973	8	.535	.980	.811	1.231	6.11	3.28	20.0	.60
61	.447	.960	6	.551	.973	.822	1.219	6.36	3.14	20.0	.63
62	.454	.994	7	.546	.996	.802	1.248	6.40	3.13	20.0	.64
63	.464	.994	7	.536	.995	.792	1.262	6.28	3.18	20.0	.62
64	.476	.997	8	.520	.995	.750	1.346	6.40	3.12	20.0	.64
1965	.531	.994	8	.471	.993	.649	1.536	6.29	3.19	20.1	.62
66	.503	.963	7	.497	.963	.682	1.467	6.50	3.08	20.0	.65
67	.397	.972	10	.603	.988	.940	1.062	6.47	3.09	20.0	.65
68	.468	.997	8	.533	.998	.772	1.296	6.39	3.13	20.0	.64
69	.448	.993	8	.611	.945	.768	1.123	7.00	2.94	20.6	.72

Table 2. Hydraulic geometry of Big Lost River at Howell Ranch, Idaho, 1904–82—Continued

[r^2, correlation coefficient for depth regression and velocity regression]

Year	F'	Depth r^2	Number of samples	M'	Velocity r^2	C'	K'	Velocity (ft/s)	Depth (ft)	Unit discharge [(ft³/s)/ft]	Froude number
1970	.459	.987	7	.540	.991	.755	1.325	6.68	2.99	20.0	.68
71	.470	.991	7	.530	.993	.772	1.295	6.34	3.15	20.0	.63
72	.456	.993	8	.544	.995	.751	1.331	6.79	2.95	20.0	.70
73	.466	.948	6	.536	.962	.750	1.331	6.62	3.03	20.1	.67
74	.499	.995	6	.501	.995	.743	1.347	6.04	3.31	20.0	.59
1975	.479	.999	4	.546	.996	.752	1.248	6.40	3.16	20.2	.63
76	.500	.987	6	.499	.987	.703	1.424	6.35	3.15	20.0	.63
77	.429	.975	6	.571	.987	.751	1.329	7.36	2.72	20.0	.79
78	.477	.982	6	.521	.986	.721	1.393	6.64	3.01	20.0	.67
79	.497	.989	7	.504	.989	.702	1.423	6.43	3.11	20.0	.64
1980	.457	.993	4	.542	.995	.775	1.293	6.57	3.05	20.0	.66
81	.551	.994	8	.449	.991	.716	1.397	5.36	3.73	20.0	.49
82	.501	.993	7	.499	.993	.730	1.369	6.10	3.28	20.0	.59

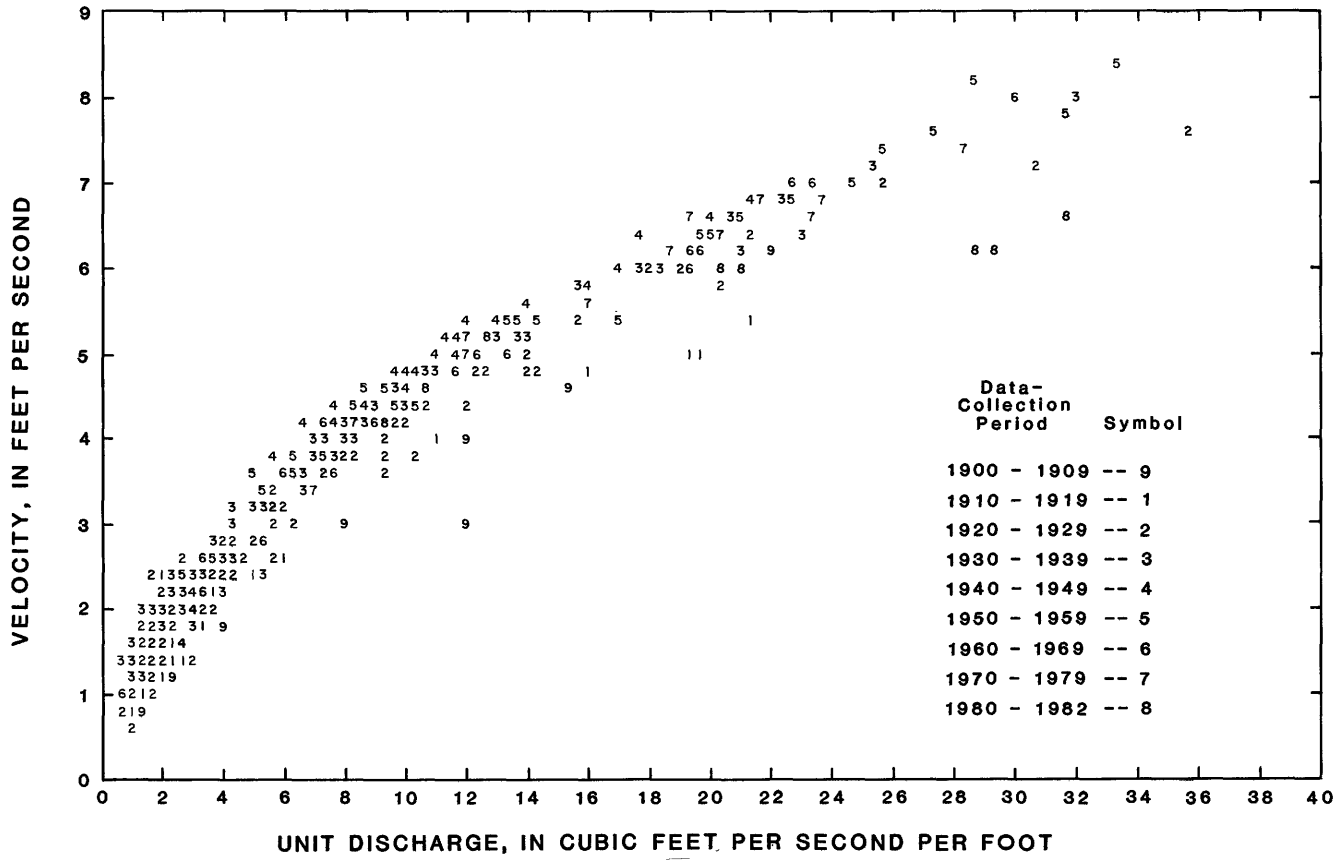

Figure 8. Relation of velocity to unit discharge, Big Lost River at Howell Ranch, Idaho.

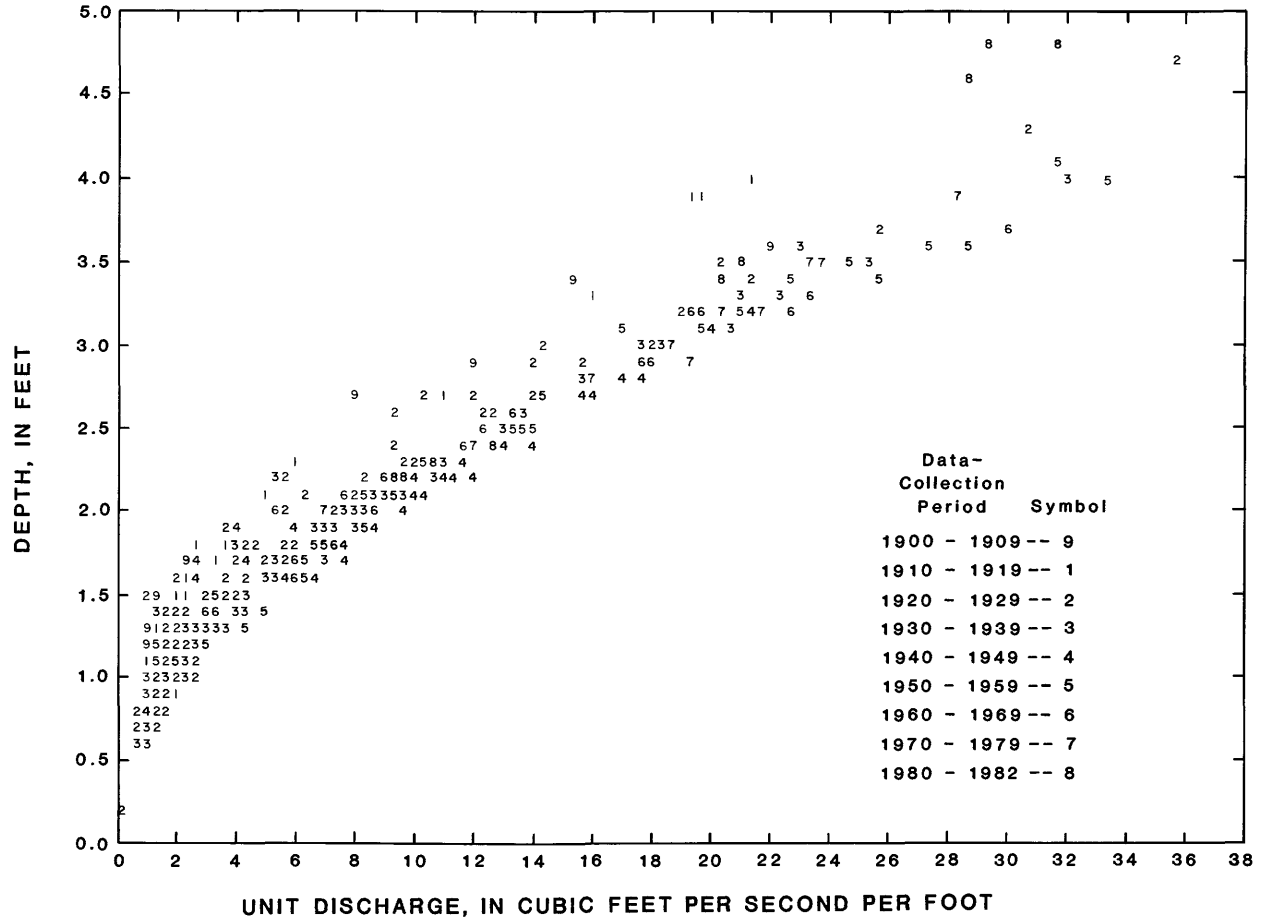
DEPTH, IN FEET
UNIT DISCHARGE, IN CUBIC FEET PER SECOND PER FOOT
Data-Collection Period Symbol
1900 - 1909 -- 9
1910 - 1919 -- 1
1920 - 1929 -- 2
1930 - 1939 -- 3
1940 - 1949 -- 4
1950 - 1959 -- 5
1960 - 1969 -- 6
1970 - 1979 -- 7
1980 - 1982 -- 8

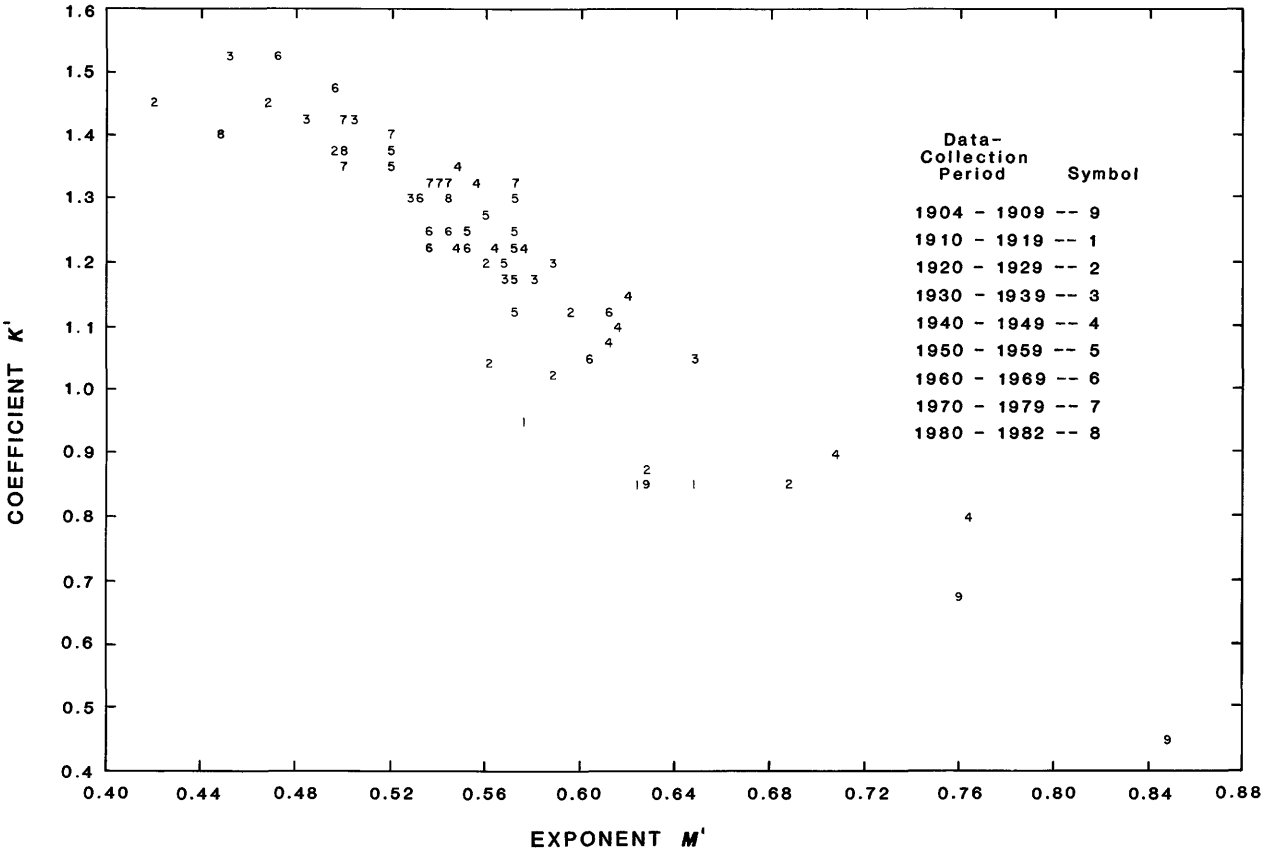
COEFFICIENT K'
EXPONENT M'
Data-Collection Period Symbol
1904 - 1909 -- 9
1910 - 1919 -- 1
1920 - 1929 -- 2
1930 - 1939 -- 3
1940 - 1949 -- 4
1950 - 1959 -- 5
1960 - 1969 -- 6
1970 - 1979 -- 7
1980 - 1982 -- 8

Figure 9 (upper left). Relation of depth to unit discharge, Big Lost River at Howell Ranch, Idaho.

Figure 10 (lower left). Yearly velocity relations, Big Lost River at Howell Ranch, Idaho, 1904–82.

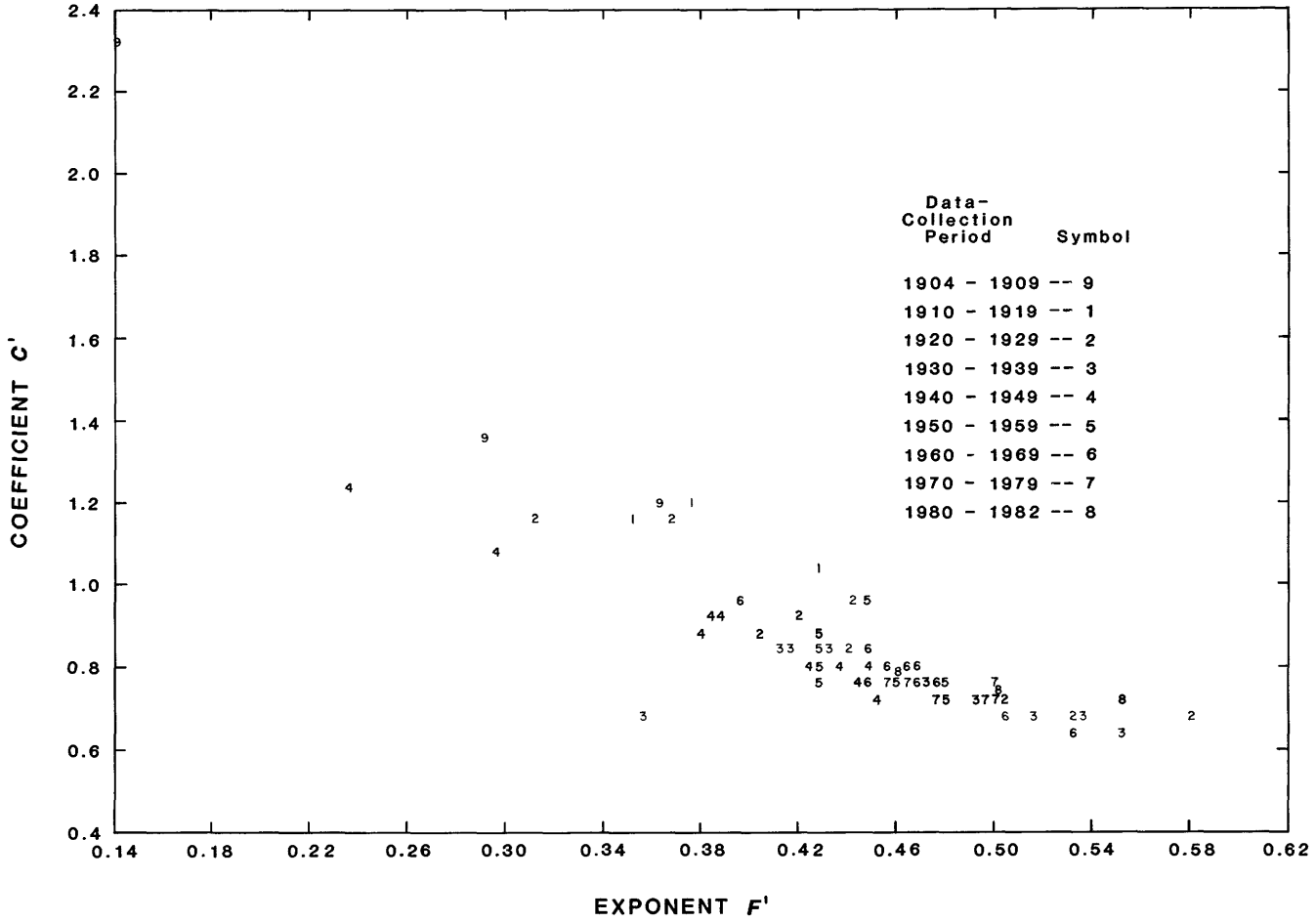

Figure 11. Yearly depth relations, Big Lost River at Howell Ranch, Idaho, 1904–82.

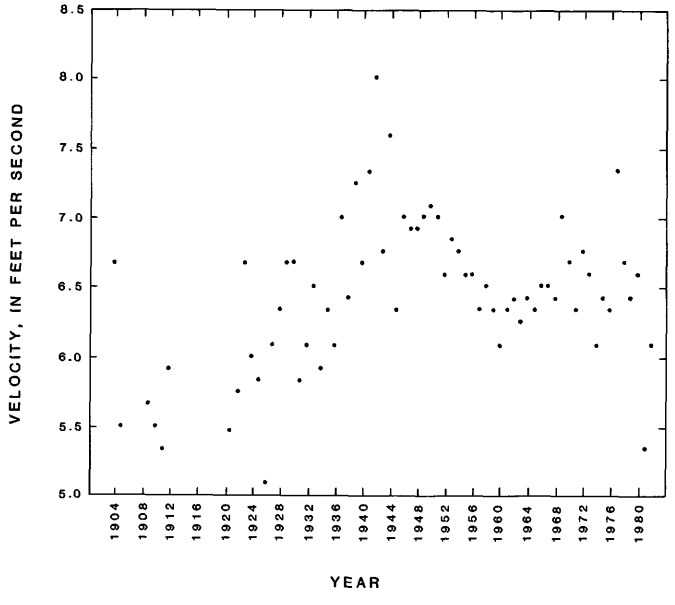

Figure 12. Velocity, determined from yearly regression for unit discharge equal to 20 (ft^3/s)/ft, Big Lost River at Howell Ranch, Idaho, 1904–82.

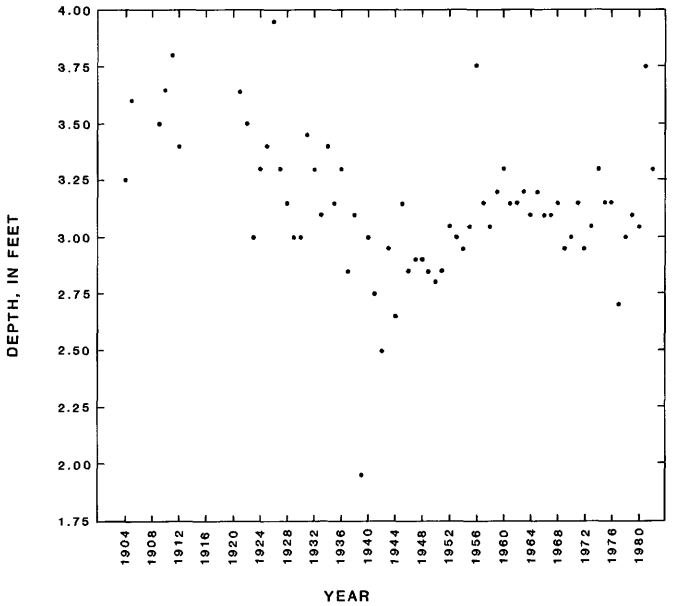

Figure 13. Depth, determined from yearly regression for unit discharge equal to 20 (ft^3/s)/ft, Big Lost River at Howell Ranch, Idaho, 1904–82.

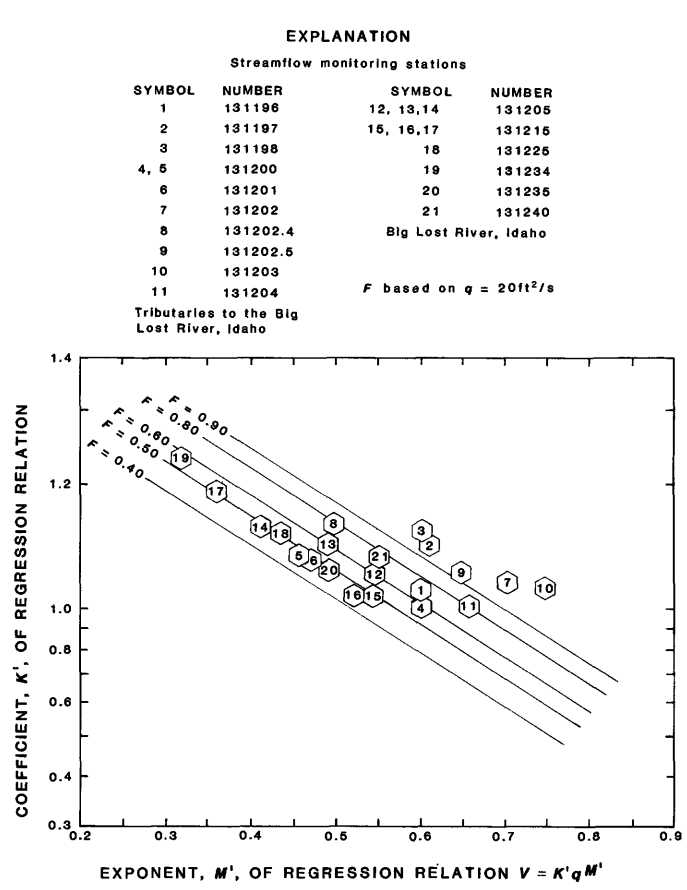

Figure 14. Average velocity relations, Big Lost River basin, Idaho.

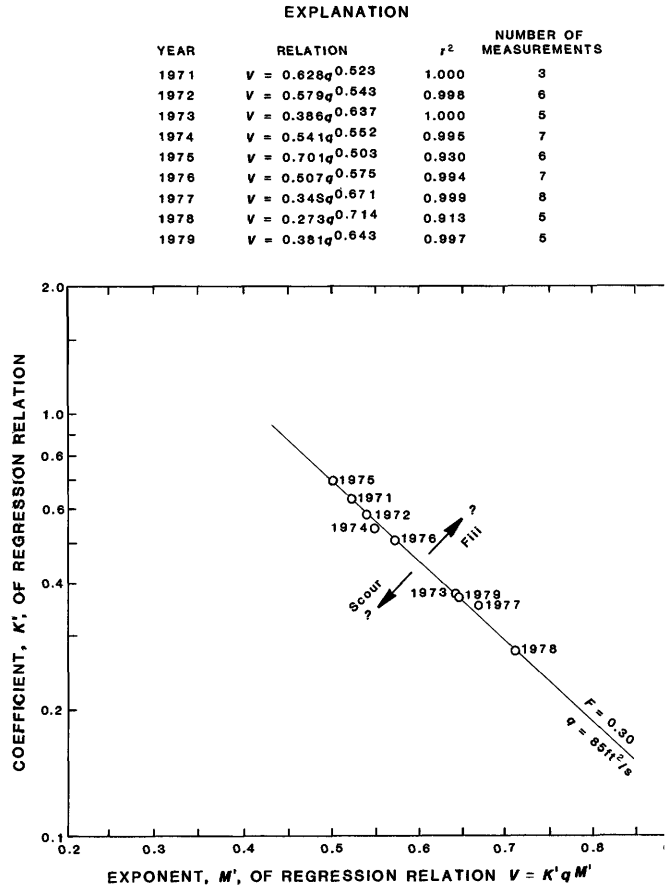

Figure 15. Relation of velocity coefficients and exponents for Snake River at Anatone, Washington.

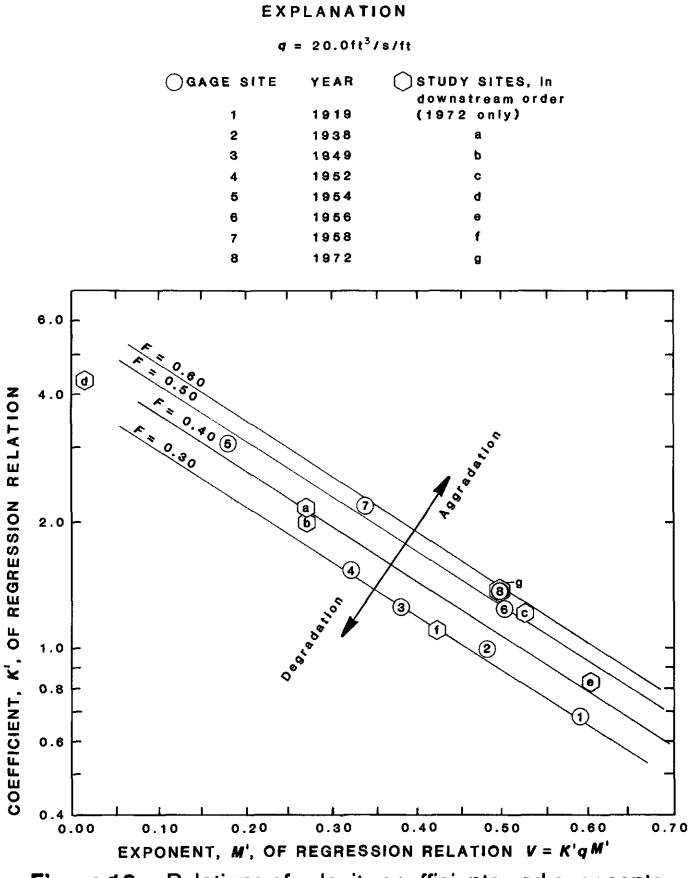

Figure 16. Relations of velocity coefficients and exponents, Owens River near Bishop, California.

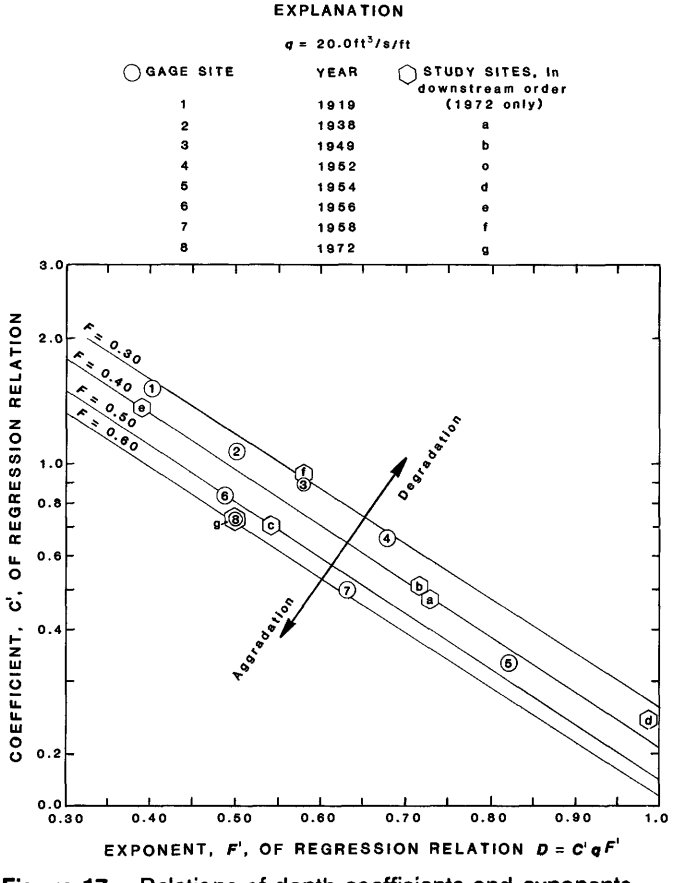

Figure 17. Relations of depth coefficients and exponents, Owens River near Bishop, California.

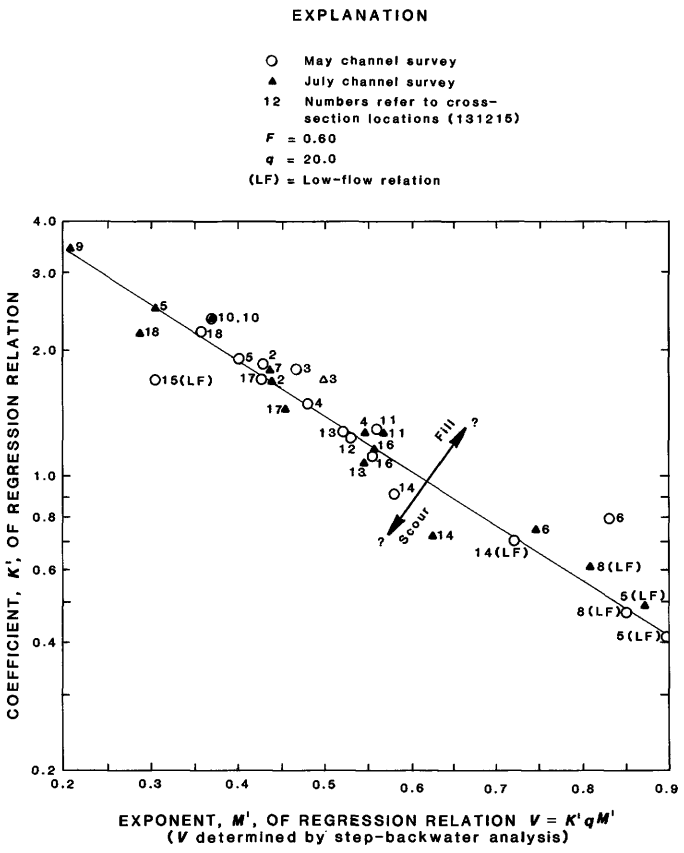

Figure 18. Relations of velocity coefficients and exponents for the surveyed reach near station 131215, Big Lost River, Idaho.

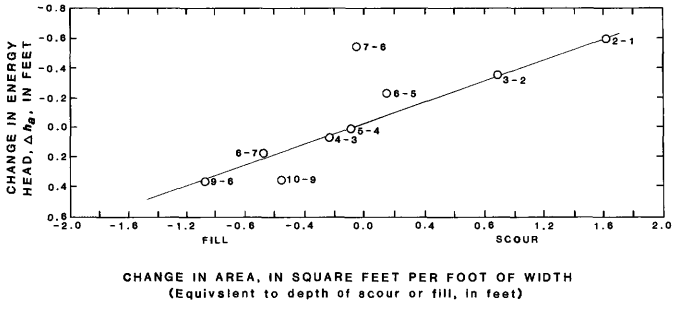

Figure 19. Relation of change in energy head to change in area per foot of channel width, North Fork Teton River, Idaho, 1976–78.

comparison of V and D (table 2) determined from yearly regression for q equal to 20 (ft^3/s)/ft is given in figures 12 and 13. Considerable differences in velocities and depths for same unit discharge exist, on the basis of yearly relations.

Plotted relations appear to be consistent, whether grouped by year or site, to the extent that a family of lines representing various hydraulic regimes of streams, including tributaries to the Big Lost River, within the Big Lost River basin can be drawn (fig. 14). Figure 14 gives the "average" V relations at each station in the Big Lost River basin for various periods of record. The lines represent multiple combinations of K' and M' for the V relations such that similar values of V are computed for a characteristic q value. This value of q was determined by equating two arbitrary points on the established line such that $V_1 = V_2$ and $D_1 = D_2$. The q calculated consistently represented near-bankfull Q for the stream analyzed. Different values of V and D can be computed for any other q by using the regression equations of plotted points. Lines defined by an F and a q may represent continuity between sections under uniform flow criteria, such that a constant F implies little variation in the ratio of S_e to n at near-bankfull Q.

Plots of V and D (figs. 9–14) from yearly hydraulic-geometry relations (table 2) compared with streambed changes (Williams and Krupin, 1984) indicated slower average velocities (fig. 12) and greater depths (fig. 13) at higher (near bankfull) flows in 1981 than occurred in the past 20 years. This may suggest decreased competency of the river section and a concurrent decrease in coarse sediment transported. It may also suggest that bedload-transport curves based on 1 or 2 years may not be representative of long-term transport.

Trends in changing coefficients and exponents relative to scour and fill on large rivers are difficult to detect. Analysis of figure 5 suggests little noticeable change in relations at low F and high q. An example of a large river is the Snake River near Anatone, Wash. (fig. 15). Although plots of hydraulic geometry clearly define a linear relation of yearly hydraulic coefficients and exponents, a high runoff year (1974) with a noted increase in bedload rate at the section plots to the left of the assumed equilibrium relation. Its plotting position suggests scour as D increased and V decreased. During the 1977 drought, the plotting position moved slightly above the established relation, which suggests a temporary fill condition, possibly owing to below-normal flushing flows.

Modified hydraulic geometry (figs. 16 and 17) of Owens River data (Williams, 1975) suggests natural changes at the gage site for observations 1 to 4, followed by aggradation, 5 to 8, resulting from upstream dam construction during the period 1953–54. Changes in channel sections in years 1919–52 (points 1–4) are termed "natural regime," whereas changes during 1954–58 (points 5–7) represent a period of aggradation below the dam. Analyses of hydraulic changes during a sediment-transport study in 1972–73 suggested sites a, b, d, and e had reestablished equilibrium conditions at higher bankfull Q and higher F. Site c, located downstream from site g, was artificially constrained from lateral bank changes. The natural tendency of sites c and g would have been to degrade to reach new equilibrium; however, armoring of the local streambed had resulted in erosion of downstream banks. Aggradation at site f

(about 5.5 mi downstream from gage) may be expected in response to upstream erosion.

Application of Hydraulic Geometry to Step-Backwater Analysis

If the hydraulic variables and boundary conditions of figure 1 are reasonably assumed in time and space, step-backwater techniques should be applicable for analysis of channel behavior on ungaged reaches. Steady-state or quasi-equilibrium conditions are assumed during dates of survey.

Hydraulic-geometry analysis was applied to a surveyed reach of the Big Lost River, after estimating variables by step-backwater analysis, to determine channel changes between May and July 1981. Figure 18 shows hydraulic-geometry relations for the reach where the fill totaled 4,400 ft^3 in 1981. Analysis of channel changes at several sections suggests ongoing adjustments. From the established regression equations, V and D were calculated for a q of 20 $ft^3/s/ft$, and comparisons were made of increases or decreases in V and D between the May and July surveys. Cross-sectional changes calculated from surveyed data were compared to exponents and coefficients in figure 18. Generally, channel-section areas scour if D increases and V decreases or fill if D decreases and V increases. These types of channel adjustments normally are expected as hydraulic variables seek equilibrium in the channel.

A 10-section stream reach, 1,400 ft in length, on the North Fork Teton River in Idaho was analyzed by using step-backwater techniques. Channel changes were occurring because the river had been rechanneled after the Teton Dam failure and flood in 1976. The approach used was a comparison of changes in energy heads attributed to h_a and h_f with surveyed channel changes during 1976–78. A constant n (0.030) was selected (determined from gaged reach upstream) and assumed to be representative of the stream reach. A step-backwater computer program (Shearman, 1976) was used to determine near-bankfull discharges. Values of h_f from computer printouts were adjusted by first subtracting a constant value for boundary roughness (minimum value of h_f from 10-section slope-area reach) selected as a constant h_f of 0.10 ft through the stream reach, and then subtracting any additional computed losses because of expansions or contractions. It was assumed that the remaining part of the h_f between sections should be equal to h_a and therefore proportional to the work done (or not done) per foot of channel width between sections.

Figure 19 illustrates the comparison of the estimated change in h_a from 1976 to 1978 to change in cross-sectional area per foot of channel width (scour and fill) between sections. A zero change in h_a would have corresponded to a zero change in scour and fill if the portion of h_f attributed to boundary friction had been 0.13 ft (by raising n). Inspection of figure 19 suggests sections 1 to 10 along the stream reach changed from degradation to aggradation. Sections 6, 9, and 10 were still (1979) subject to change if not physically constrained by riprap. Sections 1 and 2 had eroded their left banks by 40 to 50 ft.

IMPLICATIONS BASED ON OBSERVATIONS OF CHANGING HYDRAULIC GEOMETRY

Initial changes in exponents and coefficients of hydraulic-geometry relations resulting from scour and fill may not be indicative of long-term adjustments of degradation and aggradation. A shift or change in plotting position with time *along a line* of constant F is assumed to indicate a change in energy and possibly channel slope (thus hydraulic relations) caused by a recurring and seasonal variation of scour and fill. However, this shift does not indicate a long-term change in independent variables such as Q and supply of sediment from the drainage basin. Movement *along lines* can occur with changes in velocity and roughness distributions as cross-sectional and channel controls experience seasonal changes.

A change in plotting position to *another line* of different F may signal or suggest a long-term shift in independent variables and may be caused by a persistent change in either streamflow characteristics or sediment supply. A change in plotting position of V relation above an established line may indicate initial aggradation followed by an increase in coarse-sediment transport relative to a decrease in Q (as might result from a drought). Relations of D that plot below the established relation would reflect shallower D, while at the same time, V would be expected to increase.

A change in plotting position of the V relation below the established F line suggests initial scour and a short-term or temporary increase in coarse-sediment transport as D initially increases, but followed ultimately by quasi-equilibrium as degradation and coarse-sediment transport decrease.

Closer examination of the hydraulic geometry may explain subtle differences in observed bedload rates between channel sections. For example, channel hydraulics during peak runoff periods at several sections may have changed in response to decreases in coarse-sediment loads (during high Q) caused by slower rates of increase in average V. Upon a decrease in peak Q during recession of flow, the hydraulic-geometry relations may return to former conditions, which would flush bed material previously deposited at higher Q out of the

immediate stream reach. Such assumptions suggest that two hydraulic relations, possibly represented by a change from sectional to channel control, may be needed to adequately define a section.

Although the rate of increase of coarse-sediment loads varies as a function of $\frac{\Delta V}{\Delta D}$, further analysis of h_a and with V and D may help to quantify short-term channel changes of scour and fill.

SUMMARY

Prior to inferences of past, present, or future predictive model transport rates of coarse sediment, it is important first to understand how hydraulics in stream sections and reaches have changed. Techniques described in this article provide a means of tracking scour, fill, aggradation, and degradation in channels and can be used to imply changes in the stream competency to transport coarse-sediment loads. However, stream systems are dynamic in that a change in controlling variables of the water-sediment mixture requires an alteration in energy distribution associated with those variables that will accommodate the change. The results of these alterations are often scour and fill. Long-term channel adjustments such as aggradation and degradation (and probably meandering) are ultimately controlled by persistent changes in flow and in the rate, mode, and size of material carried into the reach. These changes may alter the velocity, depth, slope, width, roughness, and velocity distribution along the affected stream reach. These changes, with time, are not equally distributed among the hydraulic-geometry exponents.

REFERENCES CITED

Chow, V.T., 1959, Open-channel hydraulics: New York, McGraw-Hill, 680 p.

Colby, B.R., 1964, Discharge of sands and mean-velocity relationships in sand-bed streams: U.S. Geological Survey Professional Paper 462–A, 47 p.

Culbertson, D.M., Young, L.E., and Brice, J.C., 1967, Scour and fill in alluvial channels: U.S. Geological Survey Open-File Report, 58 p.

Emmett, W.W., 1976, Bedload transport in two large gravel-bed rivers, Idaho and Washington: Third Federal Inter-Agency Sedimentation Conference, Denver, Colo., Mar. 22–26, 1976, Proceedings, p. 4.100–4.113.

Jones, M.L., and Seitz, H.R., 1980, Sediment transport in the Snake and Clearwater Rivers in the vicinity of Lewiston, Idaho: U.S. Geological Survey Water-Resources Investigations Open-File Report 80–690, 179 p.

Leopold, L.B., and Maddock, Thomas, Jr., 1953, The hydraulic geometry of stream channels and some physiographic implications: U.S. Geological Survey Professional Paper 252, 57 p.

Morris, M.H., and Wiggert, J.J., 1972, Applied hydraulics in engineering: New York, Ronald Press Company, 629 p.

Nordin, C.F. Jr., 1977, Graphical aids for estimating general scour in long channel contractions: U.S. Geological Survey Open-File Report 77–837, 12 p.

Shearman, J.O., 1976, Computer applications for step-backwater and floodway analyses: U.S. Geological Survey Open-File Report 76–499, 103 p.

Williams, R.P., 1975, Erosion and sediment transport in the Owens River near Bishop, California: U.S. Geological Survey Water-Resources Investigations 49–75, 49 p.

———1979, Sediment discharge and channel change in the North Fork Teton River, 1977–78, Fremont and Madison Counties, Idaho: U.S. Geological Survey Open-File Report 79–1335, 81 p.

Williams, R.P., and Krupin, Paul, 1984, Erosion, channel change, and sediment transport in the Big Lost River, Idaho: U.S. Geological Survey Water-Resources Investigations Report 84–4147, 87 p.

Changes in Dissolved Organic Material in Spirit, South Fork Castle, and Coldwater Lakes, Washington, Summer of 1980 through Summer of 1983

By Diane M. McKnight, Kevin A. Thorn, *and* Robert L. Wershaw

Abstract

One of the important changes in the water chemistry of Spirit Lake and other lakes located in the area devastated by the eruption of Mount St. Helens was an increase in the concentration of dissolved organic carbon. Aquatic fulvic acid was a major fraction of this organic material. The data in this report show that aquatic fulvic acid in Spirit Lake underwent significant chemical changes from September 1980 to July 1983. These changes were (1) decrease in sulfur content, (2) increase in carboxylic-acid content, (3) decrease in phenolic-hydroxyl content, and (4) increase in the heterogeneity of the fulvic-acid material. Exposure to sunlight and oxygenated conditions are probable explanations for these changes.

INTRODUCTION

The eruption of Mount St. Helens on May 18, 1980, drastically changed lakes within the blast-zone area devastated by the volcano (fig. 1; Dion and Embrey, 1981). Pyroclastic- and debris-avalanche deposits entered Spirit Lake, raising the level of the lake and expanding its boundaries. Volcanic deposits in the Toutle River valley dammed two watersheds and formed two new lakes, South Fork Castle Lake and Coldwater Lake. During the summer of 1980, these lakes contained significant concentrations of many inorganic constituents from dissolution of lava and surface deposits and also contained significant concentrations of dissolved organic material from leaching of pyrolyzed plant and soil material (Wissmar and others, 1982a; McKnight and others, 1982; Pereira and others, 1982). Prolific microbial activity also occurred in these lakes, resulting in anoxic conditions even in near-surface waters (Wissmar and others, 1982b). The magnitude of these chemical and biological changes generally was greatest in those lakes most directly associated with pyroclastic- and debris-avalanche deposits.

These lakes in the blast zone of Mount St. Helens have provided scientists from several universities and the U.S. Geological Survey a unique opportunity to study the recovery of lake ecosystems. The approach taken by these scientists has been to characterize and quantify the chemical and biological processes taking place and then to relate these observations to undisturbed lake ecosystems. This report describes how the large quantities of dissolved organic material introduced into Spirit Lake, South Fork Castle Lake, and Coldwater Lake chemically changed from the summer of 1980 through the summer of 1983. Merrill Lake, 7 km southeast of Mount St. Helens, only received light ashfall and was sampled in 1981 and 1983 as a comparative reference.

CHARACTERIZATION OF DISSOLVED ORGANIC MATERIAL

Dissolved organic carbon (DOC) was measured with a Technicon DOC analyzer when DOC concentrations were less than about 10 mg/L, and with a Beckman 915C DOC analyzer when DOC concentrations were greater than about 10 mg/L. DOC fractionation analyses were performed by Huffman Laboratories, which used the methods described by Leenheer and Huffman (1976). Dissolved aquatic humic substances were isolated from water samples collected in 1980 and 1981 by using methods described by Thurman and Malcolm (1981), with the exception that fulvic and humic acids were not separated and the low-molecular-weight acids were not separated on an Enzacryl Gel Column because of the small size of the sample. In 1983, fulvic, humic, and hydrophilic acids were isolated from Spirit Lake by using the method described by Leenheer (1981). The fulvic acids obtained by these two methods were comparable. Elemental analysis of the aquatic fulvic-acid samples was performed by Huffman Laboratories, which used various combustive and oxidative techniques. Potentiometric titration was performed, as described by Thurman and Malcolm (1983), to determine the concentration of carboxylic-acid groups (titrated below pH 8) and

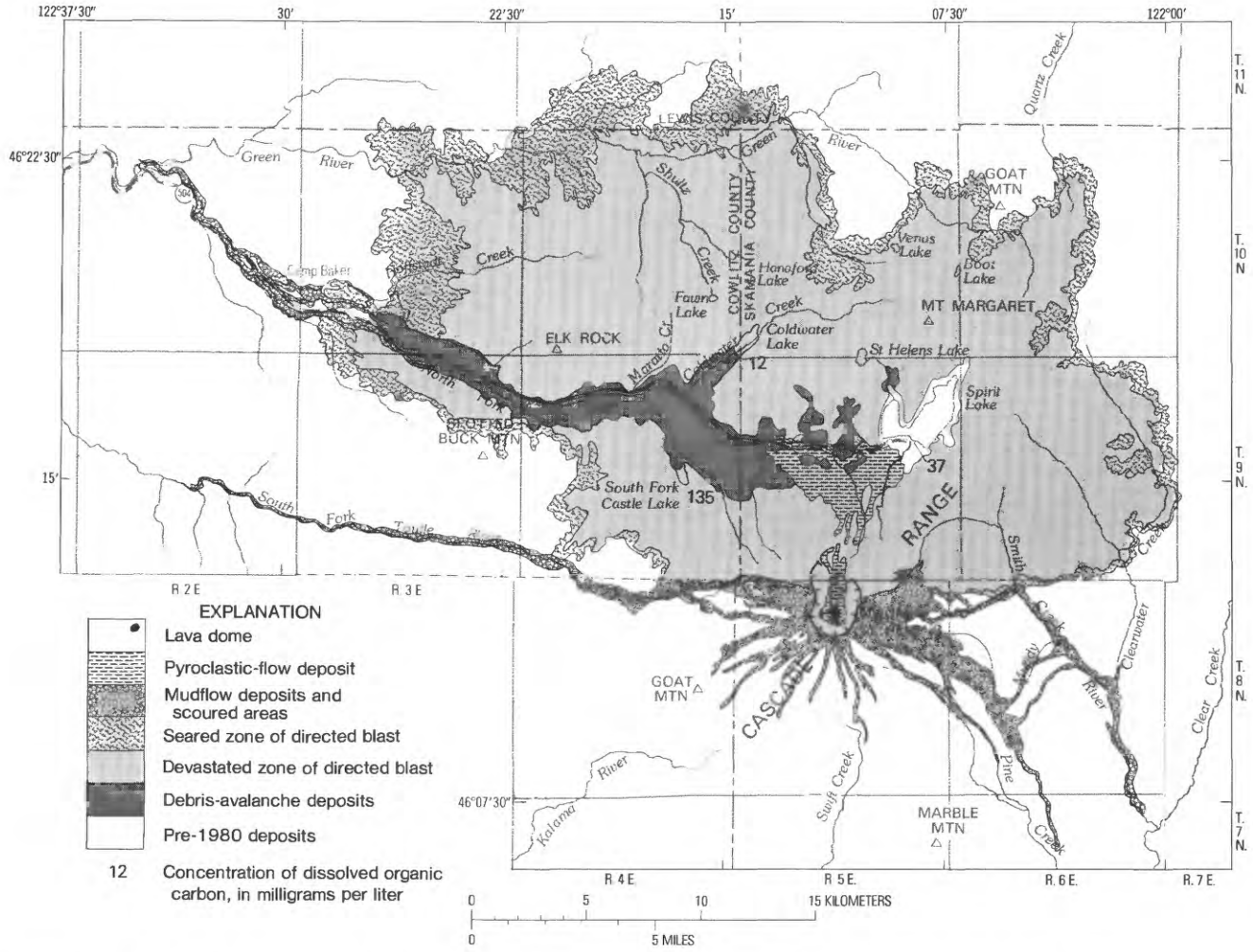

Figure 1. The blast zone of Mount St. Helens and concentration of dissolved organic carbon in several lakes.

phenolic-hydroxyl groups (one-half of which are assumed to be titrated between pH 8 and pH 10). Liquid state ^{13}C Nuclear Magnetic Resonance (NMR) spectra were obtained with a Varian FT-80A-NMR spectrometer from fulvic-acid samples derivatized with ^{13}C diazomethane as described by Wershaw and Pinckney (1978), Mikita and others (1981), and Wershaw and others (1981).

Table 1. Changes in concentration of dissolved organic carbon in South Fork Castle, Spirit, and Coldwater Lakes

Date	Dissolved organic carbon (mg/L)		
	South Fork Castle Lake	Spirit Lake	Coldwater Lake
September 1980	135	37	12
May 1981	10	17	7
September 1981	7.4	15.0	5.6

CHANGES IN DISSOLVED ORGANIC MATERIAL

The maximum concentration of DOC in Spirit Lake occurred in the summer of 1980 immediately after the major eruptions of Mount St. Helens, (fig. 1 and table 1). The pyrolytic origin of this DOC was indicated by the significant concentrations of free phenol, cresol, and other compounds produced by pyrolysis (Pereira and others, 1982). Identified compounds accounted for less than 10 percent of the total DOC. The major DOC fractions were aquatic fulvic acid and hydrophilic acids, which are the two major DOC fractions in most aquatic environments (McKnight and others, 1982; table 2).

By the following summer, the DOC concentration in all three of these lakes had decreased significantly (table 1); water-budget estimates showed that the decrease primarily was explained by dilution of the DOC

Table 2. Fractionation of dissolved organic carbon in South Fork Castle and Spirit Lakes

Lake	Date	Aquatic fulvic acid (percent)	Hydrophilic acids (percent)
South Fork Castle Lake	September 1980	24	63
	April 1981	36	47
	July 1981	40	44
Spirit Lake	September 1980 to July 1981	40–41	40–46

Table 3. Elemental analysis of aquatic fulvic acid isolated from Spirit and Merrill Lakes

Lake	Date	Zone	Carbon	Hydrogen	Nitrogen	Sulfur
			(percent by weight)			
Spirit	September 1980	Epilimnion	51.6	4.9	1.0	4.3
	April 1981	Epilimnion	50.6	4.9	.36	2.3
	July 1981	Epilimnion	50.5	4.7	.63	1.9
	July 1981	Epilimnion	53.3	4.9	.64	1.6
Merrill	April 1981	Epilimnion	51.3	5.0	.73	.5

in the lake by inflowing snowmelt and rainfall in the spring of 1981 (McKnight and others, 1984). All three lakes were eventually drained by spillways or by pumping in 1981 or 1982; however, no major losses of DOC occurred previous to these activities. The lakes were oxygen saturated at the beginning of the summer of 1981, but by midsummer the hypolimnia became anaerobic from continuing degradation of organic material in volcanic deposits covering the lake bottoms. Associated with these anoxic conditions were greater DOC concentrations and greater proportions of hydrophilic acids in the hypolimnia of Spirit and South Fork Castle Lakes (McKnight and others, 1984). One possible explanation for these changes was less efficient degradation of organic material under anaerobic conditions, with a greater accumulation of the more labile, possibly low-molecular-weight, hydrophilic-organic acids than would have accumulated under aerobic conditions. In 1982 and 1983, the same summer depletion of hypolimnetic oxygen occurred in these lakes, but in 1983 the hypolimnia did not become completely anaerobic (C.D. Dahm, Oregon State University, oral commun., 1983).

Aquatic fulvic acid, which accounted for about 40 percent of the DOC, (a slightly smaller fraction than the hydrophilic acids), was studied to see if the exposure to oxygenated conditions and sunlight from spring 1981 through summer 1983 had caused any discernible changes in its chemical characteristics. Possible reactions that would be expected to alter humic substances under these condiiton were chemical or microbial oxidation, phenol-condensation reactions, and photolytic degradation.

One of the first pieces of information used to characterize humic substances is their elemental analysis (table 3). Generally, large differences are not observed in elemental analysis for the same class of humic substances; however, there are some consistent differences between different classes of humic substances. For example, aquatic humic acid generally has a lesser oxygen content than aquatic fulvic acid (Thurman and Malcolm, 1983). Despite its unique origins, the carbon, hydrogen, and nitrogen contents of fulvic acid isolated from Spirit Lake and other blast-zone lakes were within the range reported for aquatic fulvic acids from more common environments. The exception to this was the sulfur content. Although the sulfur content in the fulvic acid from Spirit Lake had decreased from 4.3 percent in September 1980 to 2.3 percent in April 1981, the sulfur content was still much greater than that (0.5 percent) in fulvic acid from Merrill Lake outside the blast-zone in April 1981 (table 3). This sulfur may have become incorporated in the humic material from the sulfur dioxide and hydrogen sulfide present during the eruption (McKnight and others, 1984). In Spirit Lake, the sulfur content in the fulvic acid decreased to 1.9 percent by July 1981 (table 3), and in South Fork Castle Lake fulvic acid, sulfur content had decreased by the summer of 1981 to 1.0 percent. This decrease may have been a result of oxidation of reduced sulfur functional groups under oxygenated conditions. The further decrease in sulfur content that occurred between July 1981 and July 1983 was small compared to the previous decreases.

Another important way to characterize fulvic acid is to measure acidic functional groups, which are primarily carboxylic acids and phenols. These functional groups are very important in the geochemical reactivity of aquatic fulvic acid, for example, in binding dissolved trace metals and in contributing to the pH-buffering capacity of natural waters. In this study, acidic functional groups were characterized by two independent methods: (1) by direct potentiometric titration (table 4) and (2) by obtaining ^{13}C NMR spectra of derivatized fulvic acid samples (fig. 2). As determined by titration, the carboxylic-acid content of all the fulvic-acid samples from Spirit Lake were greater than the carboxylic-acid content of fulvic acid from Merrill Lake. Also, the carboxylic acid significantly increased from 5.3 to 5.8 meq/g in fulvic acid from Spirit Lake from April 1981 through July 1981. However, there was no further change in carboxylic-acid content in the fulvic acid from the epilimnion of Spirit Lake during the next 2 years. This initial increase was consistent with further oxidative degradation of fulvic acid during the first summer.

Another important result from the potentiometric-titration data was that the phenolic-hydroxyl groups of the fulvic acid from Spirit Lake isolated in 1980 were not

Table 4. Functional-group content of aquatic fulvic acid isolated from Spirit and Merrill Lakes

Lake	Date	Zone	Carboxylate (meq/g)	Phenol (meq/g)
Spirit	September 1980	Epilimnion	5.2	1.7
	April 1981	Epilimnion	5.3	1.0
	July 1981	Epilimnion	5.8	1.2
	July 1983	Epilimnion	5.8	.2
Merrill	April 1981	Epilimnion	4.3	.8
	July 1983	Epilimnion	4.5	.6

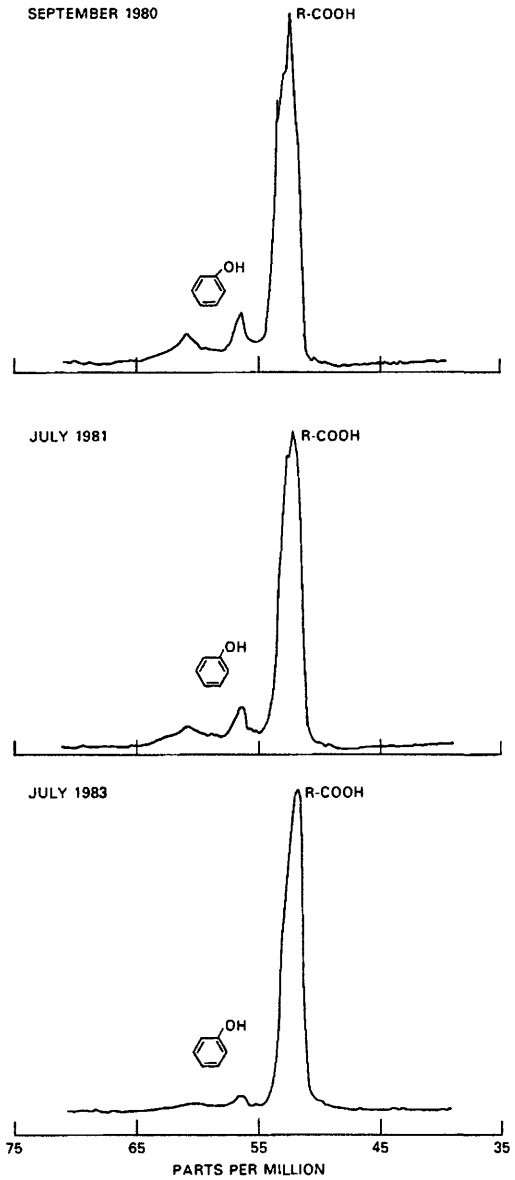

Figure 2. Liquid state ^{13}C NMR spectra of derivatized aquatic fulvic acid collected from Spirit Lake from September 1980, July 1981, and July 1983. The functional groups to which the major peaks correspond are indicated. Parts per million refers to hertz per megahertz in the NMR experiment;  represents phenolic-hydroxyl group; R-COOH represents carboxylic acid group.

stable but were degraded under the environmental conditions in the lake. In 1980, the phenolic-hydroxyl content of fulvic acid from Spirit Lake was much greater than the phenolic-hydroxyl content of fulvic acid from Merrill Lake and other aquatic fulvic acids. Between September 1980 and July 1981, phenolic-hydroxyl concentrations in fulvic acid from Spirit Lake decreased from 1.7 to 1.2 meq/g, and between July 1981 and July 1983 phenolic-hydroxyl concentrations decreased from 1.2 to 0.2 meq/g (table 4). The phenolic-hydroxyl content of fulvic acid from Spirit Lake in July 1983 was three times less than the phenolic-hydroxyl content of fulvic acid from Merrill Lake. One possible explanation for these concentrations was that the phenolic functional groups had undergone oxidative coupling or quinone formation. The changes in phenolic-hydroxyl content indicated by the titration data are confirmed by the ^{13}C NMR spectra (fig. 2). The peaks centered between 55 and 60 ppm, representing the methyl ethers of phenolic hydroxyls, are very prominent in the spectrum for the 1980 sample but are just discernible in the spectrum for the 1983 sample.

Another important conclusion can be drawn from the ^{13}C NMR spectra. In comparing the large, broad resonance centered at 52 ppm, which represents the methyl esters of carboxylic acids, we see that several discrete peaks are present within this broad resonance in the 1980 sample, fewer in the 1981 sample, and none discernible in the 1983 sample. The appearance of these discrete peaks in the spectrum for the 1980 samples indicates that this sample included some groups of molecules that were very similar to each other and that produced dicrete peaks in the spectrum. The disappearance of this fine structure in the spectrum for the 1983 sample showed that the chemical or biological "weathering" reactions or both caused the fulvic acid to become more heterogeneous; that is, fewer similar molecules were present in 1983 than in 1980. These data indicate that fulvic-acid material can undergo reactions such as photo-oxidation, biodegradation, and humification under the environmental conditions ocurring in a lake.

CONCLUSIONS

The data presented in this report show that the aquatic fulvic acid in Spirit Lake has undergone chemical changes that can be explained in a general way by exposure to sunlight and oxygenated conditions. These chemcial changes are (1) decrease in sulfur content, (2) increase in carboxylic-acid content, (3) decrease in phenolic-hydroxyl content, and (4) increase in the heterogeneity of the fulvic-acid material. Similar changes in aquatic fulvic acid might be expected to occur in other lakes that have slow flushing rates, where the incoming aquatic fulvic acid would be exposed to the chemical conditions in the lakes for several years.

REFERENCES CITED

Dion, N.P., and Embrey, S.S., 1981, Effects of Mount St. Helens eruption on selected lakes in Washington: U.S. Geological Survey Circular 850–G, 25 p.

Leenheer, J.A., 1981, Comprehensive approach to preparative isolation and fractionation of dissolved organic carbon from natural waters and waste-waters: Environmental Science and Technology, v. 15, p. 578–587.

Leenheer, J.A., and Huffman, E.W.D., Jr., 1976, Classification of organic solutes in water by using macroreticular resins: U.S. Geological Survey Journal of Research, v. 4, p. 737–751.

McKnight, D.M., Pereira, W.E., Ceazan, M.L., and Wissmar, R.C., 1982, Characterization of dissolved organic materials in surface waters within the blast zone of Mount St. Helens, Washington: Organic Geochemistry, v. 4, p. 85–92.

McKnight, D.M., Klein, J.M., and Wissmar, R.C., 1984, Changes in the organic material in lakes in the blast zone of Mount St. Helens, Washington: U.S. Geological Survey Circular 850–L, 26 p.

Mikita, M.A., Steelink, Cornelius, and Wershaw, R.L., 1981, Carbon-13 enriched nuclear magnetic resonance method for the determination of hydroxyl functionality in humic substances: Analytical Chemistry, v. 53, p. 1715–1717.

Pereira, W.E., Rostad, C.E., Taylor, H.E., and Klein, J.M., 1982, Characterization of organic contaminants in environmental samples associated with Mount St. Helens 1980 volcanic eruption: Environmental Science and Technology, v. 16, p. 387–396.

Thurman, E.M., and Malcolm, R.L., 1981, Preparative isolation of aquatic humic substances: Environmental Science and Technology, v. 15, p. 463–466.

———1983, Structural study of humic substances: new approaches and methods, *in* Christman, R.F., and Gjessing, E.T., eds., Aquatic and terrestrial humic materials: Ann Arbor, Mich., Ann Arbor Science.

Wershaw, R.L., and Pinckney, D.J., 1978, Methylation of humic acid fractions: Science, v. 199, p. 906–907.

Wershaw, R.L., Mikita, M.A., and Steelink, Cornelius, 1981, Direct ^{13}C-NMR evidence for carbohydrate moieties in fulvic acids: Environmental Science and Technology, v. 15, p. 1461–1463.

Wissmar, R.C., Devol, A.H., Nevissi, A.E., and Sedell, J.R., 1982a, Chemical changes of lakes within the Mount St. Helens blast zone: Science, v. 216, p. 175–178.

Wissmar, R.C., Devol, A.H., Staley, J.T., and Sedell, J.R.,1982b, Biological responses in lakes of Mount St. Helens blast zone: Science, v. 216, p. 178–181.

Potential for Saltwater Intrusion into the Upper Floridan Aquifer, Hernando County, Florida

By Paul D. Ryder *and* Gary L. Mahon

Abstract

There is potential for saltwater intrusion into the coastal Upper Floridan aquifer because of expected large increases in population and consequent increases in ground-water withdrawals. To gain a better understanding of the potential for saltwater intrusion, a test well was drilled to a depth of 820 feet approximately 1 mile from the coast near Aripeka in Hernando County. Freshwater was present in the carbonate rock aquifer to a depth of about 500 feet, a mixture of freshwater and saltwater occurred from 500 to 560 feet, and saltwater occurred from 560 feet to the base of the aquifer at about 750 feet. Hydraulic testing indicated a very permeable zone at a depth from about 450 to 500 feet that has a transmissivity of about 56,000 square feet per day. Water-quality data show the freshwater-saltwater transition zone in the Aripeka area to be relatively thin and to have a steep slope, compared to nearby coastal areas to the north and south.

Digital models were used to simulate the steady-state flow system and the freshwater-saltwater transition zone near Aripeka; the models were also used to simulate large hypothetical withdrawals inland from the coast. Simulation results show that coastal freshwater supply wells could experience increases in chloride concentrations as a result of increased ground-water withdrawals, depending upon distance from the shoreline, well depth, and pumping rate.

INTRODUCTION

A potential exists for saltwater intrusion into the freshwater Floridan aquifer system along the gulf coast of west-central Florida. Seasonal and long-term pumping from the Floridan aquifer system for irrigation, industrial, and municipal supplies has caused a declining altitude of the potentiometric surface near the coast. Although saltwater intrusion apparently has not occurred on a regional scale, increased mineralization of water in wells near heavy pumping centers has caused concern among water managers and planners. The problem of saltwater intrusion is expected to increase with Florida's rapidly growing population and accompanying increased demand on the water resources.

Total population in the Southwest Florida Water Management District in 1980 was about 2.5 million and is expected to increase to about 4.6 million by 2020 (Southwest Florida Water Management District, written commun., 1982). Most of this increase will be in coastal areas where the potential for saltwater intrusion is greatest and where the ground-water resources are already heavily stressed. A study by the U.S. Army Corps of Engineers (1980) projected a 380-Mgal/d (million gallons per day) increase in water demand from 1975 to 2035 for the coastal area of west-central Florida.

Recognizing that an increase in water demand would require an increased understanding of the ground-water flow system, the Southwest Florida Water Management District in 1976 initiated its Regional Observation and Monitor-Well Program (ROMP). The main objectives of the program were to collect hydrologic data and to construct and operate long-term observation wells, including wells in the freshwater-saltwater transition zone along the gulf coast. In 1980, the Southwest Florida Water Management District entered into a cooperative agreement with the U.S. Geological Survey to apply the information and resources of ROMP to study saltwater intrusion and to predict movement of highly mineralized water under new stress conditions.

Purpose, Scope, and Approach

The overall objective of the study is to better define the physics of a coastal ground-water flow system. Specific objectives are to (1) evaluate the capability and feasibility of digital models, applied in cross section, to simulate the position of the freshwater-saltwater interface and (2) simulate movement of the freshwater-saltwater interface under hypothetical stress conditions and evaluate impact of the movement on inland freshwater resources.

The focal point of the study was the ROMP well TR18–2 near the border between Hernando and Pasco Counties (fig. 1). The well was deepened to the base of the Upper Floridan aquifer, tested to determine hydrau-

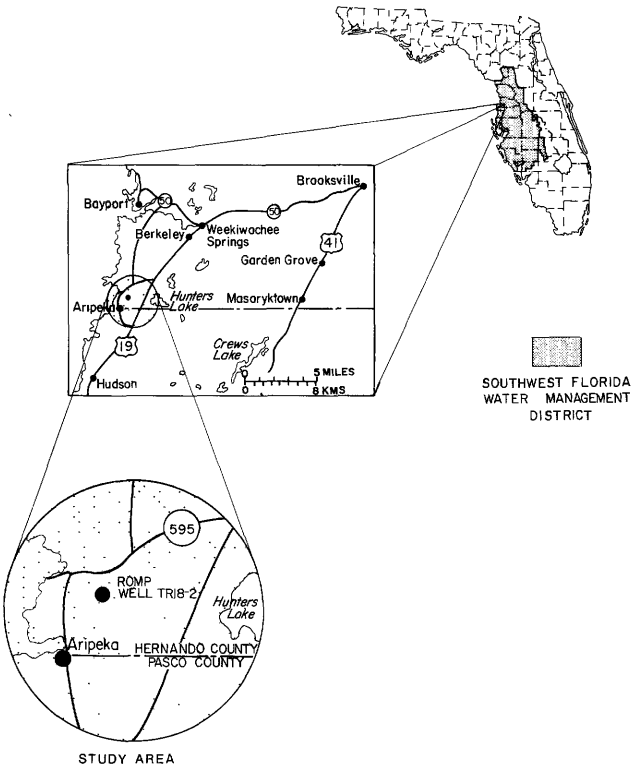

Figure 1. Location of study area.

lic characteristics and the nature of the freshwater-saltwater transition zone, and finished with multizone piezometers. This report describes the results of that testing and incorporation of test results and other field data into a digital solute-transport model.

Description of Area

The study area is centered around ROMP well TR18–2 in southwest Hernando County about 1 mi northeast of Aripeka (fig. 1). The area west of U.S. Highway 19 very nearly coincides with the physiographic unit known as the Chassahowitzka Coastal Strip (Brooks, 1981). Altitude of the land surface is generally less than 10 ft, and limestone occurs at or near the surface. Swamps and hardwood forests predominate, and saltwater marsh grasses grow at the coast among tidal flats and channels. The area is sparsely populated.

The area extending east of U.S. Highway 19 for about 9 mi is called the Weeki-Wachee Dune Field (Brooks, 1981). This is an area of sand dunes and solution basins, and land-surface altitudes are lower than 90 ft. Sand pines and long leaf pineturkey oaks occur in the area (Brooks, 1981). A prominent feature east of U.S. Highway 19 is Hunters Lake, which has a surface area of about 350 acres. Residential and commercial development is proceeding at a rapid rate near the lake and is creating an increased demand on the ground-water resources of the area.

Average rainfall for the period 1915 to 1976 at Brooksville, about 15 mi northeast of the study area, was nearly 57 in./yr (Palmer and Bone, 1977, p. 6). More than half, about 29 in., of the rainfall occurs from June to September as thundershowers (Fretwell, 1985).

Previous Investigations

Reichenbaugh (1972) discussed some aspects of saltwater intrusion and defined the freshwater-saltwater interface in the Upper Floridan aquifer in coastal Pasco County. A similar study was done by Mills and Ryder (1977) for a coastal strip north of Pasco County. Hickey (1982) made a detailed study of the saltwater part of the Upper Floridan aquifer in the Tampa Bay area (about 50 mi south of the study site) to test the feasibility of injecting sewage-treatment-plant effluent. Wilson (1982) estimated the effects of projected pumping on movement of the saltwater front in the Upper Floridan aquifer in the southern part of west-central Florida. Steinkampf (1982) discussed the origin and distribution of saline waters in the Upper Floridan aquifer for the southern area. Causseaux and Fretwell (1982, 1983) updated and expanded earlier studies that defined chloride-concentration distributions and the nature of the freshwater-saltwater interface in west-central Florida.

HYDROGEOLOGIC UNITS AND HYDRAULIC CHARACTERISTICS

The Floridan aquifer system consists of a thick sequence of carbonate rock of Tertiary age and, in descending order, is made up of the Tampa, Suwannee, and Ocala Limestones and the Avon Park, Oldsmar, and Cedar Keys Formations (Miller, 1986). In the study area, the Oldsmar and Cedar Keys Formations generally contain intergranular evaporities of low permeability and are not considered part of the ground-water flow system. The oldest rocks having any significant involvement in the ground-water flow system are within the Avon Park Formation. Thus, discussion and references to the aquifer in the report are restricted to the Upper Floridan aquifer (Miller, 1986) that includes the Avon Park Formation and younger rock units, with the exception of the Tampa Limestone, which is not present in the study area.

The geology in the study area is best described at ROMP well TR18–2, where permeable quartz sand of Holocene and Pleistocene age extends from land surface (7 ft above the NGVD of 1929) to a depth of 5 ft (J.L. Decker, Southwest Florida Water Management District, written commun., 1983). The Suwannee Limestone of

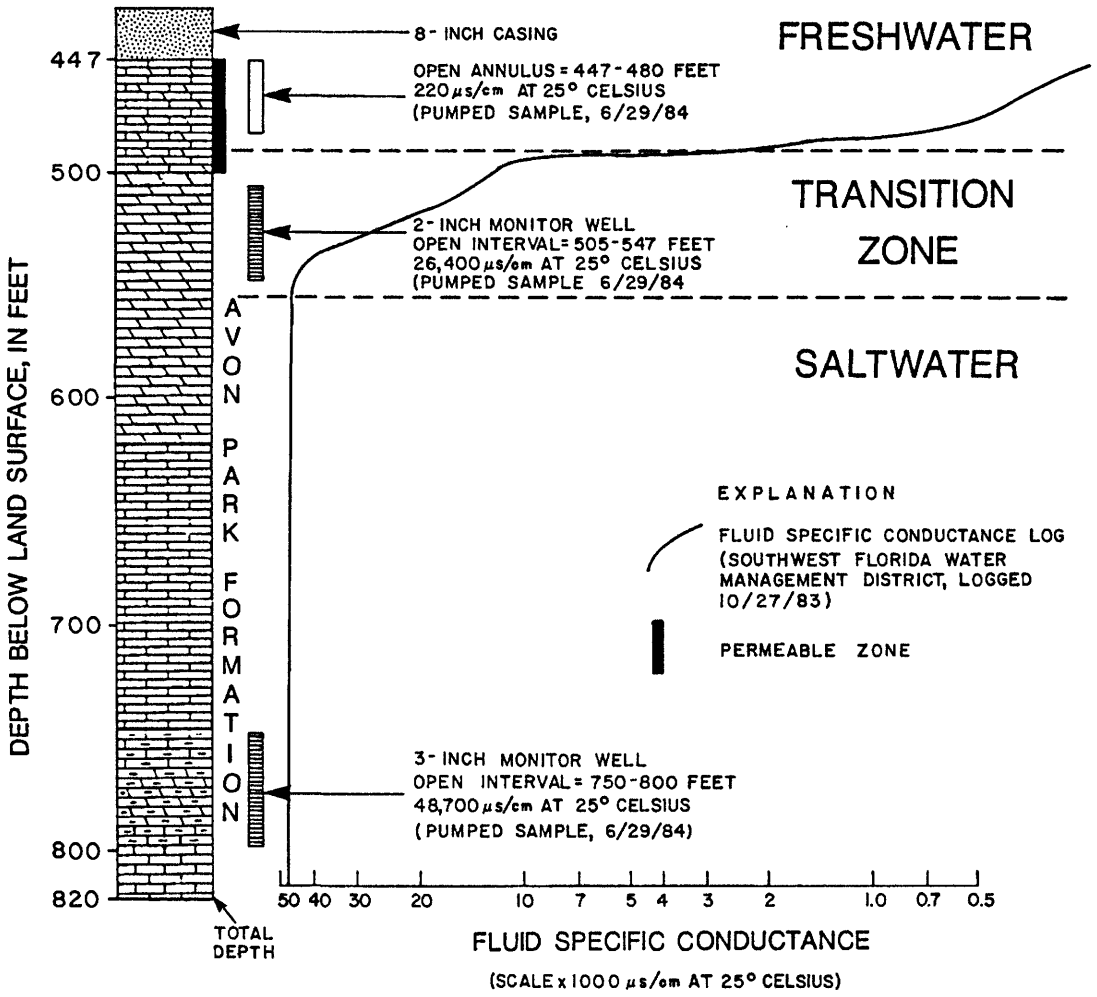

Figure 2. Permeable zone, monitored intervals, and specific conductance distribution at site TR18–2.

Oligocene age, at depths from 5 to 150 ft, is mostly limestone with some clay and sand anomalies that can be attributed to infilling of solution cavities and fractures. The Ocala Limestone of Eocene age extends from a depth of 150 to 275 ft and consists of fossiliferous limestone. The thickest unit is the Avon Park Formation of Eocene age. It is present from depths of 275 to 820 ft and consists of alternating limestone and dolomite. Intergranular gypsum and anhydrite occur within the Avon Park Formation between 745 and 807 ft and mark the base of the aquifer unit.

Well TR18–2 was initially drilled in 1981 to a depth of 498 ft, and an 8-in. casing was set to a depth of 447 ft. Hydraulic testing to determine the magnitude and distribution of rock permeability was not performed before the casing was set. In 1983, as part of this study, the well was deepened to 820 ft, and the open-hole interval from 447 to 820 ft was pumped at a rate of about 560 gal/min for 5.5 hours. A concurrent flow-meter survey was run to identify the contributing zones. The zone from which nearly all water was being produced was from the bottom of the casing at 447 ft to 500 ft (fig. 2). A transmissivity of 56,000 ft^2/d was determined from an analysis of the pumping test data (J.M. Clayton, Southwest Florida Water Management District, written commun., 1983).

Because of lack of testing in the cased-off section of rock, it is not certain that the transmissivity value represents just this interval (447 to 500 ft). At a test site about 20 mi east-southeast of well TR18–2 in Pasco County, it was determined that the better water-bearing zones are located at formation contacts between the Suwannee and Ocala Limestones and the Ocala Limestone and the Avon Park Formation. Major water-bearing zones are in dolomite of the Avon Park Formation at altitudes of 400 ft and 500 ft below the NGVD of 1929 (Ryder, 1978, fig. 3). It was also determined at the Pasco County test site that good vertical connection exists between the more permeable zones and that the entire rock column functions as a single aquifer down to the base, which was the first occurrence of intergranular gypsum and anhydrite.

WELL NO.	WELL DEPTH (ft.)	CASING DEPTH (ft.)	CHLORIDE CONCENTRATION IN MILLIGRAMS PER LITER DATE OF COLLECTION: (month/year)	
1			5(12/75)	
2	180		30(12/75)	
3	170		7(12/75)	
4	580	445	5(9/81)	
5	373	210	6(12/75)	
6	101	64	17(12/75)	
7	195	176	13,600(10/65)	18,000(11/75)
8	70	51	8200(8/84)	
Metered wells at SITE TR18-2 9a	480	465	3(6/84)	
9b	525	505	10,000(5/84)	
9c	790	760	18,200(6/84)	
10	250	81	2(12/75)	
11	73		254(?)	
12	100		35(?)	
13	111		50(9/78)	

SPRING(S)	DATE OF COLLECTION: (month/year)	DISCHARGE IN MILLION GALLONS PER DAY	CHLORIDE CONCENTRATION IN MILLIGRAMS PER LITER
Bobhill	11/64	2.4	5
	8/65	2.9	4
	12/72	1.3	8
Boat	2/62	3.9	—
	5/62	—	21
	4/64	1.0	—
	10/64	—	12

EXPLANATION

2(30) WELL NUMBER AND SAMPLE (Chloride concentration, in milligrams per liter)

(8) SPRING SAMPLE (Chloride concentration, in milligrams per liter)

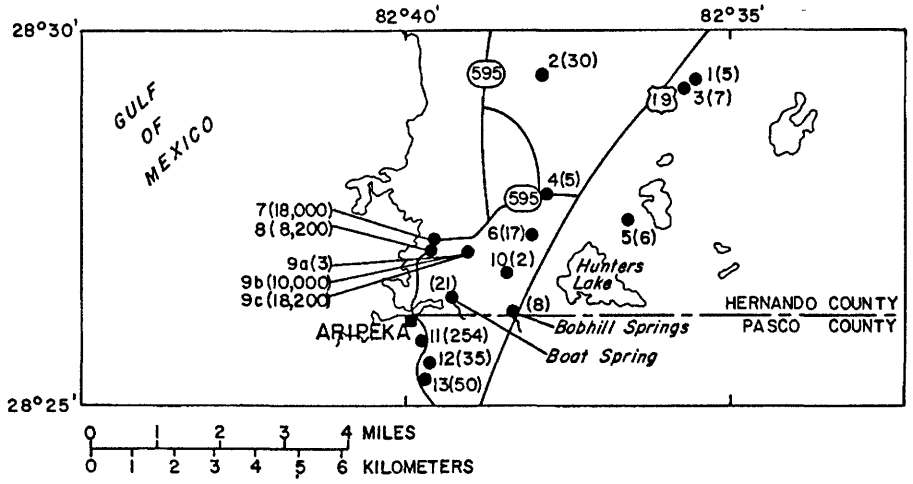

Figure 3. Chloride concentrations in wells and springs. (Modified from Mills and Ryder, 1977.)

For modeling purposes, a transmissivity of 50,000 ft^2/d was assumed and divided by 500 ft of aquifer thickness to give an estimated hydraulic conductivity of 100 ft/d for the Upper Floridan aquifer.

WATER QUALITY

Regional Variations in Chloride Concentrations

Samples of water were collected from wells, springs, and streams in the coastal Pasco and Hernando County area (fig. 3) to define the freshwater-saltwater interface in the Upper Floridan aquifer (Reichenbaugh, 1972; Mills and Ryder, 1977). Water from many of the wells had chloride concentrations of less than about 30 mg/L. Exceptions were water from wells 7 and 8 that are only a few feet from saltwater channels, site TR18–2 that consists of nested monitor wells (9a, b, and c) that are open to and below the zone of transition between freshwater and saltwater, and three wells (11, 12, and 13) in Pasco County. The two samples from Boat Spring had low chloride concentrations even though the spring is only a few hundred feet from an estuary. Perhaps the two samples collected from the spring were at low tide, whereas sampling at high tide may indicate that saltwater is mixing with freshwater in the aquifer.

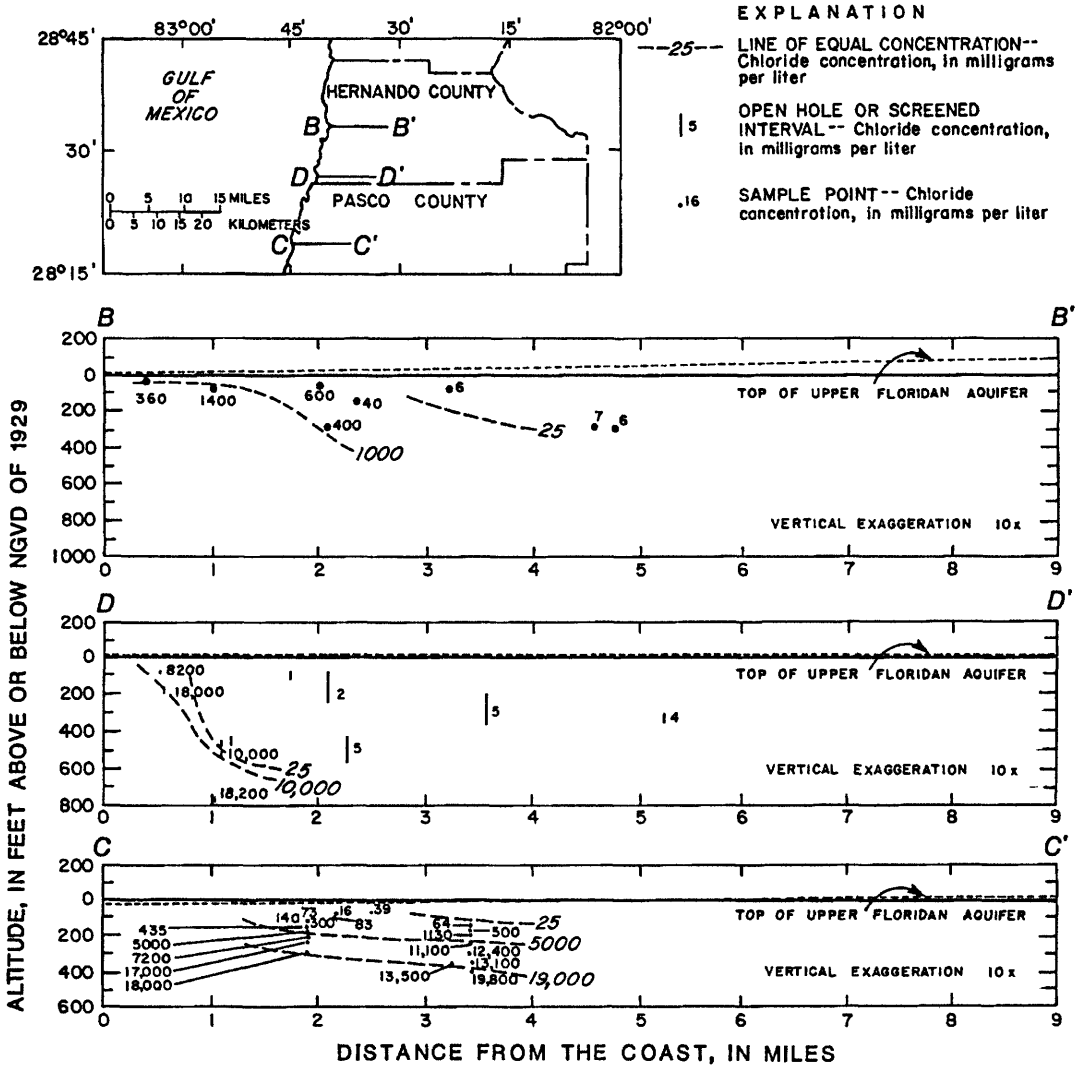

Figure 4. Sections showing chloride concentrations in the coastal margin of Pasco and Hernando Counties. (Modified from Causseaux and Fretwell, 1983, figures 7–9.)

Vertical sections of the regional distribution of chloride concentrations are shown in figure 4. Sections *B–B'* and *C–C'* are from Causseaux and Fretwell (1983, figs. 8 and 9). These sections were constructed by using chloride concentrations for water from wells located within 2 mi of the line of section. Chloride concentrations are shown at the bottom altitude of each well. Section *D–D'* was constructed from data from the TR18–2 test site and other wells that lie within 1 mi of the line of section. Chloride concentrations for section *D–D'* are shown opposite the open-hole or screened interval of each well.

The angle and width of the freshwater-saltwater transition zone in section *D–D'* is quite different from those in sections *B–B'* and *C–C'*. For section *B–B'*, freshwater discharge through large springs and a consequent lower hydraulic head for a given distance from the coastline could explain higher chloride concentrations at shallow depths. However, it is not clear why chloride distributions in the vicinity of section *C–C'* are so greatly different from those at section *D–D'*. Topographic and hydrogeologic conditions and hydraulic head as a function of distance from the coastline appear to be similar for the two areas. It is not known whether the differences are natural or are attributable to development. Pasco County has undergone more development than Hernando County. Dredging of finger canals at the coastline, large rock-quarrying operations, and significant groundwater pumpage are possible causes of saltwater intrusion.

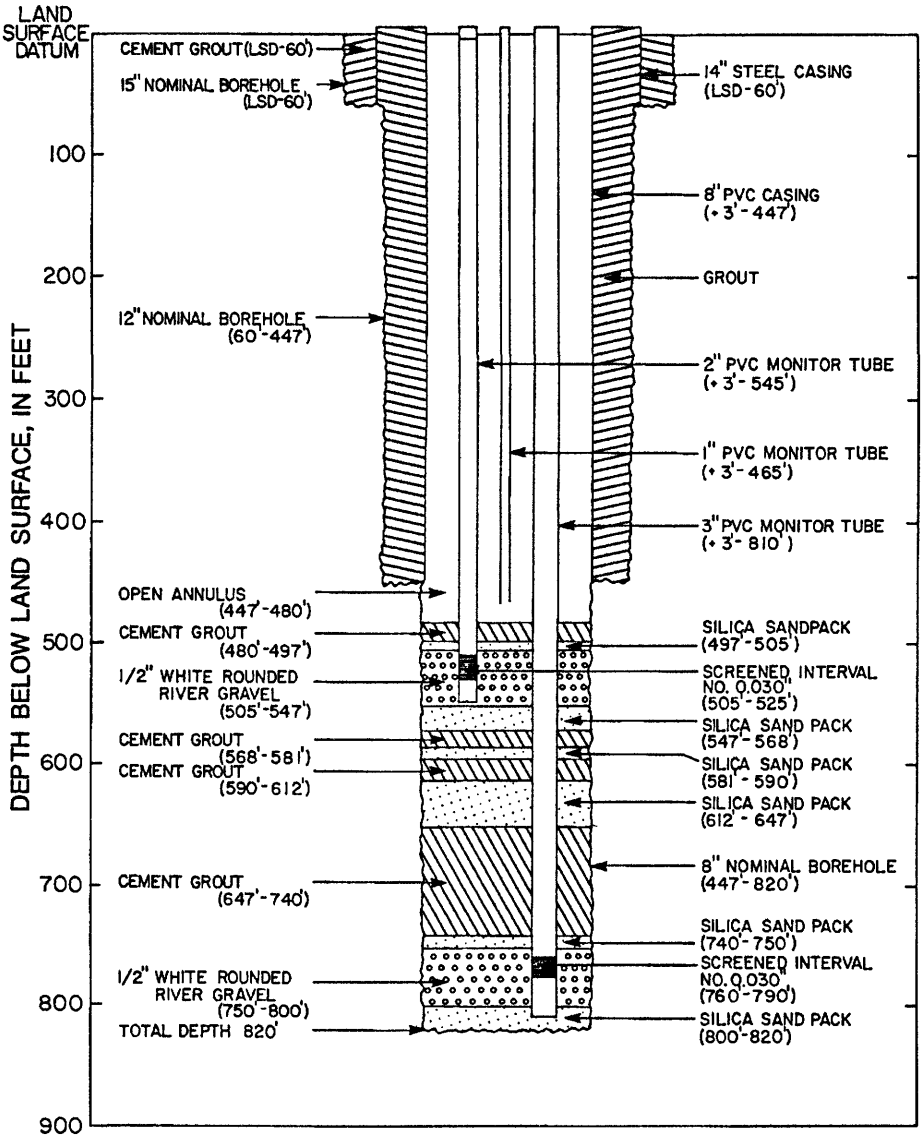

Figure 5. Monitor-well construction at site TR18–2 near Aripeka. (Modified from J.L. Decker, Southwest Florida Water Management District, written commun., 1983.)

Water Quality at Regional Observation and Monitor-Well Program Well TR18–2

As well TR18–2 was being deepened in 1983, water samples were collected at appropriate times from the bottom of the hole for determination of specific conductance and selected water-quality constituents. Upon completion of the hole to a depth of 820 ft and after stabilization of the water column, a fluid specific-conductance log was run (fig. 2). The hole was completed as a three-zone monitor well with a 3-in. monitor tube open to the saltwater zone, a 2-in. tube open to the transition zone, and a 1-in. tube open to the freshwater zone (fig. 5)

Figure 2 shows that the zone from the bottom of the casing to a depth of 480 ft is freshwater. The specific-conductance log shows a large increase in conductance at about the 500-ft depth. Figure 2 also indicates that the 2-in. monitor well is open to the transition zone. This fact is confirmed by water samples pumped from this zone that had specific conductances that were about midway between the specific conductance of freshwater and saltwater. The open interval of the 3-in. monitor well is far below the transition zone; specific conductance of water samples are nearly 49,000 μS/cm. Specific conductance of water samples obtained during drilling agree with specific conductances of the monitor-well samples and the specific-conductance log, except

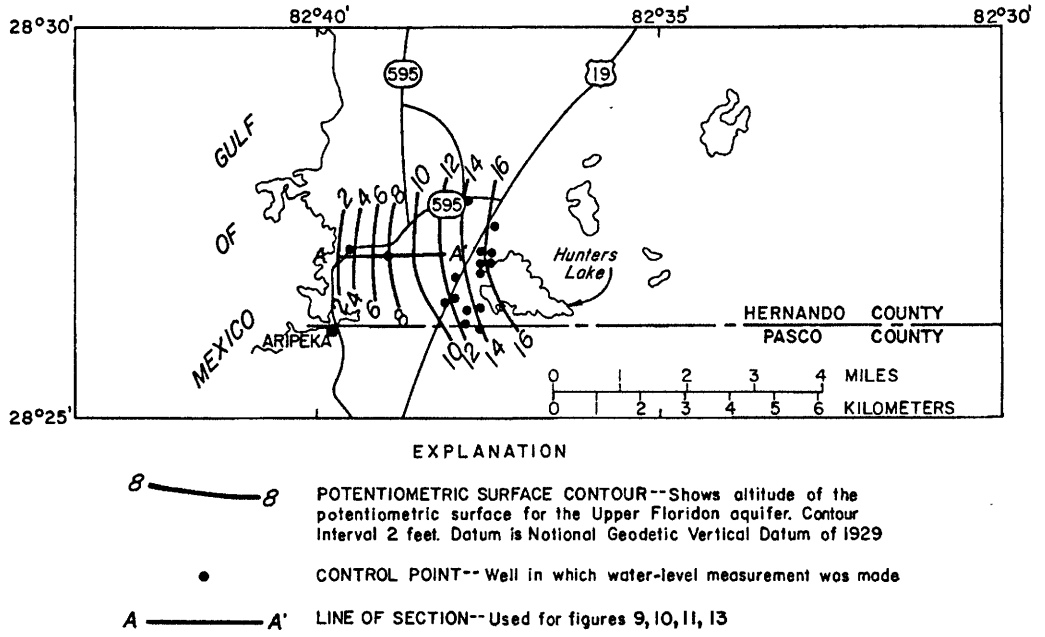

Figure 6. Potentiometric surface of the Upper Floridan aquifer near Aripeka, 1982.

below about 500 ft where water from the overlying high-permeability zone diluted the water samples obtained during drilling.

GROUND-WATER FLOW SYSTEM

Areas of Recharge and Discharge

A regional, closed high in the potentiometric surface of the Upper Floridan aquifer occurs in central Pasco County about 25 mi east-southeast of Aripeka, resulting in flow in all directions. Recharge to the aquifer also occurs between the Pasco County high and the gulf coast as downward leakage from rainfall. As a result, the general direction of ground-water flow is coastward from inland areas. Areas east of U.S. Highway 19 are generally recharge areas, with annual recharge rates of 10 to 20 in., as estimated by a regional flow model (Ryder, 1982, fig. 16). Areas west of U.S. Highway 19 are generally discharge areas, with water moving laterally toward the gulf (fig. 6) and vertically upward to discharge as springs and diffuse upward leakage into low-lying coastal swamps.

A digital flow model, developed to simulate flow along section *A–A'* (fig. 6), indicates an average upward leakage rate of about 30 in./yr. In the model, the rate of discharge increases toward the gulf, where the discharging ground water mixes with gulf water in coastal marshes, estuaries, and channels.

The potentiometric surface shown in figure 6 was constructed by using average water levels in wells for 1982. The range in water levels between the wet summer season and dry spring season in the vicinity of U.S. Highway 19 is about 3 ft. The seasonal fluctuations diminish toward the gulf and are only about 1 foot for the freshwater monitor well at site TR18–2. Ground-water pumpage in the area is not large and has no apparent effect on the regional potentiometric surface. Rock-quarrying operations just to the north of State Road 595 reportedly pump sizable amounts of water from a large open pit, but little water is used and most is returned to the pit.

Changes in Water Levels and Specific Conductance in Response to Tidal Fluctuations

In addition to water-level changes that are caused by short- and long-term variations in recharge, water levels in the coastal areas also respond to gulf tidal fluctuations. Hydrographs in figure 7 compare water levels in wells TR18–1 and TR18–2, about 11,000 and 3,700 ft, respectively, from the gulf, and tidal fluctuations at Bayport (fig. 1). Water levels in well TR18–2 indicate an average apparent tidal efficiency of about 11 percent and an average time lag of about 93 min. Tidal effects on water levels in well TR18–1 are greatly diminished because of its greater distance from the shoreline.

On March 29, 1984, after well TR18–2 was deepened and finished with multiple piezometers, a water-quality minimonitor was installed to record specific con-

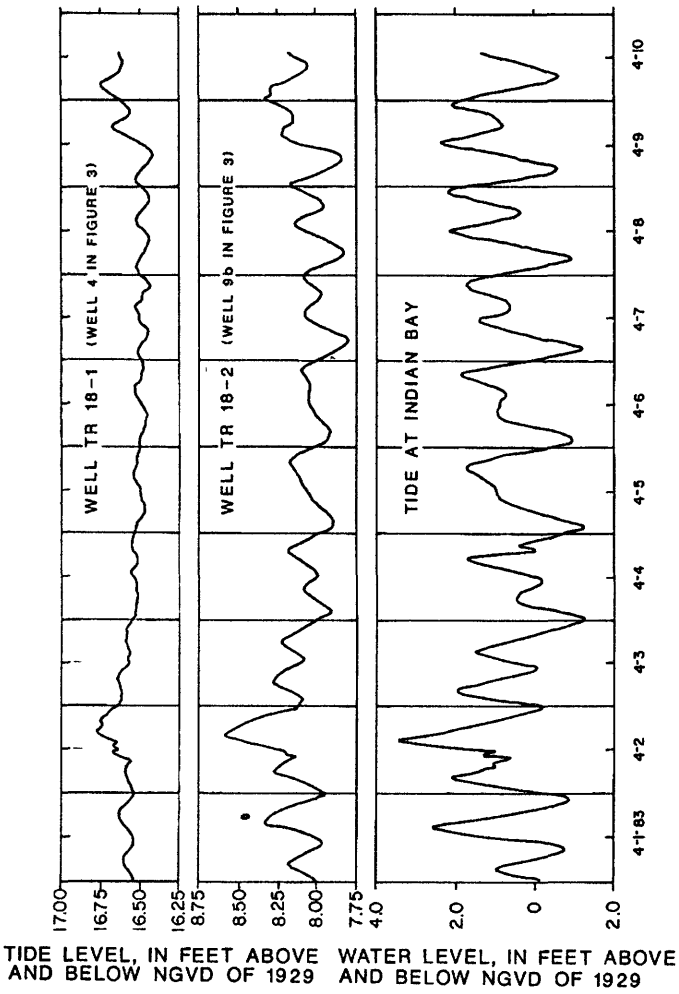

Figure 7. Water levels in wells TR18–1 and TR18–2 and tidal fluctuations at Indian Bay, April 1–10, 1983.

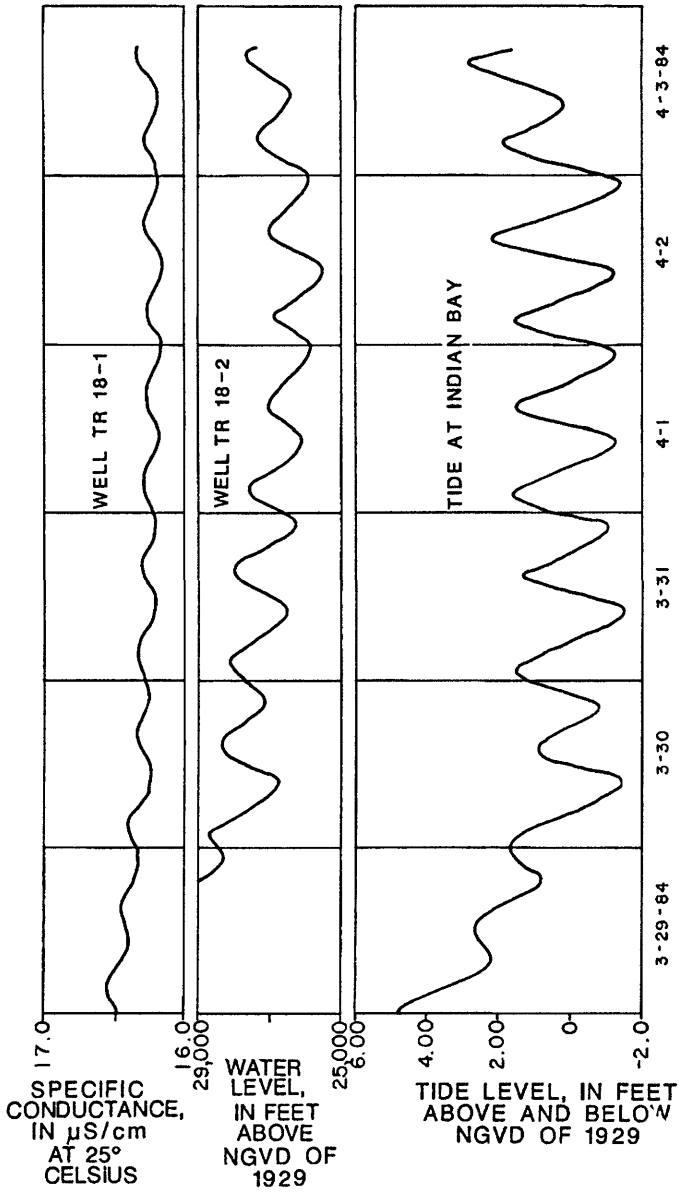

Figure 8. Relation between specific conductance in water from well TR18–2, water levels in well TR18–1, and tidal fluctuations at Indian Bay, March 29 to April 3, 1984.

ductance simultaneously with water level in the 2-in. transition zone well (fig. 2). The sensing probe was lowered to a depth of 538 ft below land surface. Specific-conductance data in well TR18–2, tidal fluctuations at Indian Bay, and water levels in well TR18–1 are shown in figure 8.

About midnight on March 28, 1984, the tide at Indian Bay peaked at nearly 5 ft, the highest tide in several years. This is reflected by the high specific conductance, 29,000 µS/cm, when the water-quality monitor was installed on March 29. As the tidal waters receded on March 29, a fairly stable diurnal pattern having tidal amplitudes that averaged about 2.8 ft was established. Specific conductance also stabilized to a fairly uniform pattern following that of the tide with an average amplitude of about 1,250 µS/cm. The range in specific conductance in well TR18–2 that was caused primarily by tidal influences was 3,500 µS/cm. This range would have been higher had the monitor been operating during the peak tidal period. Water levels in well TR18–1 remained fairly constant during the period, but small changes were caused by tides.

Flow in the Freshwater-Saltwater Zone of Transition

In the zone of transition from freshwater to saltwater, two important processes are extant. One is advection, the process by which nonreactive solutes are transported by flowing ground water at a rate equal to the average linear velocity of the water (Freeze and Cherry, 1979, p. 75). The other process is hydrodynamic disper-

sion, which causes dilution and spreading out of the solute because of mechanical mixing (mechanical dispersion) during fluid advection and because of molecular diffusion. Mechanical dispersion is caused by (1) velocity differences among water molecules in individual pore channels, (2) differences in pore sizes along the flow paths of water molecules, and (3) the tortuosity, branching, and interfingering of pore channels (Freeze and Cherry, 1979, p. 75).

Cyclic Flow of Saltwater and Interface Theory

Cooper and others (1964) postulated that, wherever a zone of diffusion exists in a coastal aquifer, the saltwater is not static but flows in a perpetual cycle from the sea floor into the zone of diffusion and back to the sea. Cooper and others further stated that the cyclic flow of saltwater may be large enough to produce head losses in the saltwater environment; this lead loss, in turn, would lessen the extent of saltwater in the aquifer. Field evidence at well TR18–2, supported by transport modeling results, indicates the applicability of Cooper's concepts to the study area.

Field data at site TR18–2 that support the concept of cyclic flow of saltwater are that (1) heads in the saltwater zone of the rock column are about 3 ft below the NGVD of 1929 and (2) water in the aquifer remains fresh to a depth of nearly 500 ft. Saltwater would have been encountered about 200 ft higher had there been static conditions in the saltwater environment. The latter point is explained in terms of interface theory.

Hubbert (1969, p. 102–104) gives the following expression for determining the altitudes of a point on an interface that separates two nonhomogeneous fluids. The interface represents a configuration of dynamic equilibrium, which means that it will adjust itself to a new position of equilibrium for each change in the state of flow of either of the fluids.

$$z=\frac{1}{g}\left(\frac{\rho_2}{\rho_2-\rho_1}\times\phi_2-\frac{\rho_1}{\rho_2-\rho_1}\times\phi_1\right) \qquad (1)$$

where z = elevation of point on interface (feet);
g = acceleration due to gravity (feet/second^2);
ρ = density of the liquid (grams/centimeter^3); and
$\phi = gh$ = potential at a point in a liquid flow system with head, h (feet), measured relative to standard datum.

Substituting the expression for ϕ into equation 1 and dividing by g yields:

$$z=\frac{\rho_2}{\rho_2-\rho_1}\times h_2-\frac{\rho_1}{\rho_2-\rho_1}\times h_1. \qquad (2)$$

Inserting values from field data collected at site TR18–2 on March 23, 1984, into equation 2 (subscript 1 data are from the 2-in. well open to the transition zone; subscript 2 data are from the 3-in. well open to the saltwater zone; NGVD of 1929) yields:

$$z=\frac{1.0210\ \text{g/mL}}{1.0210\ \text{g/mL}-1.0101\ \text{g/mL}}\times(-3.40\ \text{ft})$$

$$-\frac{1.0101\ \text{g/mL}}{1.0210\ \text{g/mL}-1.0101\ \text{g/mL}}\times(2.54\ \text{ft})$$

$$z=-554\ \text{ft}.$$

The calculated interface depth is 561 ft below land surface, within a few feet of where the saltwater environment is estimated to begin, on the basis of chemical and geophysical log data (see fig. 2). Other sets of data collected from the wells and use of heads and densities from the 1-in. freshwater well in lieu of the 2-in. transition-zone well yield virtually the same result. If the saltwater had been static ($h_2 = 0$), the first term in equation 2 would drop out, and the resulting expression would apply to the well-known Ghyben-Herzberg principle.

Simulation of Steady-State Flow with Solute-Transport Model

The U.S. Geological Survey saturated-unsaturated transport (SUTRA) model was selected to simulate the freshwater-saltwater interface in cross section along section *A–A'* (fig. 6). The section extends from the gulf inland to a point that approximately separates the aquifer discharge area from the aquifer recharge area.

The SUTRA model is a complex computer program that employs a two-dimensional, hybrid finite-element and integrated finite-difference method to approximate the equations that describe the two interdependent processes that apply in the study area: (1) fluid density-dependent saturated ground-water flow and (2) transport of a solute in the ground water. Reference is made to Voss (1984) for a complete documentation of the SUTRA model that includes physical-mathematical fundamentals, numerical methodology, simulation of field problems and comparison to analytical solutions, and setup instructions for users.

Because of the complexity of the SUTRA model, it was deemed appropriate to precede use of the SUTRA model with a U.S. Geological Survey ground-water flow model, described by Trescott (1975) and Trescott and Larson (1976), to aid in estimating input parameters.

The flow model was calibrated to quantify steady-state fluxes entering and leaving section *A–A'* (fig. 6) as follows:

1. A finite-difference grid was constructed to simulate cross-sectional flow. A uniform vertical spacing of 20 ft and a uniform horizontal spacing of 500 ft were selected. Overall grid dimensions were 740 ft deep by 8,500 ft long.
2. A sharp interface was estimated from the data in figure 4, section *D–D'*. This defined a no-flow boundary (saltwater was assumed to be static, and transmissivities on the saltwater side of the interface were equal to zero).
3. A constant-head boundary of 12 ft was imposed at A' and was assumed constant with depth.
4. A transmissivity of 50,000 ft^2/d was estimated for the upper 500 ft of aquifer, and the lower 235 ft of aquifer was estimated to have a transmissivity of 500 ft^2/d. Anisotropy (lateral to vertical ratio of hydraulic conductivity) was estimated to be 3:1.
5. Upward leakage was simulated with pumping wells in the upper layer of grid blocks. These wells can be thought of as lines of wells perpendicular to the line of section, so that flow lines are always parallel to the plane of the section.
6. Pumping rates were varied by trial and error until the heads, shown in figure 6, were simulated to within a few tenths of a foot.
7. The pumping wells were then replaced by a head-dependent sink function (Ryder, 1982, p. 32) where land surface behaves as a constant-head boundary, as described later.
8. Upward leakage rates were divided by grid-block area, so that flux per unit area could be adapted to the SUTRA model grid.

The SUTRA finite-element grid has a total length of 8,000 ft, a height of 735 ft, and uniform horizontal and vertical spacings of 266 ft and 26 ft, respectively. Thickness of the grid is 3.3 ft. There are 899 nodes (grid-line junctions) and 840 elements, or grid blocks.

Boundary conditions for the SUTRA model include a hydrostatic pressure boundary at the shoreline. The position of the boundary implies that no movement occurs in its vicinity; however, data suggest that movement is occurring inland near well TR18–2. It is assumed that the boundary is positioned sufficiently far from the mixing zone to justify its use. If data become available that indicate movement in the vicinity of the boundary, placement of the boundary farther seaward from the shoreline would be warranted. The boundary condition at the top of the model is specified flux to simulate leakage out of the aquifer with rates determined by the flow model, as discussed previously. A specified flux boundary at the landward edge of the model is used for the nodes at *A'* (fig. 6) with a total influx that approximates the total rate of upward leakage. The base of the aquifer at 735 ft below the NGVD of 1929 is simulated as a no-flow boundary. Other model input parameters are as follows:

Permeability of upper 500 ft:

$$k=\frac{K\mu}{\rho g}=3.93\times10^{-10}\,ft^2$$

Permeability of lower 235 ft: $k=3.93\times10^{-12}\,ft^2$
Anisotropy: $\frac{k_{max}}{k_{min}}=3.1$ [dimensionless]
Effective porosity: $\theta=0.15$ [dimensionless]
Freshwater density: $\rho_0=1{,}000.0\ kg/m^3$
Saltwater density: $\rho_s=1{,}021.0\ kg/m^3$
Coefficient of density change:
$\frac{\delta\rho}{\delta c}=700.00\ kg^2/(kg^3\times m^3)$
Fluid base solute concentration: $C_0=0.0$ [dimensionless]
Saltwater solute concentration: $C_s=0.0318$ [dimensionless]*
Fluid viscosity: $\mu=1.0\times10^{-3}$ kg / (m×s)
Gravitational acceleration: g = $-32.2\ ft/s^2$
Fractional upstream weighting: UP=0.0 [dimensionless]
Pressure boundary factor: GNU=0.033 ft×s
Longitudinal dispersivity: $\alpha_L=65.6$ ft
Transverse dispersivity: $\alpha_T=13.1$ ft

The initial pressures and solute concentrations were set equal to zero. The model was then run until the saltwater wedge moved inland and stabilized. This occurred after a few thousand time steps, using a time-step size of 122 days. Because of slight oscillations of computed solute concentrations (in time and space), the time-step size was reduced to 14 days and run until oscillations disappeared. Results of the steady-state model simulation are shown in figure 9.

Figure 9 shows selected salinity contours (percent saltwater salinity) superimposed on the pore-velocity field as computed by the model. The contours closely match data from observation wells. However, since there is a lack of geochemical data near the coast, there is a degree of uncertainty with respect to the actual position of the interface. Velocities computed for the centroid of each element show the saltwater moving landward, mixing with freshwater at the interface, and moving back toward the sea floor, enlarging the zone of dispersion as it returns. The highest velocity, 3.6 ft/d, occurs in the uppermost element at the shoreline. Velocities in the deeper, low-permeability zone average less than 0.01 ft/d. There is a break in the velocities and in the salinity contours at the 500-ft altitude at the contact between zones of differing permeability.

* Saltwater salinity=31.8 mg/L.

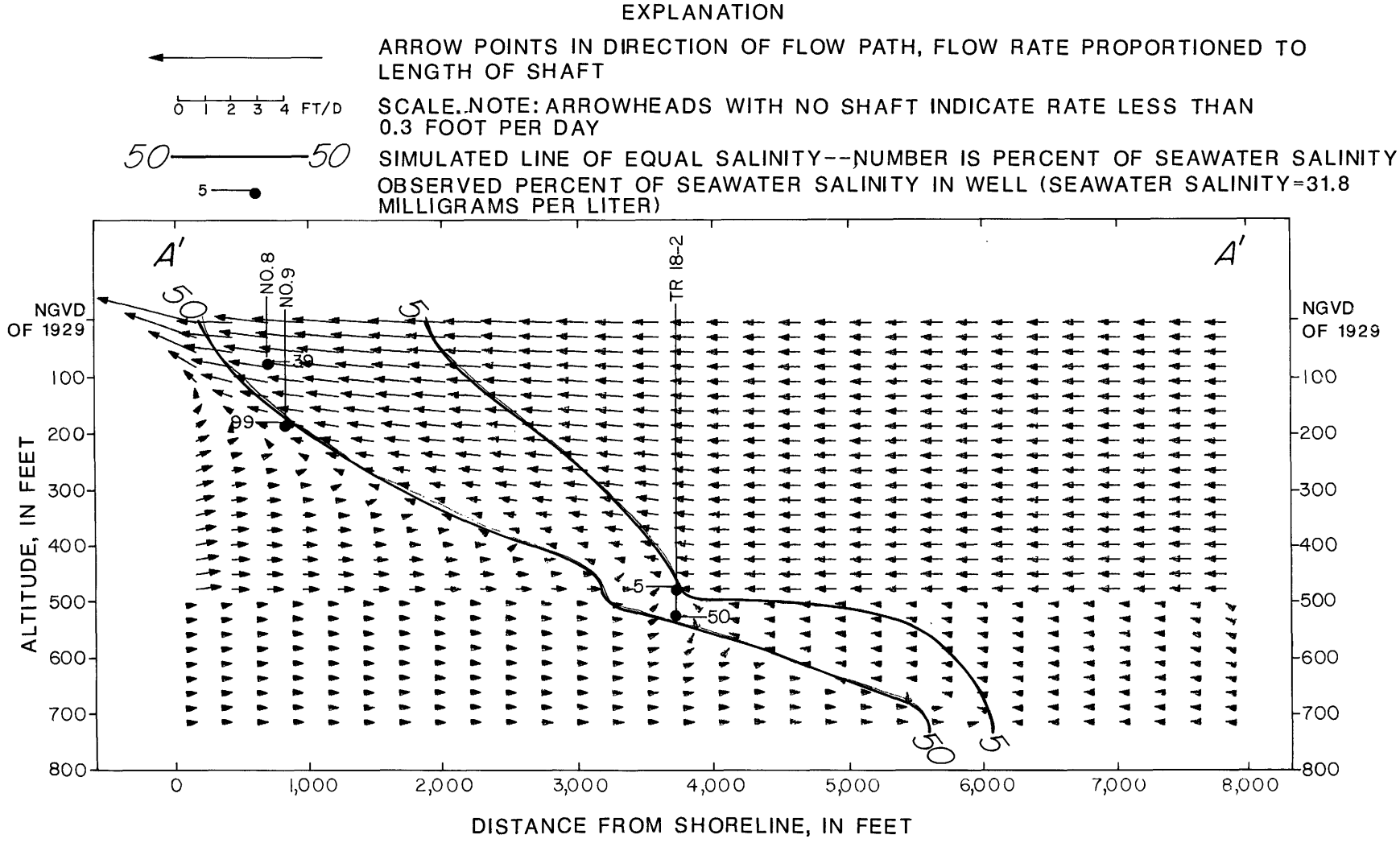

Figure 9. Modeled steady-state salinity distribution and pore-velocity field in the Upper Floridan aquifer. (See figure 6 for location of section.)

Because of the uncertanity of the values of several important input parameters, it is necessary to test the sensitivity of the model to reasonable changes in these parameters. The following parameters were changed uniformly over the modeled area: longitudinal dispersivity (±25 percent); transverse dispersivity (±50 percent); hydraulic conductivity (±100 percent); and anisotropy (changed to isotropic case). A steady-state run was made for each changed parameter while other parameters remained unchanged. The results of most of these runs are shown in figures 10 and 11. Since the flux rates used in the model simulation were derived from flow model simulations, it is also necessary to test the sensitivity of the model to changes in flux. These results can be interpreted from figure 13, which shows movement of the line of equal salinity as a result of reducing the steady-state influx. A steady-state run was also made for each reduction of influx while other parameters remained unchanged.

The 5- and 50-percent saltwater-salinity contours were chosen to show model sensitivity to the changed parameters. Contours for the ±25-percent change in longitudinal dispersivity (not shown in figs. 10 and 11) plotted almost directly on the calibration contour, thus indicating that the model was not sensitive to this range of longitudinal dispersivity. The model was sensitive to the 50-percent changes in transverse dispersivity. The contour shifted landward a few hundred feet for the reduced dispersivity and seaward a few hundred feet for the increased dispersivity. The change from anisotropic to isotropic conditions made little difference in the position of the contour. Doubling the hydraulic conductivity caused the 5-percent contour to shift landward a maximum distance of 1,700 ft and the 50-percent contour to shift landward a maximum distance of 1,300 ft. Decreasing the influx of freshwater caused the interface to move inland with the greatest changes occurring near low-concentration areas. These changes are quantified later. For nearly all sensitivity runs, the maximum differences in the positions of the contour occurred about 500 ft below NVGD where the contact between zones of differing permeability occurs.

POTENTIAL FOR SALTWATER INTRUSION

It is known that significant withdrawals of ground water in coastal lowlands in proximity to the freshwater-saltwater interface induce saltwater movement. This movement results in curtailment of pumpage or abandonment of wells because of excessively high chloride concentrations. The extent of saltwater movement due to large inland well fields and the time required for such movement to stabilize are not well known because of the complex nature of solute transport. The model developed for the Aripeka area can be used to estimate the effect of large pumping stresses located eastward of U.S. Highway 19.

Prior to the use of the SUTRA model, groundwater flow models were used to calculate flux changes caused by pumping stresses. A regional, areal flow model developed by Ryder (1982) was used to simulate a total hypothetical withdrawal rate of 60 Mgal/d eastward of U.S. Highway 19. The location and distribution of the pumpage, shown within grid blocks of the regional model in figure 12, were chosen so that the new steady-state equipotential lines near section A–A' would remain virtually parallel to the coastline and perpendicular to the line of section. This means that the assumption that flow lines are parallel to the plane of the section is still valid.

Figure 12 shows that the hypothetical pumpage caused a decline in head at A' of about 2 ft, as simulated by the regional model. The new head at A', about 10 ft, was used to define a new constant-head boundary in the cross-sectional flow model. Upward leakage rates were allowed to adjust to the new head conditions by use of a head-dependent sink function for the steady-state run. For the head-dependent sink function, land surface is specified as a constant-head boundary. The sharp-interface boundary was assumed not to have moved significantly during the short period of time (several days) that would be required for the fluxes to reach steady state. This assumption means that the observed position of the interface will not change significantly over the short period of time that the flow field equilibrates. However, over the 100-year simulation period, the freshwater flow field will decrease in size and the fluxes will consequently be redistributed. The result of not repositioning the sharp-interface boundary is that an incorrect distribution of fluxes in the flow model might minimize the landward movement of the interface in the transport model by allowing freshwater to leave the system too near the coast.

The simulated reduction in flux in the cross-sectional flow model that was caused by pumpage was about 25 percent. Specified flux in the SUTRA model was reduced by that percentage, and the model was run until changes in salinity did not occur. This required a simulation time of about 100 years. The maximum lateral and upward displacements of the 50-percent salinity contour were 450 ft and 75 ft, respectively. Pumpage in the regional areal-flow model was then doubled, with rates of 40 and 80 Mgal/d (fig. 12). This run resulted in an additional 2 ft of head decline at A' and a new head of 8 ft. Flow lines were still parallel to the plane of section A–A'. The new pumpage resulted in a 44-percent reduction of the original predevelopment flux based on the cross-sectional flow model. The SUTRA model was then run with this percentage of reduced flux; after a 100-year simulation, salinities had nearly stabilized. The maximum

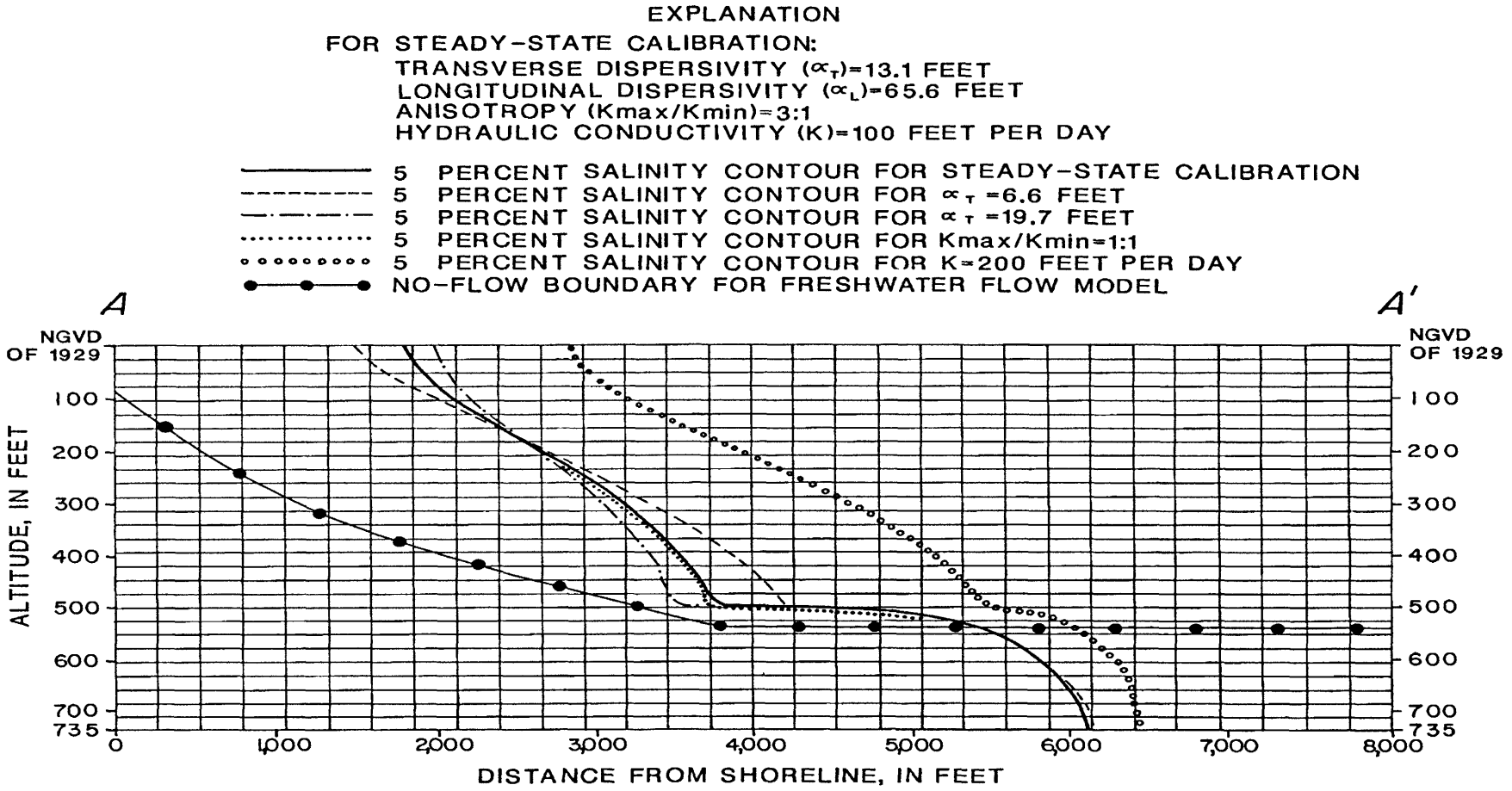

Figure 10. Positions of the 5-percent salinity contour resulting from changes in selected parameters. (See figure 6 for location of section.)

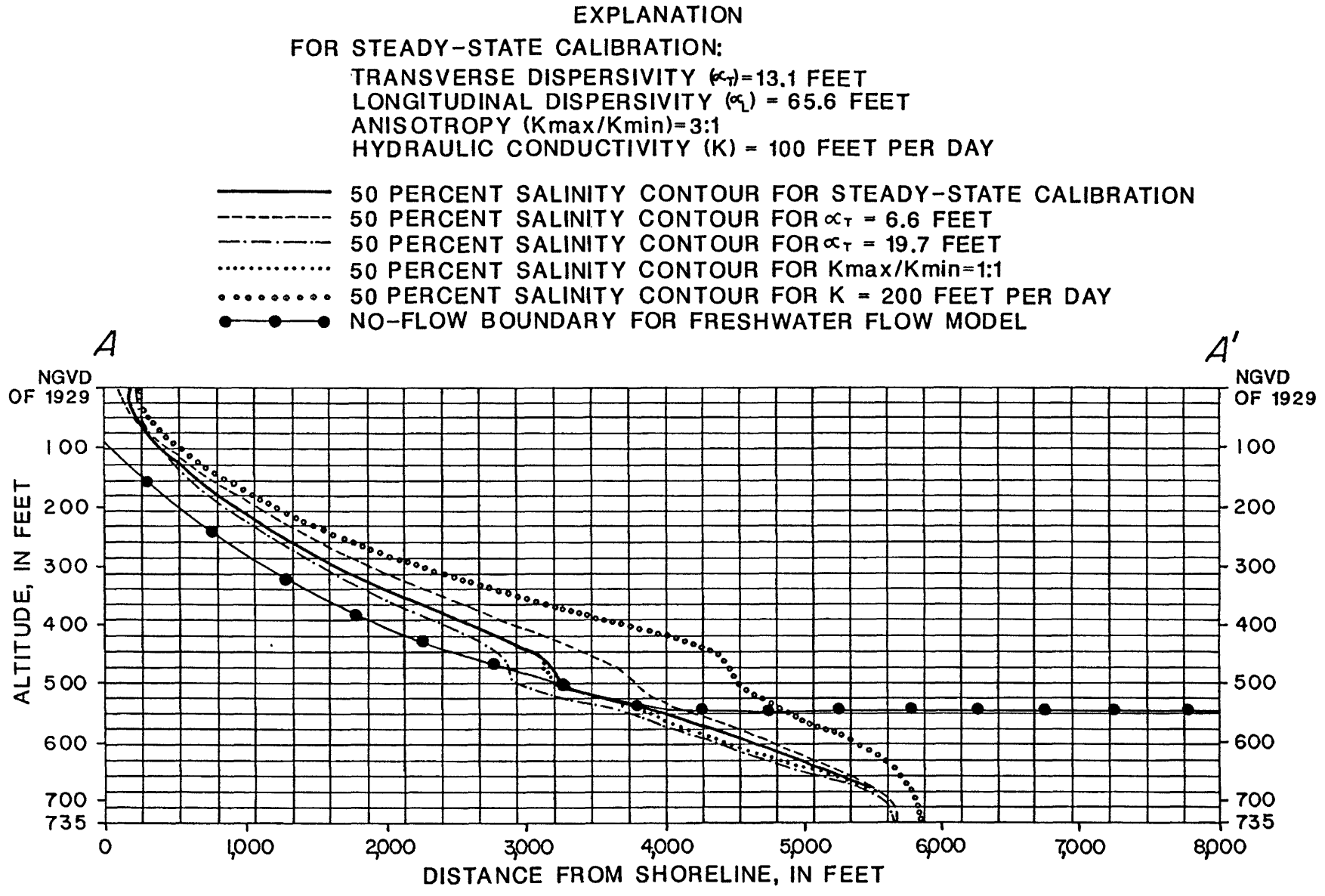

Figure 11. Positions of the 50-percent salinity contour resulting from changes in selected parameters. (See figure 6 for location of section.)

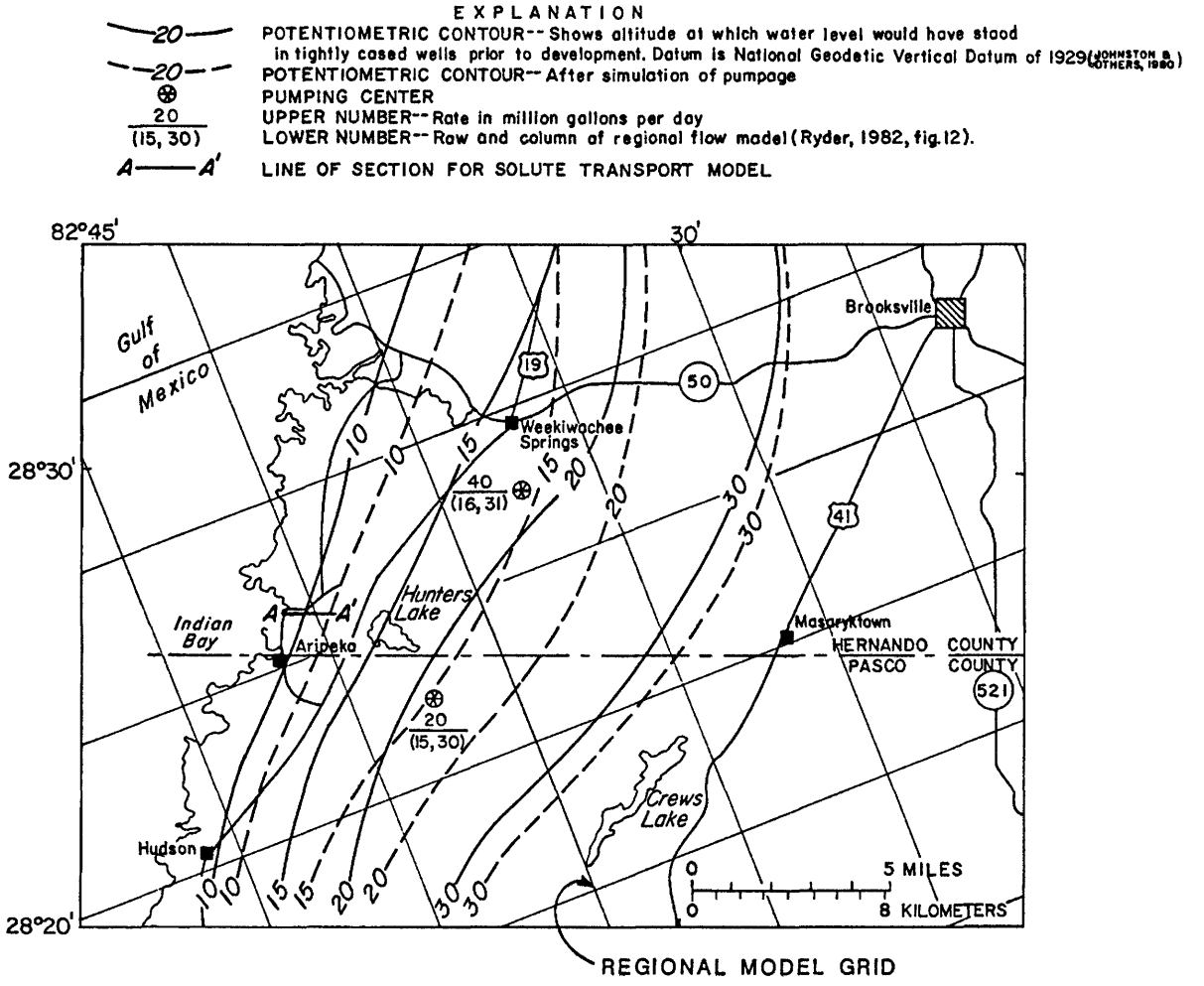

Figure 12. Potentiometric surface of the Upper Floridan aquifer prior to development and after simulation of hypothetical pumpage. (Superposed grid and regional flow model from Ryder, 1982.)

lateral and upward displacements of the 50-percent salinity contour were 900 ft and 115 ft, respectively.

The maximum lateral displacement of the 5-percent salinity contour was significantly larger than the 50-percent contour—1,200 ft compared to 900 ft (fig. 13). The same is true for maximum upward displacement—250 ft compared to 115 ft. The 5-percent contour was displaced landward fairly uniformly in the upper, more permeable zone, in contrast to the 50-percent contour. Landward displacement of both contours is relatively small in the lower, less permeable zone. Five-percent saltwater salinity is equivalent to a chloride concentration of several hundred milligrams per liter. Results of the model simulations indicate that increased pumpage east of U.S. Highway 19 could cause chloride concentrations to increase in wells west of U.S. Highway 19, depending on well depths, distance from the shoreline, and pumping rates.

SUMMARY AND CONCLUSIONS

To gain a better understanding of the phenomenon of saltwater intrusion, test well TR18–2 was drilled in coastal Hernando County to a depth of 820 feet. The following hydrogeologic data resulted:

- Except for 5 ft of permeable surficial sand, limestone and dolomite, which range in age from Eocene to Oligocene, are present to the total well depth.
- Hydraulic testing showed a permeable zone from the bottom of the casing at 447 ft to 500 ft. The estimated transmissivity of 56,000 ft^2/d probably includes effects of other permeable zones above the bottom of the casing.
- Freshwater having chloride concentrations of a few milligrams per liter was present to a depth of about 500 ft. A freshwater-saltwater transition zone occurred between 500 and 560 ft, below which saltwater was present with chloride concentrations of about 18,000 mg/L.

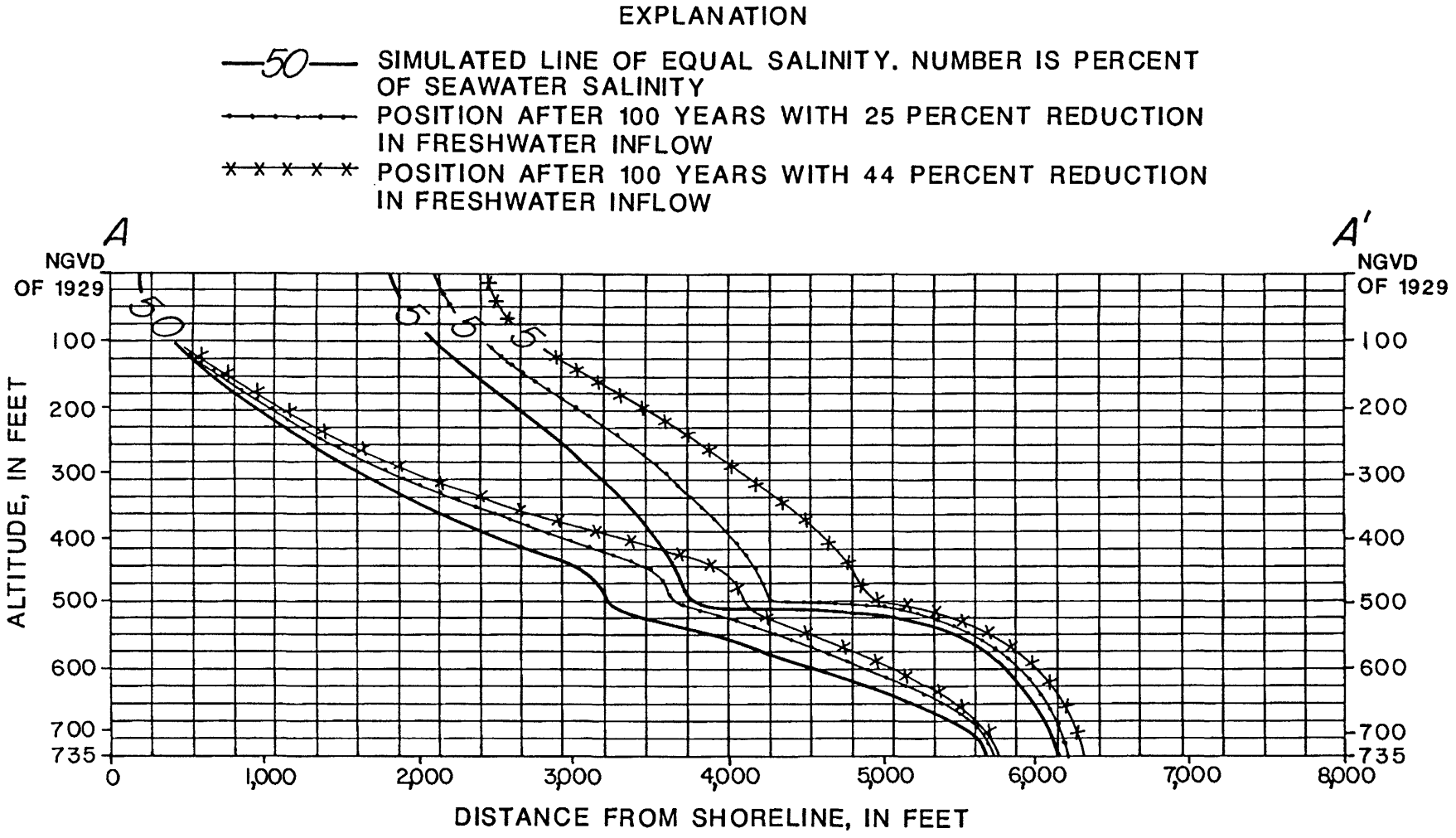

Figure 13. Simulated change in salinity with time resulting from reductions of freshwater inflow. (See figure 6 for location of section.)

- Freshwater was found at a considerably greater depth than would be expected if saltwater were static and the Ghyben-Herzberg principle were applicable. This is explained by the cyclic flow of saltwater and by interface theory.
- The freshwater-saltwater transition zone is thin and the slope of the transition zone from the shoreline inland is steep relative to coastal areas a few miles to the north and south.
- Gulf tidal fluctuations from March 29 to April 3, 1984, caused specific conductance in the transition zone to range from 25,500 to 29,000 μS/cm.

Digital models of ground-water flow and solute transport were applied in cross section to simulate 1982 steady-state flow conditions and the freshwater-saltwater transition zone. The flow model that was developed to determine flux rates for the solute transport model indicated an average upward leakage rate of about 30 in./yr. The solute-transport model closely simulated observed salinity data. A simulated pore-velocity plot shows the pattern of saltwater and freshwater flow with velocities that range from 0.01 ft/d in the basal, less permeable zone to 3.6 ft/d near the top of the aquifer at the shoreline. After the solute transport model was calibrated to 1982 conditions, hypothetical pumpages of 60 and 120 Mgal/d were simulated in an areal flow model to determine the new stress to the flow system. These stresses caused flux reductions to the solute-transport cross-sectional model of 25 and 44 percent, respectively. The latter flux reduction was applied to the solute-transport model that was run to a new quasi-steady-state condition. The maximum lateral and upward displacements of the 50-percent saltwater-salinity contour were 900 ft and 115 ft, respectively. For this condition, freshwater supply wells in the area could experience increases in chloride concentrations, depending upon distance from the shoreline, well depth, and pumping rate.

REFERENCES CITED

Brooks, H.K., 1981, Physiographic divisions of Florida: Gainesville, Florida Cooperative Extension Service, Institute of Food and Agricultural Sciences, University of Florida.

Causseaux, K.W., and Fretwell, J.D., 1982, Position of the saltwater-freshwater interface in the upper part of the Floridan aquifer, southwest Florida, 1979: U.S. Geological Survey Open-File Report 82–90, 1 sheet.

———1983, Chloride concentrations in the coastal margin of the Floridan aquifer, southwest Florida: U.S. Geological Survey Water-Resources Investigations Report 82–4070, 33 p.

Cooper, H.H., Jr., Kohout, F.A., Henry, H.R., and Glover, R.E., 1964, Sea water in coastal aquifers: U.S. Geological Survey Water-Supply Paper 1613–C, 84 p.

Freeze, R.A., and Cherry, J.A., 1979, Groundwater: New Jersey, Prentice-Hall, Inc., 604 p.

Fretwell, J.D., 1985, Water resources and effects of development in Hernando County, Florida: U.S. Geological Survey Water-Resources Investigations Report 84–4320, 83 p.

Hickey, J.J., 1982, Hydrogeology and results of injection tests at waste-injection test sites in Pinellas County, Florida: U.S. Geological Survey Water-Supply Paper 2183, 42 p.

Hubbert, M.K., 1969, The theory of ground-water motion and related papers: New York, Hafner Publishing Co., 310 p.

Johnston, R.H., Krause, R.E., Meyer, F.W., Ryder, P.D., Tibbals, C.H., and Hunn, J.D., 1980, Estimated potentiometric surface for the Tertiary limestone aquifer system, Southeastern United States, prior to development: U.S. Geological Survey Open-File Report 80–406, 1 sheet.

Miller, J.A., 1986, Hydrogeologic framework of the Floridan aquifer system in Florida and in parts of Georgia, South Carolina, and Alabama: U.S. Geological Survey Professional Paper 1403–B, 91 p.

Mills, L.R., and Ryder, P.D., 1977, Saltwater intrusion in the Floridan aquifer, coastal Citrus and Hernando Counties, Florida, 1975: U.S. Geological Survey Water-Resources Investigations Report 77–100, 1 sheet.

Palmer, C.E., and Bone, L.P., 1977, Some aspects of rainfall deficits in west-central Florida, 1961–1976: Southwest Florida Water Management District Hydrometeorological Report No. 1, 19 p.

Reichenbaugh, R.C., 1972, Sea-water intrusion in the upper part of the Floridan aquifer in coastal Pasco County, Florida, 1969: Florida Bureau of Geology Map Series 47.

Ryder, P.D., 1978, Model evaluation of the hydrogeology of the Cypress Creek well field in west-central Florida: U.S. Geological Survey Water-Resources Investigations Report 78–79, 68 p.

———1982, Digital model of predevelopment flow in the Tertiary limestone (Floridan) aquifer system in west-central Florida: U.S. Geological Survey Water-Resources Investigations Report 81–54, 61 p.

Steinkampf, W.C., 1982, Origins and distribution of saline ground waters in the Floridan aquifer in coastal southwest Florida: U.S. Geological Survey Water-Resources Investigations Report 82–4052, 34 p.

Trescott, P.C., 1975, Documentation of finite-difference model for simulation of three-dimensional ground-water flow: U.S. Geological Survey Open-File Report 75–438, 103 p.

Trescott, P.C., and Larson, S.P., 1976, Supplement to Open-File Report 75–438, Documentation of finite-difference model for simulation of three-dimensional ground-water flow: U.S. Geological Survey Open-File Report 76–591, 21 p.

U.S. Army Corps of Engineers, 1980, Water resources management study, Four River Basins Project, Florida: Department of the Army, Jacksonville District, U.S. Army Corps of Engineers, 116 p.

Voss, C.I., 1984, SUTRA; Saturated-Unsaturated TRAnsport; A finite-element simulation model for saturated- unsaturated, fluid-density-dependent ground-water flow with energy transport or chemically-reactive single-species solute transport: U.S. Geological Survey Water-Resources Investigations Report 84–4369, 409 p.

Wilson, W.E., 1982, Estimated effects of projected groundwater withdrawals on movement of the saltwater front in the Floridan aquifer, 1976–2000, west-central Florida: U.S. Geological Survey Water-Supply Paper 2189, 24 p.

Base Flow as an Indicator of Drought Occurrence

By Ronald L. Hanson

Abstract

Droughts are one of the most costly hydrologic hazards in the United States. They are generally slow in developing, frequently occur over a long period of time, and can affect a large area. In general, when the water content in streams, reservoirs, aquifers, lakes, or soils falls below the long-term average, a pending or potential hydrologic drought may exist. The severity of a hydrologic drought is not always obvious until these water supplies are seriously depleted. Base flow, which represents the ground-water discharge into a stream after all surface runoff has occurred following a storm event, can be an indicator of ground-water conditions in a river basin.

This study uses the seasonal base-flow characteristics of the Blue River, a 203 square mile unregulated watershed in south-central Oklahoma, to illustrate how a hydrologic drought can be evaluated. Base flow is selected from historic streamflow hydrographs and is used to define the frequency of occurrence of base flow for each month during the period January through September. Base-flow recession curves also are defined for this 9-month period and are used to project assured base flow from the winter season through the subsequent spring and summer months. Finally, the magnitude of monthly increases in base flow is evaluated to describe the probability that the projected assured base flow will be exceeded. Once these base-flow relations are defined for selected index streamflow stations throughout the State, they can be used to describe the severity of a hydrologic drought for the entire State.

INTRODUCTION

Droughts are one of the most costly hydrologic hazards in the United States. Compared to a flood, which is the other common hydrologic hazard in the Nation, droughts occur over a larger area and persist for a longer duration, thus usually affecting a greater number of people.

Hydrologic droughts do not occur suddenly but develop gradually over several months. Virtually all areas of the United States are vulnerable to droughts and their impact on man is dependent largely on the availability of surface reservoirs or fresh ground-water aquifers to provide water during prolonged periods of deficient precipitation. Figure 1 shows that the duration of a drought, where no alternate source of water supply exists, typically ranges from several years in the Western States to only a few months in the eastern part of the Nation. Droughts occur with some severity almost every year in parts of the Central United States.

The regional differences in drought characteristics across the United States are caused by various physical processes that affect precipitation, which include orographic lifting of air over mountain ranges, lifting by frontal activity, localized temperature differences and temperature convergence, and dynamic lifting of air. Of these processes, dynamic lifting, which is associated with surface cyclones and a broad belt of upper level westerly winds, is considered the most significant process that affects meteorological events in the United States (Perry, 1980).

Even though a hydrologic drought may be widespread, many people may not be aware of its severity or extent. Some people may not be affected either because they either live in an arid region where they have adapted to limited water supplies or because they live in areas where stored water supplies remain adequate to meet their needs during a drought.

The purpose of this study is to demonstrate how historic base flow, determined from streamflow hydrographs, can be used to (1) develop a drought index that measures the status of water availability in a basin in late winter and early spring, (2) project assured base flow to the subsequent summer months, and (3) provide estimates of spring and summer base flow in excess of the assured base flow for selected probability levels.

This report discusses some of the more common methods that are presently used to describe a drought. The report outlines the criteria used in selecting an appropriate drought-index stream, describes the technique for measuring the severity of an existing or potential drought on the basis of the base-flow characteristics of the drought-index stream, and describes how projections of subsequent drought conditions can be made on the basis of existing base-flow conditions.

ACKNOWLEDGMENTS

This study was supported by cooperative funding between the Oklahoma Water Resources Board and the

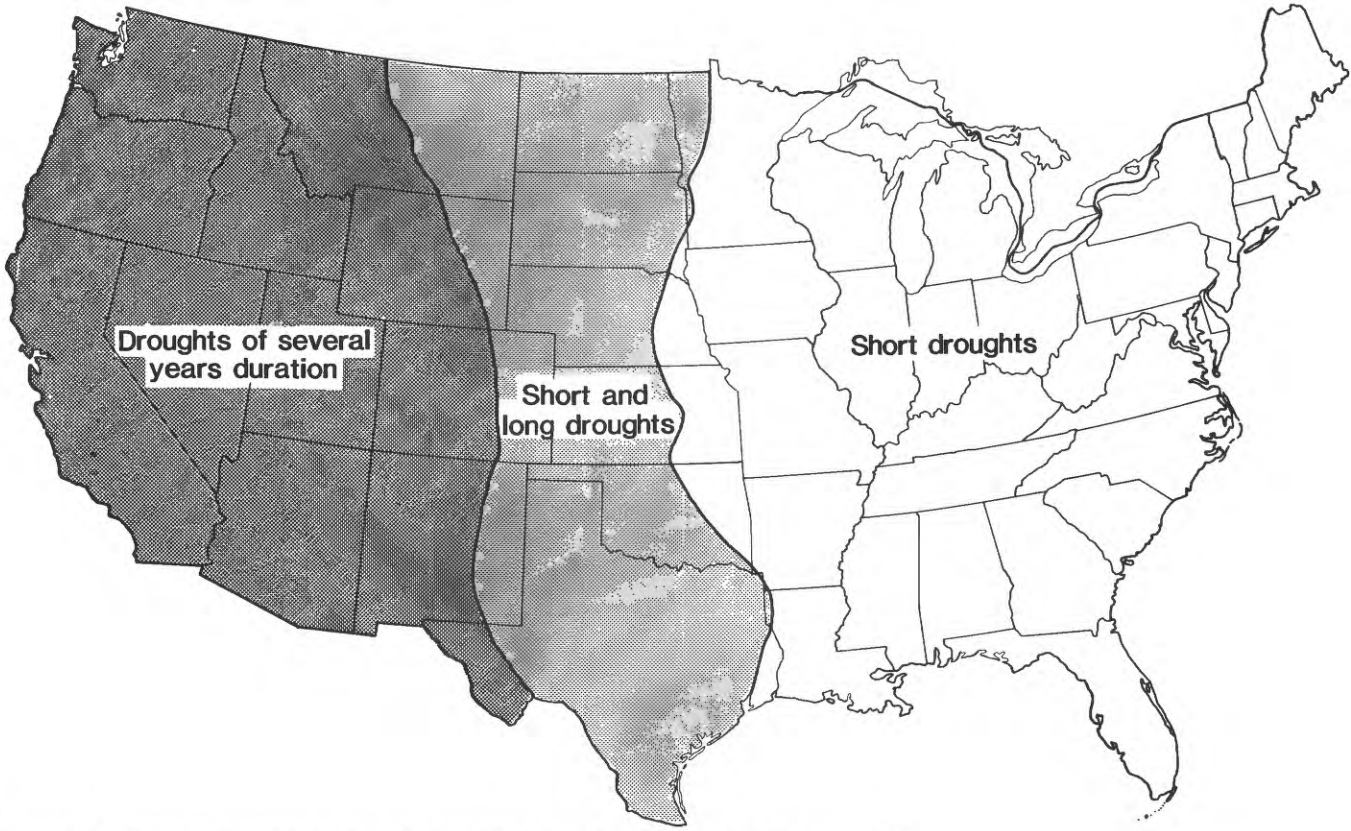

Figure 1. Areas vulnerable to drought (modified from U.S. Geological Survey, 1970).

U.S. Geological Survey, Oklahoma City, Oklahoma. The author wishes to thank J.A. Wood, Harold Springer, and James Schuelein of the Oklahoma Water Resources Board for their reviews of this report.

DEFINITIONS OF DROUGHTS

Droughts do not have the same meaning or significance to all people. No generally accepted definition is adequate nor is one practical, because a drought is the result of many different factors. In general, however, "drought is a condition of moisture deficit sufficient to have an adverse effect on vegetation, animals, and man over a sizeable area" (Warrick, 1975). Three common definitions are:

1. Meteorological drought: "A period of abnormally dry weather sufficiently prolonged for the lack of water to cause serious hydrologic imbalance in the affected area" (Huschke, 1959).
2. Agricultural drought: "A climatic excursion involving a shortage of precipitation sufficient to adversely affect crop production or range production" (Rosenberg, 1979).
3. Hydrologic drought: "A period of below average water content in streams, reservoirs, ground-water aquifers, lakes and soils" (Yevjevich and others, 1977).

CHARACTERISTICS OF HISTORIC DROUGHTS

The frequency, severity, and duration of historic droughts have been studied by several investigators. Perry (1980) related well-documented solar activity to annual precipitation for selected stations in the Central United States having more than 60 years of record and showed 11- and 22-year cycles that are nearly in phase with the solar activity cycles.

Mitchell and others (1978) used tree-ring records in the Western United States dating back to about 1600 A.D. to develop a relation between drought for a large number of areas and the 22-year cycle of sunspot minimums. Weakly (1943) examined 400-year tree-ring records for western Nebraska and found the average recurrence interval of severe droughts was 20.6 years and the average duration was 12.8 years.

A spectral density analysis of tree-ring widths dating back to 1640 A.D. in the northern Great Plains by

Meko (1982) indicates a significant 55-year cycle of severe droughts, with the most significant drought probably occurring in the late 1750's. His study also shows that droughts more severe than the well-known and widespread 1930's drought occurred in the northern Great Plains in the 1820's, the 1860's, and the 1950's.

DROUGHT INDEXES

Numerous drought indexes have been developed to provide farmers, water managers, meteorologists, and hydrologists a measure of the severity of a drought. The most widely used index is the Palmer Drought Severity Index (Palmer, 1965), which provides a quantitative assessment of periods of prolonged meteorological anomalies. This index includes antecedent precipitation and the duration and magnitude of the abnormal moisture deficiency (or excess).

Another widely used drought index is the Crop Moisture Index developed by the National Weather Service (1977), which provides information about prevailing soil-moisture conditions. The Crop Moisture Index is based on information from the Palmer Drought Severity Index and measures current changes in soil moisture over a large region.

The U.S. Geological Survey, Water Resources Division, publishes a monthly report entitled "National Water Conditions" that describes the monthly status of surface water in the Nation's principal rivers and reservoirs and the status of ground-water levels in some of the Nation's representative aquifers. Selected long-term index stations in each State are used to compare existing streamflows, reservoir storage, and ground-water levels with normal and extreme recorded values.

Numerous statewide studies of the magnitude and frequency of annual low flows have been made to provide information about the likelihood of occurrence of drought-related low flows (Singh and Stall, 1973; Huntzinger, 1978).

All of the above techniques have significant limitations for adequately describing the status of an existing or pending drought, one of the major limitations being that they do not always consider the status of available ground water. This is particularly true if the period of record does not include a prolonged severe drought. In general, these techniques measure only the deficiency in shallow soil moisture and antecedent precipitation of recent weeks and do not reflect availability of the deeper ground-water supplies that result from the previous months or year of precipitation.

Not only is it important to know the status of an existing drought, it is important to know the probability of drought conditions prevailing for several months. Few existing drought studies provide a method of making reliable predictions several months in advance of the potential for a severe hydrologic drought. Hirsch (1981) describes a stochastic technique for predicting several months into the future the likelihood of the occurrence of various streamflow rates. Riggs and Hanson (1969) developed base flow recession curves to project minimum assured flows several months into the future for the condition of no significant rainfall during the projection period.

The base-flow component of streamflow in unregulated basins is generally a good indicator of water availability in the basin. Base flow is essentially discharge in the stream derived from ground-water sources. For some regions, late winter and early spring base flow includes discharge from ground water stored during the preceding summer and fall season.

CRITERIA FOR SELECTING DROUGHT-INDEX STREAMS

Three criteria must be considered in selecting an appropriate streamflow gaging station to be used as a drought-index stream. First, man's activities in the basin should not appreciably affect the natural flow characteristics in the stream. Thus, no significant upstream regulation, diversions, large ground-water withdrawals, or other manmade alterations that may affect the low-flow regime should exist. Second, perennial flow should exist for most years so that the magnitude and recession rates of base flows occurring during the winter, spring, and summer can be evaluated. Finally, at least 15 years of continuous streamflow record should be available at the streamflow-gaging site to provide sufficient record for making reliable estimates of the frequency of occurrence of base flow for each month during the winter, spring, and summer. Generally, a 15-year period of record will involve at least one significant drought for inclusion in the analysis.

The streamflow-gaging station Blue River at Milburn (station number 07332400) in south-central Oklahoma (fig. 2) is used in this report to illustrate the technique for applying base flow to evaluate the drought characteristics of that region of the State. The Milburn station was established October 1, 1965, and the subsequent 16 water years of streamflow record (1966–81) were used to develop the relations describing the base-flow characteristics of the stream. Drainage area at this site is 203 mi^2, flow is sustained throughout the year by numerous spring flows in the basin, and no significant regulation or withdrawals from the river occur upstream from the gaging station. Minimum daily flow measured during the period of record was 15 ft^3/s during August 22, 24, 25, and September 1, 1980.

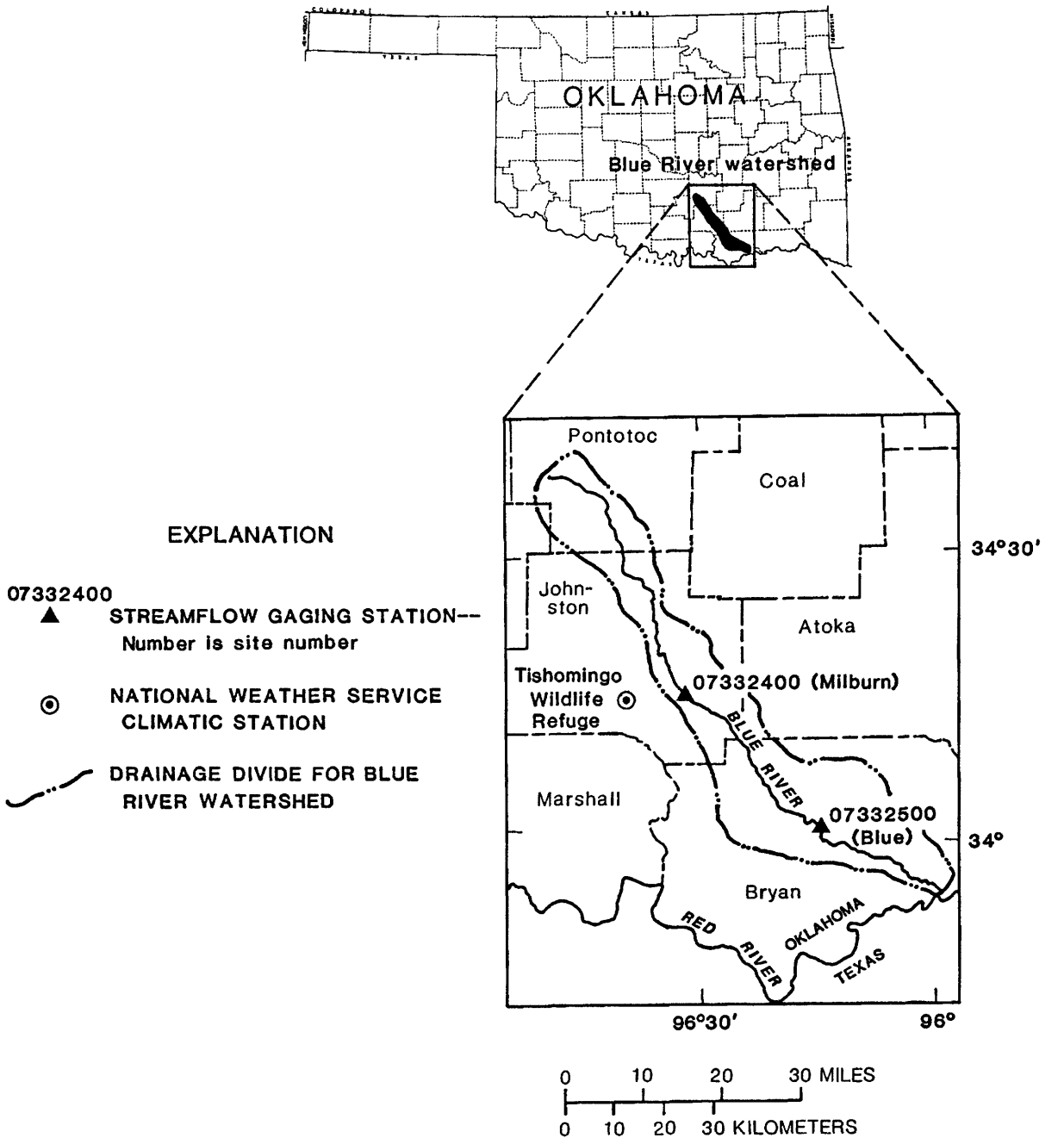

Figure 2. Location of Blue River watershed, Blue River gaging stations, and National Weather Service climatic station at Tishomingo Wildlife Refuge, Oklahoma.

OCCURRENCE OF SIGNIFICANT DROUGHTS DURING THE STREAMFLOW RECORD

The reliability of the base-flow relations derived for evaluating the severity of an existing or potential drought are dependent on the length of record available for analysis and on the severity of droughts during the period of record. A continuous streamflow record of 15 years or more will usually include at least one significant drought and is generally of sufficient duration to define adequately the base-flow characteristics of the stream. However, this period of record may not be sufficient to include the more severe droughts if they do, in fact, tend to occur in approximately 22-year cycles as suggested by Mitchell and others (1978) and Weakly (1943).

Thus, the 16-year streamflow record at the Milburn station was compared with the longer streamflow record of 45 years (1937–81) at a downstream gage, Blue River near Blue, Oklahoma (station number 07332500),

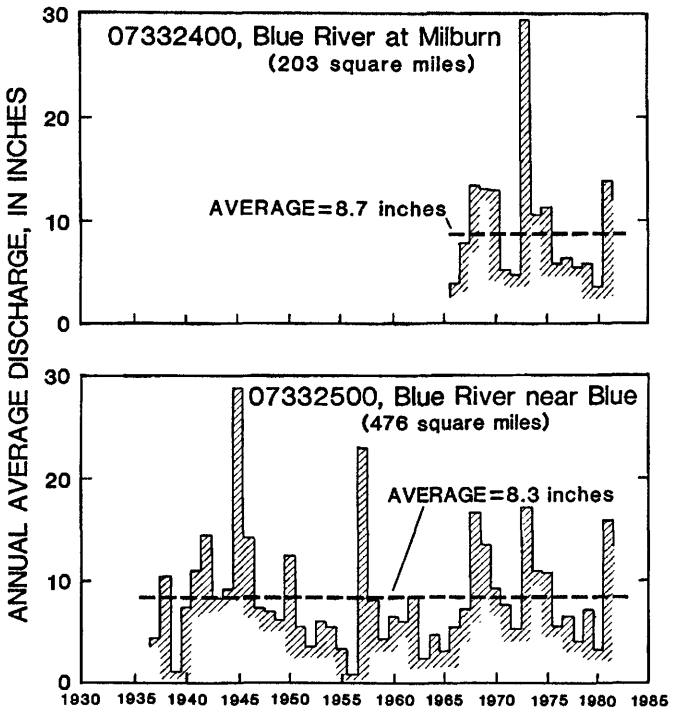

Figure 3. Calendar year average discharges for Blue River at Milburn, Oklahoma, gaging station (1966–81) and Blue River near Blue, Oklahoma, gaging station (1937–81).

shown in figure 2. (This long-term station was not used to develop the base-flow relations described in this report because low flows are affected by some regulation between the Milburn and Blue stations.) The annual discharges at the Blue River near Blue gaging station correlate closely with those for the Blue River at Milburn for most years during the common period of record 1966–81. The graphs of annual average (calendar year) discharge for both the Milburn and Blue stations for their respective periods of record (fig. 3) indicate that three relatively dry years occurred during the 16-year common period of record (1966–81)—1966, 1978, and in particular, 1980. The graph for the Blue River near Blue also indicates that annual discharge, and possibly seasonal base flows, were lower in 1939 and 1956 than were recorded during the subsequent common period of record.

A further indication of the severity of hydrologic droughts that occurred during the period of streamflow record can be made by evaluating a longer period of historic climatic droughts observed in the area of study. Figure 4 shows a graph of annual precipitation for 79 years of record (1903–81) at the National Weather Service climatic station at the Tishomingo Wildlife Refuge located 12 miles west of the Milburn gage. This graph indicates that the 45-year period (1937–81) that is common to the streamflow record at the Blue River near Blue station includes the relatively significant dry years of the late 1930's, mid-1950's, mid-1960's, and the late 1970's. Only the prolonged period of deficient precipitation during 1909–12 was dryer than the 45-year period of streamflow recorded at the Blue gaging station. Also, the graph suggests that the prolonged period of significantly below-normal precipitation during 1976–78 and 1980 may compare with the prominent drought of the late 1930's.

This overview of significant droughts during the past 79 years suggests that at least one drought—that of 1980—during the 16-year study period may be representative of the severe drought that occurred during the 1930's. Documentation of the occurrence and severity of droughts prior to the 1900's in the Central and Western United States is limited because of sparse streamflow and precipitation data prior to the turn of the century. However, the analysis by Meko (1982) of tree-ring data in the northern Great Plains over the past 300 years indicates that hydrologic records collected since the early 1900's may not reflect droughts of the severity of those of the 1750's, 1820's, and 1860's.

CHARACTERISTICS OF BASE FLOW

One of the objectives of this study is to use the status of known winter or early spring moisture conditions in a watershed as a basis for projecting subsequent summer moisture conditions. Because base flow of an unregulated stream represents inflow to the stream from the ground-water system, this flow is an indicator of the status of ground water in the watershed. Total flow in the stream following prolonged dry periods, particularly during the summer, generally represents base-flow conditions.

The source of base flow usually is an unconfined aquifer where the stream channel partially penetrates the aquifer. In many instances, however, the stream channel lies above the principal aquifer and base flow is derived from perched ground-water sources or slow (delayed) seepage from shallow soil moisture that has been recharged by precipitation during a previous wet period. If the quantity of water stored in the perched zones is limited, and no significant rainfall occurs during the late spring and summer season, flow in the stream can be expected to cease. The use of this type of stream as an index for evaluating drought conditions should be avoided, particularly if base flow is depleted early in the summer.

Daily flow-duration hydrographs, which define the frequency characteristics of daily flows, provide an indication of the seasonal variation in minimum flows and may approximate base-flow conditions for some periods during the year. The flow-duration hydrographs for the Blue River at Milburn, Oklahoma, for water years

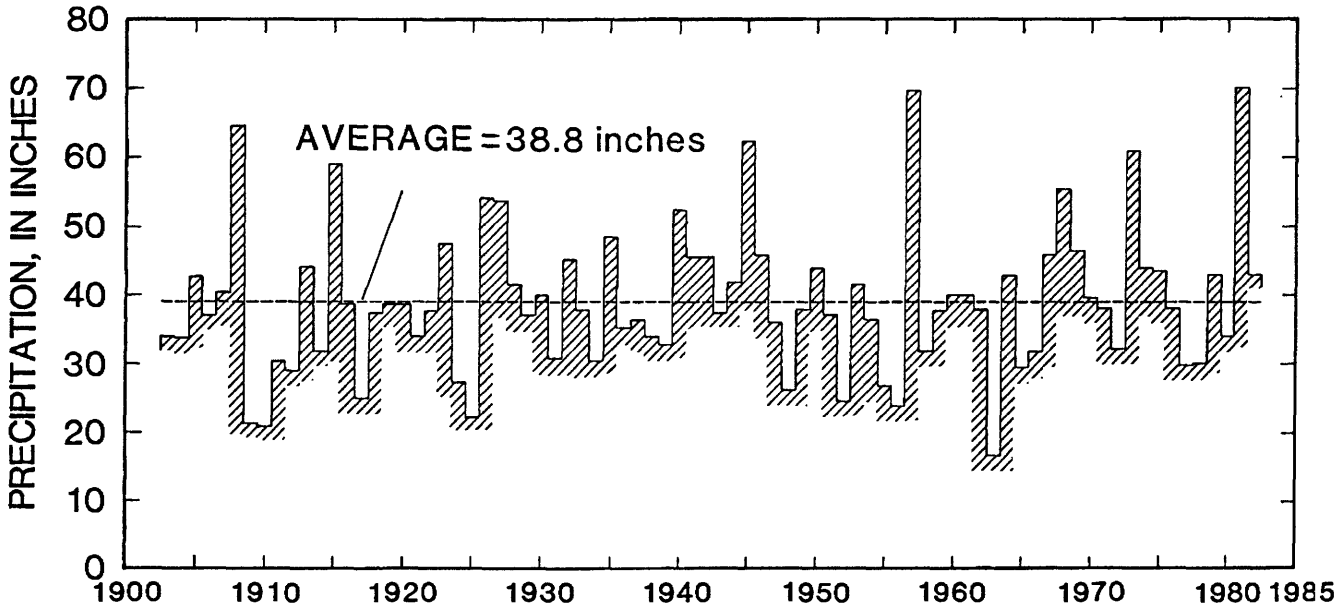

Figure 4. Annual calendar year precipitation for National Weather Service climatic station at Tishomingo Wildlife Refuge, Oklahoma, 1903–81.

1970–78 (fig. 5) give the daily discharge for three percentage levels of exceedance—20, 50, and 100 percent. The lower hydrograph, which defines daily flows that were exceeded 100 percent of the time, reflects the low-flow characteristics of the stream. This hydrograph shows that the minimum flow observed on October 1 during 1970–78 was 29 ft^3/s and that this value was equaled or exceeded 100 percent of the time for all October 1's during this 9-year period. The smooth curve drawn through the troughs of this hydrograph approximates the minimum low flows of record but may not always reflect base flow, particularly during the spring and early summer months when streamflow may never recede to base-flow levels.

Work by several investigators (Barnes, 1939; Riggs, 1963; Rorabaugh, 1964) has shown that when the streamflow recession following a runoff event approaches a straight line on a semilog plot, the flow is considered to be derived entirely from ground-water discharge. An idealized streamflow hydrograph with straight-line base-flow recession segments delineated on the lower end of selected hydrograph recessions is shown in figure 6. In each instance, the hydrograph is considered to represent base flow only after surface runoff, bank storage, and channel storage following a storm event have been depleted and the recession approximates linearity.

The first step in defining a base-flow recession curve was to select 10-day linear base-flow recession segments from all appropriate hydrograph recessions observed during the 16-year period of record. A logarithmic plot of the beginning-day base-flow value versus the base-flow value 10 days later was then prepared for each month from January through September as described by Riggs (1963). Examples of these 10-day base-flow relations are illustrated in figure 7 for January and July for the Blue River at Milburn station. These relations were determined for each month and then used to construct—by 10-day increments—the family of continuous base-flow recession curves for the 9-month period, January through September, as shown in figure 8.

For example, the recession curve in figure 8 that begins on January 1 with 150 ft^3/s was drawn by first entering at 150 ft^3/s on the abscissa axis of the 10-day base-flow relations in figure 7, moving up to the January relation, and across to the ordinate axis to obtain the January 11 base flow of 125 ft^3/s. Then the January 11 value of 125 ft^3/s was entered on the abscissa axis to obtain the January 21 value of 106 ft^3/s. Similarly, the January 21 value of 106 ft^3/s was entered on the abscissa axis to obtain the January 31 value of 93 ft^3/s, thus defining the recession curve for January. Continuation of this curve through February and all subsequent months to September 30 was determined in a similar manner by using the appropriate 10-day base-flow relation for each month.

Because each of these 9-month base-flow recession curves is derived from linear segments, which represent periods of no rainfall and thus represent only ground-water discharge to the stream, the curves are considered to approximate the minimum flow that would occur throughout the 9-month period. These curves are, therefore, referred to in this report as "assured" base-flow recession curves. The lower dashed portions of these

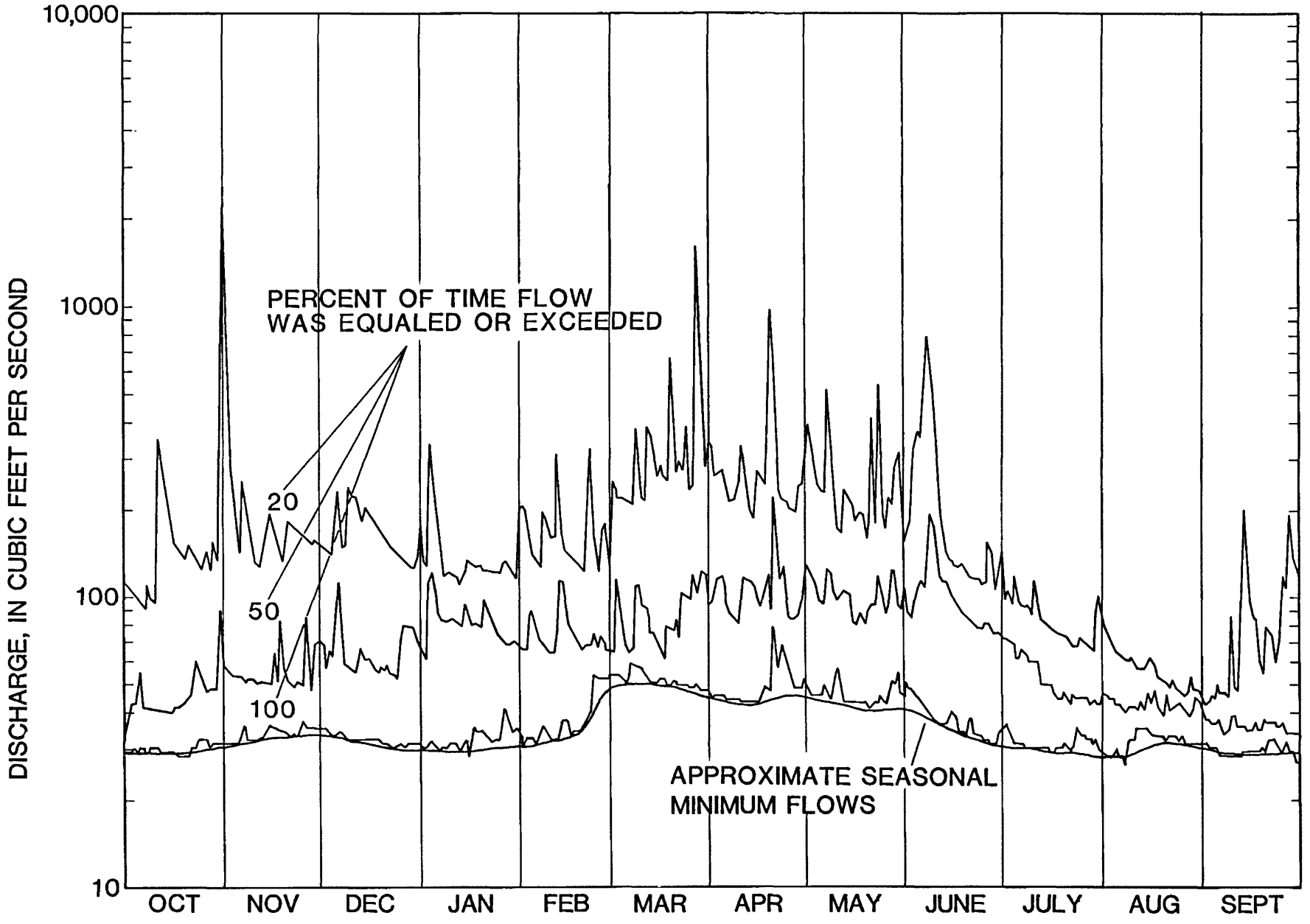

Figure 5. Daily flow-duration hydrographs for Blue River at Milburn, Oklahoma, for 20, 50, and 100 percent exceedance levels and approximate seasonal minimum flows (1970–78).

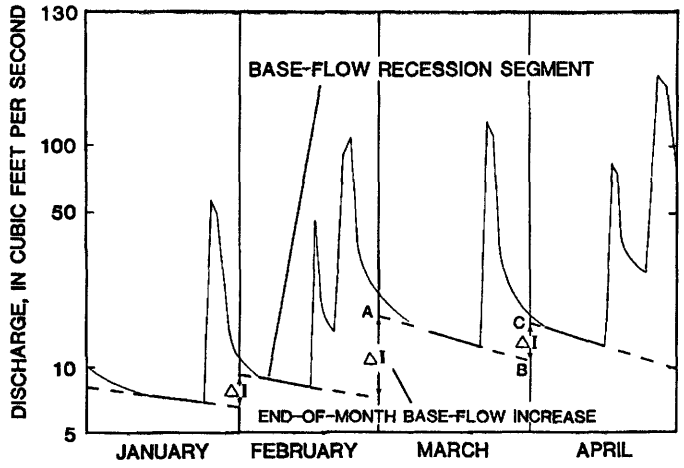

Figure 6. Typical streamflow hydrograph showing base-flow recession segments (solid lines), estimated assured base flow projected from the recession segments (dashed lines), and end-of-month base-flow increase (ΔI). A, beginning-month base flow; B, end-of-month assured base flow; and C, end-of-month increase in base flow for March.

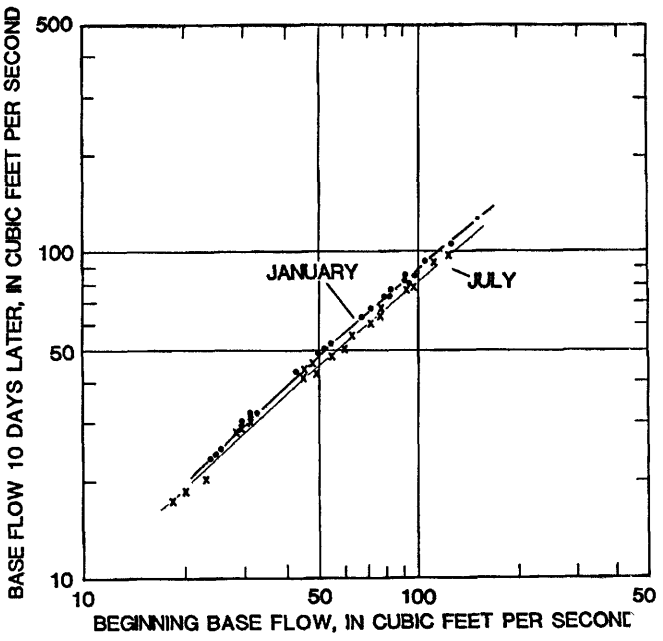

Figure 7. Relation between beginning base flow and base flow 10 days later for January and July, Blue River at Milburn Oklahoma, 1966–81.

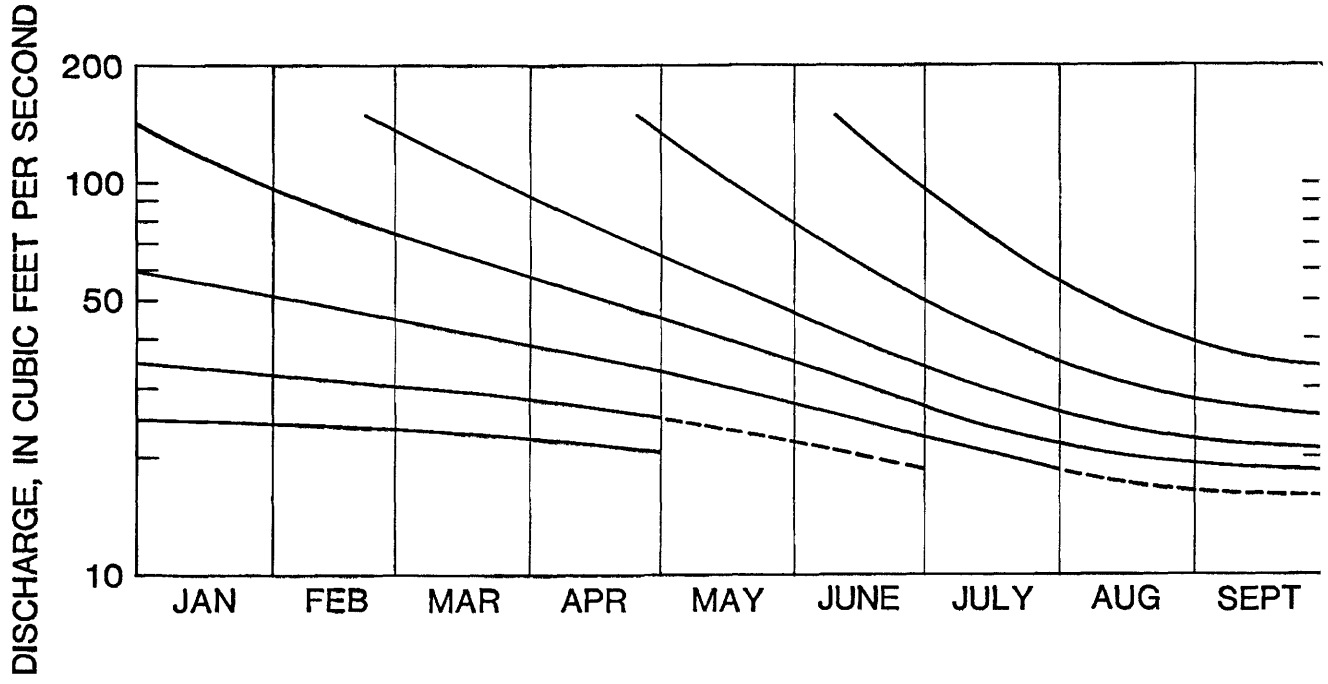

Figure 8. Family of base-flow recession curves, Blue River at Milburn, Oklahoma. Dashed lines are estimated on the basis of downward projections of relation between beginning base flow and base flow 10 days later.

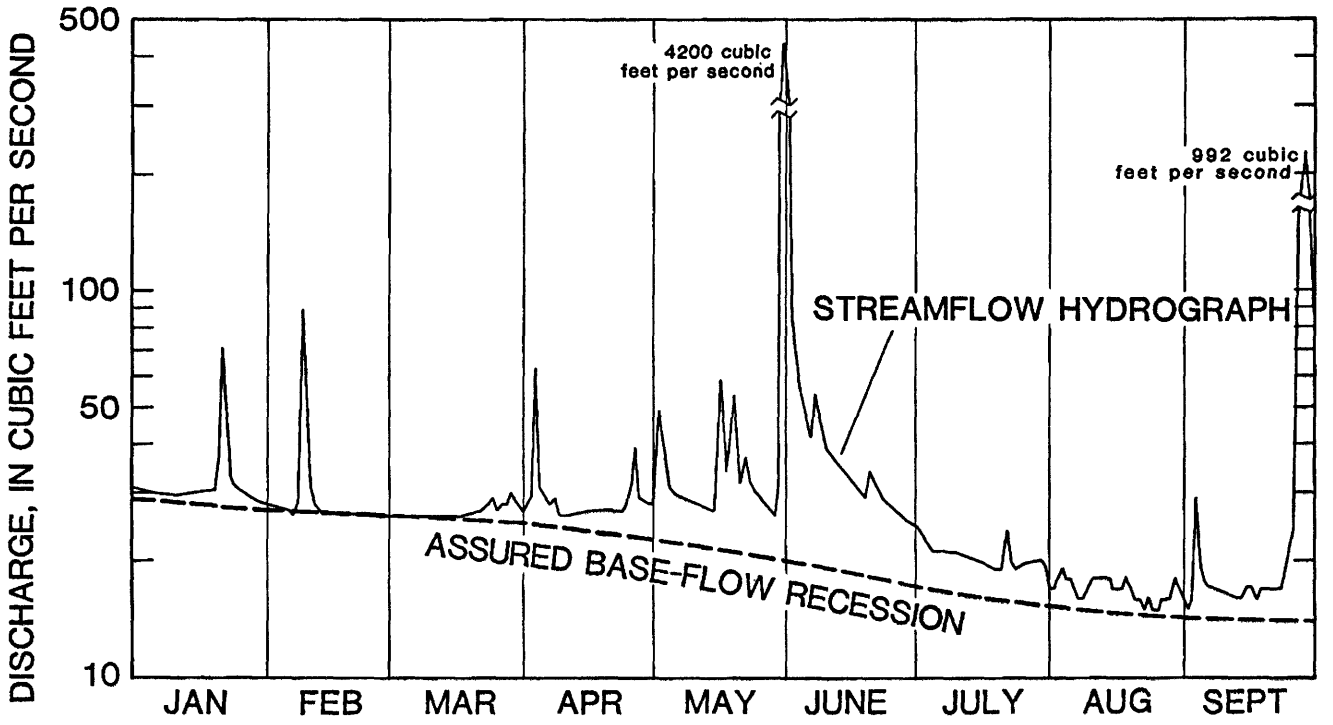

Figure 9. Comparison of assured base flow with streamflow hydrograph for period of record minimum flow, January to September 1980, Blue River at Milburn, Oklahoma.

assured curves indicate that no base-flow data have been recorded at these levels for the periods shown. Estimates for these periods are based on downward projections of the appropriate 10-day relations for each month.

One may expect that these base-flow recession curves, derived from 10-day linear segments, also would be linear throughout the 9-month period. However, several hydrologic factors affect the shape of these curves. First, some of the base-flow segments may include discharge into the stream from delayed or prolonged bank and channel storage that will define a slightly steeper recession rate than the rate defined solely from ground-water discharge. In fact, the selection of representative linear base-flow segments from the streamflow hydrograph can be a particular problem during the spring because of intermittent rainfall limiting the duration of the base-flow recession. The slope of the recession curve will also be relatively steep, as shallow perched ground water is depleted. In addition, summer recession slopes are typically steeper than winter slopes because of the increased evapotranspiration by riparian vegetation during the summer. The effect of evapotranspiration on the recession hydrograph is shown in figure 7 by the displacement of the July base-flow relation to the right of the January relation. The effect of evapotranspiration also is shown in figure 8 by steeper recession slopes during the summer than during the winter, for a given discharge level.

Finally, these recession curves show that base flow for the Blue River does not drop below about 15 ft^3/s and remains relatively sustained during the winter and summer months. This reflects a large ground-water supply from the Arbuckle aquifer, which underlies the Blue River watershed (Fairchild and others, 1982).

It is important to emphasize that these base-flow recession curves are a composite of many 10-day base-flow segments—some of which are influenced by runoff from delayed storage or depletion from evapotranspiration—and that the curves are only an approximation of ground-water discharge. Their use, however, in defining assured base flow is appropriate as long as these constraints are recognized and the curves are used, in a consistent manner, to make projections of assured base flow only for the period in which the curves have been defined.

A measure of the reliability of these derived recession curves for making projections of assured base flow for several months into the future is difficult in regions where rainfall commonly interrupts the streamflow recession during the spring and summer months. An indication of their reliability can be shown, however, by comparing the recession curves with a period of record low streamflow. Figure 9 shows this comparison for the streamflow hydrograph of the Blue River at Milburn for the 1980 water year, which was a year of record minimum streamflows (33 percent of normal). The assured base

flow lies below the observed hydrograph throughout the entire 9-month recession period and is considered to approximate that flow which would occur with little or no rainfall during the 9-month period.

FREQUENCY OF OCCURRENCE OF BEGINNING-MONTH BASE FLOW

One of the principal objectives of this study is to establish ground-water conditions for any given month expressed in terms of base-flow levels. This information is particularly important in the winter and early spring (January through May) prior to the subsequent summer months, when the demand for water becomes high. This was accomplished by defining the frequency of occurrence of base flow at the beginning of each month from January through May.

Beginning-month base-flow values were selected for each month from the streamflow hydrograph for all years of record. These values define, for each month, the full range of beginning-month base flows during the period of record. If the flow on the first day of the month is representative of a prolonged dry period, it may be considered to approximate ground-water discharge only, and base flow can be obtained directly from the streamflow hydrograph. In many instances, however, the hydrograph includes some surface runoff, and base flow at the beginning of the month must be approximated by projecting the appropriate predetermined base-flow recession curve (such as defined in figure 8) under the hydrograph as illustrated by the dashed lines in figure 6.

By arranging the beginning-month base-flow values in order of magnitude (m) with the smallest value assigned $m=1$, their recurrence intervals (frequency of occurrence, in years) can be computed from the ratio $RI=(n+1)/m$, where RI is the recurrence interval and n is the total number of years of record ($n=16$ for the Blue River at Milburn site). The January 1 base-flow values for the Blue River at Milburn and their corresponding order number and recurrence interval are listed in table 1 for water years 1966–81.

A plot of the January 1 base-flow values is shown in figure 10 with discharge plotted along the ordinate axis (logarithmic scale) and RI plotted along the abscissa axis, which is based on the normal probability distribution. A curve of best fit has been drawn through these values (curve 1 in figure 10) to define the frequency curve for January 1 base flows. This curve indicates, for example, that a January 1 base flow can be expected to be less than 25 ft^3/s at intervals averaging 10 years. This relation also can be expressed in terms of probabilities where the probability of exceedance is defined as $[1-(1/RI)]$. Thus, if a January 1 base flow is observed to be 25 ft^3/s, this flow can be expected to be equaled or exceeded about 90 percent of the time, which indicates that ground-water conditions are significantly below normal and that drought conditions may exist or be imminent. Beginning-month base-flow frequency curves have been developed for each month of the winter and spring (January through May) as indicated in figure 10. This 5-month period is the most likely to be used in Oklahoma for establishing the status of base flow prior to the subsequent typical dry summer months, when drought conditions have the greatest impact on farmers and municipal water users.

Table 1. January 1 base-flow values for the Blue River at Milburn and their corresponding recurrence interval, water years 1966–81

Water year	January 1 base flow (ft^3/s)	Order number, m	Resource interval, RI (years)
1966	28	2	8.50
1967	24	1	17.0
1968	74	10	1.70
1969	102	13	1.31
1970	96	12	1.42
1971	78	11	1.55
1972	123	15	1.13
1973	46	8	2.12
1974	132	16	1.06
1975	110	14	1.21
1976	57	9	1.89
1977	43	7	2.43
1978	30	4	4.25
1979	31	5	3.40
1980	28	3	5.67
1981	42	6	2.83

Application of the base-flow frequency curves for establishing the status of base-flow conditions on January 1, 1984, for Blue River at Milburn is illustrated in figure 11. The streamflow hydrograph, recorded to January 1, 1984, indicates that base flow as of January 1, 1984, is about 45 ft^3/s. The base-flow frequency curve in figure 10 shows that a January 1 base flow will be less than 45 ft^3/s at intervals averaging every 2.2 years, or that the probability of exceedance of a January 1 base flow of 45 ft^3/s is 55 percent, indicating a slightly below-normal base flow for this time of the year. Figure 10 indicates that normal base flow ($RI=2.0$ years) on January 1 is about 54 ft^3/s.

PROJECTIONS OF SPRING AND SUMMER BASE FLOW

Once the magnitude of winter (or early spring) base flow has been established as described above, the predetermined base-flow recession curves of figure 8 can be used to project minimum "assured" base flow into the subsequent summer months.

Figure 11 shows this projection of the assured base flow from the January 1, 1984, base flow of 45 ft^3/s through the subsequent spring and summer months to September 30. This projection was made by first selecting

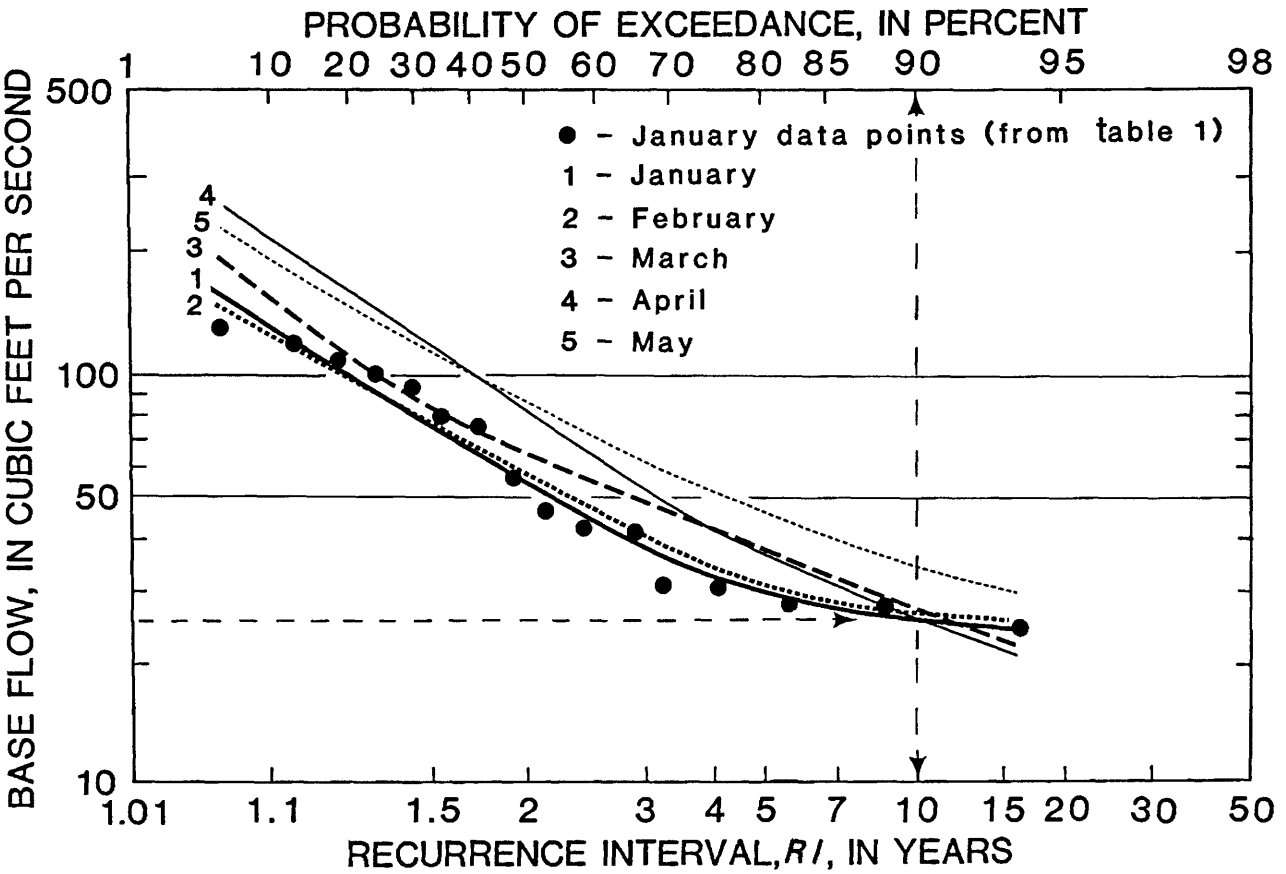

Figure 10. Frequency curves of beginning-month base flows for January to May, Blue River at Milburn, Oklahoma (1966–81).

the two base-flow recession curves in figure 8 that lie immediately above and below the January 1 discharge of 45 ft^3/s. In this instance, interpolation between the curves with January 1 base flows of 60 ft^3/s and 35 ft^3/s was made to define the desired recession curve, which begins with 45 ft^3/s on January 1.

The assured recession in figure 11 represents the minimum flows that would be expected to occur through the projection period (January through September) when the January 1 base flow is 45 ft^3/s. This assured flow reflects essentially ground-water discharge from the regional aquifer system and assumes that little or no significant rainfall will occur during the 9-month projection period to recharge the regional aquifer. The assured recession, therefore, is considered to define the "worst condition" or lower limit of base flow expected for this 9-month period, given a measured base flow of 45 ft^3/s on January 1.

The likelihood that no precipitation will occur throughout the spring and early summer months is generally quite small in Oklahoma. Thus, there is a very low probability that the 9-month projection of assured base flows as indicated in figure 11 will actually occur. The probability, however, that the projected assured base flows will be exceeded as a result of rainfall can be estimated for any given month by evaluating the distribution of historic end-of-month increases in base flow (ΔI). To determine this distribution, the increase in base flow was estimated from the streamflow hydrograph by projecting base-flow recessions under the hydrograph using the recession curves of figure 8. The increase, ΔI, for a given month, i, as shown for March in figure 6, is defined as:

$$\Delta I_i = C_i - B_i$$

where B_i is the "assured" end-of-month base flow projected from the beginning-month base flow (A_i), and C_i is the "adjusted" end-of-month base flow that must be equal to or greater than B_i.

During a month when no recharge occurs because of little or no precipitation, $C_i = B_i$, and $\Delta I_i = 0$. To determine the subsequent month increase in base flow $\Delta I_{(i+1)}$, C_i becomes $A_{(i+1)}$ and the appropriate recession curve (which must be extrapolated from the assured curves in figure 8) is projected from $A_{(i+1)}$ to define $B_{(i+1)}$. For months during which little or no precipitation occurs, ΔI is relatively easy to define, but accurate definition of ΔI during periods of significant runoff is more difficult and requires some subjective interpretation of the base-flow recession under the hydrograph. However, this problem is not critical because only order-

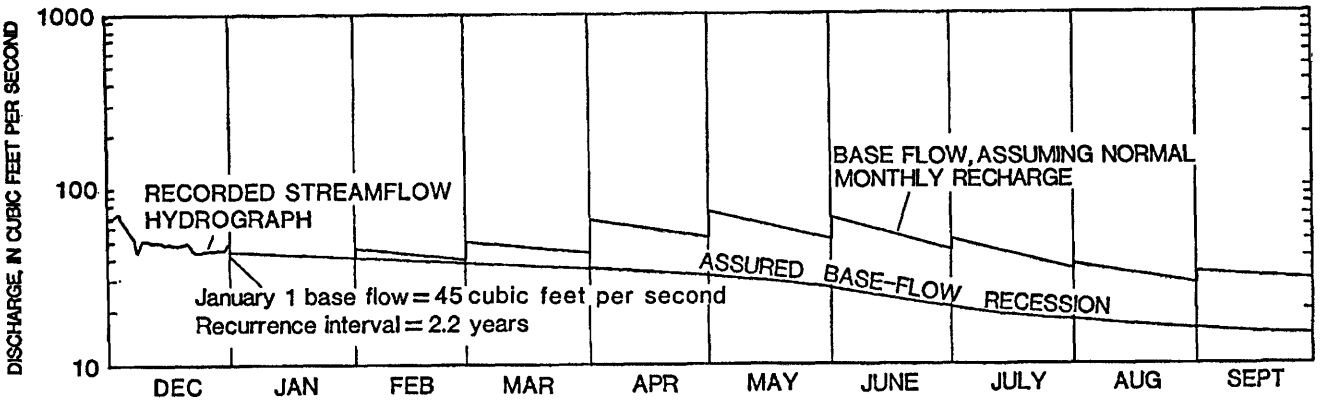

Figure 11. Recorded streamflow of Blue River at Milburn, Oklahoma, defined to January 1, 1984, projected assured base-flow recession from January 1, and projected base flow from January 1, assuming normal monthly recharge.

of-magnitude estimates of ΔI are needed for this analysis, and when ΔI is large, which indicates that significant precipitation has occurred to recharge the regional ground-water system, the potential for hydrologic droughts is reduced.

Estimates of ΔI were obtained from the annual hydrographs for each month from January through September and their probability of exceedance curves were computed in the same manner as described previously for the beginning-month base-flow values. Figure 12 shows the probability curve of exceedance for base-flow increases (ΔI) for the end of each month during January–September. For example, the January curve indicates that an end-of-month increase in base flow of 5 ft^3/s will be exceeded, on the average, 50 percent of the time for January.

If probabilities of recharge are assumed for each month during a projection period such as the 9-month recession period for water year 1984 in figure 11, then the ΔI probability curves in figure 12 can be used to estimate increases to the assured base flow throughout the recession period. For example, if the end-of-month increase is assumed to occur at the 50 percent probability level for each month (normal monthly recharge), then the projected base flow will define the incremental base-flow recessions shown in figure 11. Table 2 lists the beginning-month and end-of-month base-flow values and the corresponding monthly base-flow increases at the 50 percent probability level (taken from figure 12). These monthly base-flow increases were used to define the incremental base-flow recessions in figure 11.

RELIABILITY OF PROJECTED BASE FLOWS

A measure of the reliability of the derived base-flow recession curves and the ΔI probability curves for projecting base flow through the spring and summer months was made by comparing the recorded 1984 streamflow hydrograph with the derived base-flow recession curves adjusted to reflect monthly recharge from excess runoff. Excess runoff is defined in this analysis as the volume of water above the assured base flow—that is, above the base-flow recession unadjusted for recharge (recession A–B in figure 6). Work by the author in relating monthly excess runoff (RO) to the corresponding end-of-month increase in base flow (ΔI), in this study and in previous studies (Riggs and Hanson, 1969), indicates that RO is a good indicator of base-flow increase. Excess runoff was estimated for each month (January through September) for water years 1966–81 and their probabilities of occurrence were computed in the same manner as for the end-of-month increase in base flow. Table 3 lists the probability of exceedance (P) of excess runoff (RO) for each month during January through September 1984.

Because RO relates closely to ΔI, the probability distributions of RO and ΔI should be similar. The

Table 2. Projection of 1984 base flows from January through September, assuming monthly recharge at 50 percent probability level, Blue River at Milburn, Oklahoma

[A is beginning-month base flow; B is projected end-of-month assured base flow; ΔI is end-of-month base-flow increase at 50 percent probability level; C is the end-of-month adjusted base flow;–, no data]

Month	A (ft^3/s)	B (ft^3/s)	ΔI (ft^3/s)	C (ft^3/s)
January	45	41	5	46
February	46	40	11	51
March	51	44	24	68
April	68	53	21	74
May	74	51	17	68
June	68	44	7	51
July	51	35	2	37
August	37	29	4	33
September	33	30	4	34
October	34	--	--	--

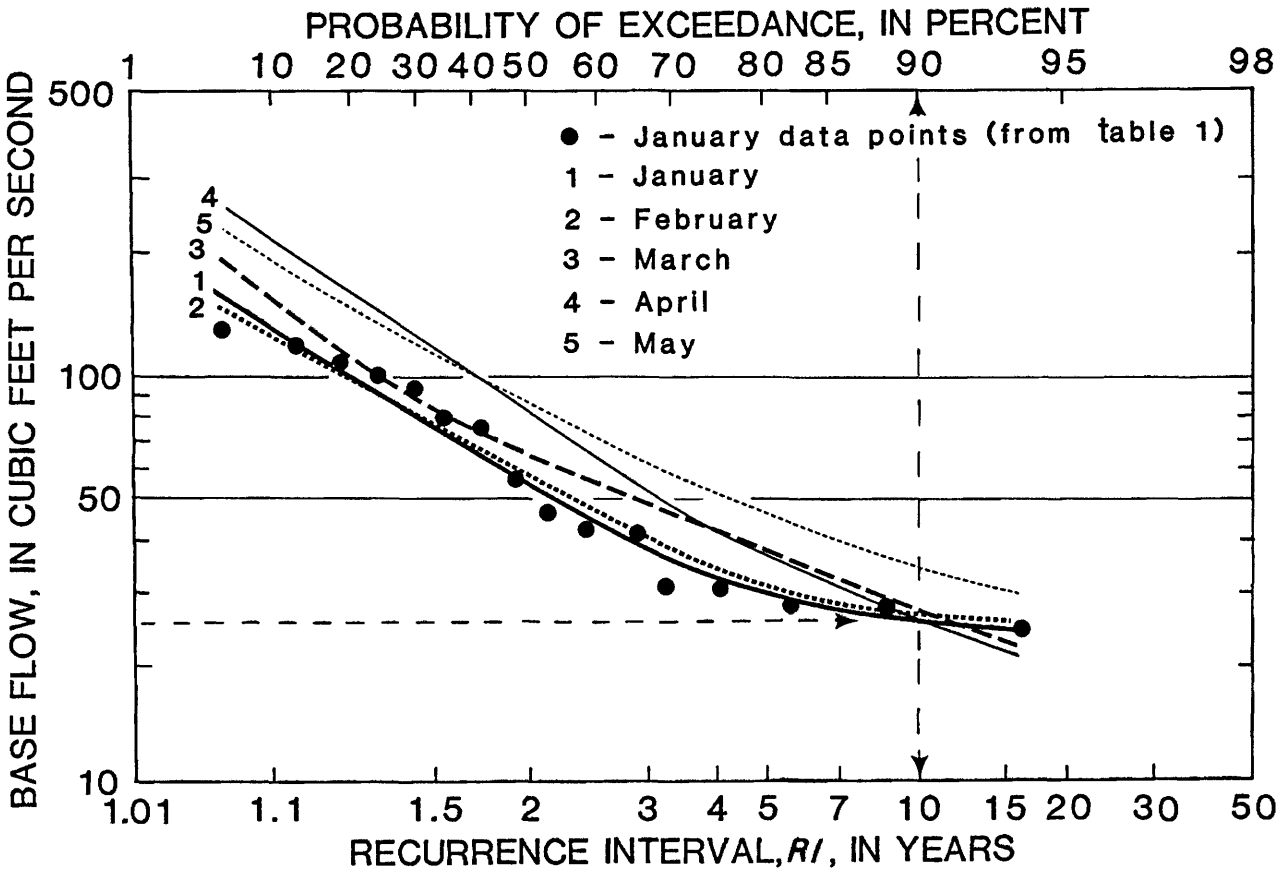

Figure 12. Curves defining probability of exceedance of end-of-month base-flow increase, ΔI, for January to September, Blue River at Milburn, Oklahoma (1966–81).

Table 3. Estimates of end-of-month base-flow increase for each month from January through September 1984 derived from corresponding probability of exceedance of excess runoff for each month, Blue River at Milburn, Oklahoma

[*RO* is monthly excess runoff; *P* is probability of exceedance corresponding to each *RO* value; and ΔI is estimated end-of-month base-flow increase (from figure 12) associated with each probability value]

Month	*RO* (ft^3/s)	*P* (percent)	ΔI (ft^3/s)
January	6	65	2
February	9	70	4
March	98	40	40
April	58	55	16
May	14	90	2
June	5	80	1
July	5	40	3
August	1	90	0
September	3	85	0

probabilities of exceedance determined for each monthly *RO* were substituted in the probability of exceedance curves of figure 12 to obtain estimates of ΔI for each month during 1984. These ΔI values, which are included in table 3, were then used to compute the adjusted base-flow recession segments shown in figure 13. The graph shows significant base-flow increases at the end of March (40 ft^3/s) and April (16 ft^3/s) in response to the large volume of surface runoff during these two months, followed by relatively minor increases during the subsequent summer months. The base-flow recession from May through September 1984, when precipitation at the Tishomingo Wildlife Refuge was 20 percent below normal, follows the recorded streamflow recession closely, indicating that the derived relations do describe base-flow recession rates (fig. 8) and base-flow increases (fig. 12) reasonably well. Included on the graph is the assured base-flow recession for no recharge during the 9-month recession period.

CONCLUSIONS

This study shows that base flow, which approximates ground-water discharge to the stream, varies both seasonally and annually and is dependent on the volume of seasonal and annual recharge to the ground-water system. Base flow from an unregulated watershed can be used to estimate future streamflows characterized by prolonged periods when little or no precipitation occurs. Relations that describe the frequency of occurrence of

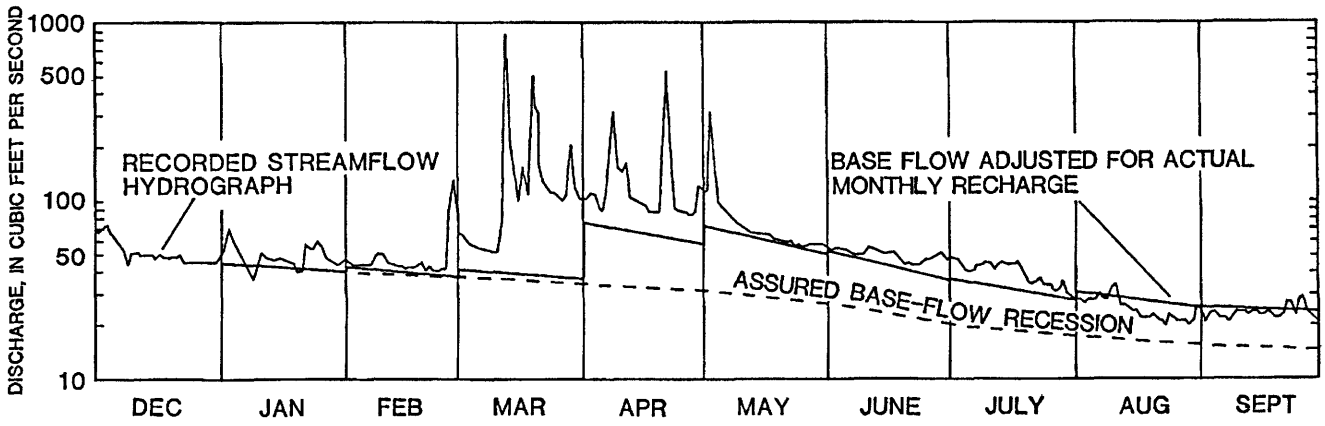

Figure 13. Recorded streamflow of Blue River at Milburn, Oklahoma, December 1983 to September 30, 1984, assured base-flow recession projected from January 1, and base flow adjusted for actual monthly recharge.

beginning-month base flows for the winter and spring months are good tools for evaluating the relative amount of streamflow available at the time and the status of an impending or potential hydrologic drought.

Base-flow recession curves developed from recorded streamflow hydrographs can be used to project base flow from the winter through the subsequent spring and summer months, thus giving an estimate of the spring and summer assured minimum flows. Assured flows approximate streamflow, assuming no rainfall during the projection period and, therefore, are considered to define the minimum quantity of streamflow available. Projection of base flow in excess of the assured flow that results from recharge by rainfall also may be made for any desired (or assumed) probability. These projections are not considered "forecasts" of base flow and should not be applied as such, unless reliable climatological forecasts are available to indicate what the future runoff is expected to be.

Application of these techniques to evaluate existing and potential drought conditions for an unregulated 203-mi^2 watershed in south-central Oklahoma indicates that the techniques give reliable results. A base-flow analysis of other unregulated streams throughout the State can provide index sites for monitoring the status of ground-water conditions statewide. The regional extent and severity of a pending or potential hydrologic drought can then be evaluated for the entire State.

REFERENCES CITED

Barnes, B.S., 1939, The structure of discharge recession curves: American Geophysical Union Transactions, v. 20, pt. IV, p. 721–725.

Fairchild, R.W., Hanson, R.L., Davis, R.E., 1982, Hydrology of the Arbuckle Mountain area, south-central Oklahoma: U.S. Geological Survey Open-File Report 82–775, 156 p.

Hirsch, R.M., 1981, Stochastic hydrologic model for drought management: American Society of Civil Engineers, Journal of Water Resources and Planning Management Division, v. 107, no. WR2, p. 303–313.

Huntzinger, T.L., 1978, Low-flow characteristics of Oklahoma streams: U.S. Geological Survey Open-File Report 78–166, 93 p.

Huschke, R.E., ed., 1959, Glossary of meteorology: Boston, American Meteorological Society, 638 p.

Meko, D.M., 1982, Drought history in the Western Great Plains from tree rings, *in* Proceedings of the International Symposium on Hydrometeorology, June 13–17, 1982: Denver, Colorado, American Water Resources Association, p. 321–326.

Mitchell, J.M., Jr., Stockton, C.W., and Meko, D.M., 1978, Evidence of a 22-year rhythm of drought in the western United States related to the Hale solar cycle since the 17th century, *in* McCormac, B.M., and Seliga, T.A. eds., Proceedings of the Symposium on Solar-Terrestrial Influences on Weather and Climate, Ohio State University, July 24–28, 1978: Boston, D. Reidel Publishing Co., p. 125–143.

National Weather Service, 1977, Crop moisture index: Technical Procedures Bulletin No. 204, 7 p.

Palmer, W.C., 1965, Meteorological drought: U.S. Department of Commerce Research Paper 45, 58 p.

Perry, C.A., 1980, Preliminary analysis of regional-precipitation periodicity: U.S. Geological Survey Water-Resources Investigations 80–74, 26 p.

Riggs, H.C., 1963, The base-flow recession curve as an indicator of ground water: International Association of Scientific Hydrology, Publication No. 63, General Assembly of Berkeley of the International Union of Geodesy and Geophysics, p. 352–363.

Riggs, H.C., and Hanson, R.L., 1969, Seasonal low-flow forecasting, *in* Hydrologic Forecasting, Technical Note No. 92: World Meteorological Organization No. 228, T.P. 122, p. 286–299.

Rorabaugh, M.I., 1964, Estimating changes in bank storage and ground-water contribution to streamflow: International Association of Scientific Hydrology Symposium—Surface Waters, Publication No. 63, p. 432–441.

Rosenberg, N.J., ed., 1979, Drought in the Great Plains—Research on impacts and strategies: Proceedings of the Workshop on Research in Great Plains Drought Management Strategies, University of Nebraska, Lincoln, March 26–28: Littleton, Colorado, Water Resources Publications, 225 p.

Singh, K.P., and Stall, J.B., 1973, The 7-day 10-year low flow of Illinois streams: Illinois State Water Survey, Department of Registration and Education, Bulletin 57, 24 p.

U.S. Geological Survey, 1970, The National Atlas of the United States of America: p. 121.

Warrick, R.A., 1975, Drought hazard in the United States: A research assessment: Boulder, Colorado, University of Colorado, Institute of Behavorial Science, Monograph no. NSF/RA/E-75/004, 199 p.

Weakly, H.E., 1943, A tree-ring record of precipitation in western Nebraska: Journal of Forestry, v. 41, p. 816–819.

Yevjevich, Vujica, Hall, W.A., and Salas, J.D., eds., 1977, Drought research needs, *in* Proceedings of the Conference on Drought Research Needs, December 12–15, 1977: Colorado State University, Fort Collins, Colorado, 276 p.

*U.S. G.P.O. 1988-242-338:80043

SELECTED SERIES OF U.S. GEOLOGICAL SURVEY PUBLICATIONS

Periodicals

Earthquakes & Volcanoes (issued bimonthly).
Preliminary Determination of Epicenters (issued monthly).

Technical Books and Reports

Professional Papers are mainly comprehensive scientific reports of wide and lasting interest and importance to professional scientists and engineers. Included are reports on the results of resource studies and of topographic, hydrologic, and geologic investigations. They also include collections of related papers addressing different aspects of a single scientific topic.

Bulletins contain significant data and interpretations that are of lasting scientific interest but are generally more limited in scope or geographic coverage than Professional Papers. They include the results of resource studies and of geologic and topographic investigations; as well as collections of short papers related to a specific topic.

Water-Supply Papers are comprehensive reports that present significant interpretive results of hydrologic investigations of wide interest to professional geologists, hydrologists, and engineers. The series covers investigations in all phases of hydrology, including hydrogeology, availability of water, quality of water, and use of water.

Circulars present administrative information or important scientific information of wide popular interest in a format designed for distribution at no cost to the public. Information is usually of short-term interest.

Water-Resources Investigations Reports are papers of an interpretive nature made available to the public outside the formal USGS publications series. Copies are reproduced on request unlike formal USGS publications, and they are also available for public inspection at depositories indicated in USGS catalogs.

Open-File Reports include unpublished manuscript reports, maps, and other material that are made available for public consultation at depositories. They are a nonpermanent form of publication that may be cited in other publications as sources of information.

Maps

Geologic Quadrangle Maps are multicolor geologic maps on topographic bases in 7 1/2- or 15-minute quadrangle formats (scales mainly 1:24,000 or 1:62,500) showing bedrock, surficial, or engineering geology. Maps generally include brief texts; some maps include structure and columnar sections only.

Geophysical Investigations Maps are on topographic or planimetric bases at various scales; they show results of surveys using geophysical techniques, such as gravity, magnetic, seismic, or radioactivity, which reflect subsurface structures that are of economic or geologic significance. Many maps include correlations with the geology.

Miscellaneous Investigations Series Maps are on planimetric or topographic bases of regular and irregular areas at various scales; they present a wide variety of format and subject matter. The series also includes 7 1/2-minute quadrangle photogeologic maps on planimetric bases which show geology as interpreted from aerial photographs. Series also includes maps of Mars and the Moon.

Coal Investigations Maps are geologic maps on topographic or planimetric bases at various scales showing bedrock or surficial geology, stratigraphy, and structural relations in certain coal-resource areas.

Oil and Gas Investigations Charts show stratigraphic information for certain oil and gas fields and other areas having petroleum potential.

Miscellaneous Field Studies Maps are multicolor or black-and-white maps on topographic or planimetric bases on quadrangle or irregular areas at various scales. Pre-1971 maps show bedrock geology in relation to specific mining or mineral-deposit problems; post-1971 maps are primarily black-and-white maps on various subjects such as environmental studies or wilderness mineral investigations.

Hydrologic Investigations Atlases are multicolored or black-and-white maps on topographic or planimetric bases presenting a wide range of geohydrologic data of both regular and irregular areas; principal scale is 1:24,000 and regional studies are at 1:250,000 scale or smaller.

Catalogs

Permanent catalogs, as well as some others, giving comprehensive listings of U.S. Geological Survey publications are available under the conditions indicated below from the U.S. Geological Survey, Books and Open-File Reports Section, Federal Center, Box 25425, Denver, CO 80225. (See latest Price and Availability List.)

"Publications of the Geological Survey, 1879- 1961" may be purchased by mail and over the counter in paperback book form and as a set of microfiche.

"Publications of the Geological Survey, 1962- 1970" may be purchased by mail and over the counter in paperback book form and as a set of microfiche.

"Publications of the U.S. Geological Survey, 1971- 1981" may be purchased by mail and over the counter in paperback book form (two volumes, publications listing and index) and as a set of microfiche.

Supplements for 1982, 1983, 1984, 1985, 1986, and for subsequent years since the last permanent catalog may be purchased by mail and over the counter in paperback book form.

State catalogs, "List of U.S. Geological Survey Geologic and Water-Supply Reports and Maps For (State)," may be purchased by mail and over the counter in paperback booklet form only.

"Price and Availability List of U.S. Geological Survey Publications," issued annually, is available free of charge in paperback booklet form only.

Selected copies of a monthly catalog "New Publications of the U.S. Geological Survey" available free of charge by mail or may be obtained over the counter in paperback booklet form only. Those wishing a free subscription to the monthly catalog "New Publications of the U.S. Geological Survey" should write to the U.S. Geological Survey, 582 National Center, Reston, VA 22092.

Note.--Prices of Government publications listed in older catalogs, announcements, and publications may be incorrect. Therefore, the prices charged may differ from the prices in catalogs, announcements, and publications.